**UNIVERSIDADE DE SÃO PAULO**

**INSTITUTO DE QUÍMICA**

**Programa de Pós-Graduação em Química**

LETÍCIA FRANCINE MENDES

# Development of portable electrochemical devices on polymer materials using $CO_2$ laser for analytical applications

Versão corrigida da Tese defendida

SÃO PAULO

Data de depósito na SPG:

27/07/2023

LETÍCIA FRANCINE MENDES

# Desenvolvimento de dispositivos eletroquímicos portáteis em materiais poliméricos usando laser de $CO_2$ para aplicações analíticas

*Tese apresentada ao Instituto de Química da Universidade de São Paulo para a obtenção do título de Doutora em Ciências (Química).*

Orientador: Prof. Dr. Thiago Regis Longo Cesar da Paixão

SÃO PAULO

- 2023-

Universidade de São Paulo
Instituto de Química

# "Desenvolvimento de dispositivos eletroquímicos portáteis em materiais poliméricos usando laser de $CO_2$ para aplicações analíticas"


## LETÍCIA FRANCINE MENDES


**Tese de Doutorado submetida ao Instituto de Química da Universidade de São Paulo como parte dos requisitos necessários à obtenção do grau de Doutora em Ciências - no Programa de Química.**

_____

**Prof. Dr. Thiago Regis Longo Cesar da Paixão**
**(Orientador e Presidente)**

**APROVADO(A) POR:**

_____

**Prof. Dr. Lucio Angnes**
**IQ - USP**

_____

**Profa. Dra. Maiara Oliveira Salles**
**UFRJ**

_____

**Profa. Dra. Pollyana Souza Castro** *(por videoconferência)*
**UFRN**

**SÃO PAULO**
**29 de agosto de 2023**

Ficha Catalográfica elaborada eletronicamente pelo autor, utilizando o programa desenvolvido pela Seção Técnica de Informática do ICMC/USP e adaptado para a Divisão de Biblioteca e Documentação do Conjunto das Químicas da USP

Bibliotecária responsável pela orientação de catalogação da publicação:
Marlene Aparecida Vieira - CRB - 8/5562

M538d

Mendes, Letícia Francine
Development of portable electrochemical devices on polymer materials using CO2 laser for analytical applications / Letícia Francine Mendes. - São Paulo, 2023.
203 p.

Tese (doutorado) - Instituto de Química da Universidade de São Paulo. Departamento de Química Fundamental.
Orientador: da Paixão, Thiago Regis Longo Cesar

1. Laser-scribing technique. 2. electrochemical sensor. 3. portable devices. 4. low-cost material. 5. polymeric platforms. I. T. II. da Paixão, Thiago Regis Longo Cesar , orientador.

*Dedico este trabalho primeiramente a Deus que me presenteia todos os dias com o dom da vida e me dá forças e coragem para atingir os meus objetivos. Também à minha querida família: meus pais (Marco e Walkiria), irmã (Larissa) e meu noivo (Vinícius), sem os quais a realização desse sonho não seria possível.*

*Amo vocês imensamente!*

# ACKNOWLEDGMENTS

This thesis is dedicated first to God, Who has given me strength and encouragement throughout all the challenging moments of completing this dissertation. Furthermore, He has opened many doors in my extensive path, and during this stage of my life, He has been by my side, illuminating and protecting me.

I would also like to thank my parents and sister for all their support, affection, and dedication. They always believed in me, even when I did not, and did their best to help me in my achievements. I love you so much! Furthermore, with affection, I would like to thank my fiance, who has been there for me and extraordinarily supportive throughout this process. His love was essential to show me the beauty and opposite side of life and keep me moving forward during my thesis's challenging times.

I also thank Professor Dr. Thiago Regis Longo Cesar da Paixão, my supervisor, who, with wisdom, knew how to direct my steps and thoughts to reach my goals. He was essential in my formation, sharing his knowledge and friendship with me during this time.

I thank my colleagues and friends from $L_2$ESQ lab for all the help and shared knowledge. Especially to Professor Dr. William Reis de Araujo, for helping me at the beginning of the Ph.D., for sharing with me his knowledge, and for his friendship. I also dedicate a special thanks to Vanessa Neiva de Ataide, Lauro Pradela Filho, Iana Arantes, Juliana, William, Davi, Bruno, Diele, Thiago Matheus Guimarães Selva, José Ricardo, and Akira Ameku for their friendship and support.

I thank my colleagues and friends from other labs, especially Jéssica Soares Guimarães Selva, Gilberto, and Raphael Bacil de Prata, for all the moments, coffee

requests, and friendship. They are my second family who have contributed significantly throughout my professional and personal formation.

From all of them, I could not particularly thank Vanessa and Jessica for always being there for me during these years. We have shared great moments and the same home for a few years. I am so grateful for all their support and friendship! Also, to Raphael, who is like a brother to me and had so much patience in sharing his knowledge and friendship all these years.

To my friends from abroad, I would like to thank Maria José, Amal, Kittiya, Chochanon Moonla, and Pedro for all the shared knowledge. To Professor Dr. Joseph Wang for receiving me in his lab, at the University of California San Diego, for one year.

To Professors from other laboratories, in special Professor Dr. Silvia Serrano and Professor Dr. Mauro Bertotti, for the welcome, all the help, knowledge shared, and the friendship.

To Maria Cristina and Lucia, laboratory technicians, for all the friendship, affection, encouragement, and help they gave me during this stage of my life.

To FAPESP for the Ph.D. scholarship (Process: 2018/16250-0), for giving me the opportunity of going to my research internship abroad (Process: 2021/10523-7), and for all the financial support granted, as well as to CAPES and CNPq for financial support to the laboratory.

To my other colleagues for their usual companionship, for always supporting me, and for giving me the pleasure of friendship, making this stage of my life much more unique and fun.

And to everyone who directly or indirectly contributed to the completion of this thesis.

“Alguns homens vêem as coisas como são, e dizem ‘Por quê?’ Eu sonho com as coisas que nunca foram e digo ‘Por que não?'”

**(George Bernard Shaw)**

# ABSTRACT

Mendes, L. F., **Development of portable electrochemical devices on polymer materials using $CO_2$ laser for analytical applications**, 2023, 203 p. Ph.D. Thesis - Graduate Program - Chemistry, Institute of Chemistry, University of São Paulo (USP), São Paulo, Brazil.

This work is divided into two parts. First, I studied the use of two different non-conductive polymeric platforms to develop portable electrochemical devices using the laser-scribing technique as a scalable, low-cost, easy method to fabricate portable devices. Phenolic paper, a low-cost, rigid board that can easily be bought or recycled from used systems, as another alternative material for fabricating laser-scribed electrochemical divices, provided a conductive carbon-based material containing a porous structure with graphene-like domains. Furthermore, an electrochemical treatment on the fabricated material provided excellent conductivity and low charge-transfer resistance. Thus, great potential for on-site analytical applications was observed when using these devices, achieving better performances than conventional carbon electrodes. Polyimide is another polymeric material widely used to obtain electrochemical devices using laser-scribing. In this work, a low-cost polyimide source, Kapton tape, was also used to fabricate a flexible device. This device was applied using static conditions and a paper-based platform to obtain a microfluid system using hydrodynamic conditions. A low-cost, flexible, and versatile electrochemical platform was obtained, where the analytical performance of the system was evaluated in both static and hydrodynamic modes, presenting great potential for analytical applications when compared to conventional platforms. In the second part of this work, an initial study with microneedles to learn about wearable sensors was carried out in my research internship abroad. A hollow microneedle array-based electrochemical sensor was studied, aiming at minimally invasive monitoring of propofol drug. Although more studies are necessary, the new microneedle array sensing platform holds excellent potential for continuously monitoring the anesthetic propofol drug during surgical procedures.

**Keywords:** Laser-scribing technique, electrochemical sensor, portable devices, low-cost material, polymeric platforms, wearable sensors.

# RESUMO

Mendes, L. F., **Desenvolvimento de dispositivos eletroquímicos portáteis em materiais poliméricos usando laser de $CO_2$ visando a aplicações analíticas**, 2023, 203 p. Tese de Doutorado - Programa de Pós-graduação em Química, Instituto de Química, Universidade de São Paulo (USP), São Paulo, Brasil.

Este trabalho está dividido em duas partes. Primeiro, estudamos o uso de duas plataformas poliméricas não condutoras diferentes para o desenvolvimento de dispositivos eletroquímicos portáteis usando a técnica de gravação a laser como um método escalável, de baixo custo e fácil para fabricação dos dispositivos portáteis. Uma placa rígida de fenolite de baixo custo que pode ser facilmente comprada ou reciclada de sistemas usados, foi usada como outro material alternativo para a fabricação de dispositivos eletroquímicos usando a técnica de gravação a laser, fornecendo um material condutor à base de carbono contendo uma estrutura porosa com domínios semelhantes ao grafeno. Além disso, um tratamento eletroquímico no material fabricado proporcionou excelente condutividade e baixa resistência à transferência de carga. Assim, ao usar esses dispositivos, observou-se um grande potencial para aplicações analíticas in loco, obtendo desempenhos melhores do que os eletrodos de carbono convencionais. A poliimida é outro material polimérico amplamente utilizado atualmente para a obtenção de dispositivos eletroquímicos pelo método de gravação a laser. Neste trabalho, uma fonte de poliimida de baixo custo, fita Kapton, também foi utilizada para fabricar um dispositivo flexível. Este dispositivo foi aplicado usando condições estáticas e combinado com uma plataforma baseada em papel para obter um sistema microfluídico usando condições hidrodinâmicas. Obteve-se uma plataforma eletroquímica flexível, versátil e de baixo custo, onde o desempenho analítico do sistema foi avaliado nos modos estático e hidrodinâmico, apresentando grande potencial para aplicações analíticas quando comparado a plataformas convencionais. Na segunda parte deste trabalho, em meu estágio de pesquisa no exterior, foi realizado um estudo inicial com microagulhas para aprender sobre sensores vestíveis. Um sensor eletroquímico baseado em arranjo de microagulhas ocas foi estudado, visando o monitoramento minimamente invasivo da droga propofol. Embora mais estudos ainda sejam necessários, a nova plataforma de detecção, uma matriz de microagulhas, possui excelente potencial para monitorar continuamente o anestésico propofol durante procedimentos cirúrgicos.

**Palavras-chave:** Técnica de gravação a laser, sensor eletroquímico, dispositivos portáteis, material de baixo custo, plataformas poliméricas, sensores vestíveis.

# LIST OF FIGURES

# LIST OF TABLES

# TABLE OF CONTENTS

# CHAPTER 1

## 1. Introduction

## 1.1. Portable analytical platforms

The search for fast diagnoses [1], real-time food safety monitoring [2], quick inspections of crime scenes [3], and environmental supervision [4], among others, has attracted attention to the fabrication of portable analytical platforms since most of the used analysis techniques are time-consuming and requires laboratories with very qualified technicians [5]. Therefore, different ways to fabricate these portable analytical platforms have been studied using various techniques and materials. And the search for miniaturization and simplification in the fabrication process has been intensified to provide accessible devices with lower cost and establish the possibility of coupling more sensors on the same platform [6–9].

In this direction, a significant number of platforms have been explored, such as silicon, glass, ceramics, dimetil polissiloxano (PDMS), Polyimide, and polimetilmetacrilato (PMMA), among others, including paper [10], which has aroused great interest and gained strength in the last years [11]. The paper has been a tool used since 79 AD, where there are reports of a colorimetric test for ferrous sulfate performed with papyrus [12]. In the 1950s, paper was widely used for electrophoresis, for example, in separating proteins [13], and in 1957 J. Kohn described the first application of the paper as a colorimetric test for detecting glucose in urine [14]. In contrast, the first commercial pregnancy test was made available only in 1988 [15], and in 2007, Prof. Whitesides presented devices based on paper using photoresist as a patterning technique [16]. Since then, the use of this type of platform for the fabrication of colorimetric sensors has increased, not only due to its excellent properties, such as high porosity and flexibility, in addition to the low cost, but also due to the advancement

in micro and nanotechnology, which provided the fabrication of new types of devices [17].

Paper is composed of cellulosic fibers, which give it several essential properties, including microfluidics due to capillarity providing easy transport of the analyte through the paper's fibers without the need for analytical instrumentation to carry it out as, for example, peristaltic pumps. Hydrophilicity and compatibility with biological samples are essential properties observed on paper platforms besides the high porosity and flexibility already mentioned. Another great point is the low cost of this material due to its abundance, which characterizes it as a good platform for developing simple and portable analytical devices [18–22].

Both colorimetric and electrochemical analyzes can be performed on these platforms, depending on the preparation and application of the devices [10,11,16,23–25]. For fabrication, different types of paper have been used, such as filter paper, chromatography paper, and cardboard, among others [7,19,26]. Furthermore, a hydrophobic barrier is usually created to delimit the reaction area for electrochemical and colorimetric paper-based analysis. This barrier can be produced using polymers, such as polydimethylsiloxane, polystyrene, polyurethane[19], permanent marker[27], wax printing [19,28], and even school glue [29]. Physical barriers are also reported in the literature by cutting the paper where the microstructures formed create the physical boundaries [30]. This procedure can be realized using a laser cutting machine or a cutter plotter with X-Y axis control [30], handheld blades, and hole punches [31].

Associated with electrochemical detection techniques, the obtention of miniaturized, portable, and disposable paper-based devices is more accessible due to being more sensitive techniques and reaching lower detection limits than the colorimetric methods [32]. These advantages lead to the facility to use the devices for

point-of-care (POC) analysis, which has been widely investigated [17,32,33] since portable devices have gained significant attention, especially in the clinical analysis due to the possibility of real-time monitoring of patients undergoing treatment. These are the so-called wearable sensors, in addition to health conditions for preventing and controlling diseases without the need for sophisticated apparatus, trained technicians or sophisticated laboratory facilities [17,22,34].

In 2009, Dungchai and collaborators [35] reported the first paper-based electrochemical device containing three electrodes system and three separate test zones. In this case, the fabricated device was tested for clinical application to determine ascorbic acid, uric acid, and glucose in serum and human urine. The electrodes were modified using enzymes, and the respective detection limits reached were 0.21, 0.36, and 1.38 mmol $L^{-1}$, for glucose, lactate, and uric acid, respectively.

Since then, several electrochemical paper-based devices have been fabricated following the same direction, aiming for better responses and limits of detection. Moreover, these devices have been studied to be used in the detection of other analytes of interest, such as cholesterol [36], cortisol [37], metabolites [38], and even cancer biomarkers [39], aiming at expanding analytical applications.

Besides the different methods and techniques proposed to isolate the reaction zones, a diversity of techniques has been presented for the fabrication of the conductive tracks, so-called electrodes, in the electrochemical paper-based devices (ePDAs), building upon the initially used screen-printing approach and followed by stencil-printing, inkjet-printing, photolithograph, drop-casting, pencil drawing, filtration, pyrolysis, and laser-scribing method [8]. A timeline of the different approaches applied to the ePDAs fabrication from 2009 to 2019 is presented in Figure 1.

**Figure 1 –** Timeline with the main techniques used to fabricate electrochemical paper-based devices (ePADs) reported from 2009 to 2019. **a)** screen-printing technology, **b)** stencil-printing approach, **c)** Inkjet printing, **d)** Photolithography, **e)** Drop casting, **f)** Pencil lead, **g)** Pencil drawing, **h)** Filtration, **i)** Microwire incorporation, **j)** Paper pyrolysis, **k)** Direct laser scribing on paper[8].

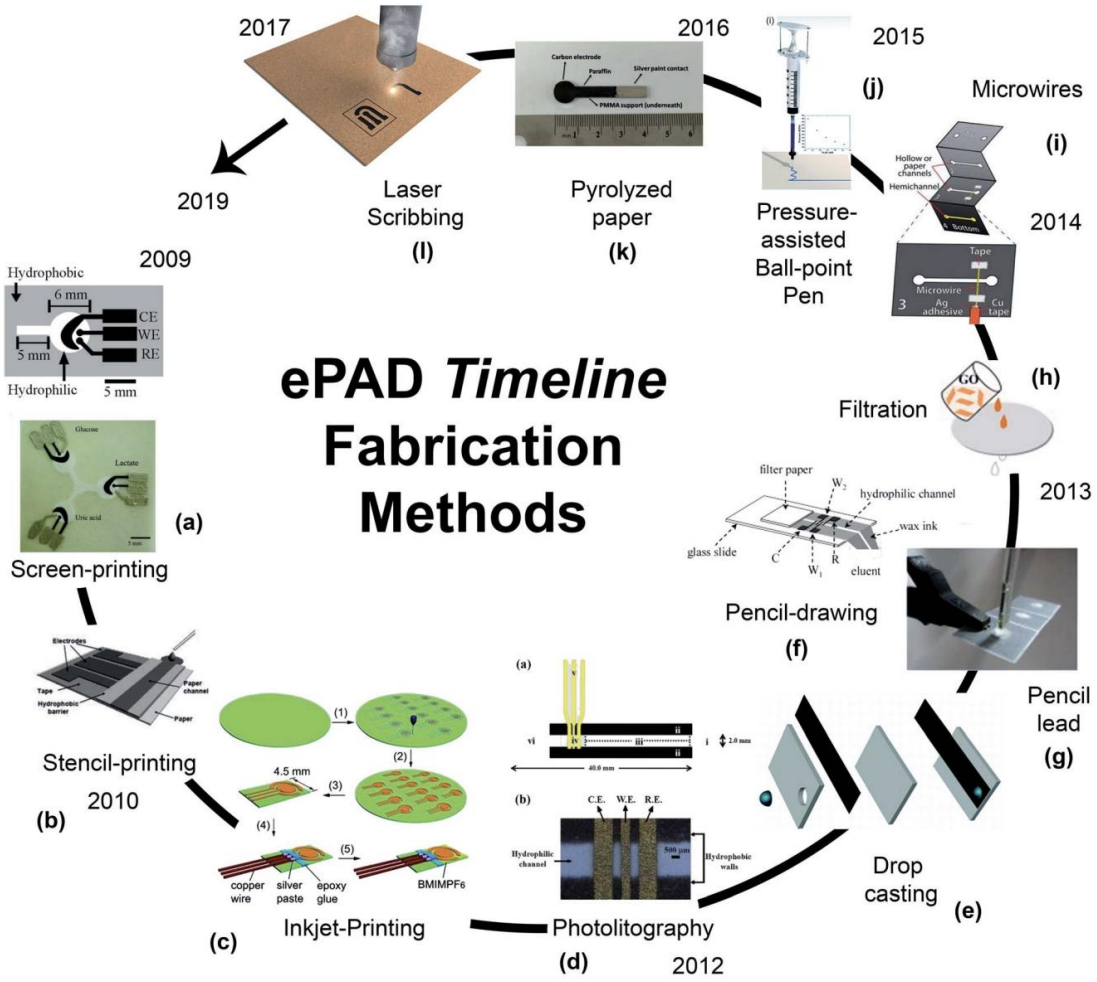


The latter approach, laser-scribing, represents one of the essential methods because it is a scalable, manageable, and low-cost method to fabricate carbon-based electrodes. Furthermore, it can be applied not only on paper platforms but also on polymeric materials. Although the paper has some advantages and is widely used in fabricating portable analytical devices, polymeric materials can guarantee flexibility to the devices, which is essential when talking about “wearable sensors” type, besides the robustness and physical stability compared with paper [17].

## 1.2. Laser-scribing technique

Laser-scribing represents one of the most required fabrication methods for portable electrochemical devices. It is a scalable, manageable, and low-cost method to fabricate carbon-based electrodes that can be applied to various platforms. The technique only requires a print-shop-grade $CO_2$ laser engraver to carbonize the material's surface, rendering a conductive carbon track [40].

The main point is to provide better sensitivity, selectivity of portable analytical devices, and several groups have modified the electrodes' surface with different materials. Among them are functional carbon nanomaterials such as graphene or carbon nanotubes [41], which have interesting properties due to their type of hybridization, and one of the most exciting materials used by researchers of different areas is the Graphene Oxide (GO). Thus, distinct ways to fabricate the material and its derivative have been studied and utilized [42]. Most of these techniques are limited by availability, cost, variability in the composition, and the chemistry used to immobilize the final obtained material. Furthermore, a laser-based method has also been used, where direct laser scribing is applied on hydrated GO to obtain the reduced one (rGO). This technique provides a simple method to reach a 3D graphene pattern [43]. In 2014 researchers dispersed GO upon a polyimide (PI) surface and applied the laser-scribing technique to the material. However, the $CO_2$ infrared laser occasionally reached the PI surface, where a black carbonized material was obtained, as observed in Figure 2 [44,45].

The carbonized trail observed was studied and characterized, and a porous graphene-like material was noticed. Unlike the other techniques involving time consumption and reagent use, a new, simple, low-cost route was found to fabricate

the material. Therefore, a graphene-like platform could be obtained directly from laser-scribing polymers. The most common terms found in the literature to refer to the materials produced by this technique are Laser-Scribed Graphene (LSG), Laser-Induced Graphene (LIG), and Laser-Derived Graphene (LDG) to describe graphene-based materials fabricated from laser scribing, regardless of the type of laser or the precursor material used [46–48]. For clarity, throughout the text, we will use LSG to refer to carbon materials obtained by the laser-scribing technique.

**Figure 2 – a)** Schematic figure of the laser-scribing process on PI substrate using $CO_2$ laser machine. **b)** SEM images of the LSG pattern obtained from the process (scale bar, 1 mm) and **c)** an ampliation of the image of the LIG film circled in **b)** (scale bar, 10 µm). **d)** Cross-sectional SEM image of the LSG material obtained (scale bar, 20 µm). With permission [44].

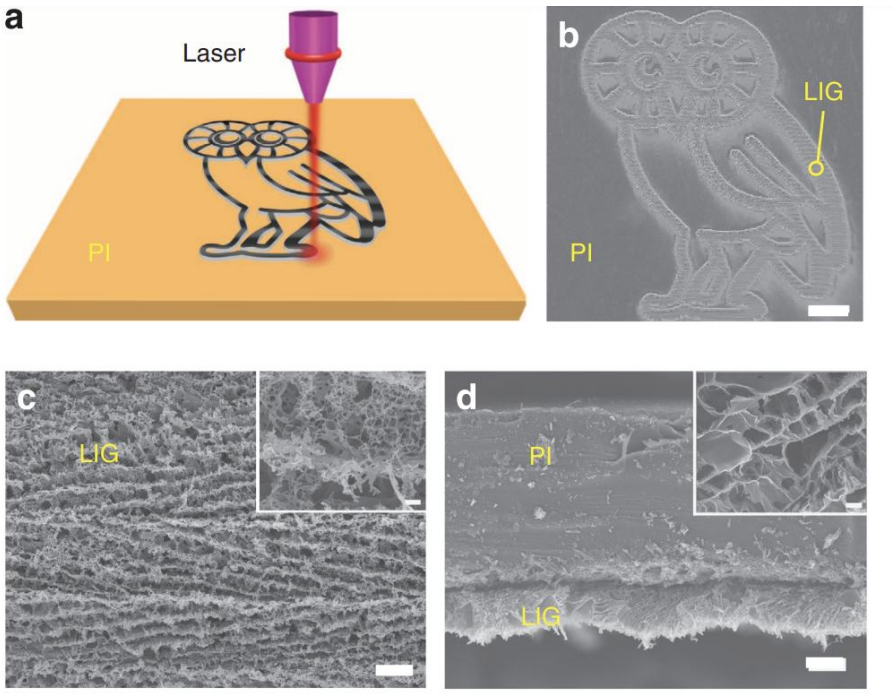


In this area, the first fabricated device was applied as a supercapacitor in energy storage [44]. Then, different applications have emerged, such as microfluidic devices [49,50], electrocatalysts [51] and portable analytical sensors [52–55].

Among the sensors fabricated using this technique, it is possible to observe the physical ones based on capacitance[53] and resistance measurements [54–56], and the electrochemical ones [57,58]. And as already mentioned above, herein we will focus on the electrochemical-based sensors.

One of the first electrochemical devices based on laser-scribed graphene was reported in 2016 for the simultaneous determination of ascorbic acid, dopamine, and uric acid [52]. On this occasion, Pranati Nayak and collaborators fabricated the electrodes using direct laser writing on polyimide under ambient conditions. The parameters used in the laser machine were optimized, and a conductive porous material was obtained with a thickness of 33 μm. Posteriorly, PDMS was used to delimitate the reaction area, and the working electrode was modified with Pt nanoparticles by electrodeposition. The devices showed very high flexibility and potential to be applied as electrochemical sensors, besides an electrocatalytic activity observed due to the modification using Pt nanoparticles, which provided better results than in previously reported graphene-based electrodes [52].

In terms of electrochemical sensors fabrication, the laser-scribing technique presents some advantages when compared with others, such as low-cost, mask-free, template-free patterning method, besides the simple and green synthesis of the electrode material directly on the platform and the obtention of a porous, conductor and mechanically stable material with a large surface area[40]. Due to the characteristics of the method, it has been attracting more attention, and the studies have increased in this direction.

### 1.2.1. LSG precursors platforms

Although the first device had been fabricated using polyimide as a precursor for the obtained material, other polymeric platforms were studied, such as polyetherimide (PEI) [44] and PDMS [59]. Moreover, cloth, paper, food [60], and wood [61] were also explored as other LSG precursors. Among these materials, a multiple laser step could be used to achieve the objective, and materials based on cellulose are usually pretreated with a flame retardant to avoid the decomposition of the material and to provide the obtention of LSG [45].

For the fabrication of the electrochemical sensor, in 2017, a single-step reagentless laser-scribing method was employed for the very first time in a paperboard platform [26]. The $CO_2$ laser machine parameters were optimized and applied to carbonize the material surface using single-step laser-scribing without pretreatments, as is demonstrated in the scheme presented in Figure 3. Besides the fabrication of the electrodes, the devices were cut and separated one by one using the laser machine, applying a higher power. The simple and low-cost electrochemical paper-based device was applied to detect ascorbic acid and caffeic acid as a proof-of-concept for its application potential [26].

**Figure 3 – a)** Schematic presentation of the fabrication process of the LSG ePAD and the **b)** dimensions of the device. **c)** The comparison of the LS-ePAD dimension with the hand size. **d)** SEM image of the obtained carbon-based material. With permission [26].

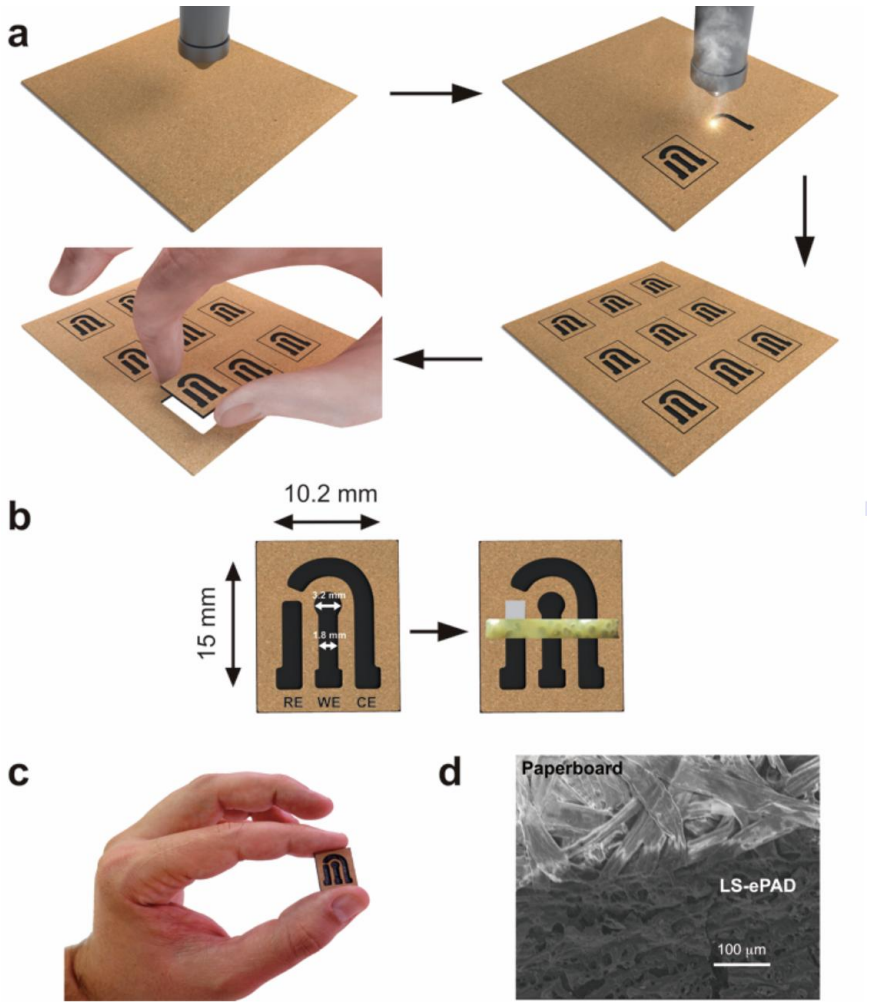


Polyimide, paper, and PDMS have been used as a platform to fabricate electrochemical sensors. The polyimide was the precursor material, and the laser-scribed tracks were easily transferred to a PDMS film. The transference was made by pouring the PDMS onto the carbonized polyimide, and after, it was thermally cured to accomplish the procedure. At the end of the process, the working electrode was modified with electrodeposited Pt-Au nanoparticles. A highly flexible electrochemical

device was obtained, presenting a high selectivity to other molecules, such as ascorbic and uric acid [62].

Another precursor material to obtain LSG applied as an electrochemical sensor was phenolic resin [63]. In 2018 this platform was used for this purpose and presented the advantages of good solubility in different solvents and the facility to form films. These allow its doping with other materials to obtain LSG with distinct and particular properties, besides being also a low-cost material. With this material, Zhuchan Zhang and collaborators fabricated electrochemical devices using an inexpensive 405 nm laser under ambient conditions. After the laser-scribing, the working electrodes were modified using glutaraldehyde and applied as electrochemical glucose sensors [63].

In this direction, lignin was also used as a platform to fabricate electrochemical devices based on the laser-scribing method [64]. This is another platform with the potential to fabricate doped laser-scribed graphene. In this work, a polymeric film using lignin, poly(vinyl alcohol) (PVA), and urea was achieved, and the $CO_2$ laser machine was used to carbonize the tracks. Then, nitrogen-doped laser-scribed graphene was observed and modified using a nanomaterial based on Ti and Prussian Blue, besides the functionalization with specific enzymes to detect glucose, lactate, and alcohol, showing a great potential to be applied in personalized electrochemical sensors for health care[64].

Eventually, in other works, doped laser-scribed graphene was fabricated using polyimide platforms with a controlled atmosphere during the laser-scribing process. One example is the nitrogen-doped porous graphene obtained during the LIG fabrication in $N_2$ controlled atmosphere [65]. In this work, Zhengfen Wan and collaborators obtained a self-N-doped only using polyimide as a precursor polymer for the laser-scribed graphene and specific laser-scribing parameters, such as high

velocity and laser power [65]. The devices were applied as an electrochemical biosensor for mRNA detection since the final N-doped material enhanced interaction with nucleic acids. In another work, Zhang and coworkers developed a 3D graphene doped with high nitrogen concentration using a single-step laser scribing on a urea-containing polyimide substrate [66]. The device was fabricated aiming for applications as Na-ion battery anodes.

The direct fabrication of carbon-based materials modified with metals using the laser-scribing technique as a single step has also been scarcely reported. Yong-il Ko and coworkers used a spin-coated film based on a mixture of Cu particles, polyimide, and N-methyl-2-pyrrolidone under a quartz surface as the substrate for laser-scribing [67]. The obtained carbon nanomaterial presented a high sensitivity for $NO_2$ gas sensing using electrical resistance measurements. In addition, Er-Chieh Cho et al. developed Ag-decorated graphene using a laser-scribing technique under a polyimide surface previously chemically treated with ions $Ag^+$ [68]. This material was applied as a flexible temperature sensor. In another example, Arantes and collaborators [69] used $CO_2$ laser reduction of a precursor solution ($HAuCl_4$) over kraft paper to directly produce Au structures embedded in the carbonized paper matrix generated by the laser-scribing technique. The laser-scribing gold-modified electrodes were applied for hypochlorite (NaClO) detection using the batch-injection analysis (BIA) technique reaching low detection limits.

A different precursor reported for laser-scribing electrode's obtention is the 3D printed platforms. Since the thermoplastic material usually used in the 3D printer is partially insulant, a sub-minute laser-scribing treatment was applied after printing. For example, Rocha and coworkers developed a disposable electrochemical sensor using a carbon-black/PLA-based 3D-printed electrode [70]. This device was used to determine

$Cd^{2+}$, $Pb^{2+}$, and $Cu^{2+}$ simultaneously. Veloso and collaborators also applied the laser-scribing technique to a carbon-black/PLA-based 3D-printed electrode using a similar approach. They used an electrochemical treatment over the device in an alkaline solution (NaOH) to promote the growth of $Na_2O$ nanoflowers [71]. These nanoflowers enhanced the electrochemical response, and the devices were applied for the non-enzymatic quantification of tyrosine in human urine samples.

Thus, another advantage of laser-scribing use would be the controlled, direct, and in-situ synthesis of conductive carbon domains with adequate electrochemical reactivity, besides the possibility of obtaining a doped carbon-based material.

### 1.2.2. Laser sources and other parameters used for LSG fabrication

In addition, besides the different platforms used to develop these electrochemical LSG-based devices, it is possible to notice other variables in the fabrication method. LASER is an acronym for Light Amplification by Stimulated Emission of Radiation [72]. As discussed, the laser-scribing technique consists of the controlled carbonization of precursor materials, such as carbon, polymers, and biopolymers, which generally have insulating characteristics, into conductive materials (graphitic materials) [73–75].

The most commonly used lasers for the fabrication of LSG are $CO_2$ (infrared region (IR)), visible, and ultraviolet [72,76]. The mechanism involved in forming carbon materials or reducing GO depends on the type of laser used in the procedure. The definition of a mechanism as photochemical or photothermal is related to the laser wavelength and pulse duration. A photochemical process occurs using lasers with

short wavelengths and ultra-short pulse widths. The photothermal process is characterized by long wavelengths and pulses (in the order of μs) [44].

IR lasers can reach a smaller spatial resolution, with laser spots of tens and hundreds of micrometers, compared to visible and ultraviolet ones, with few micrometers [77]. This is responsible for the fabrication of smaller electrochemical devices. Moreover, the locally reported temperature during the laser-scribing process can reach up to 2500 ºC depending on the laser type used, which leads to gas generation and, consequently, the formation of a porous carbon-based structure[44]. Santos and collaborators have compared LSG fabricated using UV and IR laser sources[78]. Both devices were applied for quantifying dopamine and presented similar electrochemical responses except for the lower sensitivity observed on the LSG obtained using a UV laser. The porous structure formed was micron-sized for the fabrication using an IR laser and nano-sized using a UV laser.

In addition to the laser source, other parameters also play a vital role during the LSG obtention, such as scanning speed, laser power, and focal distance[79]. It has been reported that a variation in the laser power, for example, can directly alter the ratio of each element observed on the obtained LSG material [65]. Furthermore, Chen and coworkers noticed an effect on the conductivity and wettability of fluorine-doped laser-induced graphene by varying the focal distance [80]. And it was observed that the scanning speed could also influence the structure of the obtained LSG due to the change in the gas evolution. Andrea Lamberti and collaborators observed an order porous LSG with a high hydrophobic behavior using a scan speed of 160 mm $s^{-1}$ and a repetition frequency of 20 kHz [81].

### 1.2.3. LSG electrochemical sensors application

As observed, devices fabricated using the laser-scribing technique were successfully employed for different analytical applications as a proof-of-concept, spatially as electrochemical sensors. A diversity of electrochemical techniques is used in this case, such as differential pulse voltammetry (DPV), square wave voltammetry (SWV), amperometry, potentiometry, and electrochemical impedance spectroscopy (EIS). Tutku Beduk and coworkers developed an LSG-based electrochemical device for environmental monitoring [82]. A Bisphenol A (BPA) sensor was fabricated using polyimide as an LSG precursor platform. A $CO_2$ laser was used to carbonize the material's surface to obtain a laser-scribed three-electrode system containing a working, a reference, and a counter electrode. Then, the reaction area was isolated from the electrical contact area using PDMS. After the development of the electrochemical device, the working electrode was modified using Molecular Imprinted Polymer (MIP) by the electropolymerization of pyrrole monomer. The electropolymerization was performed in the presence and absence of BPA to obtain the control devices. An acetic acid/methanol (3:7) solution was used to remove the BPA from the MIP-specific cavities. Lastly, the electrochemical sensor was used to detect BPA in tap, mineral water, and plastic samples using the DPV technique. The authors observed that the devices presented good reproducibility, besides the capability to be reused up to 4 times. Furthermore, the method represented a simple and easy way to develop the electrodes with great biorecognition [82].

In another work, Raquel R. A. Soares and collaborators developed a safety control sensor using the laser-scribing method [83]. They reported using a three electrodes system where only the working electrode was fabricated employing the

carbonization of polyimide, and counter and reference electrodes were part of the electrochemical analyzer instrument used in the measurements. The working electrode was obtained using a $CO_2$-cutting laser machine in ambient conditions, and the reaction area was isolated from the electric contact by a fast-drying lacquer. Then, the LSG working electrode was modified with a polyclonal antibody anti-Salmonella to detect and monitor *Salmonella enterica* in chicken broth. After the modification of the device, it was applied in real food samples using electrochemical impedance spectroscopy technique for *Salmonella* detection. The sensor presented a good LOD ((13 ± 7) CFU $mL^{-1}$) in a complex sample matrix compared to those fabricated using carbon-based transducers. Moreover, without pretreatment, the time needed to perform the analyses is relatively low when literature shows the time demanded from other carbon-based electrodes used for *Salmonella* detection [83].

Another important application for this type of device is in point-of-care analyses for clinical diagnoses due to its low-cost, disposability, and flexibility. Sharat Chandra Barman and coworkers developed a highly selective electrochemical device to detect Immunoglobulin (IgG), an important biomarker for some diseases [84]. The devices were fabricated using polyimide as an LSG platform, where a three electrodes system was developed by the laser-scribing method in a $CO_2$ laser machine. The reaction area of the electrodes was delimitated using a passivation layer. Then, the electrodes were modified using polyallylamine (PAAMI) to introduce the chemical groups -$NH_2$ on the surface, which would provide the antibody immobilization. Pt nanoparticles were electrodeposited on the working and counter electrode simultaneously. Finally, the working electrode was functionalized by dropping casting technique with the IgG antibody solution. The DPV technique was used to detect IgG, and the sensor platform presented a low LOD (0.006 ng $mL^{-1}$) in human serum samples when confronted with

other carbon-based devices, besides its simplicity, good reproducibility, and high selectivity [84].

In another work, Lima and collaborators fabricated an LSG device to detect xylazine, a drug of abuse, in urine and beverage samples as a POC sensor [85]. This veterinary drug is usually used to facilitate crimes (robbery and rape cases). The device was developed using a polymeric polyetherimide (PEI) platform and $CO_2$ laser. A sensitive device was obtained for xylazine detection, where a highly porous material was observed enhancing the electroactive area. After the carbonized surface was fabricated, an anodic treatment was applied to the working electrodes (2 V for 120 s in 0.1 mol $L^{-1}$ NaOH), which improved the electrochemical performance. The sensor platform was applied on commercial beverage and synthetic urine samples for xylazine detection using SWV electrochemical technique and showed recoveries of 96.0 and 114.8%, respectively, representing a good response. Besides the sensitive electrochemical detection, the devices presented a low-cost (US$0.12) and good reproducibility (RSD 2.56%), essential in POC analysis.

Furthermore, the fabrication of LSG-based sensors was also reported in the literature aiming at wearable sensors application. Wang et al. developed an LSG flexible sensor for simultaneous glucose and pH detection [86]. The electrodes were fabricated using polyimide as a precursor, where a platinum hydroxyethyl cellulose-based hydrogel was deposited over the polyimide surface using the blade coating method. After the precursor material preparation, an one-step direct laser-scribing was applied to the surface using a $CO_2$ laser to generate the electrodes system. The non-carbonized hydrogel was removed from washing using ultrapure water. One of the sided electrodes was modified using Ag/AgCl paste to become the reference electrode, PANI (polyaniline) was electrodeposited on the first working electrode to

obtain a sensible pH sensor, and using the drop-casting technique GOx was immobilized on the second working electrode, using Nafion as a permselective membrane to obtain a glucose selective electrode. After being prepared, the dual electrochemical sensor was applied to analyze glucose and the pH in the human sweat during physical exercise. The results showed a low LOD of 0.23 μmol $L^{-1}$ for glucose quantification using the amperometry technique and a highly sensitive (72.4 mV/pH) in the linear range of pH 4–8 for the pH determination using potentiometry. Furthermore, the device presented good reproducibility, biocompatibility, stability, and flexibility, also the interference effect test presented a good response. Thus, a flexible printed circuit board was coupled to the device to make the entire wearable platform a miniaturized system.

Vivald and coworkers also developed a wearable sensor using an LSG device [87]. The device was fabricated using polyimide as a precursor and a $CO_2$ laser to detect different molecules in human sweat collected through a paper sampler coupled to the device. Characterization of the fabricated carbon-based materials showed a better electrochemical response for the reported analyses when using porous LSG structure. After the fabrication of the device, a sheet of adhesive medical polyurethane (PU) was put over the sensor leaving only the electrical contact exposed. With the bare electrode, both uric acid and tyrosine were detected using electrochemical oxidation, and a modification on the working electrode surface was applied using indoaniline derivative [4-((4-aminophenyl)imino)-2,6-dimethoxycyclohexa-2,5-dien-1-one] to provide selective pH measurements. The multifunctional sensor was tested on-body during exercise and presented great responses. Moreover, cytotoxicity analyses were performed, showing good biocompatibility and the viability of applying the LSG

wearable sensor on the skin, besides the numerous advantages of using the laser-scribing technique for fully laser-manufactured devices.

One of the advantages of the laser-scribing approach would be the controlled, direct, and in-situ synthesis of conductive carbon domains with adequate electrochemical reactivity. More developments in this area would simplify and speed up the fabrication and applicability of laser-scribing electrochemical-based devices, providing the community with new technology.

### 1.3. Wearable sensors

Recently, this other portable analytical device called wearable sensors, consisting of sensors coupled on-body directly, has attracted considerable interest in the real-time monitoring of patients undergoing treatment, health risk, performance, and nutrition markers [88]. Compared to analyses carried out in the laboratory, these devices can be used to monitor health conditions besides control diseases, without needing sophisticated apparatus, trained technicians, or sophisticated laboratory facilities [89]. In this perspective, the electrochemical detection methods also have been widely applied in this case due to the facility of devices miniaturization, fast response, and the possibility to attain lower limits of detection. This is essential for the measurement of important biomarkers since it usually exists in low concentrations in non-invasive body fluids (sweat, saliva, tears,etc.) [88–90].

Wearable sensors are divided into minimally invasive and non-invasive ones, depending on which body fluid is used for monitoring the molecule of interest [91]. For example, different wearable sensors for monitoring the markers contained in sweat

using a non-invasive way have been reported, including temporary tattoos, epidermal patches, clothes-based sensors, and various accessories. Among analytes present in the sweat are glucose, lactate, alcohol, uric acid, tyrosine, sodium, potassium, chloride, and cortisol, where the concentration could be directly correlated to those observed in the blood [91].

Another body fluid for non-invasive measurements using wearable sensors is saliva. Mouthguards, implantable teeth, dental adhesives, and devices outside the mouth have been developed in this case. Nonetheless, the use of this body fluid can be challenging for long-term measurements due to the interference caused by food ingestion, the difficulty of maintaining the sensor over an extended period inside the mouth, the biocompatibility of the device, and the sensor surface fouling induced by the number of macromolecules present in saliva [88]. Tears, on the other hand, are a less complex fluid that contains a lower number of proteins limiting analyses to fewer molecules when compared to the other body fluids. For this reason, this approach has been interesting for analytes with a low molecular weight where devices such as contact lenses, fluidic channels for insertion in the tear canal, and a fluidic sensor coupled in an eyeglass have been used for the detection [88].

Lastly, interstitial fluid (ISF) is one of the most attractive mediums to perform analysis in the biomedical field due to its similarity with blood composition [92]. Thereby, to have access to this fluid, usually, two methods are applied: Reverse iontophoresis (RI) or epidermal microneedles devices [88]. The first one consists of the application of an electrical current on the skin using two electrodes, which causes the ions migration from the inside to the outside skin leading either to the migration of small non-charged molecules, such as glucose [93]. However, this method can imply a dilution of the

analyte's real concentration due to paracellular diffusion, besides the possibility of contamination with skin sweat [91].

The second method, epidermal microneedles, although considered a minimally invasive method, allows the combination of different microneedle sensors in a single array leading to multiple analyses. Moreover, the microneedles enable access to the outer skin layer, and consequently the ISF, with no pain for the biomarkers monitoring [94].

### 1.3.1. Microneedles

Microneedles are used for sensor applications, cosmetics, and therapeutic purposes, such as drug delivery. However, herein, we will focus on microneedle electrochemical sensors. These devices can be fabricated using different materials, such as polymers, silicon, metal, ceramics, hydrogels, and glass, the variety of configurations depends on the application [95]. For transdermal detection, the most used microneedles are both hollow and solid microneedles, although there are also other classes, including dissolvable, coated, and porous microneedles [96].

Solid and hollow microneedles can be fabricated using a mix of microfabrication processes (photolithography, deep reactive ion etching, wet etching, and plasma-enhanced chemical vapor deposition) [96–98], drawing photolithography [99], micromolding [100] or 3D printing [101] techniques. Microfabrication processes, micro-molding, and photolithography, for example, provide high repeatability and high resolution to produce microneedles using different materials. However, it consists of high-cost and time-consuming techniques. On the other hand, in the 3D printing technique, the software can be used to design the object, divide it into a bunch of digital slices, and

to be printed in the 3D printer. In this case, the most used materials are hydrogel, plastic, metal powder, and resin, leading to a low-cost technique, although its resolution is still an issue to be improved [96].

A solid electrochemical microneedle example is represented in Figure 4A. Usually, the microneedles are modified pos-fabrication for electrochemical applications if the precursor material is not conducive [102]. Noble metals are metalized over the microneedle surface using e-beam evaporation and sputtering techniques. Furthermore, a biorecognition modification layer is also used to improve specific interaction between the electrode surface and the analyte [96]. The solid microneedles are easy to use and produce. In addition, they can be reused [103]. However, biorecognition layer modification is more exposed in this microneedle kind which can lead to the leaching of the recognition biomaterial.

Hollow microneedles can also be fabricated using the same techniques used to produce the solid ones, as listed previously. Those needles are hollow and can be filled using different materials, such as metal wires, nanostructured materials, and carbon paste [102]. An example of hollow microneedles is represented in Figure 4B before and after being packed with a conductivity material for being applied as an electrochemical sensor. This example presents a hollow microneedle for apomorphine monitoring, a therapeutic drug used in Parkinson's management [104]. In this case, the hollow microneedles were packed with carbon paste to obtain a three-electrode system, where the working electrode was modified with rhodium nanoparticles and Nafion. The electrochemical oxidation of the apomorphine drug generates the signal response according to the drug concentration in the medium, which was also tested in a skin mimic environment. Hollow microneedles are not as simple as solid ones due

to the connections needed between transducer materials inside the hollows and the electrical connections in the back of them [96]. However, they can better store the materials after modification and allow packing inside microneedles materials such as carbon paste base, which are difficult to use in solid microneedles due to leaching.

**Figure 4 - A)** Schematic representation of the skin layers, a solid microneedle device in the dermal interstitial, and a simple representation of data collected and transmitted to a phone. Adapted from [105]. **B)** Schematic representation of a hollow microneedle filled with a conductor material (carbon paste) to provide an electrochemical sensor for apomorphine drug monitoring. The microneedle is also represented before and after being packed with the conductive material, adapted from [104].

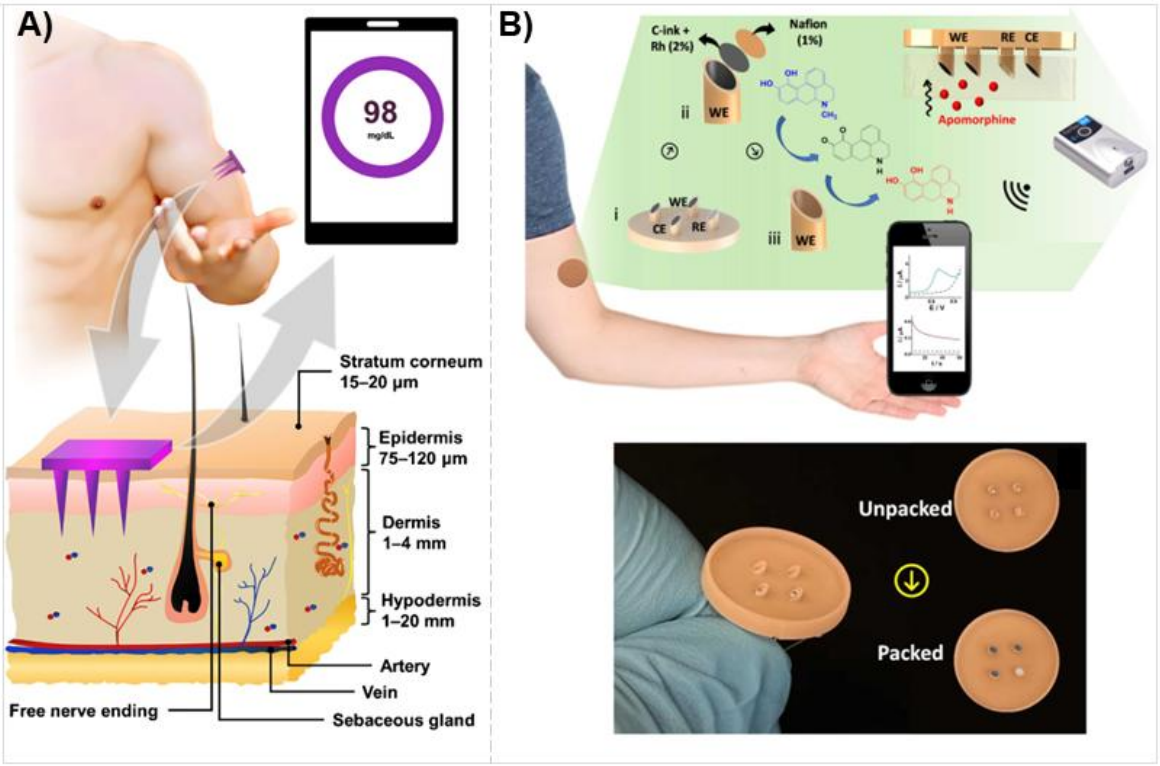


### 1.3.2. Health risk markers monitoring

First, wearable sensors' development focused on monitoring simple markers, such as metabolites and electrolytes. However, monitoring more complex biomarkers

(hormones and proteins) using these platforms has emerged recently due to the possibility of controlling essential diseases and their earlier diagnoses [106]. The pioneers in this category are the wearable sensors for monitoring glucose levels in the body fluids of Diabetics patients [107]. Nevertheless, the interest in developing wearable sensors for non-invasive glucose measurements is still extensive and necessary in this area [108]. Muamer Dervisevic and coworkers developed a high-density silicon microneedle for glucose monitoring due to the material's biocompatibility, high rigidity, and mechanical strength [108]. It improves skin penetration with no breaking needles and accumulation of the material inside the skin, which prevents unwanted immune responses or health problems. The solid microneedles were coated with a thin layer of gold and modified using ferrocene-cored poly(amidoamine) dendrimers [Fc-PAMAM], which is a redox mediator and the glucose oxidase as a bioreceptor; when tested in mice, the device presented a great response corresponding to glucose blood concentration measured using a glucometer [108].

In addition, there are other exciting diseases markers, such as cholesterol [109], cortisol for chronic stress monitoring as a biomarker of depression [110], dopamine monitoring as a Parkinson's disease marker [111], nitrotyrosine monitoring as a biomarker for neurodegenerative diseases [112], essential proteins biomarkers for early diagnosis of aggressive diseases such as cancer [113], among others.

As of today, only a handful of studies have shown the application of wearable sensors in detecting molecules that do not correspond only to simple metabolites and electrolytes. Yang and coworkers, for example, developed in 2019 a wearable electrochemical sensor for detecting and quantifying low concentrations of uric acid and tyrosine in sweat [114]. These biomarkers are associated with gout disease and metabolic disorders, respectively. A microfluidic and flexible device was fabricated

using the laser-scribing technique to carbonize a polyimide sheet to obtain the conductive tracks for electrochemical detection. In addition, double-sided adhesives were used to manufacture the microfluidic channels, which are essential for the constant measurements of the analytes. The device presented great potential for application in the personalized monitoring of uric acid and tyrosine on sweat [114].

In another work, Goud and collaborators developed a wearable sensor to detect Levodopa (L-Dopa) for effective Parkinson's disease management [115]. In this case, a microneedle sensor was used to fabricate a minimally invasive system for continuous electrochemical detection. The measurements were performed in interstitial fluid, and the hollow microneedle was fabricated using polymer material and a microfabrication system. The devices demonstrated an excellent performance for the wearable sensor application in quantifying Levodopa, a drug used in Parkinson's disease, to optimize the personalized required dose of the drug in the medical treatments [115].

In addition, a wearable microneedle sensor was also proposed by Samuel M. Mugo and coworkers for simultaneous pH and cortisol detection in sweat aiming at stress monitoring [116]. This device was obtained using conductive microneedle polydimethylsiloxane (PDMS) flexible substrate modified by printing layer by layer (LbL). The pH detection chamber was modified using polyaniline (PANi), whereas the cortisol detection chamber was modified using molecularly imprinted polymer (MIP). The final wearable sensor was tested for in-situ and ex-situ monitoring of real human sweat samples for accurate simultaneous detection of pH and cortisol [116].

### 1.3.3. Therapeutic drugs monitoring

Besides biomarkers monitoring, wearable sensors have been developed for therapeutic drug monitoring in body fluids. This provides benefits such as patient-specific dose optimization and monitoring the dynamic changes of the drug inside a patient's body. The drug distribution on body fluids depends on its pharmacokinetics, which will lead to the choice of the fluid to be analyzed, and, consequently, the kind of device to be used [91]. Nonetheless, the Interstitial fluid (ISF) has attracted attention and demonstrated a good correlation with blood for small drug molecule concentration [117]. However, limited therapeutic drugs have been studied and reported in ISF [91]. For example, Rupesh Kumar Mishra and collaborators developed a hollow microneedle sensor array for fentanyl and organophosphate (OP) nerve agent detection in ISF [118]. Fentanyl is used as an analgesic and, together with other drugs for anesthesia, besides being an opioid even more potent than morphine. Due to the similarity of the effects, it is difficult to distinguish opioid overdose and nerve agent poisoning, which leads to the importance of fentanyl and OP detection on a single patch platform. In this work, carbon paste was used as a transducer for a non-enzymatic platform, and a study was performed in a skin-mimicking phantom gel, demonstrating the device's suitability for on-body dual sensing.

Goud and coworkers developed a hollow microneedles device for apomorphine monitoring in ISF, a therapeutic drug used in Parkinson's disease control [104]. The microneedles were packed with carbon paste to obtain a three-electrode system, where the working electrode was modified with rhodium nanoparticles and Nafion, and the reference electrode Ag/AgCl based. The electrochemical signal was generated by the electrochemical oxidation of the apomorphine, where the signal is proportional to

the drug concentration in the medium. The device presented a good linear correlation and LOD. It was tested in phantom gel as a skin mimic environment, showing attractive analytical performance in this medium, consequently, a powerful candidate for being used in the skin.

Although different types of wearable sensors have been developed using a diversity of techniques for monitoring health risk markers, therapeutic drugs, and others, detecting analytes present in the boby in extremely low concentrations is still a challenge. Furthermore, the development of multiple-tasking platforms is needed to combine sensing, processing, communication in the same place. And using these devices for daily application requirements leads to a mass production need where disposable and low-cost chemical sensors are ideal in this case [119].

# CHAPTER 2

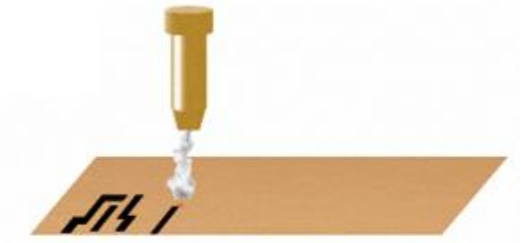

## 2. Fabrication of Portable Electrochemical Devices Using Laser-Scribing Technique on Phenolic Paper Sheets

## CHAPTER 2

In this chapter, we proposed fabricating a portable electrochemical device on non-conductive phenolic paper using this substrate as an alternative polymer platform. The devices were obtained using the $CO_2$ laser-scribing technique as a simple, low-cost, and easy method to fabricate portable devices. A conductive carbon-based material was observed after the polymer carbonization, and the tracks were characterized using Raman spectroscopy, XPS, XRD, SEM, and EIS techniques. A porous structure with graphene-like domains was noticed, presenting a predominance of carbon double bonding ($sp^2$) after the photo-thermal process induced by the $CO_2$ laser radiation, which, combined with an electrochemical treatment, provided an excellent conductivity and low charge-transfer resistance to the obtained material. The devices were fabricated containing a three-electrode system for electrochemical applications and also presented physical stability, besides the great reproducibility and repeatability. They also showed great potential for on-site analytical applications achieving better performances than conventional carbon electrodes.

This work has been published in journal Carbon (Volume 159, Pages 110-118, 2020, DOI: 10.1016/j.carbon.2019.12.016) and counted with the help of Professor Dr. Abner de Siervo, who has contributed to the XPS data analysis and Professor Dr. William Reis de Araujo who has helped in experimental suggestions and discussions.

## 2.1. Introduction

As mentioned above, the laser-scribing technique has been emerging as a low-cost, scalable, and interesting fabrication method of a conductive carbon-based material (LSG) for electrochemical devices [48,120]. This leads to the search for different and alternative precursor platforms, including paper and mainly polymeric ones, which have in common flame retardancy, high-temperature resistance, or thermoplastic materials, to guarantee the LSG formation [121]. The use of distinct platforms can guarantee different properties for the obtained device and carbonized material, depending on the application.

One of the materials mentioned in the literature for LSG obtention is the phenolic resin, a heat-resistant polymer that is either thermosets or thermoplastic [63]. This material has been widely used to fabricate carbon composites and activated-carbon materials for different [122,123] applications. However, the fabrication process evolves severe conditions such as a controlled atmosphere and very high temperature [122]. Zhang and collaborators have explored an alternative method by carbonizing the material and applying the laser-scribing technique. They have used phenolic resin to fabricate new electrochemical devices on various revested substrates [63]. Unlike polyimide, a common polymer used for LSG obtention, the phenolic resin can be easily synthesized with distinct properties, using phenols and formaldehyde, besides the low cost [124]. This work showed that the carbon-based material obtained from the carbonization of phenolic resins generated a porous structure with low resistance and great applicability as an electrochemical sensor as well [63].

In this chapter, we propose using another alternative material, phenolic paper (Figure 5), in the LSG fabrication. This material consists of a tough board made of

wood fiber and phenolic resin applying heat and pressure [125]. It is usually used as a platform to print circuit boards due to its properties, such as good electrical insulation, dimensional stability with temperature variation, and good mechanical strength, besides the facility to manufacture and the low cost. It can also be applied in automotive, industrial control, medical, and others [126].

**Figure 5 –** In brown, the phenolic paper is represented as a platform for a circuit board.

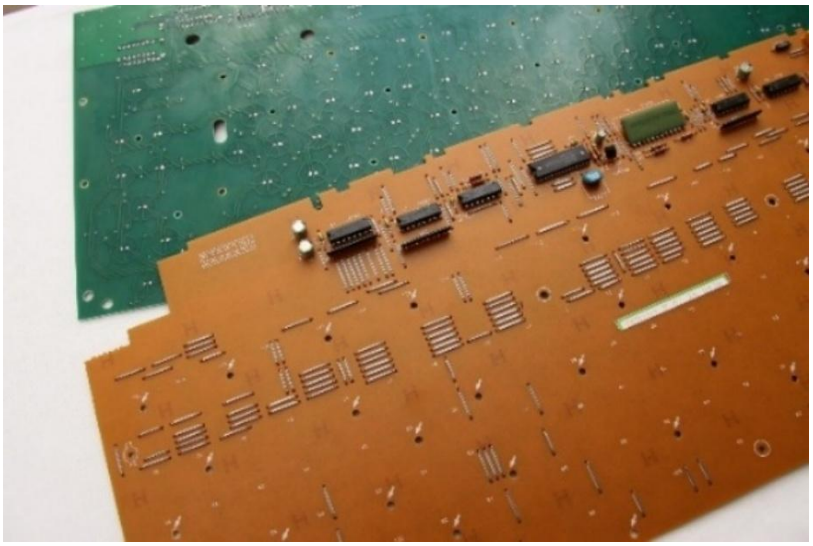

Considering the low cost and the format of the tough board, which can easily be bought or recycled from used systems, we proposed the fabrication of a new electrochemical sensor. We developed the electrochemical device using a single-step $CO_2$ laser-scribing method on a phenolic paper platform as a simple and scalable way to fabricate carbon-based electrochemical sensors. This leads to the possibility of an electrochemical sensor obtention directly coupled with an electrical circuit board, such as a miniaturized potentiostat system. Moreover, as already discussed, although paper platforms are another interesting material for the fabrication of portable electrochemical sensors, the use of paper-based devices exhibits some drawbacks,

such as physical and mechanical resistance and stability, besides the wettability of the substrate, which could compromise the handling and performance for in-field analysis [17]. Thus, phenolic paper, as a polymeric material, could be an alternative substrate for developing these devices.

Herein, estradiol or the so-called β-Estradiol hormone (E2) was used to evaluate the fabricated devices' electrochemical performance. This steroid is known as the main female sex hormone, and although it is present at higher levels in women, it plays also an important role in males. The excess of this compound in human bodies can cause serious damage, such as congenital malformation in children, male fertility problems, breast and prostate cancer, or sexual disorders, and the development of abnormal thyroid function in animals [127].

The main source of this hormone in the environment is generated by human activities, and this pollutant can be found in higher concentrations in aquatic mediums [128,129]. Therefore, new detection methods without sample pretreatment necessity for simple and fast E2 quantification have been investigated [130,131], and in this regard, electrochemical methods have attracted attention [132]. The E2 chemical structure is presented in Figure 6, and its electrochemical oxidation is usually observed in carbon-based sensors, which is ideal for evaluating the electrochemical performance of the laser-scribing carbon-based fabricated sensor in river water samples.

**Figure 6 –** β-Estradiol molecule chemical structure.

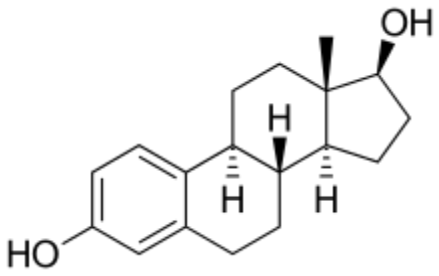

## 2.2. Materials and methods

### 2.2.1. Reagents and materials

The phenolic paper (printed circuit boards) were obtained from Pertech in Brazil (São Bernardo do Campo, Brazil). Before being used, these boards were cleaned with water and detergent, rinsed with deionized water, and dried at room temperature (25°C). All reagents used were analytical grade without the need for any prior purification. The solutions were prepared by dissolving the reagents in appropriate electrolytes and deionized water (Direct-Q® 5 Ultrapure Water Systems, Millipore, MA, USA). The potassium ferricyanide ($K_3[Fe(CN)_6]$), potassium chloride (KCl), acetic acid, boric acid, acetonitrile, and sodium hydroxide (NaOH) were obtained from Merck (Darmstadt, Germany). Phosphoric acid, hexaammineruthenium(III) chloride ($[Ru(NH_3)_6Cl_3]$), and β-Estradiol (98%) were obtained from Sigma-Aldrich (St. Louis, MO, USA). In addition, the silver ink was purchased from Joint Metal Comercio LTDA (Diadema-SP, Brazil). The Britton-Robinson buffer solution was prepared by mixing 0.1 mol $L^{-1}$ acetic acid, boric acid, and phosphoric acid each, where a concentrated NaOH solution was used to adjust the pH values from 2.0 to 12.0.

### 2.2.2. Devices fabrication

#### *2.2.2.1. Fabrication*

Initially, the devices based on phenolic paper platforms were fabricated using the laser-scribing method to obtain a three electrodes system on the substrate, as shown in Figure 7.

**Figure 7 –** Representation of the device's fabrication process and the dimensions of the electrodes (working (WE), counter (CE), and reference electrodes (RE)).

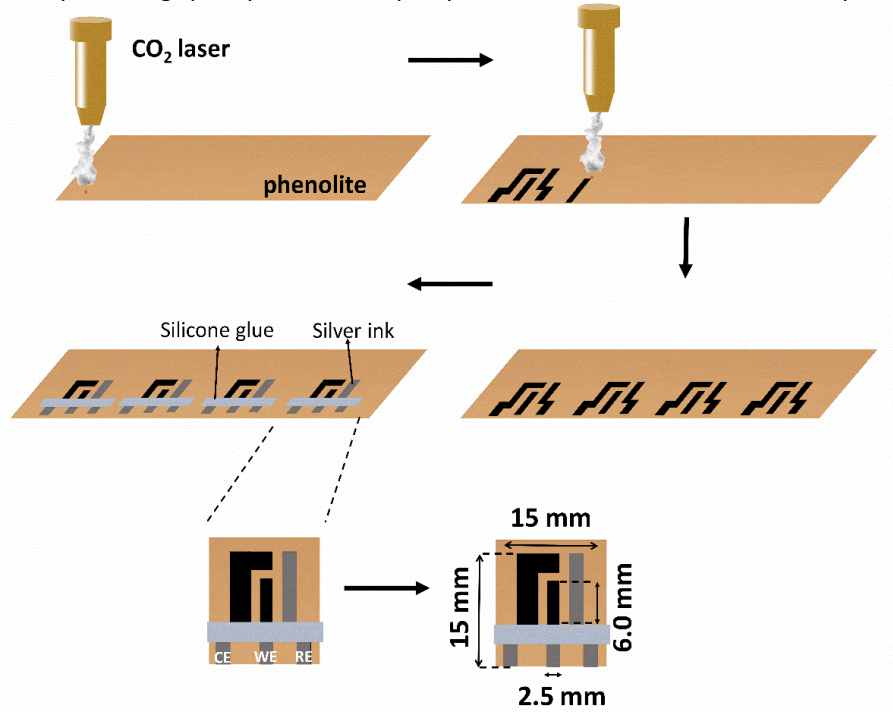


A $CO_2$ cutting laser machine from Work Special Laser (wavelength of 10.6 pm and a pulse duration of approximately 14 µs) was used for the fabrication process. The laser parameters were optimized: 7.5–10%, speed 4.0–12.0 mm $s^{-1}$, and Z distance (focal distance) 8.0–14.0 mm under ambient conditions. The optimal conditions were 8.8% (~2.1 W), 8.5 mm $s^{-1}$, and 12.0 mm. The three electrodes system was drawn using the equipment's software, and the electrodes' dimensions are shown in Figure 7.

Subsequently, silver ink was applied over the electrode contacts and the reference electrode to ensure the electrical connection and form a pseudo silver

reference electrode, providing electrochemical stability. Finally, Silicone glue (Tek Bond- transparent silicone sticker) was used to delimit the electrochemical reaction area, protecting the electrical contacts from contacting the electrolyte, where only 500 mL of solution is needed for the electrochemical measurement.

The optimization of the laser conditions for the electrode fabrication was evaluated using electrochemical characterization by obtaining electrodes under different conditions of power, speed, and Z distance. Electrochemical measurements were performed in 1.0 mmol $L^{-1}$ hexaammineruthenium(III) chloride and 1 mol $L^{-1}$ KCl, using the cyclic voltammetry technique from 0.0 to -0.4 V and scan rate of 20 mV $s^{-1}$. For this purpose, an Autolab potentiostat PGSTAT128N (Eco Chemie, Utrecht, The Netherlands) was used coupled with the NOVA 1.11 software.

#### *2.2.2.2. Electrochemical treatment*

An electrochemical treatment was applied to ensure better electrochemical performance of the devices. The treatment conditions were optimized using positive and negative potential ranges in 1.0 mol $L^{-1}$ KCl electrolyte solution, also varying the period. First, the potential range was studied using cyclic voltammetry, applying ten cycles at 20 mV $s^{-1}$ and different potential ranges (from -0.4V to 0.8V, or 0.0 to 0.8 V, or 0 to -0.4 V). After a potential range was chosen, and using the chronoamperometry technique, different potentials (0V, -0.4, -1.0, -1.5V) were applied during 30 s in 1.0 mol $L^{-1}$ KCl. Finally, the electrochemical treatment time was optimized using 0V and varying the time to 30, 60, 90, and 120 s.

Cyclic voltammograms were obtained in 1 mmol $L^{-1}$ potassium ferrocyanide as a redox probe and 1.0 mol $L^{-1}$ KCl as electrolyte solution with voltage potential ranging

from 0.7 to -0.2 V, and a scan rate of 20 mV $s^{-1}$, to evaluate the quality of the electrochemical treatments applied on the devices. Then the defined conditions were the application of -1.0 V for 60 s in 1.0 mol $L^{-1}$ KCl solution. Furthermore, the treatment quality was followed over the days to observe the duration.

### 2.2.3. Physical, chemical, and electrochemical characterizations of the material

The material was characterized before and after carbonization, with and without electrochemical treatment, using physical, chemical, and electrochemical techniques. All the electrochemical measurements were obtained using a potentiostat and the NOVA 1.11 software. For electrochemical characterization, only the conductive surfaces were characterized using cyclic voltammetry in 1 mmol $L^{-1}$ potassium ferrocyanide and 1mol $L^{-1}$ KCl from 0.7 to -0.2 V, varying the scan rate from 2 to 500 mV $s^{-1}$. The EIS plots were recorded in a mixture of 1 mmol $L^{-1}$ potassium ferricyanide/ferrocyanide with frequencies between $10^5$ and $10^{-1}$ $s^{-1}$ for a sinusoidal signal applied using a typical open circuit potential (OCP) of 0.22 V and 10 mV amplitude at ambient temperature.

The morphology of the samples was characterized using TEM (Jeol JEM 2100 equipment) and SEM images (Jeol J6360 LV in secondary electron mode (ETD detector)). The sample preparation for TEM characterization was carried out by scraping off the laser-scribed material and dispersing it in chloroform solution to be transferred onto a C-flat TEM grid. Top-of-view and cross-section images were obtained using the SEM, and the film dimensions were measured using ImageJ software. The interlayer distance was obtained from the X-ray diffraction (XRD)

patterns (using a diffractometer Shimadzu XRD7000 Diffractometer with Cu Kα radiation of 1.54 Å. Parameters: voltage of 40 kV, current of 30 mA, scan speed of 1.00 deg/min and a 2 theta range of 5º - 90º) by Bragg's law:

$$2d \sin\theta = n\lambda$$

Where $d$ is the interlayer distance, θ is the scattering angle, $\lambda$ is the incident wavelength, and $n$ is the number of $\lambda$. Moreover, the TEM images also estimated the interlayer distance to compare values.

Raman spectra were obtained using a (Horiba Scientific T64000, spectrometer equipped with an objective lens with 100 x magnifications. Parameters: green laser with a wavelength of 532 nm and a power of 22 mW, integration time of 30 s, and 3 accumulations). Whereas the XPS analyses were conducted using a SPECS Phoibos 150 hemispherical analyzer with multi-channeltron detection, the Mg Kα radiation was maintained at a constant energy mode of 10 eV pass energy. Lastly, contact angle measurements were collected using a goniometer couple in a home-built apparatus. The measurements were obtained using a 10 µL drop of deionized water (after drop stabilization) under the non-carbonized, carbonized, and electrochemically treated material. The captured images were treated using ImageJ software, whereby the contact angle between material/water interfaces was calculated.

Reproducibility and repeatability of the electrochemical devices were studied using electrochemical measurements and expressed in % RSD. Cyclic voltammograms were recorded in potassium ferricyanide as a redox probe (1 mmol $L^{-1}$ ferrocyanide + 0.1 mol $L^{-1}$ KCl at 20 mV $s^{-1}$, from 0.7 to -0.2 V) using ten different fabricated electrodes, for reproducibility, or fifty measurements in the same electrode,

for repeatability. After, the RSD values were calculated from the variation in the Ip of the obtained cyclic voltammograms. Additionally, using the same approach and conditions, cyclic voltammetry was used to evaluate the durability of the electrochemical treatment in the electrodes over 21 days and expressed in %RSD (Relative Standard Deviation). The measurements were obtained using electrochemically treated and non-treated electrodes stored in ambient conditions. Also, the storage of the electrochemically treated electrodes in 0.5 mol $L^{-1}$ sulfuric acid was evaluated.

### 2.2.4. Analytical application

The electroanalytical performance of the devices was evaluated using estradiol. First, the voltammetric profile of the hormone in 0.1 mol $L^{-1}$ Britton-Robinson buffer solution pH 6.0 was observed using the cyclic voltammetry before and after the electrochemical treatment. The voltammograms were recorded in the presence and absence of 50 µmol $L^{-1}$ estradiol diluted in the buffer solution, from 0.2 to 0.7 V, using a scan rate of 20 mV $s^{-1}$.

The study of the pH variation on the estradiol electrochemical oxidation response using the fabricated devices was observed by cyclic voltammetry. The measurements were carried out varying the pH values from 2.0 to 12.0 in 0.1 mol $L^{-1}$ Britton-Robinson buffer, containing 50 µmol $L^{-1}$ estradiol, from -0.2 to 1.0 V, at a scan rate of 20 mV $s^{-1}$, at room temperature.

Finally, the electrochemical quantification of the estradiol was performed using differential pulse voltammetry (optimum step and amplitude values of 10 mV and 80 mV, respectively) and a concentration range from 0.10 to 1.0 µmol $L^{-1}$ estradiol in 0.1

mol $L^{-1}$ Britton-Robinson buffer (pH = 6.0), from 0.2 to 0.8 V. The recovery tests were performed by spiking 10 and 30 µmol $L^{-1}$ estradiol into river water, where the sample was used as received and diluted 1:1 (v/v) in 0.1 mol $L^{-1}$ Britton-Robinson buffer (pH = 6.0) before the analysis.

## 2.3. Results and Discussion

### 2.3.1. Electrochemical material characterization

First, the laser-scribing fabrication of the new material, using phenolic paper as the platform, was optimized using the cyclic voltammetry technique. Hexaammineruthenium (III) chloride was employed as a redox probe to evaluate the electrochemical responses obtained from different fabricated materials by varying the $CO_2$ laser conditions. The power, scan rate, and Z-distance of the laser machine were varied one by one, where the Z-distance parameter represents the focal distance between the laser tip and the platform. The parameters variation ranges were from 7.5 to 10 %, 4.0 to 12.0 mm $s^{-1}$, and 8.0 to 14.0 mm, respectively, for the power, scan rate, and Z-distance. The cyclic voltammogram responses are observed in Figure 8, where the typical electrochemical behavior expected for hexaammineruthenium (III) chloride in carbon-based electrodes is noticed. From these results, the cathodic current peak (Ip) values were obtained, and the Ip *vs.* laser power, Z-distance, and scan rate plots showed in Figure 8 (d), (e), and (f). Using these plots, it is easier to observe the responses with the variation of each laser parameter, where the electrochemical process presented a higher cathodic current peak in certain conditions.

**Figure 8 –** Cyclic voltammograms of laser-scribed electrodes in 1 mmol $L^{-1}$ $[Ru(NH_3)_6]Cl_3$ at 20 mV $s^{-1}$ with a potential range from 0.0 to -0.4 V for different laser-scribing conditions of (a) laser power, (b) Z-distance and (c) scan rate. The Ip *vs.* (d) laser power, (e) Z-distance, and (f) scan rate plots for the cathodic process of $[Ru(NH_3)_6]Cl_3$ obtained from the cyclic voltammograms in (a), (b), and (c).

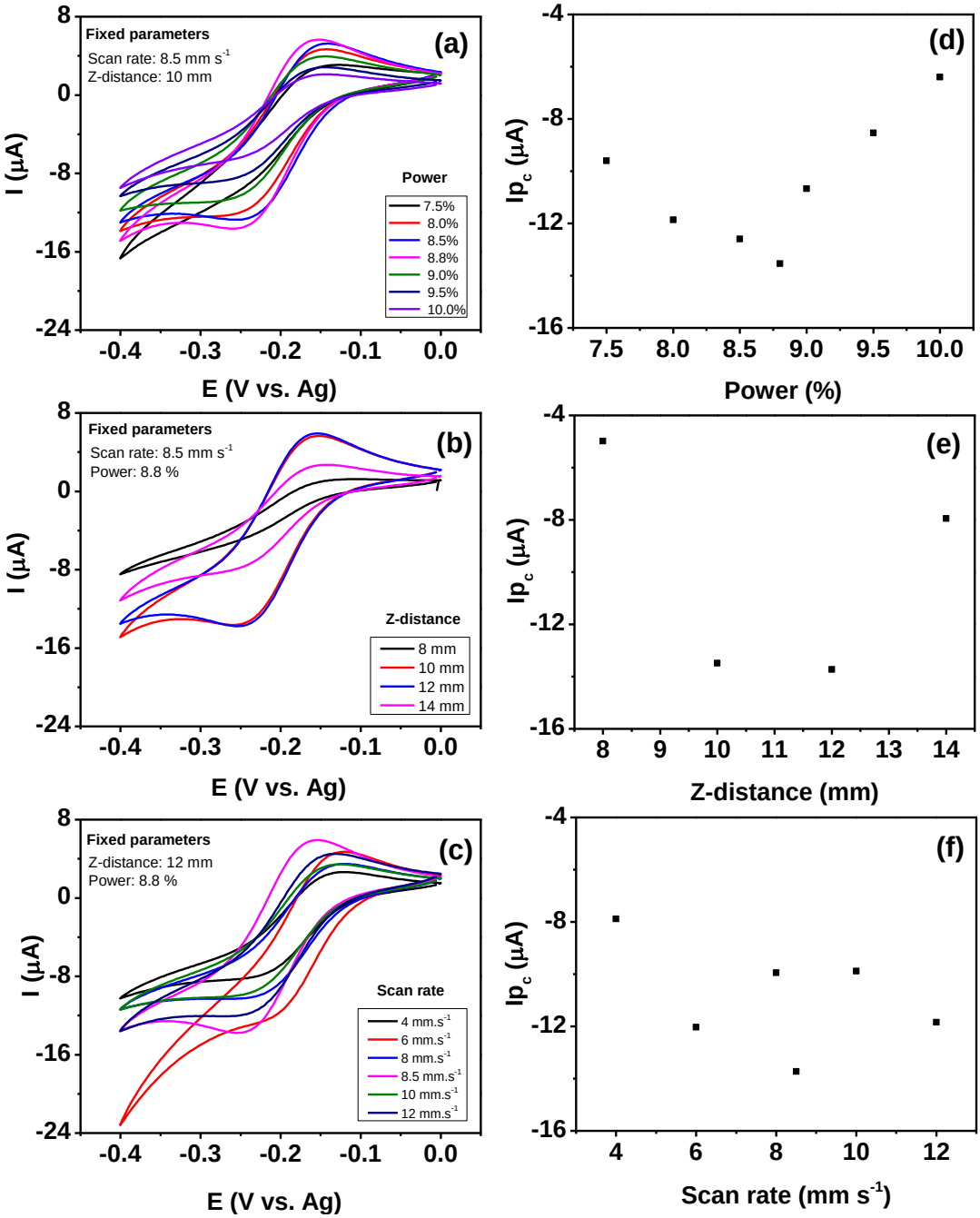


The results showed that the phenolic paper was turned into a conductive material after laser-scribing. In parallel, the electrical resistance was also measured,

using a multimeter, for the obtained carbonized track in each condition. The results are presented in Table 1.

**Table 1 –** Optimization parameters for laser-scribing fabrication of the devices

| **Scan rate: 8.5 mm $s^{-1}$ Z-distance: 10 mm** | | **Scan rate: 8.5 mm $s^{-1}$ Power: 8.8 %** | | **Z-distance: 12 mm Power: 8.8 %** | |
|---|---|---|---|---|---|
| **Power %** | **Resistance Ω $cm^{-2}$** | **Z-distance mm** | **Resistance Ω $cm^{-2}$** | **Scan rate mm $s^{-1}$** | **Resistance Ω $cm^{-2}$** |
| **7.5** | 154 ± 1 | **8** | 68 ± 1 | **4** | 64 ± 6 |
| **8.0** | 84 ± 13 | **10** | 56 ± 2 | **6** | 49 ± 1 |
| **8.5** | 64 ± 1 | ***12*** | *41 ± 1* | **8** | 55 ± 4 |
| ***8.8*** | *56 ± 2* | **14** | 41 ± 1 | ***8.5*** | *41 ± 1* |
| **9.0** | 47± 3 | | | **10** | 52 ± 3 |
| **9.5** | 37 ± 1 | | | **12** | 59 ± 1 |
| **10.0** | 33 ± 1 | | | | |

The optimized conditions for laser-scribing electrode fabrication were chosen in a compromise between the electrochemical response observed in Figure 8 and the lower electrical resistance observed in Table 1. Therefore, the better-obtained conditions were laser power of 8.8 %, scan rate of 8.5 mm $s^{-1}$, and Z-distance of 12.0 mm. It is important to highlight that although the use of higher powers lead to materials with lower electrical resistances, it comprises the mechanical resistance of the material. The electrical resistance of the carbonized tracks in the optimized condition was around 40 Ω $cm^{-2}$ and was often used to verify the reproducibility of the material during the fabrication process.

After optimizing the conditions, the obtained material was also electrochemical characterized using another redox probe, potassium ferrocyanide, which is more sensible to carbon materials surfaces than hexaammineruthenium (III) chloride. Potassium ferrocyanide is an inner-sphere electrochemical redox probe; in other words, in this compound, the electron transfer occurs through the ligands present around the metallic ion of the complex on the electrode surface. Thereby, the electron transfer, in this case, is also dependent on the electronic structure and the electrode surface of the carbon material, such as the edge plane like-sites and the oxygenated species [133,134]. On the other hand, for the hexaammineruthenium (III) chloride, which is an outer-sphere redox probe, the electron transfer depends only on the electronic structure of the carbon material since this process occurs directly between the electrode and the oxidant or reductant specie.

The electrochemical characterization of the electrode using potassium ferrocyanide is presented in Figure 9 - A).

**Figure 9 – A)** Cyclic voltammograms of optimized laser-scribed electrodes in a mixture of 1 mmol $L^{-1}$ ferricyanide/ferrocyanide at 20 mV $s^{-1}$ with a potential range from 0.7 to -0.2 V for carbonized and electrochemically treated material. **B)** Electrochemical impedance spectroscopy (EIS) at frequencies between $10^5$ and $10^{-1}$ $s^{-1}$ with a sinusoidal signal applied using a typical open circuit potential (OCP) of 0.22 V and 10 mV amplitude in a mixture of 1 mmol $L^{-1}$ ferricyanide/ferrocyanide + 0.1 mol $L^{-1}$ KCl for carbonized and electrochemically treated material. Inserted the zoom plot of electrochemically treated electrode measurement. **C)** Cyclic voltammograms of electrochemically treated electrode in 1 mmol $L^{-1}$ ferricyanide + 0.1 mol $L^{-1}$ KCl at different scan rates (2, 5, 10, 15, 20, 30, 40, 50, 75, 100, 150, 200, 300, 400, 500 mV $s^{-1}$). Inserted the logarithm plot of the anodic process current peak versus the logarithm of the scan rate.

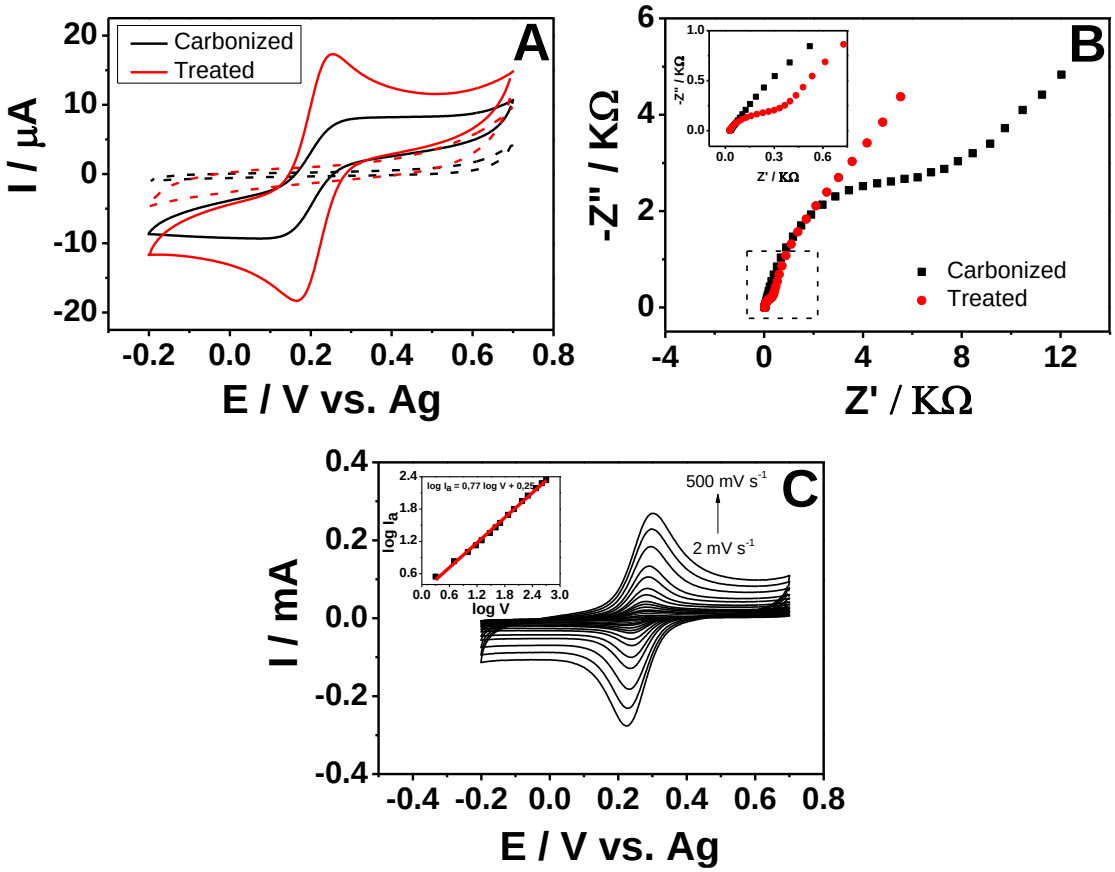


For the carbonized material, the cyclic voltammetry showed a low background current in the absence of ferrocyanide, while in ferrocyanide, oxidation, and reduction peaks were observed, demonstrating a typical electrochemical behavior for this redox probe. However, the peak-to-peak separation is noticed 142 mV, and the voltammogram profile is poorly defined. To enhance the electrochemical performance

of the device, the application of an electrochemical treatment was studied. The cyclic voltammogram of the device in potassium ferrocyanide after electrochemical treatment demonstrated better reversibility of the electrochemical signal with a decrease of peak-to-peak separation value to 73mV, besides better-defined peaks with a higher current signal (sensibility).

To define the better condition, the potential and duration of the electrochemical treatment were optimized. First, the electrochemical treatment was applied using cyclic voltammetry in 1 mol $L^{-1}$ KCl medium to study the best potential range. Three different potential's range were chosen: from -0.4V to 0.8V, from 0.0 to 0.8 V, or from 0 to -0.4 V. The electrochemical performance of the treated devices was also evaluated using cyclic voltammetry in ferrocyanide, as a redox probe and observed in Figure 10 - A).

**Figure 10 —** Cyclic voltammograms of laser-scribed electrodes in 1 mmol $L^{-1}$ ferrocyanide + 0.1 M KCl (20 mV $s^{-1}$, from 0.7 to -0.2 V). B) Electrochemical treatment applying fixed negative potentials of 0V, -0.4, -1.0 or -1.5V for 30s (Electrochemical treatment: chronoamperometry in 0.1 KCl solution). C) And electrochemical treatment time optimization applying -1.0V for 30, 60, 90 or 120s (Electrochemical treatment: chronoamperometry in 0.1 KCl solution).

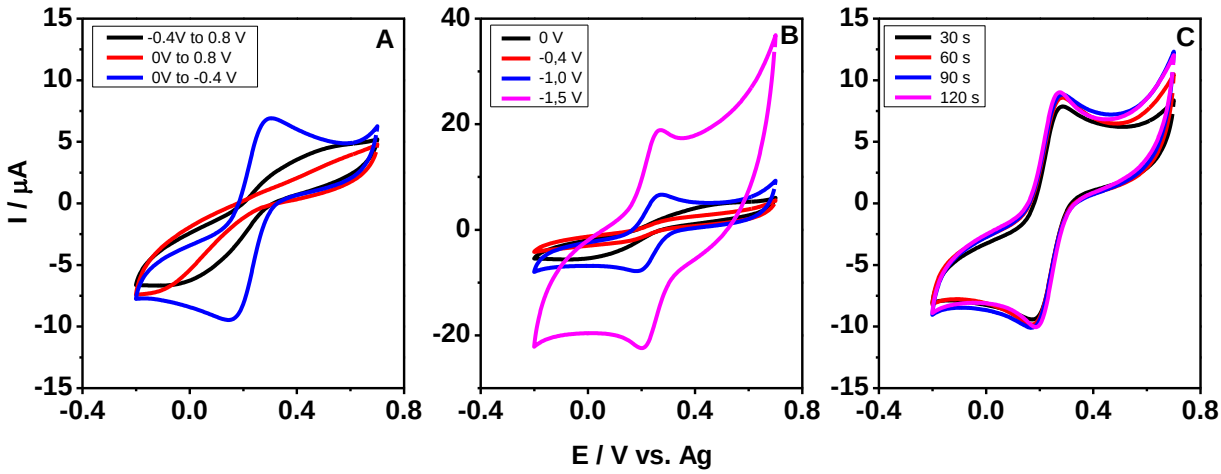

In Figure 10 - A) it is possible to observe that the treatment applying negative potentials presented better results than the others, where the electrochemical performance of the treated devices in this condition showed a typical reversible (Nernstian) electrochemical process. Thus, this potential range was chosen to perform the electrochemical treatment.

After choosing the potential range, the chronoamperometry technique in 1 mol $L^{-1}$ KCl medium was also used to analyze the best potential to apply during the electrochemical treatment. Different potentials (0, -0.4, -1.0, -1.5V) were applied during 30 s, and the treated devices' electrochemical behavior were evaluated using ferrocyanide, as observed in Figure 10 - B). The results showed that when applying -1.0 V during the electrochemical treatment, the electrochemical signal was improved. Finally, the electrochemical treatment time was optimized by applying -1.0 V, varying the time in 30, 60, 90, and 120s, and the electrochemical responses of the obtained devices are presented in Figure 10 - C). In this case, the cyclic voltammograms did not show a great variation in the electrochemical behavior of the devices, and the time of 60 s was chosen.

In Figure 9 – B), the EIS of the carbonized material before and after electrochemical treatment is observed. This technique was used to investigate the material's resistance and to evaluate the effect of the electrochemical treatment on the resistance to charge transfer ($R_{CT}$). The Nyquist diagrams showed a typical semicircle profile corresponding to the charge transfer resistance-limiting process at high frequencies. From this semicircle, it was possible to obtain the $R_{CT}$ values of 1375 ± 13 and 69 ± 1 Ω $cm^2$ for the carbonized material before and after electrochemical treatment, respectively. With these results, it is possible to observe that the $R_{CT}$ value decreased by around 95% when compared with the raw carbonized material in the

electrochemically treated material. This $R_{CT}$ value is similar to the typical obtained from carbon-based electrodes [135,136], although in this case, a simple, fast and inexpensive fabrication method has been used to obtain the devices.

After the optimization of the electrochemical treatment, cyclic voltammograms of the electrode in 1 mmol $L^{-1}$ ferricyanide were recorded at different scan rates (v) 2, 5, 10, 15, 20, 30, 40, 50, 75, 100, 150, 200, 300, 400, 500 mV $s^{-1}$, as observed in Figure 9– C). In this figure, an inset presents a logarithm plot of the anodic current peak process ($I_a$) versus scan rate, often used to distinguish a diffusional electrochemical process from an adsorptive one. In this case, the slope of the curves is used to determine the nature of the electrochemical process. For the adsorption-controlled process, the $I_a$ is proportional with u, which results in a slop of 1.0. In contrast, in diffusion-controlled processes, the $I_a$ is proportional with $v^{1/2}$, which results in a slope of 0.5 [137]. A slope of 0.77 was obtained for the data presented here, suggesting an adsorption-controlled process, different from the observed for the potassium ferrocyanide redox probe in the conventional carbon-based electrodes. This can be related to the characteristic of the material surface, which can provide the confinement of the electrogenerated species with lower diffusion in the solution, and this can give the idea of an adsorption-controlled electrochemical process.

To better understand the carbon-based material obtained from the laser-scribing carbonization of the phenolic paper platform, some physical and chemical characterizations of the material were also studied and presented below.

### 2.3.2. Physical and chemical characterizations

First, SEM images were obtained to characterize the surface morphology of the materials. In Figure 11 is presented the SEM images before and after phenolic paper laser-scribing, as well as after electrochemical treatment.

**Figure 11 –** SEM images at different magnifications of the flat morphology on the a) - c) non-conductive phenolic paper and of the porous morphology on the laser scribed phenolic paper-based electrodes d) - f) before and g) - i) after electrochemical treatment. Cross-section SEM images of the electrochemical treatment laser scribed phenolic paper-based electrodes j) - l). TEM images different magnifications of organized and amorphous carbon domains on the devices m) - o).

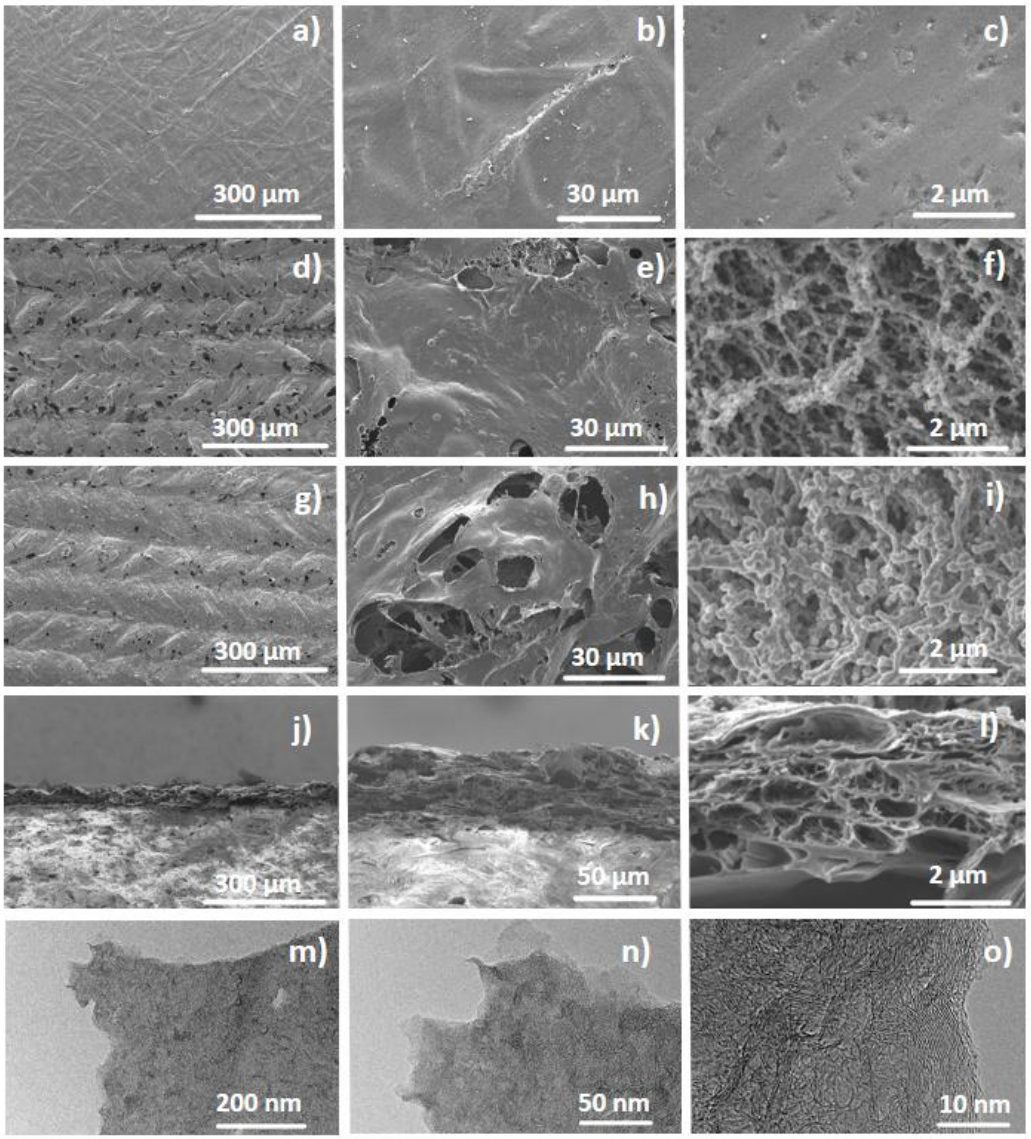

Figure 11 – a)-i) illustrate the top of the view and Figure 11 – j)-l) cross-section SEM images. And as a complement, TEM images are also observed in Figure 11 – m)-o) at different magnitudes.

In the SEM images, a flat (Figure 11 – a)-c)), and a porous morphology are observed for the raw phenolic paper and carbonized surfaces (Figure 11 – d)-i)), respectively. The porous structure can be explained due to the high local temperature (> 2500 °C) achieved with the incident laser on the phenolic paper surface. This process is responsible for the carbonization of the material, which provides gas realese and leads to the formation of a porous structure [34]. The result corroborates with the electrochemical behavior discussed above, which suggested the adsorptive-controlled process when using the ferrocyanide as an electrochemical redox probe. In this case, the obtained material's porous surface can imply the confinement of electrogenerated species on the porous surface. Furthermore, when comparing the carbonized material surface before (Figure 11 – g)-i)) and after the electrochemical treatment (Figure 11 – d)-f)) no significative differences in the morphology are noticed, and, interestingly, at a smaller magnitude, the laser tracks the direction it is observed. Finally, the cross-section images illustrated a porous material over the entire length of the laser-scribed surface, where the thickness was calculated using the Image J software and estimated at (51 ± 8) µm.

Furthermore, different information can be extracted from the obtained material using TEM as another microscopy technique. In the TEM images (Figure 11 – m)-o)) the presence of organized carbon domains is observed. These structures are typically observed in laser-scribed carbon-based materials [138,139], which are so-called graphene-like domains. The interlayer distance was measured from this structure presented in the TEM images, obtaining the value of 3.6 Å. The Raman spectroscopy

analysis presented in Figure 12 substantiated the presence of the graphene-like material.

**Figure 12** – Raman spectra of raw phenolic paper, laser-scribed material (carbonized), and carbonized material after electrochemical treatment (treated).

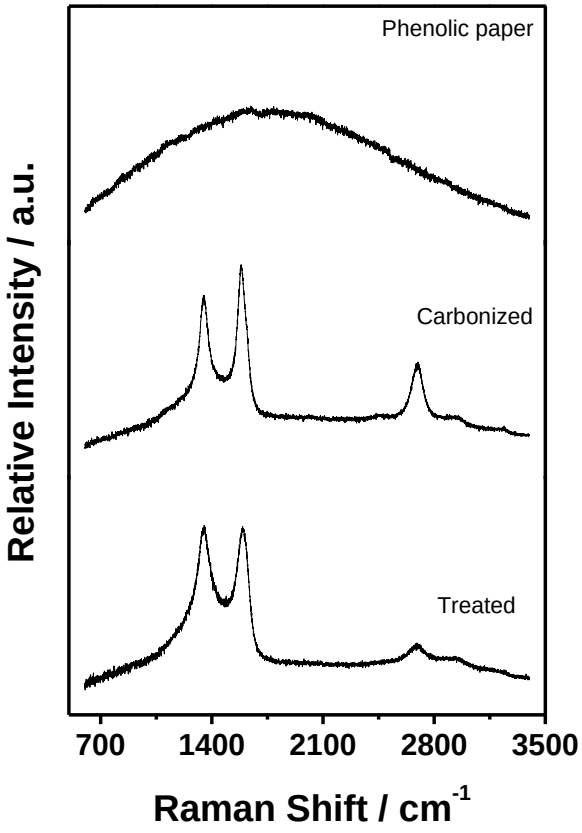


Characteristic bands (the D band in 1350 $cm^{-1}$, the G band in 1582 $cm^{-1}$, and the 2D band in 2700 $cm^{-1}$) are usually present in Raman spectra collected from carbon-based materials. The G band is related to the vibrations in the plane of $sp^2$ hybridization carbon bonds. In contrast, the D band is associated with structural defects in the material since it is resulted from the vibrational of the hybridized modes in the edges, which indicates the disorder in the material structure [140–142]. In Figure 12 the spectrum of the raw phenolic paper did not show any characteristic band. However,

the laser-scribed material before (carbonized) and after electrochemical treatment (treated) spectra presented D, G, and 2D bands at about 1350, 1580, and 2700 $cm^{-1}$, respectively.

Another important parameter investigated was the D-peak and G-peak intensities ($I_D/I_G$) ratio. This parameter is related to the disorder degree of the material. Thus, the carbonized material's calculated $I_D/I_G$ ratio before and after electrochemical treatment was 0.88 and 1.00, respectively. These values suggested that the disorder degree on the carbonized material after the electrochemical treatment is higher than before the treatment. This result can be related to the reduction the oxygen groups on the material surface provided by the electrochemical treatment, where a negative potential is applied. In this process, some incomplete chemical bonds can be generated and possibly cause an increase in material defects. It is well known that the heterogeneous electron transfer is fast in the edges [143]. Therefore, the materials with a higher disorder degree (more defects) present an improvement in the electrochemical behavior, which is substantiated by the results observed in the electrochemical characterization section.

Furthermore, in the Raman spectra, the 2D-peak band is more intense for the carbonized material before the electrochemical treatment. Differently from the other bonds, this one is related to the layers of the carbon material and interlayer interactions since it is resulted from D-peak overtone. The 2D band usually gets proportionally larger with the increment of the layers [141]. Thereby, the 2D-peak band decreases after the electrochemical treatment can be associated with the interlayer distancing on the material surface due to the insertion of different chemical groups during the process. In this case, a smaller number of layers could be penetrated by the Raman spectroscopy analyses, and the decrease in the 2D band can be noticed.

To investigate the chemical groups and the effect of the electrochemical treatment on the material surface, XPS spectra were obtained and presented in Figure 13.

**Figure 13 –** High-resolution C1s X-ray photoelectron spectra of (a) non-treated and (b) electrochemically-treated laser-scribed electrodes. High-resolution O1s XPS spectra for (c) non-treated and (d) electrochemically-treated laser-scribed electrodes.

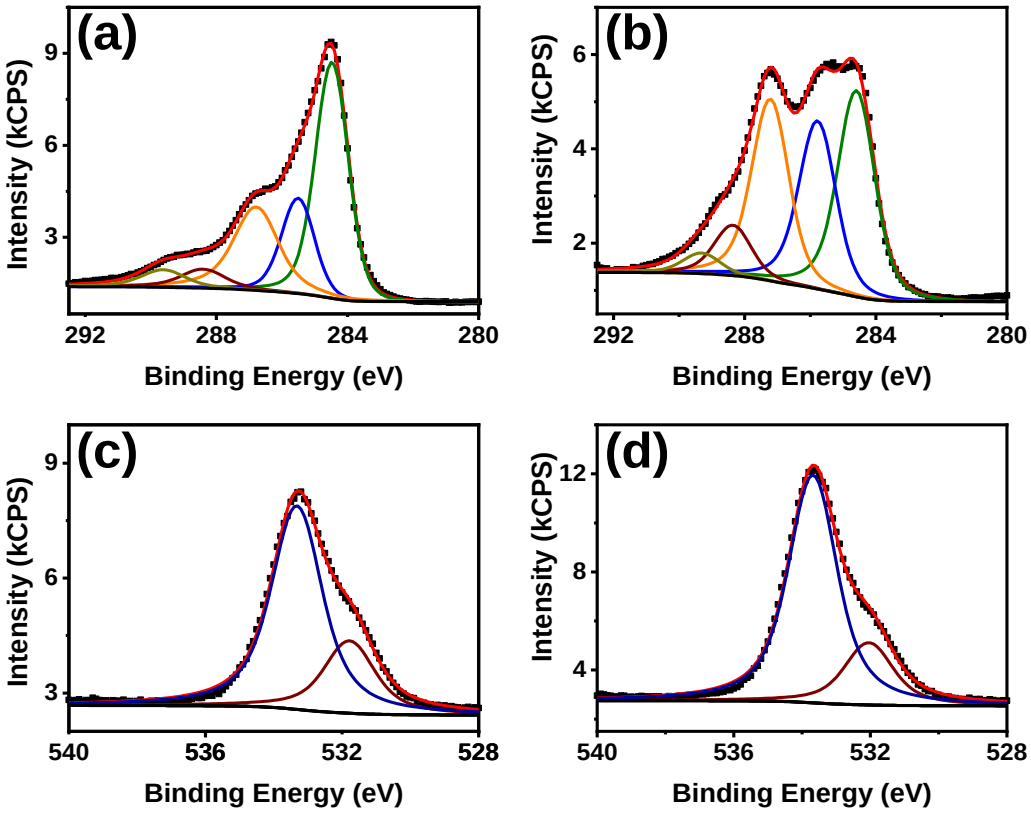


In Figure 13 – a) and b), the high-resolution C1s spectra are observed for treated and non-treated materials, respectively. In both cases, a predominant peak is noticed around 284,5 eV. This peak is related to the double bonds involving carbon, hybridization $sp^2$, which are responsible for the conductivity conferred to the material after the carbonization, transforming phenolic paper, a non-conducting material, into a conductive material. Furthermore, other peaks are also observed in 285.5, 286.8, 288.4, and 289.6 eV, and as presented in Table 2, are attributed to the C-C/C-H, C-O,

C=O, and O-C=O groups [144–147]. For the carbonized material after the electrochemical treatment, a significant increase in the intensity of the bands related to C-C/C-H, C-O groups (in 285.8 eV and 287.1 eV) was noticed. In contrast, the slight difference between the intensity of these two bands also presented a small variation when comparing the spectrum of the material before and after the electrochemical treatment.

**Table 2** – Fitting peaks for non-treated and electrochemical treated samples obtained through C1s XPS data.

| **Sample** | **Fitting peaks from C1s XPS** | | | | | **peaks from O1s XPS** | |
|---|---|---|---|---|---|---|---|
| | **C=C** | **C-C/C-H** | **C-O** | **C=O** | **O-C=O** | **C-O** | **C=O** |
| **Non-treated** | 284.5 eV | 285.5 eV | 286.8 eV | 288.4 eV | 289.6 eV | 533.3 eV | 531.8 eV |
| **Electrochemically treated** | 284.6 eV | 285.8 eV | 287.1 eV | 288.4 eV | 289.3 eV | 533.6 eV | 532.0 eV |

From the C1s spectra data, it was also possible to estimate the presence of around 36% of the oxygenized-containing functional groups in the carbonized surface. In contrast, around 40% of the oxygenated-containing groups compose the material after the electrochemical treatment. This increment in the oxygenated-containing groups value can be related to the presence of water/moisture in the porous sample since the electrochemical treatment is carried out in KCl aqueous solution. The main point is that after the treatment, the XPS analyses must be obtained as soon as

possible to avoid the change in the surface chemical groups due to the air oxygen exposure. This requirement can contribute to the insufficient drying of the samples before the analyses, and limiting, consequently, the resolution/distinguishability of the fitted peaks.

Moreover, the high-resolution O1s spectra for the carbonized material before and after the electrochemical treatment are presented in Figure 13 – d) and c), respectively. The presence of the bands related to C-O and C=O groups is observed in 533.3 eV and 531.8 eV. Thus, the quantitative distribution of the oxygenated groups on the electrode surface was determined in 26.2% of C=O and 73.8% of C-O groups for the carbonized material before the electrochemical treatment. In contrast, after the treatment, the composition turned into 21.3% of C=O and 78.7% of C-O groups. This result confirms the conversion of the oxygenated groups provided by the electrochemical treatment, which corroborates with the Raman data discussed above and the material's electrochemical characterization. It is known that a decrease in the oxygenated groups on the carbon-based electrode surface promotes the decrease in the material's electrical resistivity [148]. Thus, after the electrochemical treatment, a decrease in the $R_{CT}$ value was observed by the EIS results. This corroborates with the XPS data, and an improvement in the electrochemical performance of the devices was observed after the oxygenated groups conversion by the electrochemical treatment.

It is important to highlight that in the Raman spectra, the decrease of the 2D-peak band for the electrochemically treated electrodes indicated the increase in the interlayer distancing in the most superficial material. This data corroborates with the XPS measurements, where the oxygenated groups' reduction could contribute to the interlayer distancing in the graphene-like material observed [149]. Furthermore, as

discussed above, the suggestive co-existence of water/moisture in the porous material after the electrochemical treatment can also increase interlayer distancing.

Complementary, the contact angle images were also obtained for the raw phenolic paper, and the carbonized material before and after the electrochemical treatment, as observed in Figure 14 – a), b), and c), respectively.

**Figure 14 –** Contact angles measurements of a) raw phenolic paper, b) laser-scribed material before and c) after electrochemical treatment.

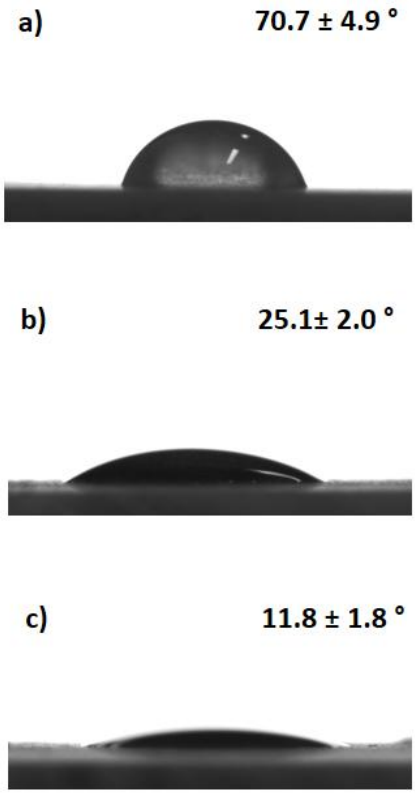


The value measured for the raw phenolic paper was about 70.7 ± 4.9°, showing poor wettability in the precursor material. On the other hand, after the carbonization, it is possible to notice the dispersion of the water droplet through the carbonized tracks, where the contact angle value obtained was around 25.1 ± 2.0°. This pointed out that the carbonization of the phenolic paper improved the wettability of the material, which

is essential for electrochemical analyses. An even higher wettability was observed for the laser-scribed material followed by electrochemical treatment, with a contact angle value of (11.8 ± 1.8)°. This could be not only attributed to the different functional groups present on the materials' surface, since it is known that the presence of the oxygenated groups on the material surface increases the water affinity [150,151], but to the porous morphology of the material responsible for the confinement of water.

The crystalline patterns of the material were also studied using XDR technique, as presented in Figure 15.

**Figure 15 –** XDR patterns of raw phenolic paper before and after laser-scribing (carbonized).

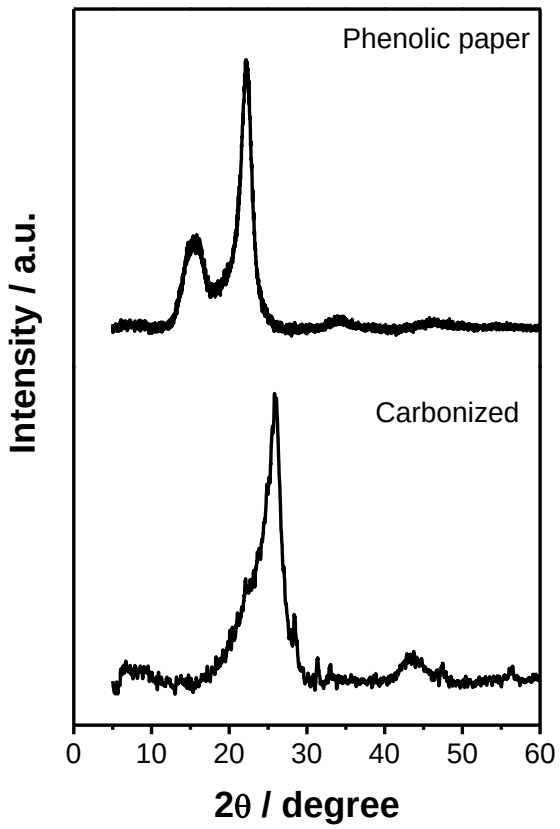


The XDR obtained from the raw phenolic paper presented the pattern observed in fiber wood [152], which was expected since this platform is mainly maid of cellulose

and phenolic resins. In contrast, the obtained material presented a different pattern after the carbonization, corresponding to the typically observed in carbon-based materials. Two peaks with 2θ maximum at 26.16° and 41.17° were observed, corresponding to the (002) and (100) planes. This is due to the obtention of a two-dimensional material, as was noticed in the SEM and TEM images. Between these peaks, the most intense one is the peak with 2θ maximum at 26.16° indicating a high graphitization of the material after the carbonization [130,153]. From this result, using Bragg's law ($2d \sin\theta = n\lambda$), the interlayer distance ($d$) between these (002) planes was calculated. The θ is the scattering angle, where 26.16° peak is correspondent to 2θ, $n$ = 1, and $\lambda$ is the incident wavelength (Cu Kα radiation with $\lambda$ =1.54 Å). Replacing all the values in the equation, the $d$ found was about 3.7 Å, corroborating with the value obtained from the TEM images (3.6 Å).

### 2.2.3. Reproducibility and repeatability study

The reproducibility and repeatability of the electrochemical performance for the treated laser-scribed electrodes were evaluated using cyclic voltammograms recorded in potassium ferricyanide as a redox probe. Ten different fabricated electrodes were used for the reproducibility measurements. For repeatability, fifty measurements were recorded using the same electrode. The obtained data are observed in Figure 16 – A and B.

**Figure 16 –** Cyclic voltammograms of laser-scribed electrodes in 1 mmol $L^{-1}$ ferrocyanide + 0.1 mol $L^{-1}$ KCl at 20 mV $s^{-1}$ with a potential range from 0.7 to -0.2 V. A) For ten different fabricated electrodes (reproducibility measurements expressed as the RSD = 4.9 %, $n$ = 10). Inset: peak current (Ip) *vs.* $n$ plot. B) Fifty measurements in the same electrode reproducibility measurements expressed as the RSD = 2.8 %, $n$ = 50). Inset: peak current (Ip) *vs.* $n$ plot.

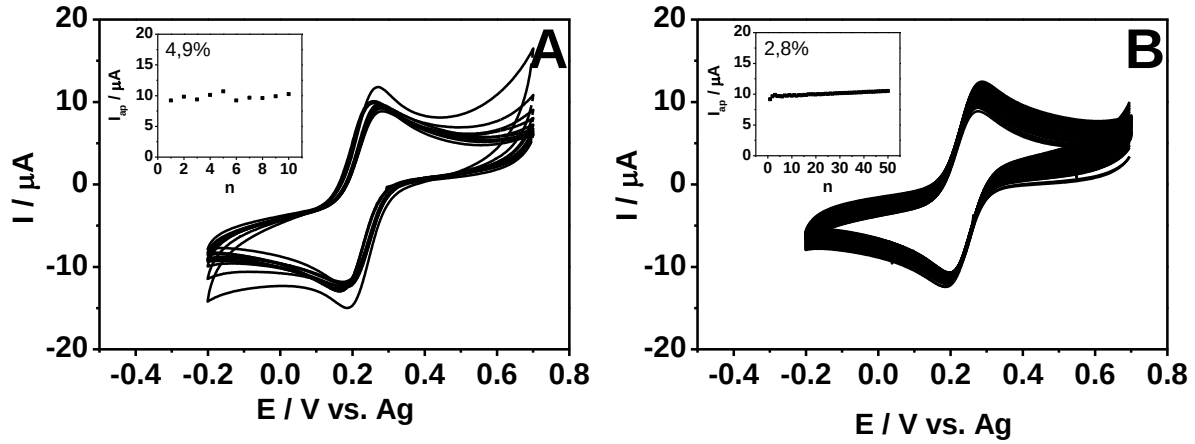


All the values were calculated through the Ip variation, using the anodic electrochemical current peak, and expressed in % RSD (Relative Standard Deviation). The % RSD obtained values were 4.9 % (n = 10) and 2.8 % (n = 50) for the reproducibility and repeatability, respectively. These represented good % RSD values when compared to those usually observed for the reproducibility and repeatability in the fabrication of electrochemical paper-based devices since RSD up to 5% have been reported [154].

Additionally, cyclic voltammograms were obtained using the same approach and conditions to evaluate the electrochemical treatment's durability expressed in %RSD. The measurements were obtained using electrochemically treated and non-treated laser-scribed electrodes over 21 days stored in ambient conditions. Also, the storage of the electrochemically treated electrodes in 0.5 mol $L^{-1}$ sulfuric acid was evaluated. The recorded voltammograms are presented in Figure 17.

**Figure 17 –** Cyclic voltammograms of laser-scribed electrodes, over the days, using 1 mmol $L^{-1}$ ferrocyanide + 0.1 mol $L^{-1}$ KCl at 20 mV $s^{-1}$ with a potential range from 0.7 to -0.2 V, for A) Electrode without and B) with electrochemical treatment stored in ambient conditions. C) Measurements using electrochemical-treated electrodes stored in 0.5 mol $L^{-1}$ sulfuric acid. Insets show the peak current (Ip) *vs.* time (days) plot, where day 0 is considered the electrode without electrochemical treatment.

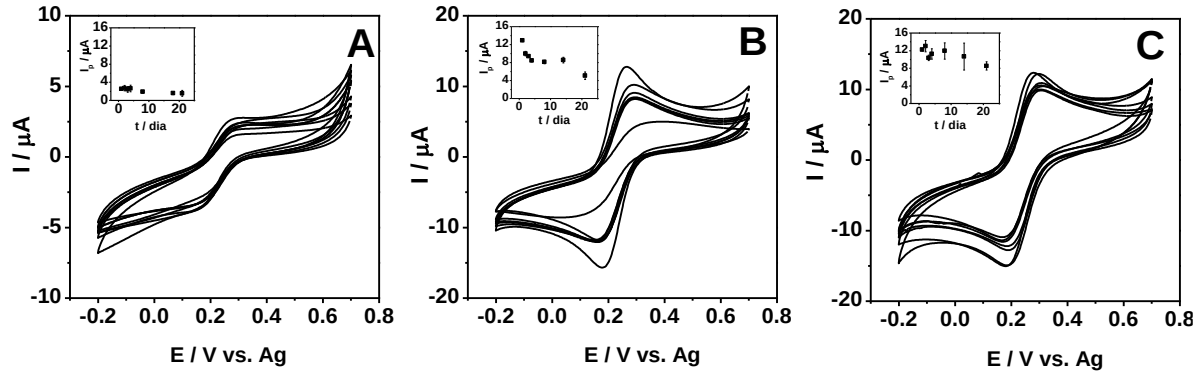


Figure 17 – A) shows the results for the non-treated laser-scribed electrodes. In this case, the electrochemical performance of the electrodes did not show a significant variation over the days after being stored in ambient conditions. This behavior is noticed in the inset figure (Ip *vs.* time (days) plot), where the oxidation current signal was not high compared to the further results. In contrast, as presented above in Figure 17 – B), the cyclic voltammograms obtained from the laser-scribed electrodes after the electrochemical treatment presented a higher current signal, as observed on the first day of the experiment (day 1). However, this Ip signal decreased over the days after storing the electrodes in ambient conditions. And on the last day of the experiment, the electrochemical behavior observed was similar to the non-treated electrodes. This is attributed to the reoxidation of the chemical groups on the electrode surface with the exposition of the electrochemical-treated devices to the air.

Thus, to prevent this oxidative process in the presence of the air over the days, the electrochemical-treated electrodes were stored in 0.5 mol $L^{-1}$ sulfuric acid. The cyclic voltammograms obtained in these conditions are reported in Figure 17 – C). The

results showed that the electrochemical treatment was conserved for a longer period when using the storage in sulfuric acid due to the oxidation delayed by the ambiance rich in $H^+$ ions. Furthermore, the electrochemical treatment is easy to apply right before using the laser-scribed electrode.

### 2.2.4. Analytical application

As a proof-of-concept, the analytical performance of the fabricated devices was also studied for detecting and quantifying β-estradiol hormone (E2). First, cyclic voltammograms were recorded in the absence and presence of 50 μmol $L^{-1}$ estradiol, using the laser-scribed electrodes before and after the electrochemical treatment. The result is presented in Figure 18 – A).

**Figure 18 – A)** Cyclic voltammograms recorded using optimized laser-scribed electrodes in 0.1 mol $L^{-1}$ Britton-Robinson buffer solution (pH = 6.0) at 20 mV $s^{-1}$ with a potential range from 0.2 to 0.7 V for carbonized (black line) and electrochemically treated devices (red line). Dotted and continuous lines represent measurements in the absence and presence of 50 μmol $L^{-1}$ estradiol hormone, respectively. B) Cyclic voltammograms recorded using electrochemical treated devices for different pH values of 0.1 mol $L^{-1}$ Britton-Robinson buffer solution containing 50 μmol $L^{-1}$ of estradiol at 20 mV $s^{-1}$. C) Ep vs. pH and Ip vs. pH plots for all oxidation processes of estradiol. Ep = -0.06 pH + 0.90.

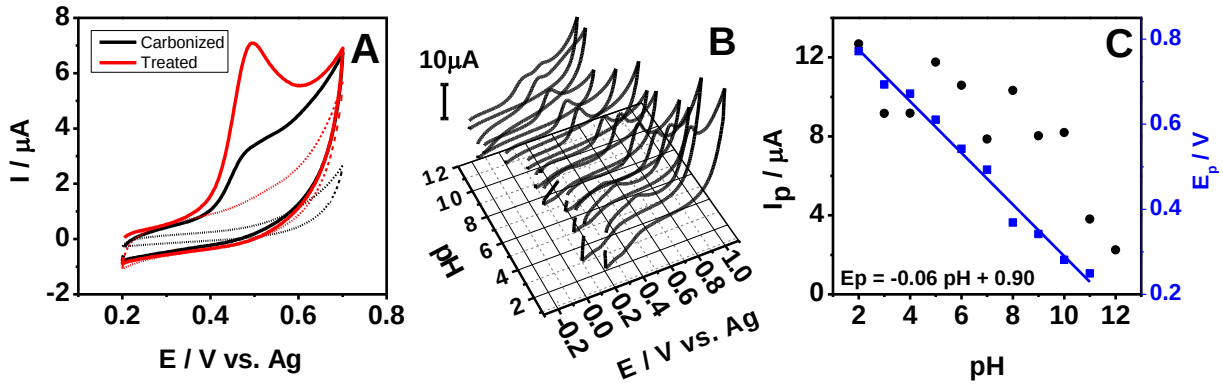

In Figure 18 – A), a typical electrochemical oxidation process is noticed for the E2 around 0.50 V. This behavior has also been reported in reduced graphene oxide modified electrodes [130], where an electrochemical oxidation process is supposed to occur in the hydroxyl group present in the aromatic ring of the E2 molecule, as shown in Scheme 1. Moreover, the results showed that the electrochemical treatment was responsible for improving the electrochemical performance of the E2 determination/quantification since the oxidation current signal increased five times compared to the signal obtained from the non-treated electrode. This behavior was similar to the observed using ferricyanide as a redox probe, which shows the importance of the electrochemical treatment for this application as well.

**Scheme 1 –** Proposed electrochemical oxidation of β-estradiol[130].

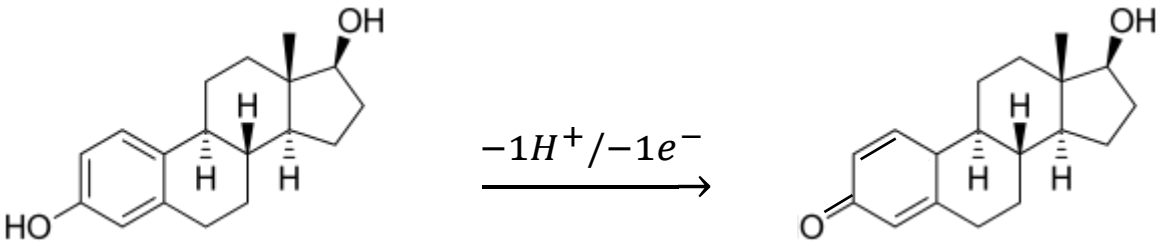


The pH variation influence on the $E_2$ electrochemical behavior was studied using cyclic voltammetry. These measurements were obtained by varying the pH values from 2.0 to 12.0 in 0.1 mol $L^{-1}$ Britton-Robinson buffer containing 50 µmol $L^{-1}$ estradiol and were presented in Figure 18 – B). The experiment was performed using electrochemical-treated laser-scribed electrodes. The results showed that the higher the $H^+$ concentrations (lower pH values) in the medium, the more the oxidation process occurs in positive potentials since the increase in the $H^+$ concentration difficult the oxidation of the molecule. This is easily observed in Figure 18 – C), where Ep *vs.* pH

plot is presented, and a linear correlation is given by the equation Ep = -0.06 pH + 0.90. The slope, in this case, is 60 mV / pH, which is close to the Nernstian value, given by 59 mV / pH. This indicates that the same ratio of protons and electrons is involved in the $E_2$ electrochemical oxidation process, which has been proposed in other works [130,155]. Furthermore, in Figure 18 – C), Ip *vs.* pH plot is also presented, where different from the Ep, the oscillation on the Ip value with the pH variation was not significative for the pH range from 2 to 10, whereas in high pH values a slight decrease on the Ip signal was observed since the oxidation process was distinguished in two peaks.

After analyzing the above data, a compromise between the current signal and lower Ep values was considered for choosing pH 6 to conduct further experiments. Furthermore, considering the fabricated devices' application for determining and quantifying E2 in the aquatic environment, the similarity with the medium was also a determinant factor in selecting the pH value.

Finally, the electrochemical quantification of the estradiol was performed using differential pulse voltammetry, as a more sensible technique, for a concentration range from 0.10 to 1.0 μmol $L^{-1}$ E2 in 0.1 mol $L^{-1}$ Britton-Robinson buffer (pH = 6.0). The amplitude and step pulse values were optimized at 80 and 10 mV, respectively. Thus, an analytical curve was obtained under the optimized experimental conditions, as presented in Figure 19.

**Figure 19 –** DPV for different estradiol concentrations (0.1 – 1 µmol $L^{-1}$). Parameters: Estep= 10 mV; Amplitude = 80 mV; Scan rate = 20 mV $s^{-1}$. Inset the Analytical curve: I/µA = 0.05+ 1.61 $C_{E2}$; $R^2$=0.99. (After electrochemical treatment).

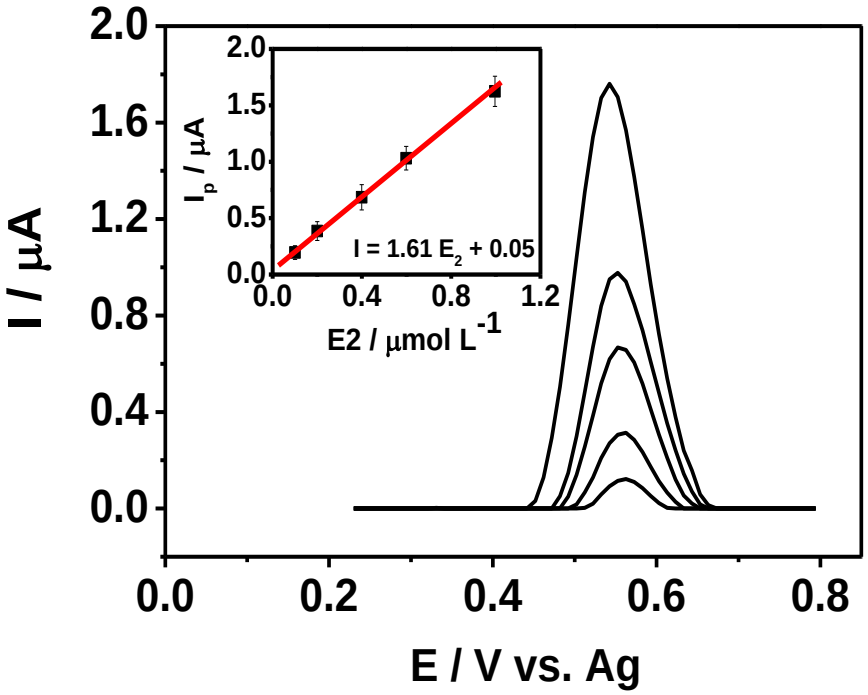


Figure 19 shows a linear correlation between the oxidation current peak and the E2 concentration, where the increase in the current signal response is noticed with the increase in the E2 concentration. The analytical curve obtained from this linear correlation was I/µA = 0.05 + 1.61 $C_{E2}$, where the correlation coefficient and sensitivity are given by 0.99 and 1.62 A $mol^{-1}$ L, respectively. From this result, the limit-of-detection (LOD) and quantification (LOQ) were calculated using LOD = 3SD/S and LOQ = 10SD/S, where SD corresponds to the standard deviation of the blank signal, and S is the slope of the analytical curve (sensitivity). The obtained values were 0.094 and 0.313 µmol $L^{-1}$ for LOD and LOQ, respectively. In the literature, bare glassy carbon electrode was reported for the E2 detection, and presented a LOD of 12.1 µmol $L^{-1}$ [155], which indicates that the developed laser-scribed electrode achieved better

performance than a conventional carbon platform. Moreover, the fabricated electrodes presented portability, low-cost, easy accessibility, and scalability in the fabrication method.

The applicability of the devices was evaluated using on-site measurements in river water. An addition and recovery test was performed by an external calibration spiking 0.1 μmol $L^{-1}$ E2 into river water, where the sample was used as received, in other words, without any previous treatment, and diluted 1:1 (v/v) in 0.1 mol $L^{-1}$ Britton-Robinson buffer (pH = 6.0) before the analysis. The obtained result for the recovery test was 94 ± 3% for n = 3 replicates. It showed the potential of the devices for on-site application in this matrix type. However, possible interfering species were not evaluated in this stage of the work. For further applications, the electrode surface modification could be considered, if necessary, to provide selectivity for the fabricated device.

Therefore, the results demonstrated the potential of the presented electrodes for analytical applications, aiming at the obtention of portable and disposable electrochemical devices using a simple and scalable method, in a low-cost polymeric material, with better electrochemical performance than conventional carbon materials.

## 2.4. Conclusion

The laser-scribed electrodes were obtained using a low-cost polymeric material and a simple, scalable method to fabricate carbon-based materials. As a result, robust devices with a porous structure and graphene-like domains were observed, presenting interesting properties, such as good conductivity. Furthermore, an electrochemical treatment was studied and demonstrated to improve the electrochemical behavior of the electrodes, decreasing the charge-transfer resistance. This is observed due to the

changes in the chemical groups on the electrode surface before and after the electrochemical treatment. Although the laser-scribing represented a scalable method to fabricate the electrodes, it did not compromise the reproducibility and repeatability of the obtained materials, where the variability expressed in RSD was calculated at 4.9 % and 2.8 %, respectively. As a proof-of-concept, the devices were applied to determine and quantify E2. Great potential was observed for on-site analytical applications, and the devices presented better electrochemical performance when compared to conventional carbon electrodes.

# CHAPTER 3

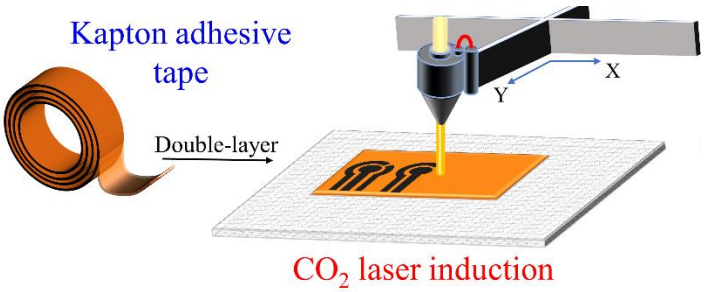


## 3. Disposable and Flexible Electrochemical Devices Fabrication Using Laser-Scribing Technique on Polyimide Tape

## CHAPTER 3

Besides the low-cost, paper-based platforms present interesting properties for fabricating portable analytical devices, including biocompatibility, recyclability, and microfluidic properties. However, as mentioned in other chapters of this work, devices made from paper can, for example, cause a compromise on the analyses due to the swelling of the platform provided by the permeation of the supporting electrolyte. In this chapter, we propose the development of an electrochemical device through the $CO_2$ laser-scribing technique based on Kapton tape to circumvent these limitations. Thus, the flexible fabricated device was applied as a static mode and combined with a paper-based platform to associate the devices to important paper characteristics such as the capillarity properties. This combination also provided the obtention of a hydrodynamic mode for microfluid analyses. The devices showed great stability, and the conductive material tracks were characterized using different techniques. The electrochemical behavior of the devices was evaluated using two different redox probes (ruthenium (III) chloride and potassium ferricyanide), presenting responses compared to the traditional electrochemical systems. The analytical performance of the system was evaluated in both static and hydrodynamic modes for 3-nitrotyrosine, presenting great potential for analytical applications when compared to conventional platforms.

This work has been published in the journal Microchemical Journal (Volume 182 (2022), 107893, DOI: 10.1016/j.microc.2022.107893) and counted with the help of Dr. Lauro A. Pradela-Filho, who has helped in experimental suggestions and discussions.

## 3.1. Introduction

As discussed in the first chapter of this work, portable analytical devices have attracted considerable attention in the last few years. Electrochemical sensors have been presenting great potential for being applied as portable analytical devices in field analyses due to the obtention of lower limit-of-detection when using electrochemical techniques and the possibility of miniaturization. In this sense, coupling microfluidic platforms to these devices has been interesting to provide the mixing of different reagents, the minimization of analyte amount necessary for the analyses from microliters to nanoliters, the employee of a single platform for both sample preparation and detection, among other benefits [156].

Different materials have been used for fabricating microfluidics electrochemical devices, such as PDMS[157], poly (methyl methacrylate)[158], glass [159], plastic[160], and paper[161]. Besides, some works have been reported in the literature on mixing materials for microfluid electrochemical device fabrication, such as paper and PDMS[162].

Among these platforms, the paper has attracted attention due to its low-cost and attractive properties presented by the material. Paper is known for its low-cost, disposability, microfluidic properties, biodegradability, and easy-to-obtain worldwide[30,163]. In addtion, different techniques can be applied to create hydrophilic/hydrophobic patterns or physical barriers to obtain microfluidic channels [30,164–167]. Furthermore, paper is an excellent platform for the fabrication of low-cost electrochemical devices. For this, various techniques can be used to obtain the conductive tracks on the paper platform, and one of the most recent ones, which has been evidenced in the last few years, is the laser-scribing method. This method characterizes a recent, scalable, manageable, low-cost method to fabricate carbon-based electrodes on paper-based platforms. The technique uses a laser machine to

carbonize the material's surface and obtain a conductive carbon track, as discussed in the first chapter [40].

Although paper-based electrodes have demonstrated satisfactory electroanalytical performance [168–170], they also present some limitations. One major drawback of this platform used for electrochemical sensor fabrication is the permeation of the supporting electrolyte into the paper through capillarity. This can cause the paper to swell, altering the sensors' electrochemical area and affecting the analytical responses' accuracy. Furthermore, this permeation can also compromise the electrical contacts of the device with the workstation instrumentation [171].

However, despite these disadvantages, paper substrates can generate flow without external pumps [172]. This property makes them highly attractive for producing microfluidic platforms, as discussed previously[173,174]. Therefore, there is a need for new electrochemical sensors that can be combined with paper structures to create versatile and efficient analytical devices.

It is known that the first laser-scribed disposable electrochemical device was fabricated using polyimide as a polymer platform, which is a good source for fabricating conductive carbon-based materials for electrocatalysis[175–178]. Thus, in this study, we presented the development of a highly versatile and flexible electrochemical sensor, which can be applied using static or hydrodynamic systems. With this purpose, an innovative combination of laser-scribing technique, Kapton adhesive tape, and a paper-based microfluidic platform is presented, where the Kapton tape is a cost-effective polyimide source commonly employed in producing flexible printed circuits.

## 3.2. Experimental section

### 3.2.1. Reagents and Materials

The Kapton adhesive tape was acquired from DS tools with dimensions of 1.8 mm x 33 M. All chemicals were analytical grade and used without additional purification. The solutions were all prepared using deionized water (Direct-Q® 5 Ultrapure Water Systems, Millipore, MA, USA) and the appropriate electrolytes depending on the experiment. Potassium ferrocyanide ($K_4[Fe(CN)_6]$), potassium ferricyanide ($K_3[Fe(CN)_6]$), potassium chloride (KCl), acetic acid, boric acid, and sodium hydroxide (NaOH) were purchased from Merck (Darmstadt, Germany). Phosphoric acid, hexaammineruthenium (III) chloride ($[Ru(NH_3)_6Cl_3]$, and 3-nitrotyrosine were acquired from Sigma-Aldrich (St. Louis, MO, USA). Silver conductive ink was obtained from Joint Metal Comercio LTDA (Diadema-SP, Brazil). The Britton-Robinson buffer 0.1 mol $L^{-1}$ was prepared by adjusting the pH values of the solution containing acetic acid, phosphoric acid, and boric acid, with the pH values varying from 2.0 to 12.0. The adjustments were realized using NaOH 6 mol $L^{-1}$ and HCl 6 mol $L^{-1}$ solution.

### 3.2.2. Fabrication of the laser-scribed sensors

Two polyimide tape parts were combined to generate a double-layer polyimide substrate. This substrate was used to fabricate the electrodes using the laser-scribing technique. The three electrodes system and the electrochemical cell were designed through software provided with the equipment. The electrodes were obtained on the polyimide tape by the carbonization of this platform. A $CO_2$ laser cutter system (Work Special Laser) characterized by a wavelength of 10.6 pm and a pulse duration of ~14

μs was used to manufacture the devices through the laser-scribing technique. The power, scan rate, Z-distance, and distance between lines used in the laser machine varied from 7.0–9%, 60.0–140.0 mm $s^{-1}$, 11.0–13.0 mm, and 0.02–0.1 mm, respectively, during the optimization of the parameters under ambient conditions. The optimized conditions for laser power, scan rate, Z-distance, and distance between lines were 8.0% (~1.4 W), 80.0 mm $s^{-1}$, 13.0 mm, and 0.04 mm, respectively.

The dimensions of the electrodes on the obtained system are observed in the scheme presented in Figure 20. After the laser-scribing, the bottom of the conductive tracks was painted with silver ink to ensure subsequent electrical contact with the electrochemical workstation. Furthermore, silver ink was also used in the reference electrode to create a silver pseudo-reference electrode which could prove more electrochemical stability. Silicon glue (Tek Bond- transparent silicone sticker) was used to delimitate the working electrode area and isolate the reaction zone.

**Figure 20 -** A) Representation of the device fabrication process and the dimensions of the electrodes (working (WE), counter (CE), and reference electrodes (RE)) for the B) Static and C) Hydrodynamic mode.

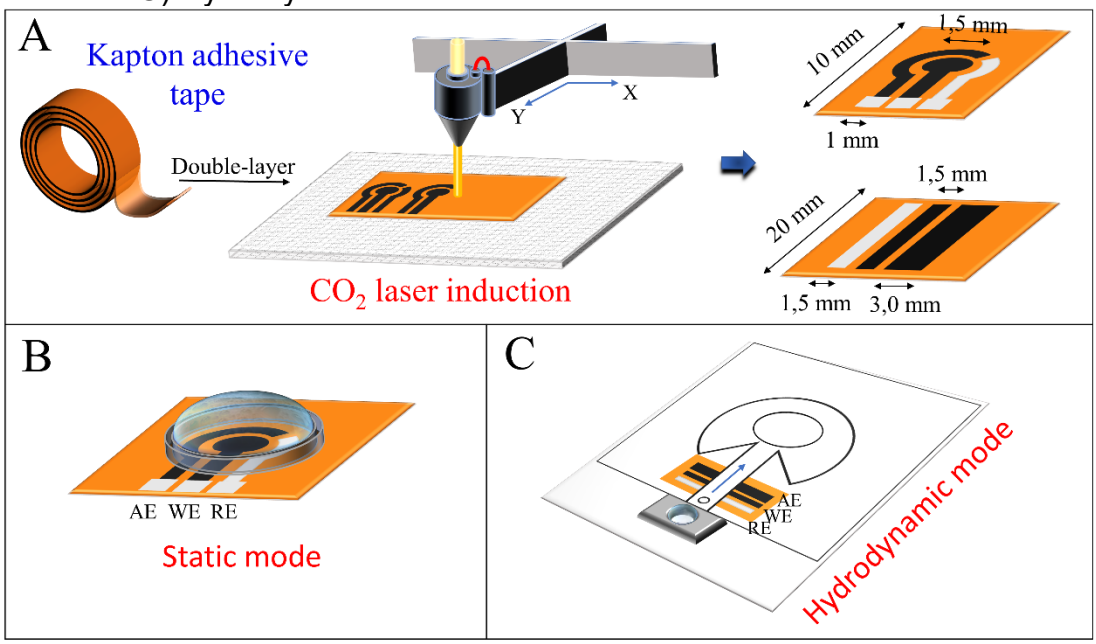

The optimization of the laser-scribing parameters for the fabrication of the devices (distance between lines, power, scan rate, and Z-distance) was evaluated using cyclic voltammetry technique and 1.0 mmol $L^{-1}$ hexaaammineruthenium (III) chloride as a redox probe in 0.1 mol $L^{-1}$ KCl electrolyte solution, with the voltage potential ranging from 0.00 to -0.45 V at 50 mV $s^{-1}$. All the electrochemical measurements were obtained using a potentiostat Autolab PGSTAT128N (Eco Chemie, Utrecht, The Netherlands) controlled by a computer running NOVA 1.11 software.

After, the versatility of the laser-scribed devices was demonstrated by combining them with a paper-based microfluidic platform. These microfluidic platforms were fabricated following the protocol presented in previous work[179]. The geometry of the microfluidic devices was designed with CorelDRAW software. ColorQube 8870 wax printer (Xerox, Connecticut) was used to deposit the wax (4-pt line thick) onto the Whatman 4 qualitative filter paper. The material obtained was transferred onto a heated plate, maintained at a temperature of 120°C for 120 seconds. This is a crucial step to facilitate the melting of the wax, thereby creating hydrophobic barriers.

Two reservoirs compound the system, as observed in Figure 20 – C). One is made from a PMMA plate with a hole of 6 mm in diameter and 3 mm in height (inlet reservoir). The other one is made from filter paper and wax in the border for the hydrophobic barrier, as the design presented in Figure 20 – C), where the semicircle has 50 mm in diameter (outlet reservoir). In addition, four pieces of paper sheets were put on top of the semicircle of this reservoir to increase the wicking capacity.

After the microfluidic device's fabrication, the device was sealed with packing tape to ensure the system's integrity, effectively preventing potential leaks. During the measurement, the inlet reservoir was constantly filled with electrolyte solution, and the

analyte injections were realized through a small cavity on the outlet reservoir distant 3 mm from the inlet reservoir. A conventional micropipette was used to inject the analyte, using a volume of 2 µL. For this hydrodynamic mode, the electrochemical measurements were conducted utilizing amperometry as the analytical technique.

### 3.2.3. Material characterization

Different techniques characterized the material before and after the laser-scribing of polyimide tape. The top-view and cross-sectional images were obtained using SEM (HITACHI / TM-3000) operated at 2 and 5 keV. The samples were metalized with a thin layer of gold using Quorum QR 150ES Metallizer.

Raman spectroscopy analyses were carried out using a spectrometer Horiba Scientific, T64000. Whereas the XPS analyses were conducted using a SPECS Phoibos 150 hemispherical analyzer with multi-channeltron detection, the Mg Ka radiation was maintained at a constant energy mode of 10 eV pass energy.

The conductive tracks were also characterized using the electrochemical technique (cyclic voltammetry), and the measurements were obtained using a potentiostat Autolab PGSTAT128N (Eco Chemie, Utrecht, The Netherlands) controlled by a computer running NOVA 1.11 software. Cyclic voltammetry technique was carried out in different redox probes, 1 mmol $L^{-1}$ $K_3[Fe(CN)_6]$ or 1 mmol $L^{-1}$ $[Ru(NH_3)_6Cl_3]$ in 0.1 mol $L^{-1}$ KCl solution. The potential range used in the first case was from 0.6 to -0.3 V and in the second one from 0.00 to -0.45 V, varying the scan rate from 2 to 500 mV $s^{-1}$ in both cases. The electrochemical impedance spectroscopy (EIS) was also used and recorded in a mixture of 1 mmol $L^{-1}$ potassium ferricyanide/ferrocyanide with frequencies varying from $10^5$ to $10^{-1}$ $s^{-1}$ for a sinusoidal

signal applied using a typical open circuit potential (OCP) of 0.22 V, and amplitude of 10 mV, at ambient temperature.

Reproducibility and repeatability were evaluated for the electrochemical measurements using cyclic voltammetry technique and potassium ferrocyanide as redox probe (1 mmol $L^{-1}$ ferrocyanide + 0.1 mmol $L^{-1}$ KCl at 50 mV $s^{-1}$). For the reproducibility test, ten different fabricated electrodes were used. In contrast, twenty measurements were obtained using the same electrode for the repeatability test. The cyclic voltammograms were recorded using a potential range from 0.6 to −0.3 V. Additionally, the electrode stability over the days was evaluated using cyclic voltammograms in 1 mmol $L^{-1}$ ferrocyanide + 0.1 mol $L^{-1}$ KCl at 50 mV $s^{-1}$, with potentials ranging from 0.7 to −0.35 V over thirty days stored in ambient conditions.

Furthermore, the stability of the devices after being banded n times was measured also using cyclic voltammograms of laser-scribed electrodes in 1 mmol $L^{-1}$ ferrocyanide + 0.1 mol $L^{-1}$ KCl at 50 mV $s^{-1}$ with potentials ranging from 0.7 to −0.35 V.

### 3.2.4. Analytical application

After the fabrication and characterization of the devices, the electrochemical performance was evaluated using hexaammineruthenium (III) chloride as a redox probe and 3-NT, dopamine, and uric acid as proof of concept. The measurements were obtained using both the hydrostatic and hydrodynamic systems.

For the hexaammineruthenium (III) chloride, a cyclic voltammetry technique was used in different concentrations (0.1 – 1.0 mmol $L^{-1}$), with potentials ranging from 0.0 to −0.45 V, to evaluate the hydrostatic system and a calibration curve was obtained. The hydrodynamic system measurements were carried out using the chronoamperometry technique, with an $E_{detection}$ = -0.4 V vs Ag pseudo-RE. The

carrier solution was 0.1 mol $L^{-1}$ KCl with injections of 2 µL of 0.2, 0.4, 0.6, 0.8, and 1.0 mol $L^{-1}$ hexaaammineruthenium (III) chloride.

For the 3-nitrotyrosine measurements, first, a cyclic voltammogram was carried out using the laser-scribed electrode as the static mode in 1 mmol $L^{-1}$ 3-nitrotyrosine + 0.1 mol $L^{-1}$ phosphate buffer solution, pH 7.4, at 50 mV $s^{-1}$, with potentials ranging from 1.0 to – 1.0 V. Furthermore, the effect of pH on the electrochemical behavior of 3-NT was observed using the laser-scribed devices and cyclic voltammetry in 0.04 mol $L^{-1}$ Britton-Robinson buffer containing 0.2 mmol $L^{-1}$ 3-NT at pH values ranging from 2.0 to 12.0. Phosphate buffer solution with pH around 7 in the same concentration was also used to compare the results with those obtained from the Britton-Robinson buffer solution. All measurements were conducted at room temperature (~25 °C).

Finally, electrochemical quantification of 3-NT was obtained using both systems (static and hydrodynamic). For the static one, the analyte was quantified using differential pulse voltammetry (DPV) in different concentrations of 3-NT (0.5 - 30 µmol $L^{-1}$) and PBS (Phosphate Buffer Solution), pH 7.4, from -0.25 V to 1.0. The optimum parameters used in the DPV technique were $E_{step}$ (step potential) = 5 mV and Amplitude = 25 mV (Scan rate = 10 mV $s^{-1}$). In contrast, the measurements for the hydrodynamic system were carried out using the chronoamperometry technique, with an applied potential of 0.8 V vs Ag pseudo reference electrode. The carrier solution was 0.1 mol $L^{-1}$ PBS pH 7.4, with injections of 2 µL with 40, 60, 80, 100 and 150 µmol $L^{-1}$ 3-NT. An interference study was performed using the static system, where the DPV measurements of the 3-NT were recorded by mixing the analyte with each interferant molecule in a proportion of 1:2. Thus, 10 µmol $L^{-1}$ 3-NT were mixed with 20 µmol $L^{-1}$ uric acid (UA), or urea (UR), or nitrite ($NO_2^-$), and caffeine (CAF). The measurements

were expressed as normalized peak current (Ip) percentage, where the 3-NT Ip corresponds to 100%.

The laser-scribed electrode was also tested in different model molecules (dopamine (DP) and uric acid (UA)) using the static conditions. The analytical performance was evaluated from 3 to 30 μmol $L^{-1}$ for DP and from 8 to 100 μmol $L^{-1}$ for the UA.

## 3.3. Results and discussion

### 3.3.1. Optimization of the carbonization process

We fabricated the electrodes using Kapton tape. This process is presented in Figure 20, including hydrodynamic and static modes. The optimization of the conditions for the laser-scribing fabrication was realized using resistance (R) of the electrodes fabricated varying the laser-scribing parameter, such as the distance between radiation lines, power of the laser, scan rate, and Z-distance. The values were measured using a multimeter, presented in Table 3.

**Table 3** - Optimization parameters for laser-scribing fabrication of the devices.

| **Distance between lines (D) mm** | **R Ω cm** | **Power (P) %** | **R Ω cm** | **Scan rate (S) mm $s^{-1}$** | **R Ω cm** | **Z-distance (Z) mm** | **R Ω cm** |
|---|---|---|---|---|---|---|---|
| **P: 8.0 % S: 80 mm $s^{-1}$ Z: 12 mm** | | **S: 80 mm $s^{-1}$ Z: 12 mm D: 0.04 mm** | | **P: 8.0 % Z: 12 mm D: 0.04 mm** | | **P: 8.0 % S: 80 mm $s^{-1}$ D: 0.04 mm** | |
| **0.02** | 79 ± 7 | **7.5** | 2792 ± 5233 | **60** | 66 ± 6 | **11** | 199 ± 79 |
| **0.04** | 80 ± 3 | **8.0** | 67 ± 5 | **80** | 83 ± 3 | **12** | 137 ± 19 |
| **0.06** | 178 ± 19 | **8.5** | 77 ± 21 | **100** | 115 ± 12 | **13** | 145 ± 12 |
| **0.08** | 165 ± 20 | **9.0** | 173 ± 78 | **120** | 142 ± 19 | | |
| **0.1** | 359 ± 135 | | | **140** | 234 ± 28 | | |

Another parameter to study the best fabrication conditions was evaluating the electrochemical responses of these electrodes using the cyclic voltammetry technique and hexaaamineruthenium (III) chloride as a redox probe. The cyclic voltammograms of PI laser-scribed electrodes for different laser-scribing conditions of the distance between radiation lines, power, scan rate, and Z-distance are presented in Figure 21 - A) B) C) e D) respectively.

The voltammograms for most fabrication conditions showed typical electrochemical behavior of the redox probe. However, a variation of the current peak values (Ip) or peak-to-peak potential distance (ΔEp) can be observed depending on the laser-scribing conditions as presented in Ip and ΔEp plots (Figure 21 - E) F) G) and H)). Higher Ip represents higher sensitivity in terms of current, which makes these devices more interesting for electrochemical applications. In Figure 21- A), and respectively in Figure 21- E), an increase in the Ip values from D=0.02 to D=0.06 mm is observed, probably due to the rise in the active electrochemical area of the sensors. In contrast, for D values higher than 0.08 mm, the spacing between the lines compromises the material's conductivity, as observed through the higher resistivity values in Table 3, and lower Ip in Figure 21 - A) and E).

**Figure 21 -** Cyclic voltammograms of PI laser-scribed electrodes in 1 mmol $L^{-1}$ $[Ru(NH_3)_6]Cl_3$ at 50 mV $s^{-1}$ with a potential range from 0.0 to -0.45 V for different laser-scribing conditions of A) distance between radiation lines, B) power, C) scan rate, and D) Z-distance. The Ip and ΔEp *vs.* E) distance between radiation lines, F) power, G) scan rate, and H) Z-distance plots for the anodic process of $[Ru(NH_3)_6]Cl_3$ obtained from the cyclic voltammograms in A, B, C, and D.

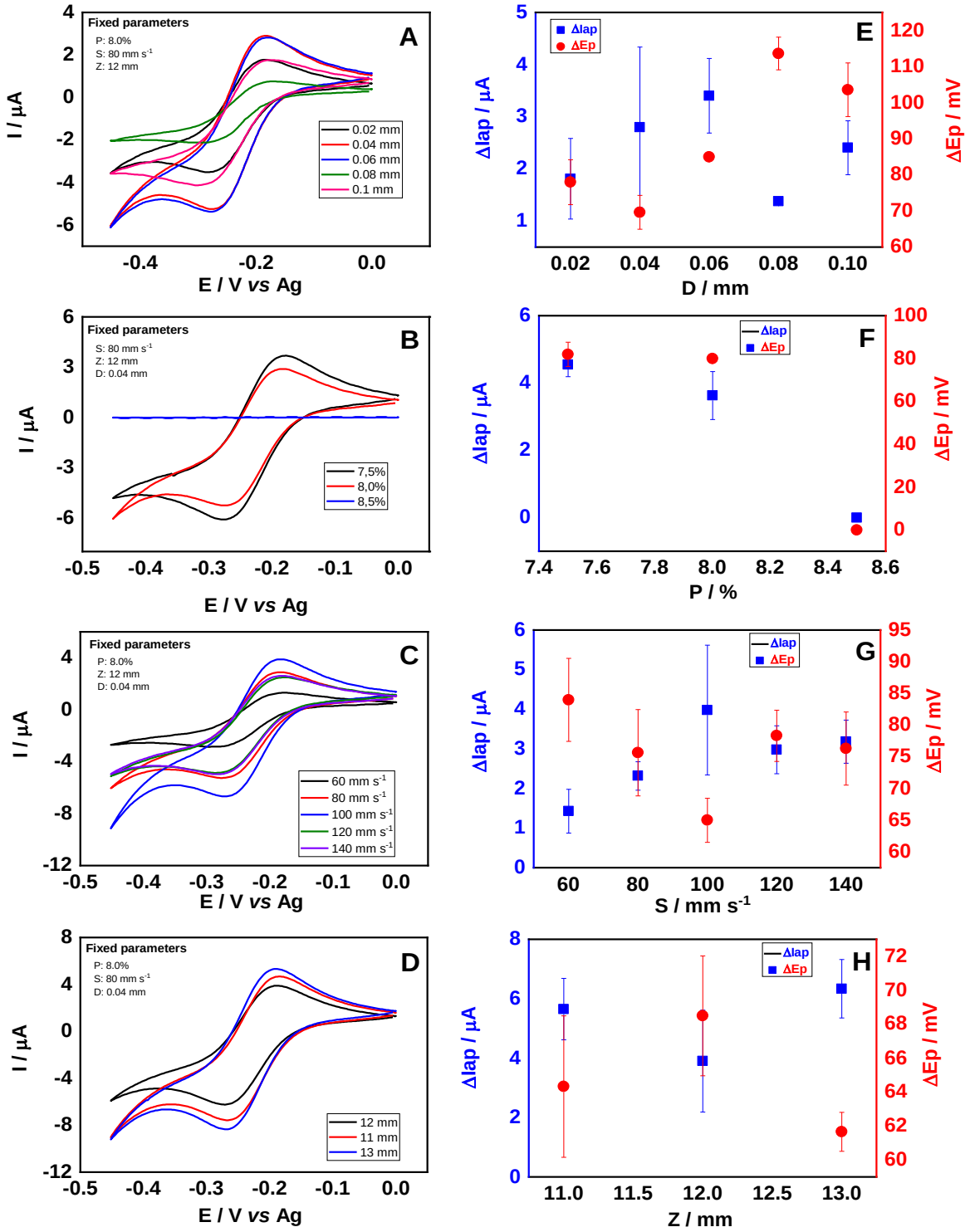

The material's conductivity also impacts the ΔEp values. For ΔEp, in conventional glassy carbon systems, this value is expected to be ideally close to 59 mV for a reversible electrochemical process, which involves only one electron, as in hexaammineruthenium (III) chloride [180]. Thus, lower ΔEp values were observed for the material using lower distances between the radiation lines during the fabrication procedure. Therefore, taking into consideration all the electrochemical measurements, higher Ip, lower ΔEp, lower resistivity values, and the mechanical stability of the material, the standard deviation error, D = 0.04 mm was chosen as the best condition to carbonize the polyimide substrate.

The other parameter investigated was the power of the laser. For power values lower than 7.5 %, the carbonization of the polyimide was not completed, while using power higher than 8.0 %, the carbon-based obtained material presented a brittle aspect with poor mechanical stability. Thus, the best-demonstrated values for the laser power were 7.5 and 8.0 %. The Ip and ΔEp obtained values (Figure 21 - B) and F)) were similar in both cases. However, the laser power of 8.0 % was selected due to the lower resistivity value in this case.

In addition, the scan rate variation of the laser was also evaluated in the electrochemical responses. In Figure 21 - C) and G), it is observed that between 80- and 120-mm s-1 scan rate values, the higher Ip and the lower ΔEp values were observed. However, the electrochemical behavior did not present significant variation. Yet higher scan rate values can make the consistent carbonization of the material difficult, providing higher resistivity to the obtained conductive tracks. Furthermore, when using 100-mm $s^{-1}$, high standard deviation values were obtained for Ip and ΔEp, which led to selecting the 80-mm $s^{-1}$ scan rate as the best condition.

The Z-distance (focal distance) was the last studied parameter. In this case, a significant variation in the electrochemical responses with the focal distance change was not observed, as noticed in the Figure 21 - D) and H). Lower ΔEp and higher Ip were observed using 11.0 and 13.0 mm Z-distances. However, lower standard deviation values on the Ip and ΔEp measurements were observed for a Z-distance of 13.0 mm. Hence this one was selected as the best focal distance for the laser-scribing procedure for the PI electrodes fabrication.

### 3.3.2. Morphological and electrochemical characterization

Finally, the optimized conditions of power, scan rate, Z-distance, and distance between radiation lines were 8.0% (~1.4 W), 80.0 mm $s^{-1}$, 13.0 mm, and 0.04 mm, respectively. After optimizing parameters, the morphology of the carbonized material in the optimized conditions was observed using SEM images (Figure 22).

First, the flat morphology of the PI tape was observed in Figure 22 A), B), and C) for different magnitudes. In contrast, a porous material was noticed for the polyimide laser-scribed-based electrodes in Figure 22 D), E), and F. As discussed above in the last chapter, it is well known in the literature that the incidence of the laser source causes the increase of the local temperature (> 2500 °C), which provides the carbonization of organic materials. This procedure is also responsible for generating gases and, consequently, the obtention of a porous carbonized surface [52].

**Figure 22 -** SEM images indicating A), B), C) flat morphology of polyimide tape and D), E), F) porous morphology of laser-scribed polyimide-based device. G), H), I) Cross-section SEM images of laser-scribed polyimide-based electrodes.

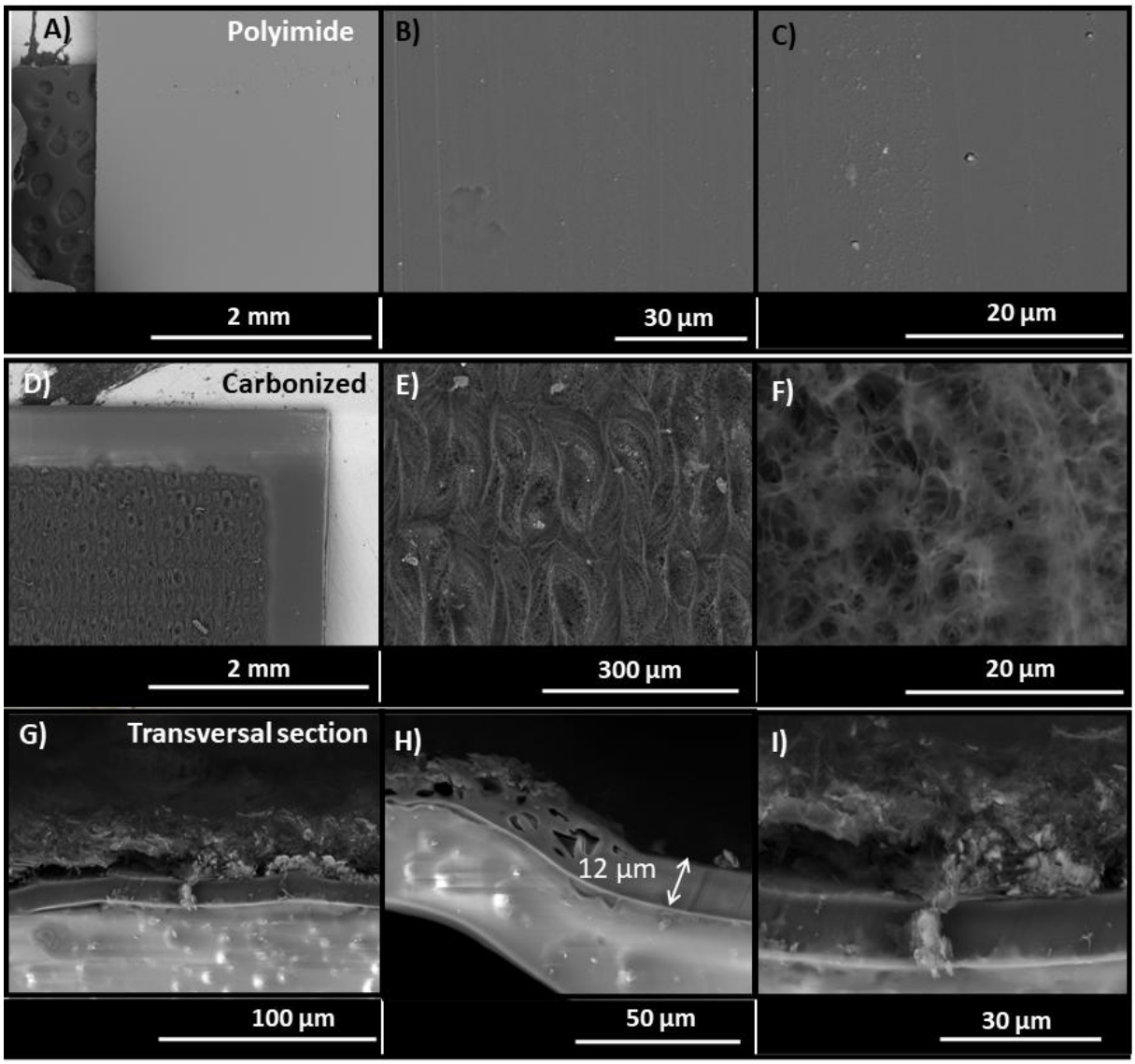


Furthermore, the cross-sectional SEM images of the carbonized material were also obtained over the entire length of polyimide laser-scribed based electrodes (Figure 22 G), H), and I)). The estimated measured thickness from these images was (12.3 ± 0.5) µm.

Raman spectroscopy technique was also used to evaluate the carbonization of the PI surface (Figure 23).

**Figure 23 -** Raman spectra of laser-scribed polyimide-based device (carbonized) and raw polyimide tape.

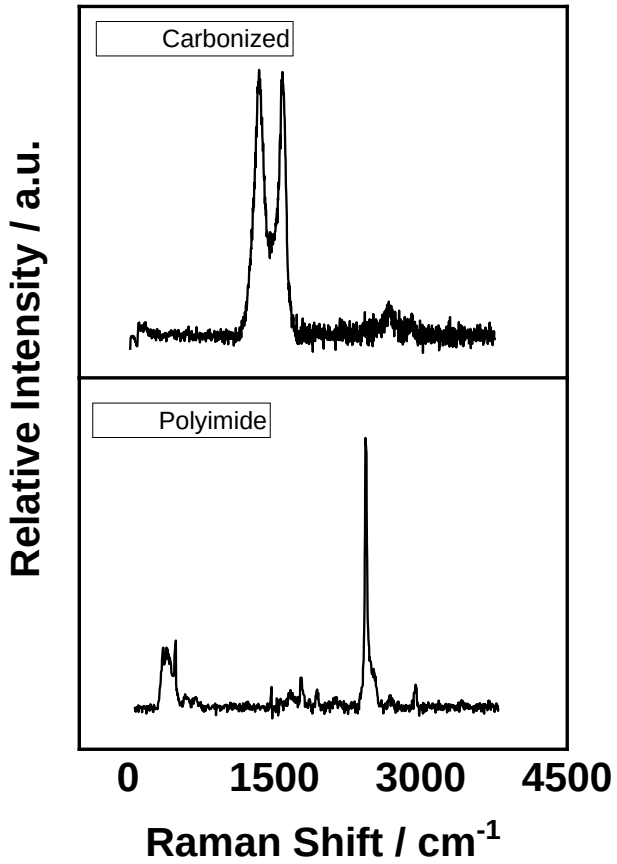


The Raman spectra of the raw PI showed no characteristic bands, whereas two bands were observed at about 1340 and 1580 $cm^{-1}$ for the polyimide laser-scribed-based electrodes. These bands are usually reported in carbon-based materials, such as graphene, representing D and G bands. In these materials, it has been reported that the vibration in the plane of the carbon bonds for $sp^2$ hybridization causes the emergence of the G band in Raman spectra. In contrast, the D band is related to the vibrational of the hybridized modes in the edges due to the structural defects in the material, which could indicate some disorder in the structure [140]. Thus, the presence of these two bands indicates the carbonization of the PI substrate after the laser-scribing treatment, obtaining a so-called graphene-like material [26,75,181]. This resulted in obtaining a conductive material, which opens the possibility of applying them as electrochemical sensors.

The literature reported a significant change in the carbon-based compounds when comparing the composition of the polyimide material before and after the carbonization [182]. To investigate the carbon-based chemical groups on the surface of the material before and after the carbonization of the Kapton tape (polyimide), high-resolution C1s XPS spectra were obtained and presented in Figure 24. Thus, it was possible to evaluate the carbonization of this Kapton tape, a low-cost and easy-to-find polyimide source.

**Figure 24 –** High-resolution C1s X-ray photoelectron spectra of (a) Kapton tape (polyimide) and (b) laser-scribed polyimide (carbonized).

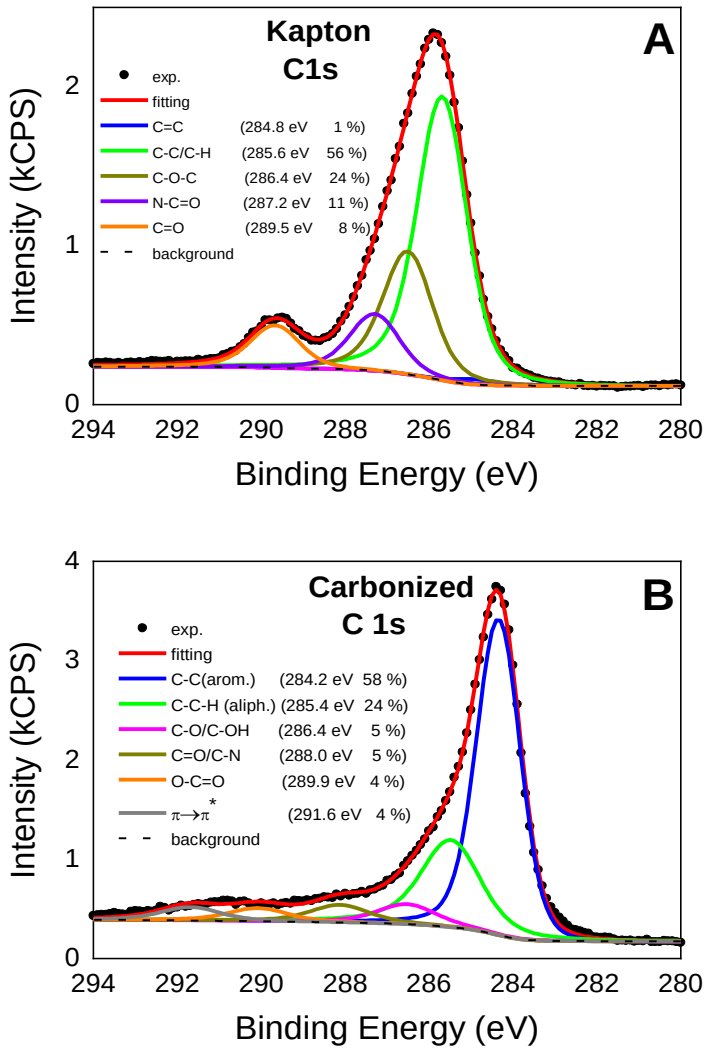

In Figure 24 – A), the high-resolution C1s spectra are observed for the Kapton tape, where a predominant peak in intensity is noticed around 285.6 eV. This peak is related to the single bonds involving carbon C-C/C-H, hybridization $sp^3$, as also observed in the literature [182], and in this Kapton tape corresponds to 56% of the carbon-containing groups. Furthermore, carbon-oxygen compounds are also observed in the composition of the material in 286.4 eV, 287.2 eV, and 289.5 eV, attributed, respectively, to C-O-C, N-C=O, and C=O [183] corresponding to 24%, 11%, and 8%. This is expected since the main composition of the Kapton is polyimide. The composition of each group and the binding energy are summarized in Table 4. The chemical structure of the polyimide is presented in Figure 25, containing C, N, and O atoms. However, impurities can also be observed in the material since the Kapton tape is a cheap not pure source of polyimide.

**Table 4 –** Summarized fitting peaks obtained from high-resolution C1s X-ray photoelectron spectra of Kapton tape (polyimide) and laser-scribed polyimide (carbonized Kapton tape).

| C 1s spectra | Contributions | | | |
|---|---|---|---|---|
| Concentrations | PI | | Carbonized | |
| | | Binding Energy | | Binding Energy |
| C-C ($sp^2$) | - | | 58% | 284.2 eV |
| C=C | 1% | 284.8 eV | - | |
| C-C-H (Aliph.) | - | | 24% | 285.4 eV |
| C-C/C-H | 56% | 285.6 eV | - | |
| C-O-C | 24% | 286.4 eV | - | |

| | | | | |
|---|---|---|---|---|
| **C-O/C-OH** | - | | 5% | 286.4 eV |
| **N-C=O** | 11% | 287.2 eV | - | |
| **C=O/C-N** | - | | 5% | 288.0 eV |
| **C=O** | 8% | 289.5 eV | - | |
| **O-C=O** | - | | 4% | 289.9 eV |
| **π→π*** | - | | 4% | 291.6 eV |

**Figure 25** - General chemical structure of a polyimide.

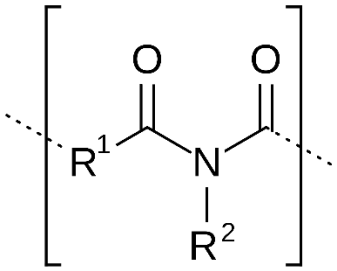


The high-resolution C1s spectra of the laser-scribed polyimide (carbonized Kapton tape) are presented in Figure 24 – B) for comparison. First, it is possible to observe a change in the functional groups contained compared to the Kapton tape before the carbonization. It is due to the breaking of carbon-oxygen and carbon-nitrogen bonds with the incidence of the laser [184]. The predominant peak in intensity is around 284.2 eV, corresponding to C-C ($sp^2$) bonds and representing around 58% of the carbon bonds in the obtained material. It shows a significant presence of $sp^2$ hybridized carbon bonds, which was not observed before and are responsible for the conductivity conferred to the material after the carbonization [185]. Thus, the Kapton

tape, polyimide, which is a non-conductive material, was transformed into a conductive material.

Other peaks are also observed in 285.4, 286.4, 288.0, 289.9, and 291.6 eV, as presented in Table 4. They are attributed to the C-C-H (Aliph.), C-O/C-OH, C=O/C-N, O-C=O, and π→π* [182,184], which are different groups from observed in the Kapton tape. Furthermore, the carbon-oxygen compounds decreased from around 43% to 14% after the carbonization of the material. It is in agreement with the literature [182]. Also, the percentage of carbon-nitrogen compounds decreased from around 11% to 5%. As mentioned above, this can be related to breaking the carbon-oxygen and carbon-nitrogen bonds, the major components of the Kapton tape, when the laser source was incident on the material since the laser irradiation results in the liberation of both gaseous oxygen and nitrogen [186].

Herein, we did not study the influence of the fabricating parameters on the carbon-based chemical groups of the carbonized material obtained. However, it was reported in the literature that the carbon bond composition varies with the laser-applied parameter, such as the power of the laser. As the laser power increases, the abundance of C=O, C−O−C, and C−N bonds decreases, whereas the percentage of C−C bonds increases. Furthermore, the conductivity of the laser-scribed samples also varies with the laser power[184]. All these variations will probably influence the electrochemical responses; thus, the modulation of the surface content is also possible depending on the necessity and electrochemical application.

Electrochemical material characterization was also obtained, as presented in Figure 26, using two redox probes, potassium ferricyanide and hexaammineruthenium (III) chloride. Potassium ferricyanide was used as a redox probe since it is more sensitive to changes in the carbon surface than hexaammineruthenium (III) chloride.

It serves as an inner-sphere electrochemical redox probe, which means that the electron transfer is not only influenced by the electronic structure but also by the carbon material's electrode surface, including edge plane-like sites and oxygenated species [133,134]. On the other hand, hexaammineruthenium (III) chloride is a redox probe less sensitive to changes in the carbon surface. It is considered an outer-sphere redox probe, where the electron transfer depends directly on the electronic structure of the carbon material. Thus, the cyclic voltammograms of optimized PI laser-scribed electrodes in potassium ferricyanide and hexaammineruthenium (III) chloride are presented in Figure 26 - A) and C).

Figure 26 – A) and C) shows a stable and low background current, where the electrodes presented a typical electrochemical behavior for both redox probes, with a reversive electrochemical process. However, the hexaammineruthenium (III) chloride peaks were more defined than potassium ferricyanide. In this case, better electrochemical reversibility was noticed since the obtained ΔEp is around 76 mV, while for the potassium ferricyanide, the ΔEp is about 246 mV. It is due to the different redox systems represented by hexaammineruthenium (III) chloride and potassium ferricyanide. As the electrochemical responses vary with the mechanisms of charge transfer in different molecules, it opens a range of applications for the polyimide laser-scribing-based electrodes since the modulation of the electrochemical surface is possible using different parameters during the electrode fabrication, as discussed above. In addition, the ratio between anodic ($I_{pa}$) and cathodic current peak ($I_{pc}$), given by $I_{pa}/I_{pc}$, values exhibited in both electrochemical probes were around 1, a characteristic behavior also observed in diffusion-controlled reversible systems.

**Figure 26** - Cyclic voltammograms of optimized laser-scribed electrodes in 1 mmol $L^{-1}$ potassium ferricyanide + 0.1 mol $L^{-1}$ KCl at 50 mV $s^{-1}$ with potentials ranging from 0.6 to -0.3V and B) at different scan rates (2, 5, 10, 15, 20, 30, 40, 50, 75, 100, 150, 200, 300, 400, and 500 mV $s^{-1}$). Inset indicates a logarithm plot of the current peak of (anodic current) versus scan rate (log Ia = 0.4 logV – 5.9). C) Cyclic voltammograms of optimized laser-scribed electrodes in 1 mmol $L^{-1}$ hexaammineruthenium(III) chloride at 50 mV $s^{-1}$ with potentials ranging from 0.0 to -0.45 V and B) at different scan rates (2, 5, 10, 15, 20, 30, 40, 50, 75, 100, 150, 200, 300, 400, and 500 mV $s^{-1}$). Inset indicates a logarithm plot of the current peak (anodic current) versus scan rate (log Ia = 0.4 logV – 5.9).

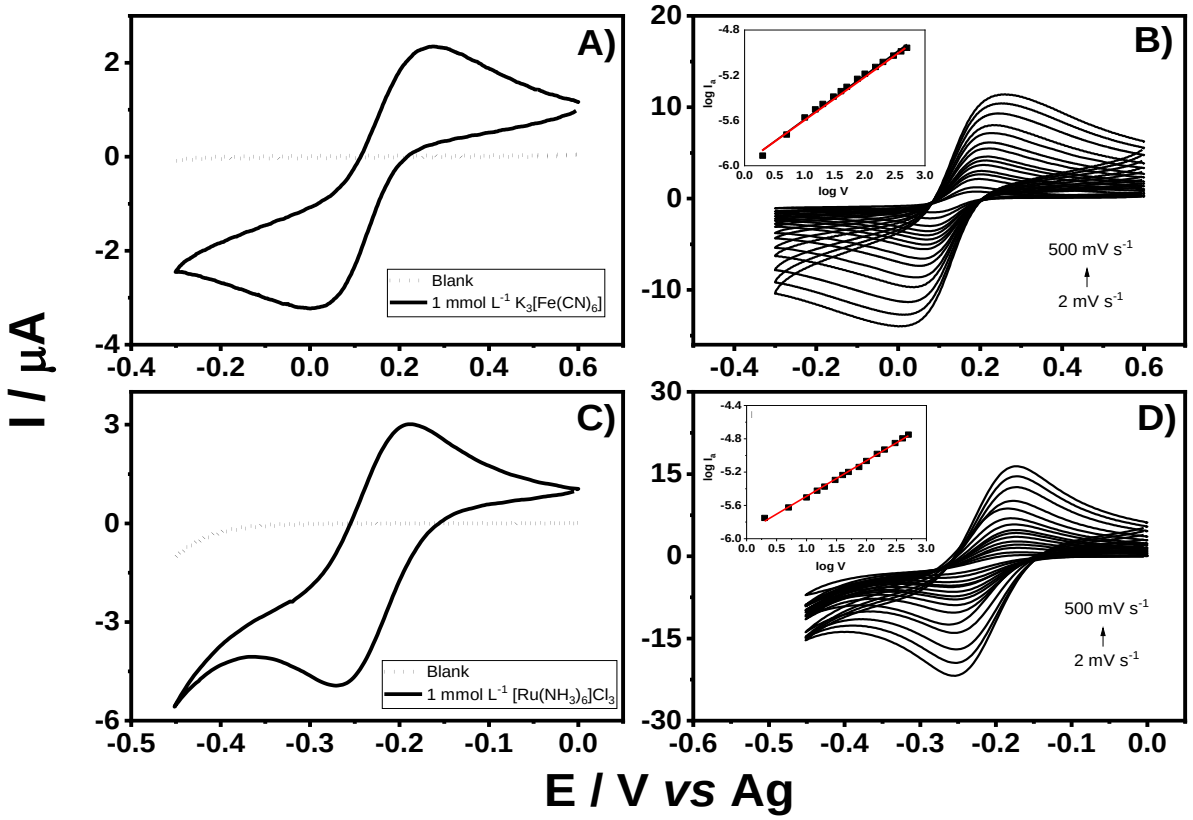


Furthermore, the scan rate influence on the electrochemical responses was evaluated using both redox systems, observed in Figure 26 - B) and D). The cyclic voltammograms of polyimide laser-scribed electrodes were recorded in a medium of 1 mmol $L^{-1}$ of ferricyanide + 0.1 mol $L^{-1}$ KCl (Figure 26 - B)) or 1 mmol $L^{-1}$ of hexaammineruthenium (III) chloride + 0.1 mol $L^{-1}$ KCl (Figure 26 - D)) using different scan rates (υ), (2, 5, 10, 15, 20, 30, 40, 50, 75, 100, 150, 200, 300, 400 and 500 mV $s^{-1}$).

The logarithm plot of $I_a$ versus scan rate insets is also observed in Figure 26 - B) and D) and is typically used to distinguish diffusional and adsorptive electrochemical processes. In this case, the nature of the electrochemical process is determined from the slope of the straight line obtained. For an adsorption-controlled process, $I_a$ is proportional to υ, resulting in a slope of 1.0. In contrast, in a diffusion-controlled process, $I_a$ is proportional to $v^{1/2}$, resulting in a slope of 0.5 [187]. Thus, the linear relationship obtained from the logarithm plots was coincidentally $\log I_a = 0.4 \log V - 5.9$ and $\log I_a = 0.4 \log V - 5.9$, when using ferricyanide and hexaammineruthenium (III) chloride. The slopes of approximately 0.4 were observed in both cases, suggesting a diffusion-controlled electrochemical process. This behavior is usually observed in traditional carbon electrode systems for ferricyanide and hexaammineruthenium (III) chloride electrochemical measurements.

Using ferricyanide as a redox probe since it is a more sensitive system to the surface chemical groups changing, the reproducibility measurements were recorded. The experiment was performed on ten fabricated electrodes using cyclic voltammetry (Figure 27 - A). When comparing the ten electrodes, the electrochemical response variation was evaluated and expressed as the Relative Standard Deviation (RSD) of the anodic current $I_p$. The obtained RSD in this case was 7.4 %. The same procedure was used for repeatability tests, and the cyclic voltammograms are presented in Figure 27 - B). However, for repeatability, twenty measurements were obtained from the same electrode. Thus, an RSD = 3.6 % was obtained, indicating good reproducibility and repeatability. Good reproducibility is highly desired on electrochemical devices when thinking about analytical applications. Reproducible sensors provide reliability to the measurements, which is primordial in analytical systems. Furthermore, the

repeatability data indicates the system's stability over the electrochemical measurements.

**Figure 27** - Cyclic voltammograms of laser-scribed electrodes in 1 mmol $L^{-1}$ ferrocyanide + 0.1 mol $L^{-1}$ KCl at 50 mV $s^{-1}$ with potentials ranging from 0.7 to −0.4 V. A) Reproducibility for ten different fabricated electrodes (reproducibility measurements expressed as RSD = 7.4%, n = 10). Inset: peak current (Ip) vs. n plot. B) Repeatability for twenty measurements obtained from the same electrode (repeatability measurements expressed as RSD = 3.6%, n = 20). Inset: peak current (Ip) vs. n plot.

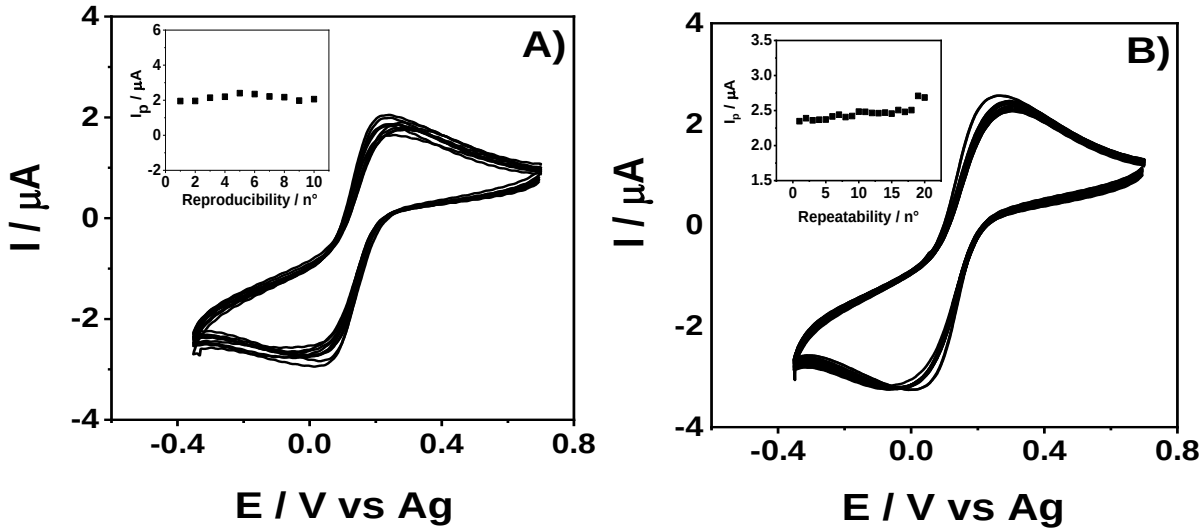


The fabricated laser-scribed electrode was compared with a screen-printed commercial electrode using cyclic voltammetry and electrochemical impedance spectroscopy (EIS) techniques and potassium ferricyanide as the redox probe. The measurements are presented in (Figure 28 - A) and B)). An electrochemical behavior similar to the commercial screen-printed electrode is observed for the proposed electrode in Figure 28 - A). It is crucial to highlight herein that, for the comparison, the normalization of the voltammograms by the geometric area was applied. Moreover, the EIS technique was used to obtain the materials' resistance to charge transfer ($R_{CT}$). Both electrodes' Nyquist diagrams (Figure 28 - B) presented the typical semicircle profile corresponding to the electron-transfer limited process observed in higher

frequencies. The diameter of these semicircles corresponds to the $R_{CT}$ values of 1.9 ± 0.3 kΩ and 10.3 ± 2.9 kΩ for the commercial screen-printed and laser-scribed electrodes, respectively. Despite the laser-scribed electrodes exhibiting higher $R_{CT}$ values, which indicates a slower charge transfer kinetic in this system, the cyclic voltammetry's electrochemical response was similar to the commercial screen-printed electrode. It highlights the potentiality of the proposed material to be studied and applied as electrochemical sensors.

**Figure 28** - A) Cyclic voltammograms of laser-scribed electrodes in 1 mmol $L^{-1}$ ferrocyanide + 0.1 mol $L^{-1}$ KCl at 50 mV $s^{-1}$ for comparison between commercial carbon screen-printed and laser-scribed PI electrodes. B) Electrochemical impedance spectroscopy (EIS) at frequencies ranging between $10^5$ and $10^1$ $s^{-1}$. A sinusoidal signal was applied using a typical open circuit potential (OCP) of 0.22 V and an amplitude of 10 mV in a mixture of 1 mmol $L^{-1}$ ferricyanide/ferrocyanide and 0.1 mol $L^{-1}$ KCl for carbon screen-printed electrode and laser-scribed PI electrode.

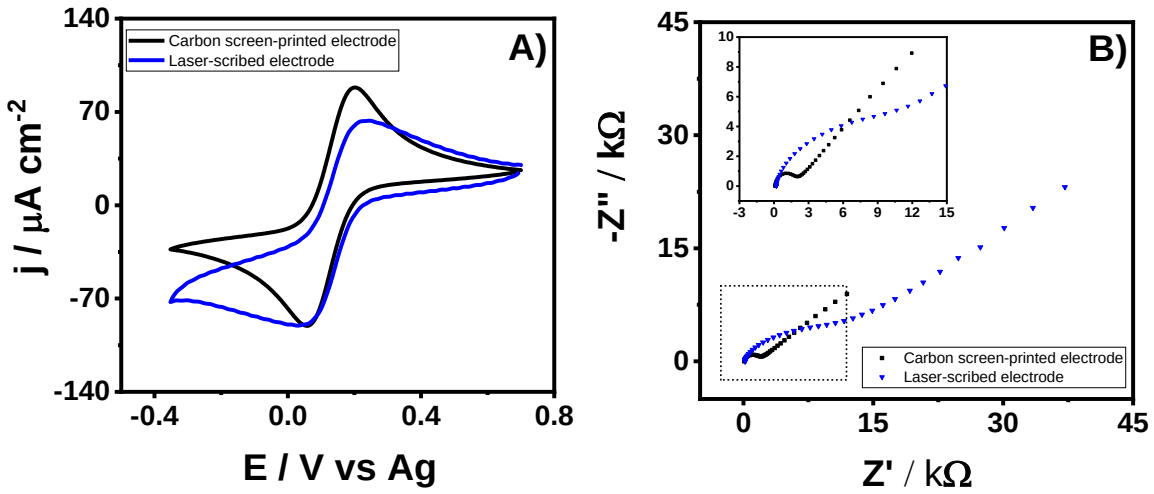


For comparison, the reproducibility and repeatability tests for the carbon screen-printed electrodes were also performed and are presented in Figure 29 – A) and B). The values were expressed regarding RSD, as described for the laser-scribed electrodes. Reproducibility and repeatability obtained values were 10.2% and 11.8%,

respectively. The values for the laser-scribed electrodes proposed herein were RSD =7.4% and 3.6%, even smaller than the obtained for the commercial screen-printed electrode. It is more evidence of the potentiality of the fabricated electrodes to be investigated as electrochemical sensors.

**Figure 29** - Cyclic voltammograms of commercial screen-printed electrodes in 1 mmol $L^{-1}$ ferrocyanide + 0.1 mol $L^{-1}$ KCl at 50 mV $s^{-1}$ with potentials ranging from 0.7 to −0.4 V. A) Reproducibility for ten different fabricated electrodes (reproducibility measurements expressed as RSD = 10.2%, n = 10). Inset: peak current (Ip) vs. n plot. B) Repeatability for twenty measurements obtained from the same electrode (repeatability measurements expressed as RSD = 11.8%, n = 20). Inset: peak current (Ip) vs. n plot.

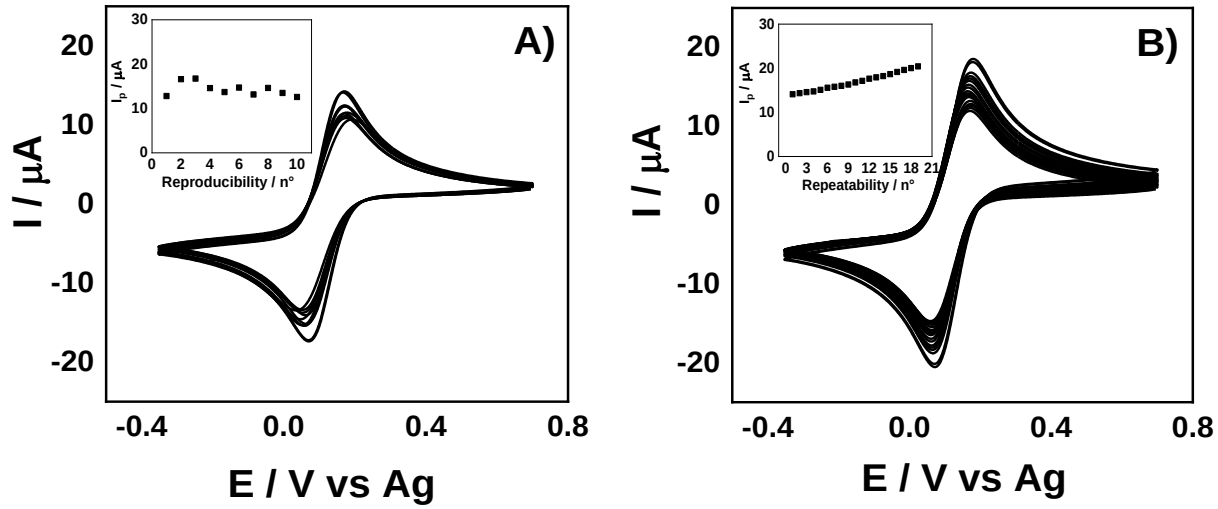


Furthermore, it is important to highlight the low cost of the proposed devices, estimated at 0.04 dollars (considering only the used materials), transforming them into viable options for single-use purposes. In addition, the fabrication method presents great scalability without the requirement of reagents. This is a highly advantageous attribute, especially compared to existing commercial sensors that rely on conductive

inks, which are susceptible to dissolving in organic solvents. In this case, no electrochemical treatment was used.

Another test performed from the laser-scribed electrodes was to evaluate the stability of the material over thirty days stored in ambient conditions. Cyclic voltammograms were recorded using ferrocyanide chloride and are presented in Figure 30 - A). A plot of the current peak (Ip) (anodic current) vs. time (in days) was obtained from these voltammograms and is presented in Figure 30 - B).

**Figure 30** - Cyclic voltammograms of laser-scribed electrodes in 1 mmol $L^{-1}$ ferrocyanide + 0.1 mol $L^{-1}$ KCl at 50 mV $s^{-1}$ with potentials ranging from 0.7 to − 0.35 V A) over thirty days stored in ambient conditions and C) after bending the device n times. B) Represents the anodic current peak (Ip) vs. time (days) plot of the data obtained in A). D) Represents the plot of anodic current peak (Ip) vs the number of times that the device was bent (n times)

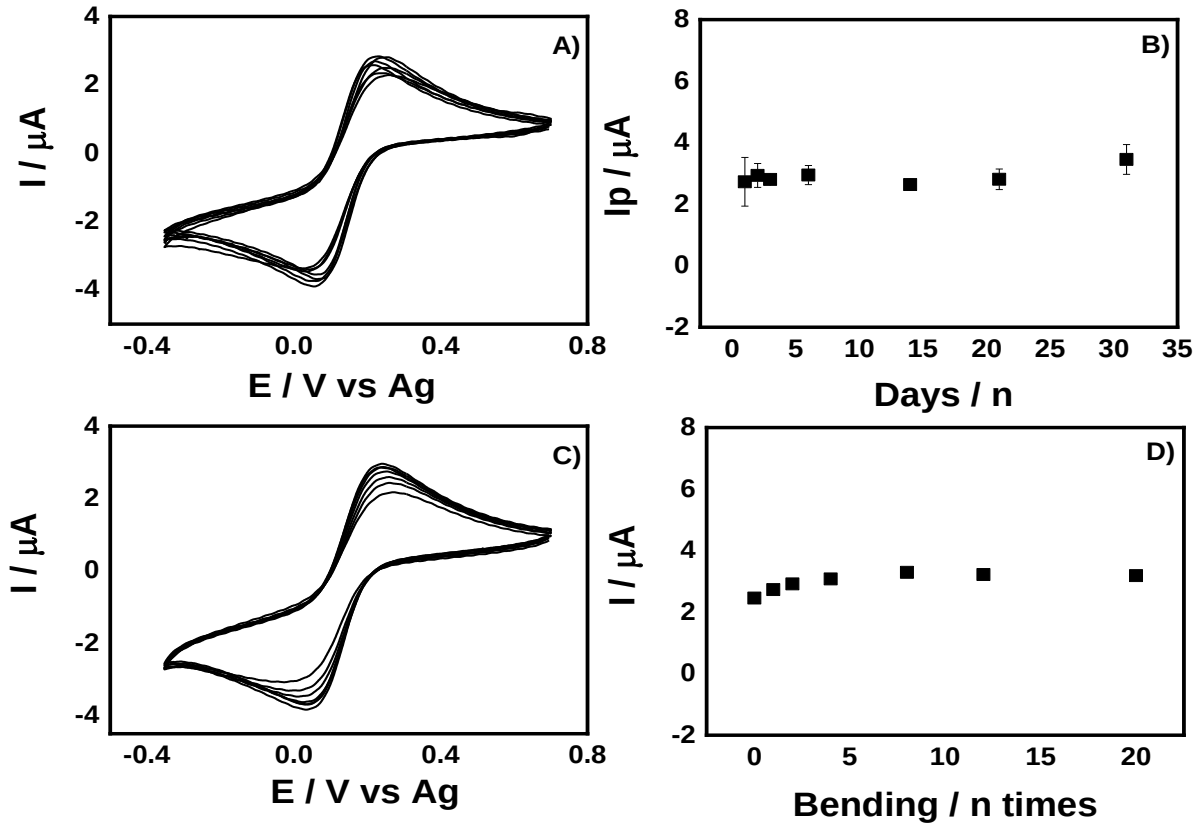

Excellent stability over these thirty days was observed with an RSD of 9.2%. Furthermore, the stability of the devices after bending them n times was also evaluated. The experiment was performed by bending the electrodes n times and recording the cyclic voltammograms after bending the material. The measurements are presented in Figure 30 - C) and the plots of the current peak (Ip) vs. the number of times that the device was bent (n times) in Figure 30 - D). The more the devices were bent, the higher the current responses. A slight increase in the current of 34.5% was observed until they reached a maximum anodic current. It is probably due to microcracks on the material generated by the bending of the device, which could provide better penetration of the solution into the material, explaining the slight improvement in the electrochemical behavior. The devices were bent twenty consecutive times without losing the electrochemical signal, demonstrating robustness.

### 3.3.3. Analytical applicability of the electrochemical devices

The applicability and versatility of the fabricated electrodes were evaluated using two systems, a static and a hydrodynamic one. For the static system, the devices were used as fabricated (Figure 31 - A). It is a miniaturized device composed of a three-electrodes system, which requires only 200 µL of solution during the analyses. Whereas for being used as a hydrostatic system, the devices were combined with a paper-based microfluidic platform. Figure 31 – B presents the microfluidic platform and fabricated following the protocol presented in previous work [179]. The combination of

the fabricated electrochemical device with the microfluidic system is presented in Figure 31 - C. In this case, a reservoir made from a PMMA to fill with the carrier solution, in Figure 31 – B demonstrated by colored solution. Moreover, in Figure 31 – C, 4 pieces of paper sheets are observed on the top of the semicircle of the main microfluidic device to increase the wicking capacity.

**Figure 31** – A) Images of the laser-scribed electrochemical devices obtained using PI as substrate, where the device's size can be noticed. B) Microfluidic paper-based system. C) Incorporation of the microfluidic paper-based system on the laser-scribed electrode.

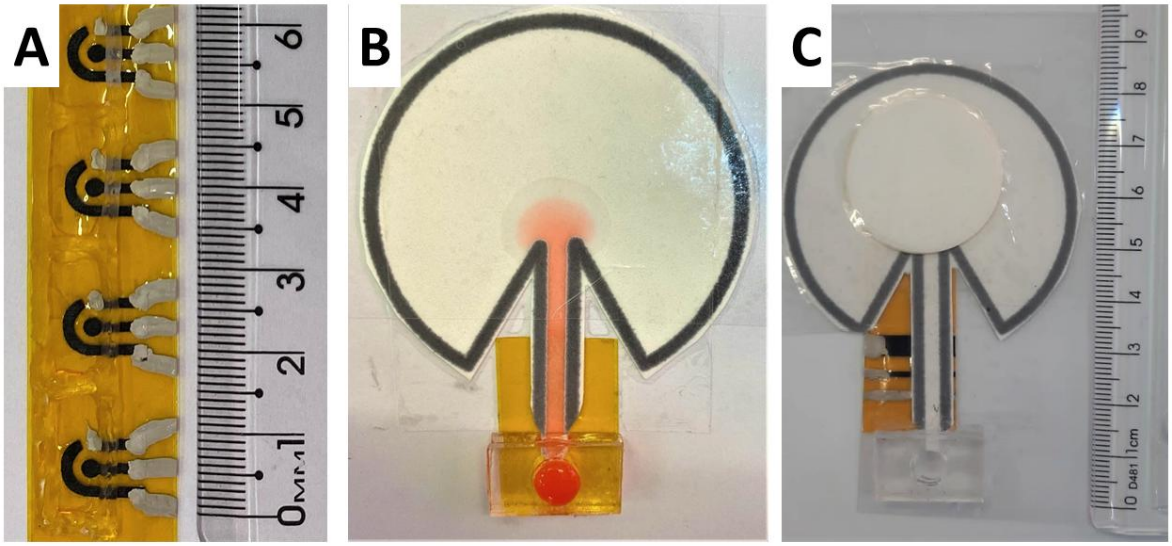


Using the proposed device as a microfluidic system is advantageous when considering in-field applications. By utilizing a paper substrate, flow generation is achieved without the need for external pumps, which makes using them simpler on this occasion. This approach offers an interesting strategy for creating portable, disposable, and microfluidic devices.

Thus, to evaluate the devices' analytical performance, the systems were applied to determine hexaammineruthenium (III) chloride (Figure 32).

**Figure 32** - A) Cyclic voltammograms recorded from the Laser-scribed electrodes in 0.1 mmol $L^{-1}$ KCl and different concentrations of $[Ru(NH_3)_6]^{3+}$ at 50 mV $s^{-1}$. B) Calibration curve for $[Ru(NH_3)6]^{3+}$ obtained by voltammetry. D) Transient current signals for injections of 0.2, 0.4, 0.6, 0.8, 1.0 mmol $L^{-1}$ $[Ru(NH_3)_6]^{3+}$ solution in 0.1 mol $L^{-1}$ KCl. Injection volume: 2 µL. $E_{detection}$ = -0.4 V vs. Ag pseudo-RE. D) Calibration curve for $[Ru(NH_3)_6]^{3+}$ obtained by amperometry.

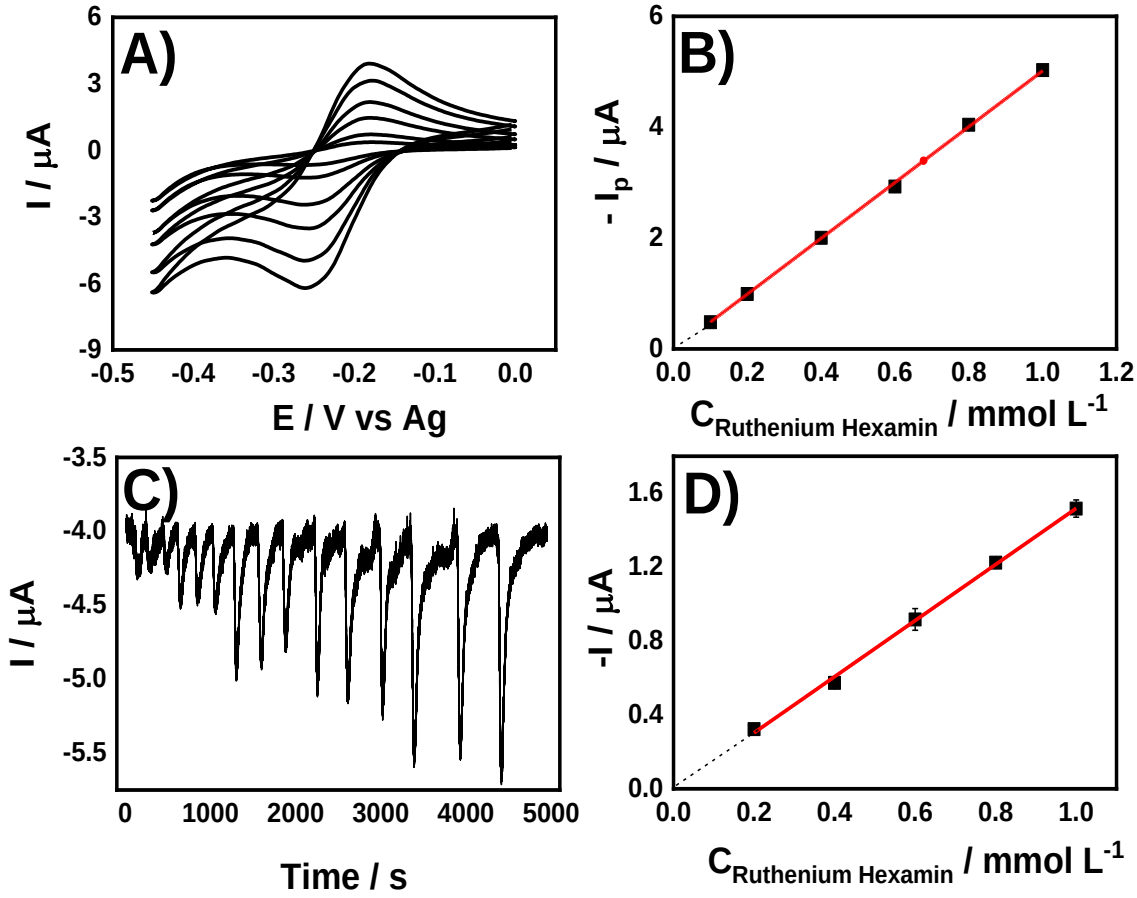


For the static system, cyclic voltammetry was recorded, varying the hexaammineruthenium (III) chloride concentration (0.1 – 1.0 mmol $L^{-1}$), as observed in Figure 32 - A). Thus, a linear correlation between the concentration and the cathodic current signal was found and is presented in Figure 32 - B). The corresponding linear equation is Ip = 5.0 $C_{hexaammin}$ – 0.018, with a correlation coefficient 0.999 and sensitivity of 5.0 µA $mmol^{-1}$ L. In addition, the hydrodynamic system was applied using

the chronoamperometry technique, as shown Figure 32 - C. The transient signal represents the injection of 2 µL of analyte solution in the microfluidic system. Also, a linear correlation is noticed between the current signal and hexaammineruthenium (III) chloride concentration as presented in the equation $Ip = 1.5\ C_{hexaammin} - 0.0006$ (Figure 32 - D)). A correlation coefficient of 0.997 and sensitivity of 1.5 µA $mmol^{-1}$ L were found.

These results showed an excellent linear correlation between Ip and hexaammineruthenium (III) chloride concentration. The device's versatility is also a great feature since its applicability can be extended. Besides being low-cost and portable, these microfluidic devices can also provide fast analyses, a great advantage for analyses performed at the point of need.

As proof of concept, 3-nitrotyrosine (3-NT) was selected as an analyte to evaluate the applicability of both systems. 3-NT is currently associated with several diseases as a biomarker of oxidative stress due to the stability of the compound, which is suitable for analysis. When its concentration is higher than the diagnosed at baseline levels, it has been related to coronary artery disease, diseases associated with immunological reactions (systemic sclerosis, asthma, kidney complications, rheumatoid arthritis, among others), and neurological diseases[188].

First, cyclic voltammograms of polyimide laser-scribed electrodes in 1 mmol $L^{-1}$ 3-NT and PBS, as presented in Figure 33.

**Figure 33 -** Cyclic voltammograms of polyimide laser-scribed electrodes in 1 mmol $L^{-1}$ 3-nitrotyrosine + 0.1 mol $L^{-1}$ PBS (pH 7.4) at 50 mV $s^{-1}$ with potentials ranging from 1.0 to – 1.0 V. Dotted line represents measurements in the absence of 1 mmol $L^{-1}$ 3-nitrotyrosine. Continuous lines represent measurements of 1 mmol $L^{-1}$ 3-nitrotyrosine for the first (red line) and second cycle (blue line).

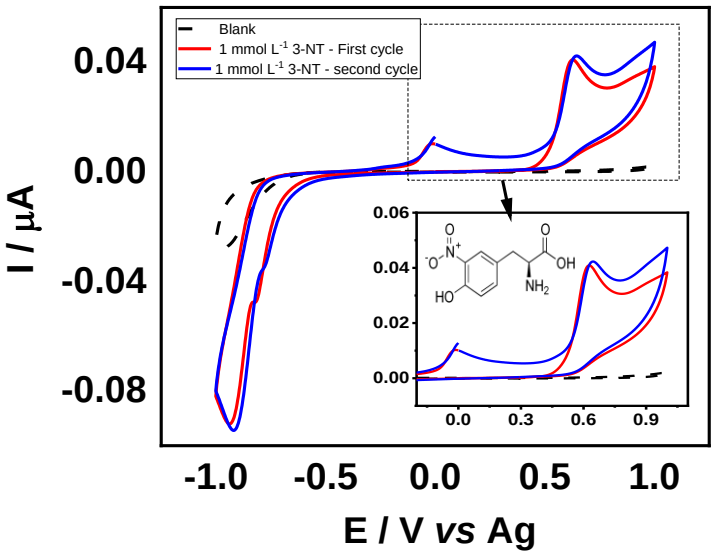


The dotted line represents measurements in the absence of 3-NT and continuous lines represent measurements in the presence of 3-NT for the first (red line) and second cycle (blue line). All the cycles started on 0 V, going to positive and after to negative potentials. In the first cycle, an electrochemical oxidation process at around 0.65 V is observed. In contrast, a reduction process is presented at -0.92 V. This result is consistent with the results observed by Martins et al. [189]. It has been reported that this electrochemical reduction process could be attributed to the $NO_2$ group involving $4H^+$ and $4e^-$ [190], while the oxidation one could be attributed to the $NH_2$ [191]. The 3-NT electrochemical behavior is not completely understood. Thus, the tyrosine electrochemical oxidation mechanism is used as a reference to propose the 3-NT electrochemical oxidation mechanism. Another oxidation peak at around 0 V is noticed in the second voltammetry cycle, dependent on the reduction process at -0.92 V.

Furthermore, a study of the pH variation using cyclic voltammograms and Britton-Robinson buffer solution from 2.0 to 12.0, presented in Figure 34.

**Figure 34 -** A) Cyclic voltammograms for laser-scribing PI electrode in 0.04 mol $L^{-1}$ Britton-Robinson buffer solution containing 0.2 mmol $L^{-1}$ 3-NT at 50 mV $s^{-1}$ and different pH values. B) Ep vs. pH and Ip vs. pH plots for all oxidation processes of 3-NT. Ep = -0.054 pH + 1.01. C) Cyclic voltammograms for laser-scribing PI electrode in 0.04 mol $L^{-1}$ Britton-Robinson buffer solution pH 7.03 (BRBS), 0.04 mol $L^{-1}$ phosphate buffer solution (PBS) pH 7.1 and pH 7.4 containing 0.2 mmol $L^{-1}$ 3-NT at 50 mV $s^{-1}$

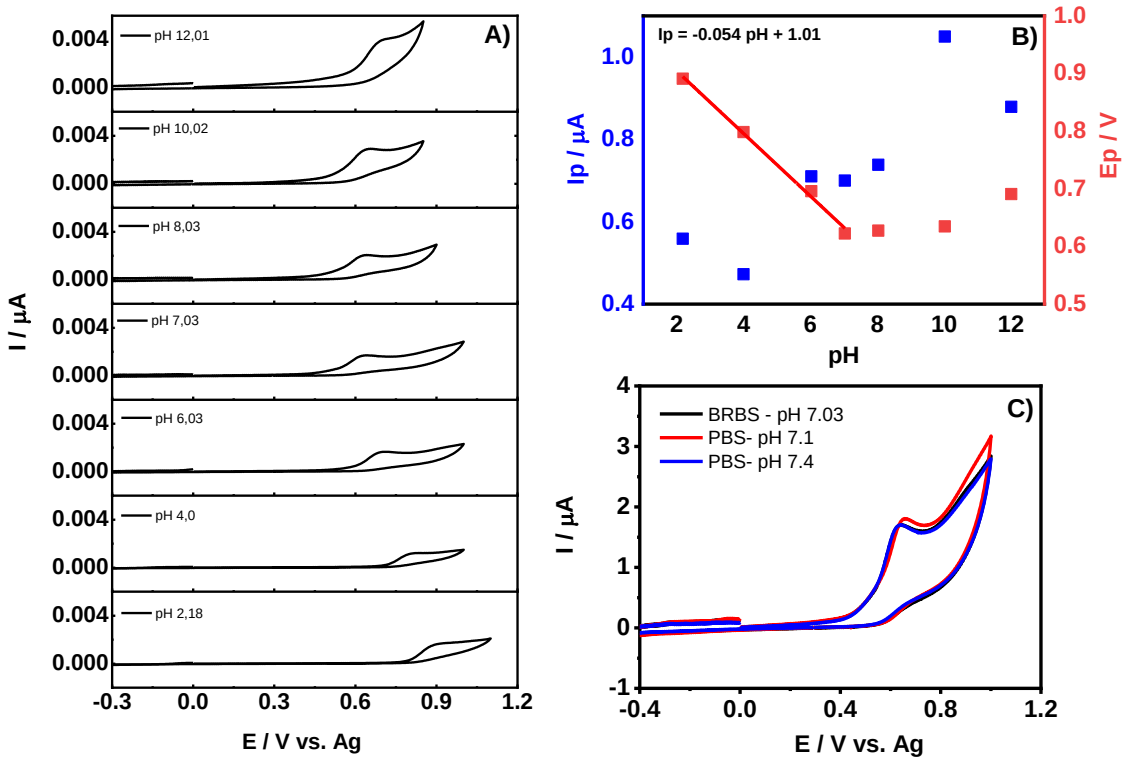


In Figure 34 - A, it is possible to observe the cyclic voltammograms recorded in each pH, and in Figure 34 – B, the influence of the pH on the electrochemical behavior of the oxidation process at 0.65 V. The potential peak (Ep) gets higher with the decrease in the pH values due to the higher $H^+$ concentration in the medium. The oxidation process is more challenging to occur in these circumstances. This electrochemical behavior is noticed up to pH 7, and a break in this pattern is observed from pH 8 to 12 due to 3-NT pKa value of 7.1 [192]. The linear correlation between the pH and the Ep is given by Ip = -0.054 pH + 1.01 with a 54 mV / pH slope, similar to the Nerstian value of 59.16 mV / pH. It indicates that the same ratio of electrons and protons is involved in this electrochemical process as observed in the tyrosine electrochemical oxidation mechanism [191].

It is essential to highlight that the pH choice of around 7 was a compromise of a low Ep (due to the selectivity) and a high sensibility expressed in terms of higher currents. The medium usually used in biological applications is PBS pH 7.4. Therefore, the cyclic voltammograms were recorded using PBS pH 7.1 and 7.4 to compare the measurements with the ones obtained in the Britton-Robinson buffer solution. The cyclic voltammograms presented a similar result in both mediums using pH around 7, where oxidation occurs at the same potential peak (Figure 34 - B). Thus, Figure 34 - C shows the buffer type did not influence the electrochemical behavior for 3-NT oxidation. Consequently, PBS pH 7.4 was selected as a supporting electrolyte.

Finally, the responses of the disposable proposed devices in this work for 3-NT determination were evaluated in static and hydrodynamic conditions. The differential pulse voltammetry was used for the static system under optimized conditions as presented in Figure 35 - A.

**Figure 35** – A) Differential pulse voltammetry for the polyimide laser scribed electrode recorded in 0.04 mol $L^{-1}$ PBS pH 7.4 with different concentrations of 3-nitrotyrosine (0.5 µmol $L^{-1}$ - 30 µmol $L^{-1}$). Parameters: ΔE = 25 mV; ΔEs = 5 mV; v = 10 mV $s^{-1}$. B) The respective calibration curve: Ip (µA) = 0.0108 $C_{3\text{-}NT}$ + 0.0006; $R^2$ 0.99.

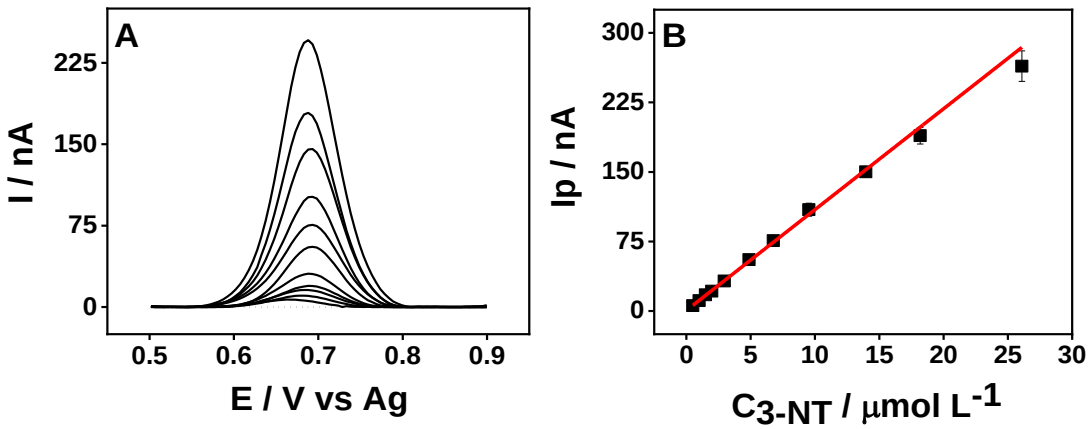


The analytical curve was constructed and is observed in Figure 35 – B. For the static conditions, a linear correlation between the concentration and the oxidation

current signal in 0.65 V was found from 500 nmol $L^{-1}$ – 27.0 µmol $L^{-1}$, according to the equation o Ip (µA) = 0.0108 $C_{3\text{- NT}}$ + 0.0006, $R^2$ = 0.99, and sensitivity of 0.0108 µA $µmol^{-1}$ L. The limit of detection (LOD) and limit of quantification (LOQ) were calculated using 3 times and 10 times the ratio of the standard deviation of the blank signal/sensitivity. In this case, the obtained values were 0.140 µmol $L^{-1}$ and 0. 468 µmol $L^{-1}$, respectively, for LOD and LOQ.

Similar analytical performance was also noticed when using carbon screen-printed electrodes to perform the same experiment in the static system. The differential pulse voltammograms recorded in different 3-NT concentration using carbon screen-printed electrode is presented in Figure 36.

**Figure 36** – A) Differential pulse voltammetry for carbon screen-printed electrode recorded in 0.04 mol $L^{-1}$ PBS pH 7.4 with different concentrations of 3-nitrotyrosine (0.5 µmol $L^{-1}$ - 30 µmol $L^{-1}$). Parameters: ΔE = 25 mV; ΔEs = 5 mV; v = 10 mV $s^{-1}$. B) The respective analytical curve: Ip (µA) = 0.022 $C_{3\text{- NT}}$ + 0.013; $R^2$ 0.99.

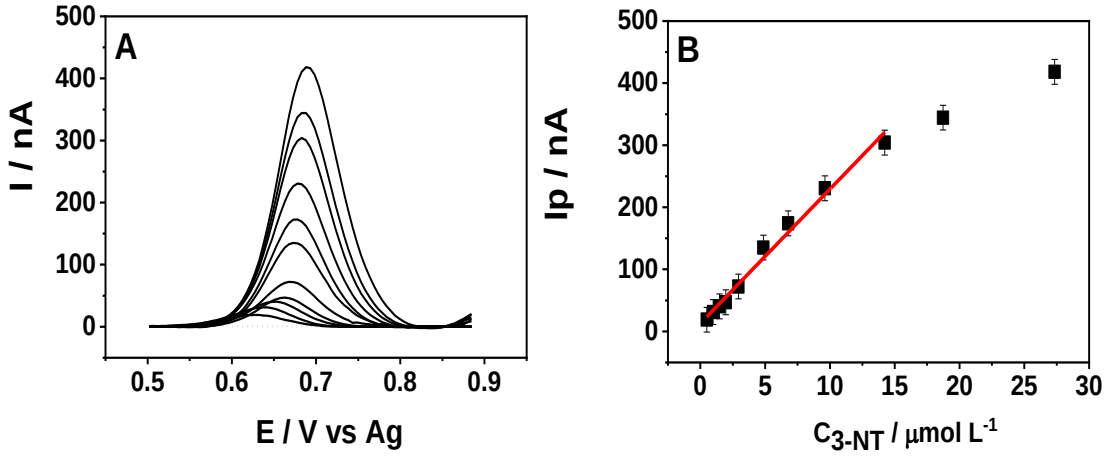


The analytical curve is presented in Figure 36 – B. However, in this case, the linear correlation was observed in a lower concentration range, from 500 nmol $L^{-1}$ to 14.0 µmol $L^{-1}$. This correlation was given by the equation Ip (µA) = 0.022 $C_{3\text{- NT}}$ + 0.013, with $R^2$ = 0.99, where the sensitivity value was 0.022 µA $µmol^{-1}$ L. The calculated LOD

and LOQ were 0.82 µmol $L^{-1}$ and 2.74 µmol $L^{-1}$. Although the polyimide laser-scribed electrode presented comparable analytical performance to the commercial carbon screen-printed electrode, lower LOD, and LOQ were obtained using the first one. Furthermore, the electrodes proposed herein have low-cost and fabricated using a scalable method, besides being flexible.

The fabricated electrode and the microfluidic paper-based system were also used to evaluate the 3-NT determination. The measurements were recorded using chronoamperometry (Figure 37 - A) for the hydrodynamic system.

**Figure 37** – A) Transient current signals for injections of 2 µL of different concentrations of 3-NT (40 µmol $L^{-1}$ - 150 µmol $L^{-1}$) using the laser-scribed electrode in the hydrodynamic system . Carrier solution: 0.04 mol $L^{-1}$ PBS pH 7.4. $E_{det}$ = +0.8 V vs Ag pseudo-RE. The respective calibration curve: Ip (µA) = 0.0009 $C_{3\text{-NT}}$ – 0.0084, $R^2$ = 0.99.

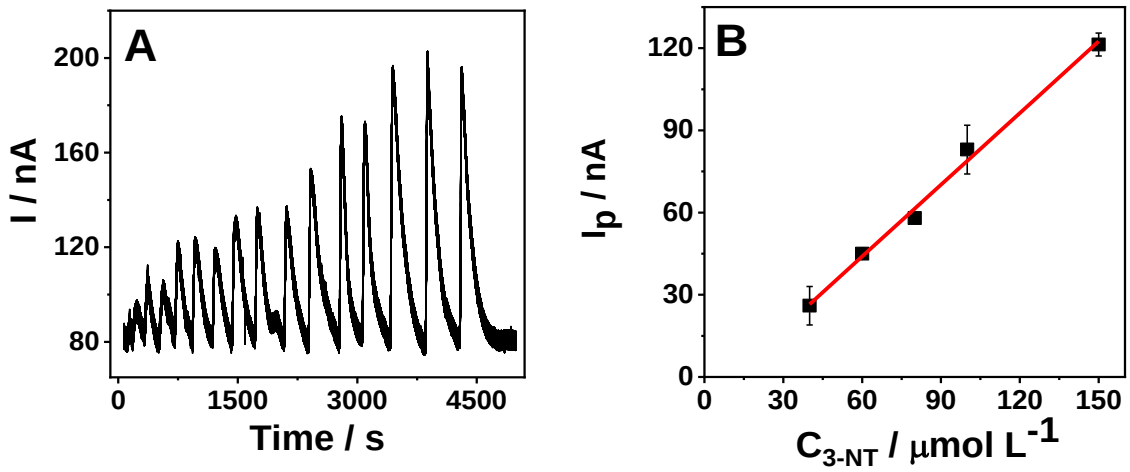


The analytical curve was constructed and is presented in Figure 37 – B. The microfluidic device had a linear correlation from 40 to 150 µmol $L^{-1}$, according to the equation Ip (µA) = 0.0009 $C_{3\text{-NT}}$ – 0.0084, $R^2$ = 0.99 and sensitivity of 0.0009 µA µmol$^{-1}$ L. The LOD and LOQ obtained were 12.4 µmol $L^{-1}$ and 41.1 µmol $L^{-1}$, respectively. The hydrodynamic system provided higher LOD and LOQ. However, it is important to highlight that only 2 µL of analyte solution was used for the microfluidic system.

Consequently, the detectability and sensibility of the proposed system can be enhanced by increasing the volume injected in the microfluidic system. The influence of the injected volume was previously reported in the literature[179].

Compared with other sensors coupled to microfluidic paper-based analytical devices, the proposed electrochemical sensors can be easily fabricated in a single step without reagents. In addition, they are ready to use after the fabrication process, dispensing the need for electrochemical pretreatments. Polishing and sanding are some pretreatments normally performed before using carbon electrodes. However, these steps can increase the time of the analytical procedure, making the analyses more laborious and time-consuming. Besides that, these steps can make the sensor surface less reproducible due to the difference in the electroactive area caused by small scratches during the polishing and sanding procedures.

The proposed electrochemical sensor has LOD and LOQ slightly higher when compared to others previously reported in the literature involving 3-NT determination (Table 5). However, most approaches involve the modification of the electrodes with some element to obtain lower LOD, while the proposed device here is a versatile and non-modified sensor. Moreover, the polyimide laser-scribed electrode is a low-cost and flexible platform, extending the possibility of analytical applications. Therefore, the proposed devices represent a promising analytical platform since other parameters and elements, such as a biorecognition component, can significantly enhance the electrochemical performance of the devices.

**Table 5** – Comparison of different sensors for 3-nitrotyrosine electrochemical detection.

| Substrate | Modified/ treated electrode | Biorecognition Element | Static (S) or hydrodynamic (Hd) system | Flexible platform | LOD | Ref. |
|---|---|---|---|---|---|---|
| **Pencil graphite electrode with Fe/Pd nanoparticles** | Yes | MIP | S | No | 1.20 μg $L^{-1}$ | [193] |
| **GCE electrode with AuNPs** | Yes | MIP | S | No | 50.0 nmol $L^{-1}$ | [194] |
| **$CdWO_4$ ND@RGO modified SPEs** | Yes | - | S | No | 3.24 nmol $L^{-1}$ | [195] |
| **$CuFe_2O_4$@ RGO composite** | Yes | - | S | No | 25.14 pmol $L^{-1}$ | [196] |
| **Glassy carbon electrode** | Yes | - | S | No | 17.0 nmol $L^{-1}$ | [197] |
| **Carbon-coated paper substrate** | No | MIP | S | No | 22.3 nmol $L^{-1}$ | [198] |
| **ZrO2@rGO composites on GCE** | Yes | - | S | No | 9 nmol $L^{-1}$ | [199] |
| **Pd/Au thin film electrodes** | Yes | - | S | No | 9 nmol $L^{-1}$ | [200] |
| **Gold-based electrodes** | No | MIP | S | Yes | 24.9 pmol $L^{-1}$ | [201] |

| | | | | | | |
|---|---|---|---|---|---|---|
| **Paper-based screen-printed electrodes** | No | - | S | Yes | 49.2 nmol $L^{-1}$ | [189] |
| **Laser-Scribed PI based electrode** | No | - | S or Hd | Yes | 0.17 µmol $L^{-1}$ / 12.4 mmol $L^{-1}$ | This work |

Different species can interfere with the 3-NT detection. An interference study was performed using the static system, where the measurement of the 3-NT was recorded by mixing the analyte with each interferant molecule in a proportion of 1:2. Thus, 10 µmol $L^{-1}$ 3-NT were mixed with 20 µmol $L^{-1}$ uric acid (UA), or urea (UR), or nitrite ($NO_2^-$), and caffeine (CAF). The measurements were expressed as normalized peak current (Ip) percentage, where the 3-NT Ip corresponds to 100%, as observed in Figure 38.

**Figure 38** - Interference study performed for 3-NT 10.0 µmol $L^{-1}$ in the presence of uric acid (UA), urea (UR), nitrite ($NO_2^-$), and caffeine (CAF). The concentration of the possible interfering species is 20.0 µmol $L^{-1}$. The signal was normalized by considering the response for 3-NT as 100%.

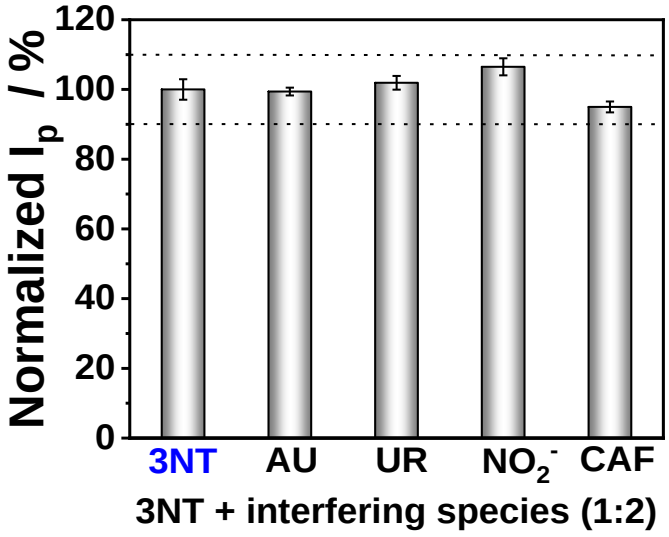

The sensors exhibited satisfactory selectivity since a 10% variation was not considered interference. However, it is possible to observe that nitrite might interfere with the 3-NT response when present in higher concentrations. If necessary, this issue could be solved by acidifying the medium since nitrite is found as HNO2 at pH < 3.3. It is a highly volatile acid that could effortlessly evaporate from the solution. Consequently, the sensitivity and selectivity towards 3-NT detection using polyimide laser-scribed electrodes could be enhanced.

The laser-scribed electrode was also tested in different model molecules (dopamine (DP) and uric acid (UA)). In this case, the static system was applied using differential pulse voltammetry to record the measurements, as presented in Figure 39 – A and C. The calibration curves were constructed and plotted in Figure 39 – B and D.

**Figure 39 -** Differential pulse voltammetry for the polyimide laser scribed electrode recorded in 0.04 mol/L PBS pH 7.4 with different concentrations of A) dopamine and C) uric acid. ΔE = 25 mV; ΔEs = 5 mV. v = 10 mV $s^{-1}$. The respective calibration curve for B) dopamine (Ip (μA) = 10.5 $C_{DP}$ − 1.4, $R^2$ = 0.99), and D) uric acid (Ip (μA) = 2.4 $C_{UA}$ − 9.2, $R^2$ = 0.99).

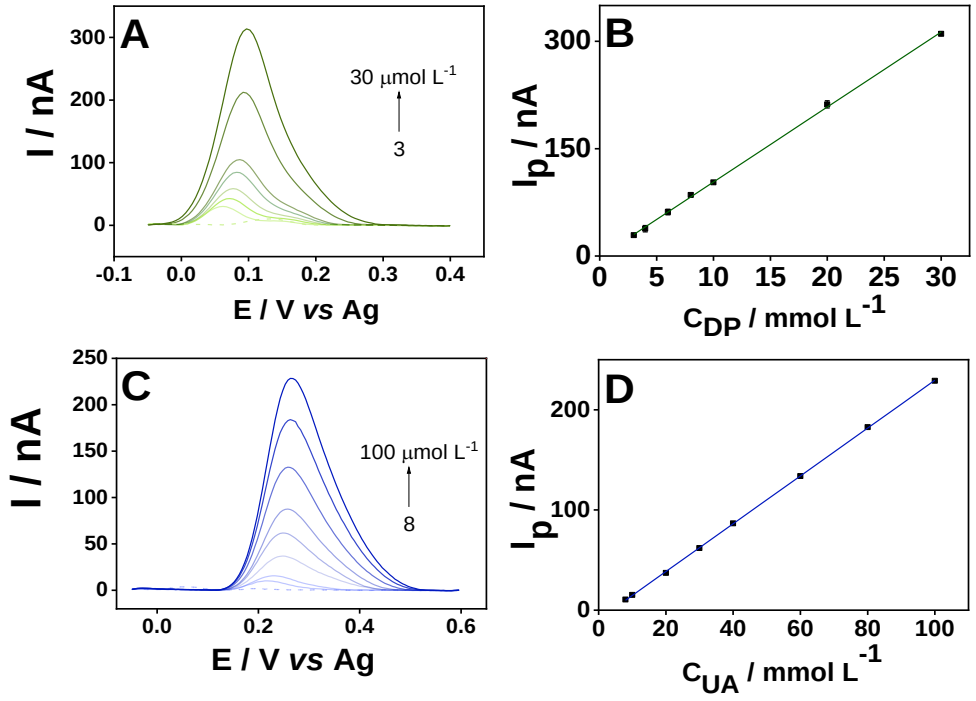

In both cases, a linear correlation was observed according to the equations Ip (μA) = 10.5 $C_{DP}$ − 1.4 ($R^2$ = 0.99) and uric acid Ip (μA) = 2.4 $C_{UA}$ − 9.2 ($R^2$ = 0.99) for dopamine and uric acid respectively. The linear correlation for dopamine was obtained from 3 to 30 μmol $L^{-1}$, and the calculated LOD and LOQ were 0.46 μmol $L^{-1}$ and 1.53 μmol $L^{-1}$, respectively. In contrast, the linear correlation for uric acid was obtained from 8 to 100 μmol $L^{-1}$, and the calculated LOD and LOQ were 0.63 μmol $L^{-1}$ and 2.12 μmol $L^{-1}$. The electrochemical oxidation signal for DP and UA were observed at +0.08 V and 0.26 V. At the same time, for 3-NT at +0.65 V. It indicates that the 3-NT could be determined in the presence of these molecules using differential pulse voltammetry since the oxidation potential for each one is different.

Moreover, the calculated LODs were comparable to the reported in the literature for DP and UA determination using carbon-based electrodes, although most use some modifiers to decrease the LOD [114,202–205]. Thus, competitive values of LOD are presented here using the proposed non-modified laser-scribed electrode. The main characteristic of the proposed material is the great potential to be used as a platform for analytical applications. Furthermore, they are versatile and simple platforms, besides being low-cost. In addition, the fabrication method used to produce the electrodes is rapid and automated, where sensors with consistent analytical responses are obtained. All these characteristics open the possibility of new analytical applications using the proposed device.

## 3.4. Conclusion

Herein we developed low-cost, versatile, and flexible devices using the laser-scribing technique and Kapton tape, an inexpensive polyimide source. A miniaturized three - electrodes system was obtained, requiring only 200 µL of solution. And due to the microfluidic properties, the devices were combined with a paper-based platform to be applied in static mode or as a hydrodynamic system. Moreover, the proposed devices dispense reagents and are single-step fabricated, presenting electrochemical responses comparable to commercial carbon screen-printed. The results also indicated the simple obtention of robust carbon-based devices with a porous structure, presenting great reproducibility, repeatability, and stability. The analytical performance of the devices was evaluated in both static and hydrodynamic systems, using a redox probe, which demonstrated a great response and versatility of the system. As a proof-of-concept, the devices were applied in 3-NT quantification, and both proposed systems showed potential for analytical applications. Furthermore, the electrochemical behavior of the devices was also evaluated using different mode molecules, dopamine, and uric acid. Although other parameters and elements, such as a biorecognition component, could enhance the electrochemical performance of the devices, the proposed analytical platforms demonstrated satisfactory analytical performance.

# CHAPTER 4

## 4. A wearable hollow microneedle array sensor for minimally invasive monitoring of propofol: Toward medical safety control during surgical procedures

## CHAPTER 4

There has been increasing evidence of the numerous benefits of using propofol-based total intravenous anesthesia, which can enhance patient outcomes, significantly reduce environmental impact, and substantially influence improved surgical outcomes compared to conventional volatile-based anesthesia. However, the lack of suitable detection techniques for continuous, real-time propofol concentration monitoring in patient blood remains a significant challenge for exploiting propofol-based total intravenous anesthesia. Herein, an initial study with solid microneedles to learn about the fabrication technique is demonstrated and applied to glucose and lactate molecules as a proof-of-concept. Thus, developing a hollow microneedle array-based electrochemical sensor was studied, aiming at minimally invasive monitoring of propofol drug. Such a propofol microneedle sensor relies on a three-electrode sensing system embedding four modified carbon paste-packed working electrodes, a carbon paste-packed counter, and an Ag/AgCl reference electrode. The proposed method enabled propofol measurements covering the μmol $L^{-1}$ concentration range of the interest analyte. The long-term monitoring capability of the sensor was evaluated in PBS and artificial ISF mediums. The potential applicability of the developed microneedle array-based sensor toward minimally invasive monitoring of propofol drug was also demonstrated by skin-mimicking phantom gel experiments. The new microneedle array sensing platform holds great potential for the continuous, real-time, in-vivo detection of the anesthetic propofol drug during surgical procedures that can significantly improve safety and efficacy for the delivery of anesthetic drugs.

This work is still in progress and counting with the help of Chochanon Moonla, Maria Reynoso, Amal Abbas, who helped with experimental data collection, suggestions, and discussions.

## 4.1. Introduction

### 4.1.2. Propofol monitoring

Propofol (2,6-diisopropylphenol) is a drug used to decrease consciousness levels for starting and maintaining general anesthesia during surgical procedures. It has been the most used compound in intravenous anesthesia due to characteristics such as short half-life and rapid induction [206]. Although it is possible to use propofol in both initiation and maintenance of the anesthesia, it is more common for its intravenous use to start the process and the sequent application of volatile-based anesthesia for the maintenance phase due to the necessity and difficulty of monitoring the real-time propofol concentration in blood [207]. The anesthesia concentration is essential during surgical procedures to prevent overdosing, which can lead to respiratory failure, a decrease in blood pressure, and, consequently, death. Furthermore, an inefficient amount of this drug can lead to significant pain [208].

The methods used for the detection and quantification of propofol involves High performance liquid chromatography (HPLC) [209], Gas chromatography-mass spectrometry (GC–MS) [210], Liquid chromatography–mass spectrometry (LC–MS/MS) [211] and optical techniques (such as, spectrophotometry [212] and fluorometry [213]). Those are time-consuming, require specialized professionals, and are difficult to miniaturize or use as portable systems.. In this perspective, electrochemical techniques have also been studied for propofol detection due to the possibility of miniaturization and reaching lower detection limits [214].

However, one of propofol's long-term electrochemical monitoring challenges is the passivation of the electrodes due to an unwanted product generated from the propofol oxidation [215]. Methods such as stripping voltammetry were reported in the literature for propofol detection, yet it requires electrode renewal or polishing every measurement. Another possibility is restricting the scanned potential window, which can interfere with specificity. [214].

Membranes such as PVC [214] and molecularly imprinted polymers (MIP) [216] have also been demonstrated, but there is the possibility of leaching the material during long term measurements. Another approach demonstrated was using boron-doped diamond or pencil graphite electrodes [217], which involves the application of treatments on the electrode surface and can be impractical for real-life long-term measurements. More recently, a catheter was developed for propofol measurement in blood and showed promising results towards progress in the obstinance of a propofol wearable sensor [218]. Nevertheless, more studies are needed in this field, including developing less invasive methods.

Wearable electrochemical sensors have become increasingly attractive due to non-invasive or minimally invasive biomarkers detection direct on-body to monitor health risks, performance, and nutrition markers. From this perspective, developing simple, low-cost, high-sensible, and long-term electrochemical wearable devices has attracted significant attention.

In addition to monitoring biomarkers, wearable sensors have been used for therapeutic drug monitoring in body fluids. It offers numerous benefits, including optimizing patient-specific dosages and tracking the dynamic changes of drugs within the body. The distribution of drugs in body fluids is influenced by their

pharmacokinetics, which determines the choice of fluid to be analyzed and the type of device required [91]. Interestingly, the interstitial fluid (ISF) has garnered attention as it has shown a strong correlation with blood in measuring concentrations of small drug molecules [117]. However, it should be noted that the research on therapeutic drugs in ISF is limited, and only a few have been studied and reported [91].

Thus, considering transdermal detection, the most used microneedle types are: hollow and solid. However, different microneedles types have been reported, such as dissolvable, coated, and porous microneedles, each one with its applicability [96].

Typically, the microneedles require post-fabrication modifications for electrochemical purposes, especially if the precursor material lacks conductivity [102]. To overcome this problem, noble metals are deposited onto the microneedle surface using advanced techniques like e-beam evaporation and sputtering. Furthermore, a biorecognition modification layer can also be employed to enhance the specific interaction between the electrode surface and the analyte [96] as propofol has demonstrated good electrochemical response in carbon-based electrodes [218]. The simplest method to propose a carbon-based microneedle array for propofol monitoring would be hollow microneedle types. Hollow microneedles present a hollow core, filling them with various materials, including carbon paste [102]. Thus, in this chapter, we propose to develop an electrochemical wearable sensor using a hollow microneedle array for long-term determination and quantification of propofol anesthesia. For this purpose, low-cost and simple methods for minimal invasive microneedle fabrication will be used.

## 4.2. Material and Methods

### 4.2.1. Chemicals and Materials

All reagents and solvents were used as received. Acetaminophen ($C_8H_9O_2N$, ≥98.0%), agarose (≥99%), L-ascorbic acid ($C_6H_8O_6$, 99%), caffeine ($C_8H_{10}N_4O_2$, anhydrous, 99%), calcium chloride anhydrous ($CaCl_2$, ≥97%), D-(+)-glucose anhydrous ($C_6H_{12}O_6$, ≥99.5%), iron (III) chloride ($FeCl_3$, 97%), L-(+)-lactic acid ($C_3H_6O_3$, ≥98%), magnesium sulfate anhydrous ($MgSO_4$, ≥99.0%), mineral oil, phosphate buffer solution (1.0 mol $L^{-1}$, pH 7.4), potassium chloride (KCl, ≥99.0%), 2,6-diisopropylphenol ($C_{12}H_{18}O$, 97%), sodium chloride (NaCl, ≥99.5%), sodium gluconate ($C_6H_{11}NaO_7$), sodium hydroxide (NaOH, ≥97.0%), sodium phosphate monobasic ($NaH_2PO_4$, ≥99.0%), sucrose ($C_{12}H_{22}O_{11}$, 99.5%), theophylline ($C_7H_8N_4O_2$, ≥99%), uric acid ($C_5H_4N_4O_3$, ≥99%), lucose oxidase (GOx, from *Aspergillus niger*, Type X-S, lyophilized powder, 100,000–250,000 units/g), and o-phenylenediamine (flaked, 99.5%) were purchased from Sigma-Aldrich. Sodium bicarbonate ($NaHCO_3$, ≥99.7%) and sodium sulfate anhydrous ($Na_2SO_4$, ≥99.0%) were procured from Fisher Scientific (Fair Lawn, New Jersey, USA). Graphite powder was obtained from Acros Organics (New Jersey, USA). Multiwalled carbon nanotubes (CNTs, > 95%, 15 ± 5 nm diameter, 1–5 μm length) were purchased from Nano Lab, Inc (Waltham, Massachusetts, USA), and silver/silver chloride (Ag/AgCl) ink was obtained from Ercon Inc. The UV resin used to glue the connections into the device was purchased from Anycubic, the DuPont wires and connections were obtained from Elegoo, and Lactate Oxidase (LOx) (108 U/mg) was purchased from TOYOBO.

### 4.2.2. Fabrication of Solid Microneedle Array Sensors, Instrumentation, and procedures

First, we have started working on solid microneedles for glucose and lactate to learn how microneedles work. The formlabs3+ 3D printer (Boston, USA) fabricated the microneedles array device (MNs). After printing, the parts were washed in an ultrasonic isopropanol bath for 60 minutes, then placed in a UV lamp for final curing for another 60 minutes. The microneedles electrodes were sputtered with chromium-supported chromium layers (1 min at 100 W) and platinum (15 min at 100 W) using a polyimide mask to define working, counter, and reference electrodes. Each MN has a height of about 2.0 mm and a base size diameter of 1.0 mm.

**Figure 40 -** Schematic fabrication of solid microneedles (MNs) sensing devices. The MNs device is integrated by 12 MNs (A), 7: 2: 3 are used for the working, reference, and counter electrodes, respectively (B). Integration with the connector and paint reference MNs using silver ink. (C) Integration of the wires on the connectors. (D) Couple the 3D printed final cover.

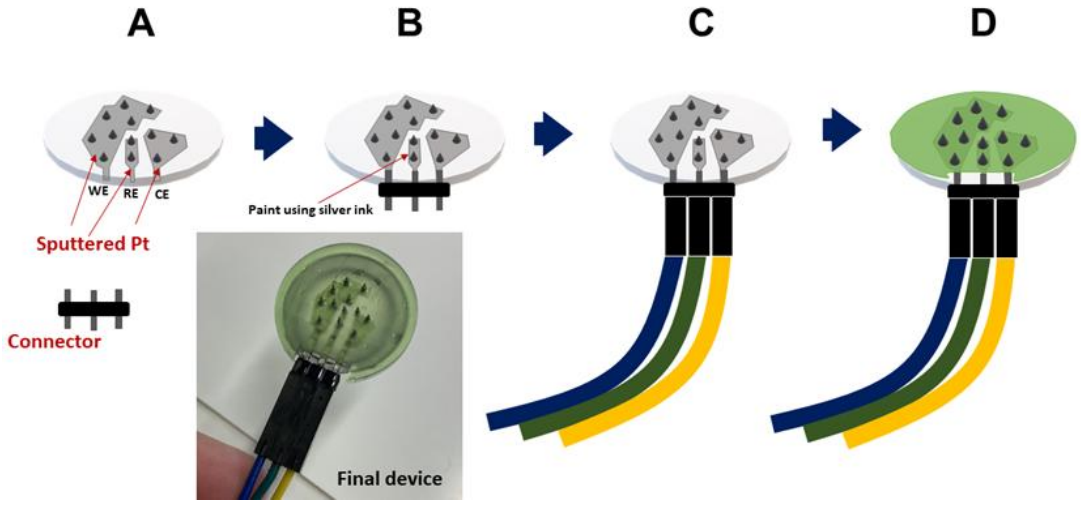

After, connectors were attached to the bottom of the device using a silver epoxy conductive paste to make an electrical connection with wires, and a 3D-printed mask was used to cover the MNs base. Finally, silver glue was used to paint the reference MN electrodes. A schematic figure of the procedure is observed in Figure 40.

Depending on the application, the working array MNs electrochemical sensors were modified using GOx or LOx. In this case, a well-known o-phenylenediamine (oPD) electrochemical enzyme immobilization protocol was used [219]. A 5 mmol $L^{-1}$ sodium sulfate solution was bubbled with nitrogen for 10 min to prepare a 10 mmol $L^{-1}$ o-phenylenediamine (oPD) solution. GOx (1600 U $mL^{-1}$) or LOx (2600 U $mL^{-1}$) were diluted in the oPD solution depending on the desired modification and used as an electrolyte solution for electrodeposition (chronoamperometry applying 0.65V Vs. Ag/AgCl (3 mol $L^{-1}$ KCl) for 900 s). After electrochemical enzyme immobilization, the MNs were left overnight inside the fridge.

All electrochemical measurements were recorded versus silver (Ag) ink-filled microneedle array sensing platform as a reference electrode and Pt as a counter and working electrode at room temperature in a 0.5 mL volume containing the analysis medium (PBS (0.1 mol $L^{-1}$, pH 7.4) using PalmSens EmStat3 Blue hand-held potentiated controlled by PSTrace software version 5.9. Data was plotted by Origin Software. The glucose (10 mM) and lactate stock solution (10 m mol $L^{-1}$) were prepared in 0.1 mol $L^{-1}$ PBS pH 7.4.

### 4.2.3. Fabrication of Hollow Microneedle Array Sensors, Instrumentation, and procedures

For the propofol experiments, hollow microneedles were used to fabricate carbon-based electrodes since this analyte presents a great response in this electrode. To fabricate the hollow microneedles devices (HMNs) formlabs3+ 3D printer (Boston, USA) was used. The same procedure used in the previous solid microneedle was applied after the printing process, where the device was washed in an ultrasonic isopropanol bath for 60 minutes and placed in a UV lamp for final curing for another 60 minutes. The HMNs have a height of 1.4 mm, a base size diameter of 1.5 mm, and the hole in the center of the microneedle has a diameter of about 1.0 mm. The area of each HMN is 0.78 $mm^2$ considering the hollow diameter and 1.77 $mm^2$ considering the base size diameter (Figure 41).

The fabricated microneedle device contains an array of 2×3 beveled-tip hollow microneedles, as observed in Figure 41 - A. Five of these hollow microneedles were packed with a freshly prepared carbon paste (60% wt. of graphite powder and 40% wt. mineral oil) containing 5% wt. of carbon nanotubes (CNTs) using a surgical blade and labeled as working electrodes No. 1–4 (WE1–4) and a counter electrode (CE), respectively (Figure 41 - B).

**Figure 41 -** Hollow microneedles (HMNs) sensing device dimensions and SEM images. The HMNs device is integrated by 6 HMNs (A), 4: 1: 1 are used for the working electrode, counter electrode, and reference electrode, respectively (B). Dupont terminal connections were integrated (C) Scale bar 1cm for the final device assembly. The SEM images showed 3D-printed hollow microneedles with a height of 1.4mm, a base diameter size of 1.5mm, and a hole size in the center of around 1mm. (D-E) Scale bar 500µm. With a space between each hollow microneedle of 3mm (F) Scale bar of 1mm.

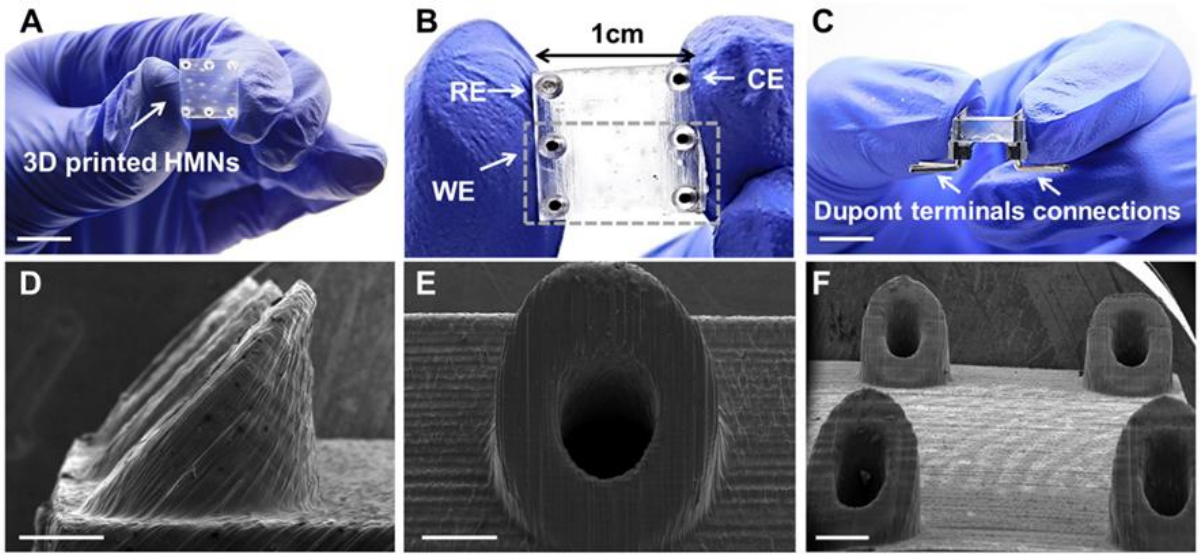


The last microneedle electrode was modified with silver/silver chloride (Ag/AgCl) ink, dried at 80 °C for an hour, and used as a reference electrode (RE). The connection integration was performed using DuPont terminals connection in the bottom of each hollow needle using carbon ink and sealed with resin in a UV lamp for 15 min (Figure 41 - C). SEM images of the needles are also demonstrated in Figure 41 – D, E, and F. After preparation; the devices were stored at room temperature for further experiments.

After microneedles array fabrication, all electrochemical experiments were recorded versus silver/silver chloride (Ag/AgCl) ink-filled microneedle array sensing platform as a reference electrode and carbon paste packed into the hollow as a counter electrode at room temperature. A 0.5 mL volume homemade cell containing

the analysis medium (PBS (0.1 mol $L^{-1}$, pH 7.4) or artificial ISF) was used coupled with a PalmSens EmStat3 Blue hand-held potentiostat controlled by PSTrace software version 5.9. Data was plotted by Origin Software. The propofol stock solution (10.0 m mol $L^{-1}$) was prepared in 0.1 mol $L^{-1}$ NaOH and diluted in PBS (0.1 mol $L^{-1}$, pH 7.4) to 1.0 m mol $L^{-1}$ or artificial ISF before use in all experiments.

### 4.2.4. Fabrication of the Phantom Gel Mimicked Skin

The phantom gel was used for mimicking the human skin and prepared following a previously reported work [115]. This procedure uses 140 mg of agarose dissolved in 10 mL of PBS or artificial ISF and stirred at 120 °C until complete dissolution (ca. 3 hours). Then, this homogeneous liquid solution was poured into 2.5 cm diameter circle-shaped molds to solidify within a few minutes at room temperature (25ºC). The obtained phantom gels were incubated in 10 mL of PBS or artificial ISF containing different propofol concentrations (0, 25, 50, 75, and 100 µmol $L^{-1}$) and kept at 4 °C for 4 days for further experimental.

### 4.2.5. In Vitro Evaluation

The electroanalytical performance of the device was tested in PBS (0.1 mol $L^{-1}$, pH 7.4) and artificial ISF (pH 7.4) as electrolyte mediums for the analysis. The artificial ISF was prepared following adjusted methods described in previous works [115,220]. Square wave voltammetric (SWV) experiments were performed using a potential range from –0.1 to 0.8 V vs. Ag/AgCl for PBS medium and from –0.1 to 1.0

V vs. Ag/AgCl for artificial ISF medium. The stability of the developed system was investigated in either artificial ISF or PBS by repetitive SWV measurements every 10 minutes for a prolonged period of up to 2 hours (120 minutes). Furthermore, the selectivity of the microneedles was also examined in artificial ISF in the presence of possible interfering species such as ascorbic acid, acetaminophen, caffeine, glucose, lactate, theophylline, and uric acid.

#### 4.2.6. Skin-Mimicking Phantom Gel Experiments

After incubating in different propofol concentrations (0–100 μmol $L^{-1}$), the previously prepared phantom gel samples were applied for skin-mimicking experiments. The sensing performance of the HMNs to detect propofol in a skin-mimic system was tested by pressing the microneedle tips into the gel and performing square wave voltammetric measurements in the potential range from –0.1 to 1.0 V vs. Ag/AgCl under the optimal conditions.

## 4.3. Results and Discussion

### 4.3.1. Introduction to solid MNs testing

#### *4.3.1.1. Glucose*

First, solid microneedles were used to learn how to fabricate microneedles and how to work with them. After fabrication, the electrochemical modification was applied on working electrode MNs for GOx immobilization using o-PD. It is one of the simplest

enzyme systems to evaluate the device's electrochemical performance to propose a biosensor. Usually, Pt electrodes are well known for hydrogen peroxide ($H_2O_2$) detection [221], and the catalytic reaction between glucose and GOx generates $H_2O_2$ as a product.

The potential of 0.3V vs. Ag reference electrode was applied to oxidize $H_2O_2$ generated after glucose additions. The measurements are observed in Figure 42 - A, and it is possible to note after each glucose addition that the current signal increases due to the $H_2O_2$ oxidation. Since the $H_2O_2$ is generated by the catalytic reaction of the glucose by the enzyme, the concentration of $H_2O_2$ in the medium is proportional to the glucose concentration.

**Figure 42 -** (A) GOxMNs chronoamperometry response for glucose in 0.1 mol $L^{-1}$ PBS pH 7.4 from 0.1 to 1 mmol $L^{-1}$. (B) Corresponding calibration plot, I = 0.212 [Glucose] + 0.016; $R^2$=0.998 (t = 60 s). Chronoamperometry parameters: 0.3V vs. Ag reference electrode for 60 s.

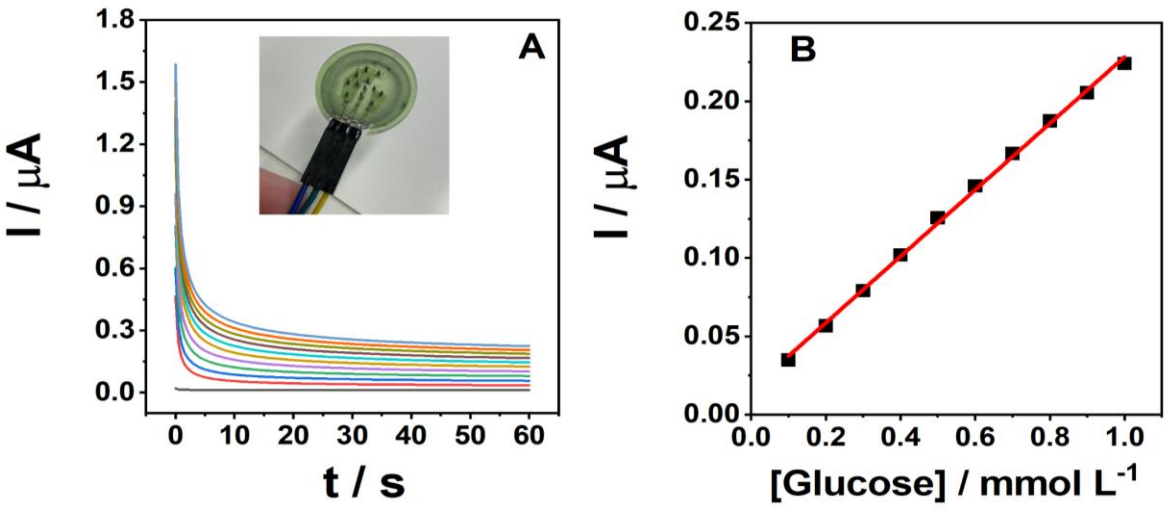


Figure 42 - B represents the corresponding calibration plot correlating the glucose concentration (from 0.1 to 1 mmol $L^{-1}$) with the current response by the

calibration curve I = 0.212 $C_{Glucose}$+ 0.016, with the coefficient of correlation ($R^2$) of 0.998, which expresses good linearity.

Besides the glucose addition measurements, we studied the electrode stability using chronoamperometry measurements in PBS containing 3.8 mmol $L^{-1}$ glucose every 5 minutes for 50 minutes. The result is presented in Figure 43 - A, which demonstrates a slight variation during this period. A bar chart plot is also presented in Figure 43 - B with current vs. stability time to evaluate the behavior. The data leads to a Relative Standard Deviation (RSD) of 3.6%, considered a slight deviation and consequently high stability.

**Figure 43 -** (A) GOxMNs stability chronoamperometry responses in 3.8 mmol $L^{-1}$ glucose + 0.1 mol $L^{-1}$ PBS pH 7.4 every 5 min during 50 min. (B) Corresponding bar chart plot (current vs. stability time) with RSD = 3.6%.

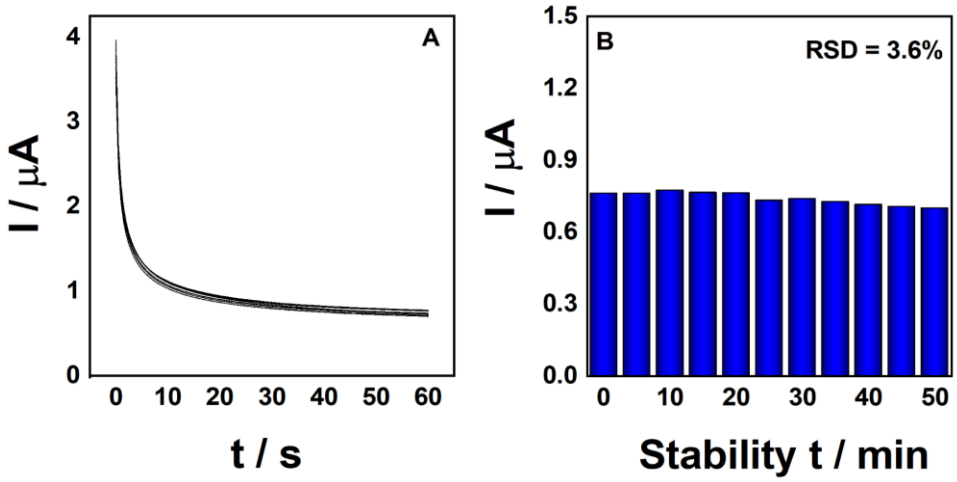


The results showed the feasibility of the device for monitoring glucose or as a biosensor. These preliminary studies were applied to verify the use of a pre-existing protocol for electrode modification on the newly fabricated microneedle device. The

idea is to adapt the procedure for lactate sensor fabrication. The MNs were modified using LOx instead of GOx, and enzyme ratio optimizations were performed.

#### *4.3.1.2. Lactate*

The catalytic lactate reaction with LOx generates the same product as the above example for glucose ($H_2O_2$). The same measurement procedure was applied in this case, which consists of using chronoamperometry to quantify lactate indirectly. After starting the parameters optimization, a chronoamperometry was carried out, and the data is presented in Figure 44 - A.

**Figure 44 -** (A) LOxMNs chronoamperometry response for lactate in 0.1 mol $L^{-1}$ PBS pH 7.4 from 0.1 to 1 mmol $L^{-1}$. (B) Corresponding calibration plot, I = 0.212 [Lactate] + 0.016; $R^2$=0.997.

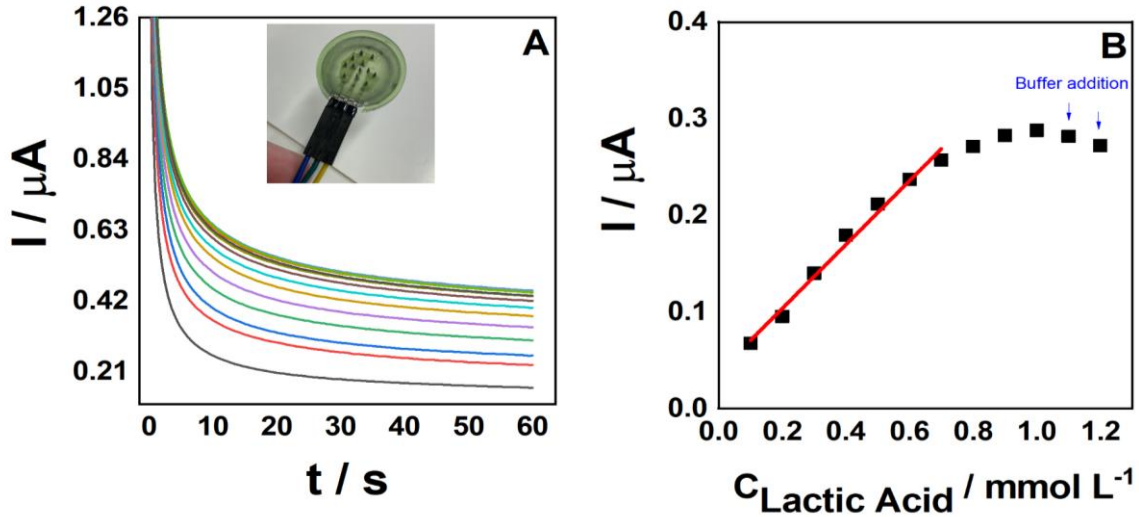


The same behavior is observed, where the current signal keeps increasing with lactate additions demonstrating the generation and, consequently, oxidation of $H_2O_2$. A corresponding calibration plot correlating the current signal and lactate concentration is presented in Figure 44 - B. A linear response is observed only

between the range from 0.1 to 0.7 mmol $L^{-1}$, with a calibration curve of I = 0.212 [Lactate] + 0.016, which provides a $R^2$ = 0.997.

In this case, problems with the electrode modification were observed since it was not reproducible. Therefore, stability tests were not performed. Further studies are required to move forward, yet the device presents a promising future to be applied as an electrochemical microneedle biosensor. Furthermore, all the procedures were used to learn about microneedle devices, fabrication, and application.

### 4.3.2. HMNs for propofol determination and quantification

#### *4.3.2.1. Principle and Design of the Microneedle Array Sensor*

The new microneedle array sensor was designed to directly measure PPF using the SWV technique as a non-enzymatic sensor, containing 4 working, 1 counter, and 1 reference electrode, as observed in Figure 41. Different designs for the hollow microneedles device, such as bases and needle size, were tested. PPF is an intravenous general anesthetic drug with the possibility of electrode passivation, so the four-working electrode array can enable a higher sensitivity or be used one at a time to ensure long-period measurements during surgery. The working and counter electrodes were packed with carbon paste, and reference electrodes were filled with Ag/AgCl.

Images of the hollow microneedles array are observed in Figure 41 (A) and (B) before and after packing with the carbon paste material. Dupont terminal connections

were used to facilitate the use of the connectors (Figure 41 (C)). SEM images of the device are presented in Figure 41 (D, E, and F), where it is possible to observe the design of the microneedles array and the hollow inside each needle. These hollows can be filled with different materials. A carbon paste was used in this study inspired by previous work [218]. This work aims to develop a device for long-term propofol monitoring.

#### *4.3.2.2. Optimization and Characterization of the Microneedle Propofol Sensors*

After fabrication, the analytical performance of the device was optimized for the hollow array MNs system (1 counter, 1 reference, and 4 working microneedles) using different ratios of graphite and mineral oil (MO). Mineral oil is a typical binder to prepare carbon paste [222,223]. Furthermore, adding carbon nanotubes (CNTs) into the carbon paste was also evaluated to enhance the device's electrochemical performance, as demonstrated in another work [224]. Thus, the best conditions to detect propofol using the carbon paste were optimized with the SWV technique in the presence of 100 µmol $L^{-1}$ PPF. First, the electrochemical behavior was tested after adding 5% CNTs w/w into the carbon paste, as presented in Figure 45 - A. In this circumstance, a significant improvement in the current signal was observed, which is better represented using the bar chart in Figure 45 - B (mineral amount vs current peak (Ip) response plot). This behavior can be attributed to the large electroactive area provided by adding the nanomaterial into the carbon paste. Thus, using 5% CNTs w/w in the carbon paste was chosen as the optimized condition.

**Figure 45 -** Investigation of CNTs amounts into carbon paste. A) SWV responses in 0.1 M PBS 7.4 medium spiked 100 µmol $L^{-1}$ PPF (5 min. Interval time each), from -0.1 to 0.8 V vs. Ag/AgCl using a frequency of 10 Hz, amplitude of 50 mV, and step potential of 6 mV. B) Corresponding SWV current peak (Ip) vs CNT percentage (w/w) plot.

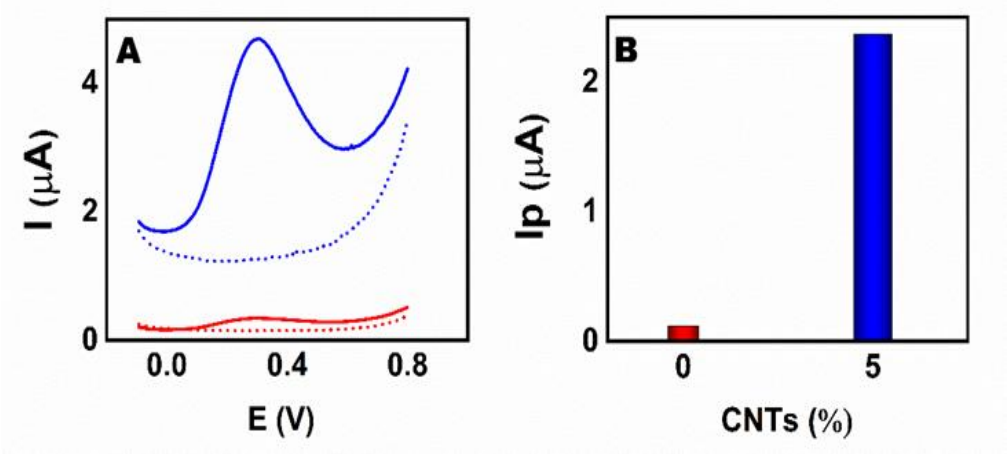


After, the electrochemical behavior of the devices was evaluated for different ratios of MO, as presented in Figure 46 - A.

**Figure 46 -** Investigation of mineral oil amounts into carbon paste. A) SWV responses in 0.1 M PBS 7.4 medium spiked 100 µmol $L^{-1}$ PPF (5 min. Interval time each), from -0.1 to 0.8 V vs. Ag/AgCl using a frequency of 10 Hz, amplitude of 50 mV, and step potential of 6 mV. B) Corresponding SWV current peak (Ip) vs. Mineral Oil amount plot (µL in 100 mg of graphite + 5%CNTs w/w).

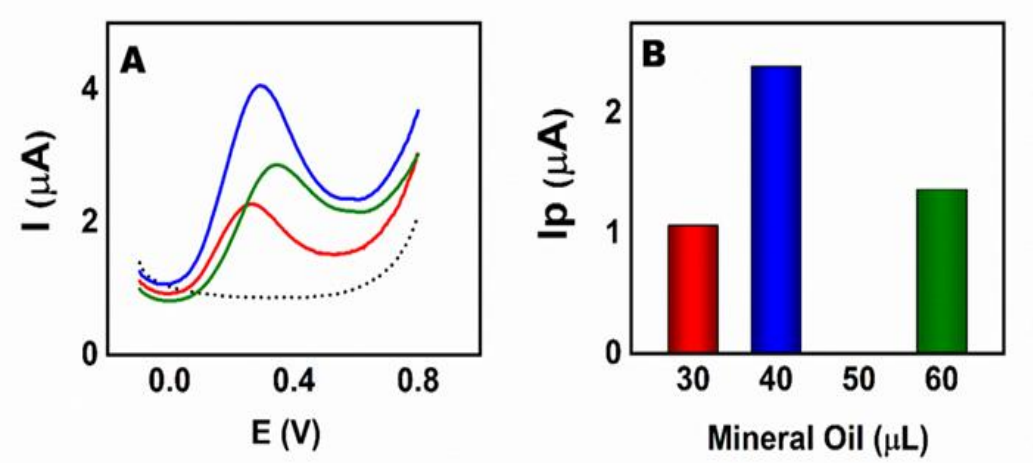


The corresponding bar chart is presented in Figure 46 - B, where it is possible to notice the mineral amount vs current peak response plot. The results demonstrated

that adding 40 µL MO in 100 mg mix of graphite powder + 5%CNTs w/w presented the highest current signal in terms of intensity. Thus, it was chosen as the optimized condition for the carbon paste in PPF detection using the HMNs (75% carbon paste and 25% mineral oil, w/w).

As observed above, PPF monitoring consists of a current signal resulting from the molecule oxidation reaction. A typical single-electron oxidation peak was observed at 0.30 V, where the phenolic group turns into phenonium ions, as shown in Figure 47 - A. The current signal generated in this reaction was recorded using the SWV technique under optimized conditions at the HMNs device for a concentration range of 5−200 µmol $L^{-1}$ PPF after optimization of the abovementioned parameters.

The experiment was conducted in both PBS (Figure 47 - B) and artificial ISF medium (Figure 47 - D). Normalization of the signal was applied by the baseline subtraction from the response signals and will also be applied in all subsequent data. An increase in the current signal was observed as the PPF concentration was raised. This pattern was noticed in both mediums, and the corresponding calibration plots are shown in Figure 47 - C and E.

**Figure 47** - Developed HMNs sensors for propofol detection. (A) The schematic representation of the developed HMNs sensors and an oxidation reaction of the target PPF onto the working electrode (WE) surface. (B) SWV responses for PPF in PBS medium from 5−200 µmol $L^{-1}$ concentrations using the developed HMNs sensor and (C) the corresponding PPF calibration plot (I = 0.022 $C_{PPF}$ + 0.318, $R^2$ 0.997). (D) SWV responses for PPF in artificial ISF medium from 5−200 µmol $L^{-1}$ concentrations using the developed HMNs sensor and (E) the corresponding PPF calibration plot (I = 0.036 $C_{PPF}$ + 0.461, $R^2$ 0.999). SWV potential range −0.1 to 0.8 V (vs. Ag/AgCl) for PBS medium and –0.1 to 1.0 V (vs. Ag/AgCl) for artificial ISF medium using a frequency of 10 Hz, amplitude of 50 mV, and step potential of 6 mV (a normalization of the signal was applied by baseline subtraction).

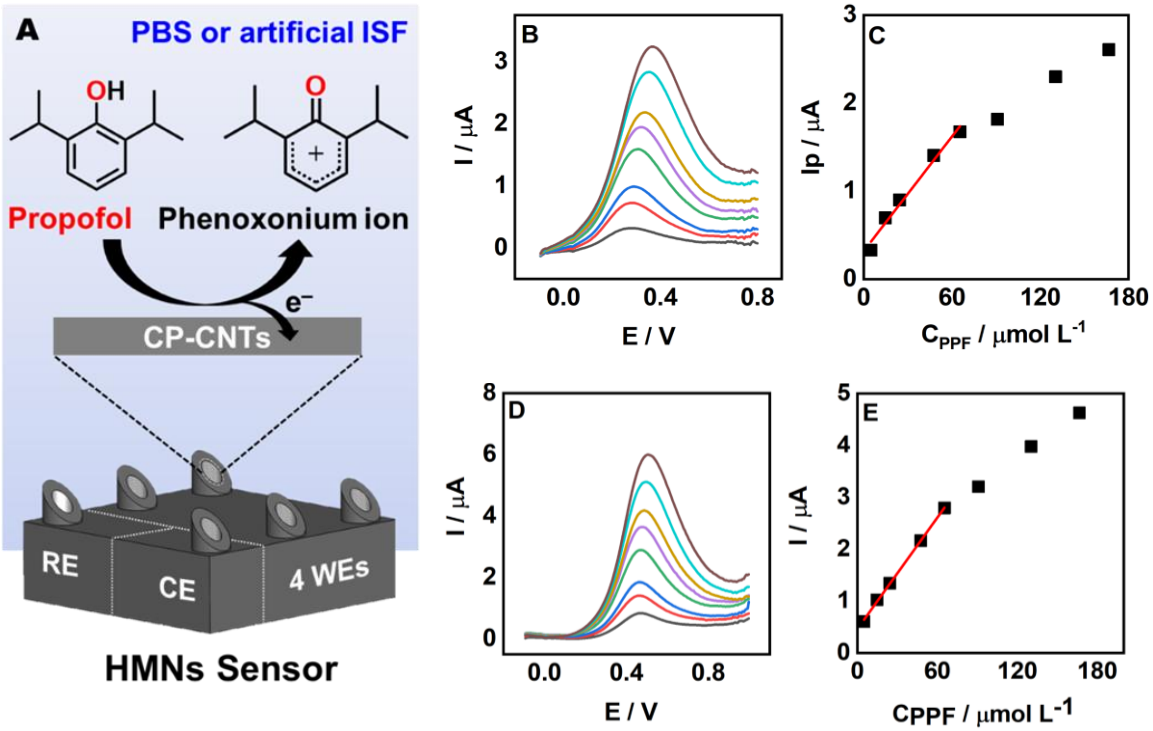


A linear relationship between PPF concentration and current response was observed in both systems from 5 to 65 µmol $L^{-1}$ PPF where the calibrations plot are I = 0.022 $C_{PPF}$ + 0.318, $R^2$ 0.997 and I = 0.036 $C_{PPF}$ + 0.461, $R^2$ 0.999, respectively for PBS and ISF. From the calibration plot, the obtained sensitivities are 0.022 and 0.036 µA $µmol^{-1}$ L, and the limits of detection (LOD) were estimated as 2.7 µmol $L^{-1}$ and 3.7 µmol $L^{-1}$, respectively, in PBS and artificial ISF. LOD = 3SD/S and LOQ = 10SD/S, where SD corresponds to the standard deviation of the intercept, and S is the slope of

the analytical curve (sensitivity). For limits of quantification (LOQ), the estimated values were 9.1 and 12.5 µmol $L^{-1}$, respectively, in PBS and artificial ISF.

Those are still preliminary studies in the development of HMNs for PPF monitoring, yet into effective plasma PPF concentration range is given between 0.25 and 10 µg/L (1– 60 µmol $L^{-1}$) [225], which is close to LOD value for artificial ISF measurements. Further studies will be applied for the electrode surface modification to improve the LOD value. Moreover, it is possible to note that LOD values obtained from measurements carried out in different electrolyte mediums differ. It can be due to the more significant complexity of the artificial ISF medium.

Furthermore, although the electrochemical PPF oxidation behavior in both mediums is similar, in artificial ISF the potential peak is shifted from 0.3 V to 0.5 V besides the higher current intensity observed comparing the same PPF concentration responses. In Figure 48 - A, it is possible to observe a comparison of SWV measurements in two concentrations for both mediums. Figure 48 - B represents the corresponding PPF current peak response in PBS medium (set as 100% in both PPF concentrations) and the relative PPF current peak response percentage in ISF medium compared to the response percentage obtained in PBS. Both behaviors, the potential shifting and the increase in the current intensity when using two different mediums during the measurement, can be caused by a pH variation.

**Figure 48 -** Comparison between PPF response in two different mediums. A) SWV responses in 0.1 M PBS 7.4 and artificial ISF medium spiked with 50 and 100 µmol $L^{-1}$ PPF (5 min. Interval time each), from -0.1 to 0.8 V vs. Ag/AgCl using a frequency of 10 Hz, amplitude of 50 mV, and step potential of 6 mV. A normalization of the signal was applied by baseline subtraction. B) Corresponding PPF response current in PBS medium (set as 100%) and PPF response current percentage in ISF medium vs. PPF concentration ($C_{PPF}$) plot.

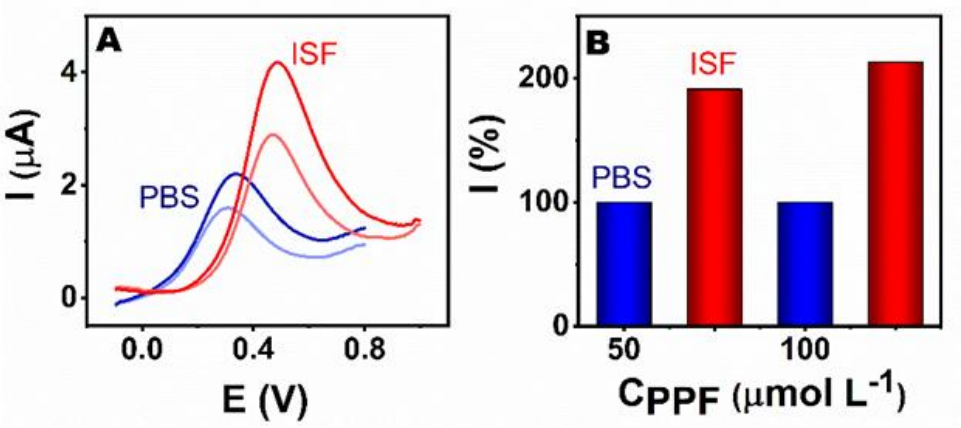


The artificial ISF composition is presented in Table 6, where a more complex medium is noticed, causing the changes in the response previously observed in pure PBS.

**Table 6 -** Composition of Artificial Interstitial Fluid*

| **Component** | **Concentration / mmol $L^{-1}$** |
|---|---|
| NaCl | 54.0 |
| KCl | 1.7 |
| $CaCl_2$ | 0.8 |
| $MgSO_4$ | 0.3 |
| $NaHCO_3$ | 13 |
| $NaH_2PO_4$ | 0.8 |
| Na gluconate | 4.8 |
| glucose | 2.8 |
| sucrose | 3.8 |

*All compounds diluted in 0.05 mol $L^{-1}$ PBS pH 7.4

After, the new devices were tested for different potential interfering species, such as ascorbic acid, uric acid, acetaminophen, caffeine, glucose, lactate, and theophylline, using artificial ISF as the electrolyte. The SWV recorded in an excessive amount (150 µmol $L^{-1}$) of each interference compound is presented in Figure 49. The data showed all the species presented oxidative electrochemical signals in different potential ranges compared to PPF response (highlighted in Figure 49 - B) by the red color), indicating this HMNs device can have a satisfactory selectivity for PPF analysis since all interfering species present oxidation signal response in different potentials.

**Figure 49 -** Selectivity investigation of the developed HMNs sensors against various potential interferers. SWV responses were recorded in (A) artificial ISF upon adding (B) 150 µmol $L^{-1}$ propofol and 150 µmol $L^{-1}$ of each interfering species, including (C) ascorbic acid, (D) acetaminophen, (E) caffeine, (F) glucose, (G) lactate, and (H) uric acid. SWV from -0.1 to 1.0 V vs. Ag/AgCl using a frequency of 10 Hz, amplitude of 50 mV, and step potential of 6 mV (normalization of the signal was applied by baseline subtraction).

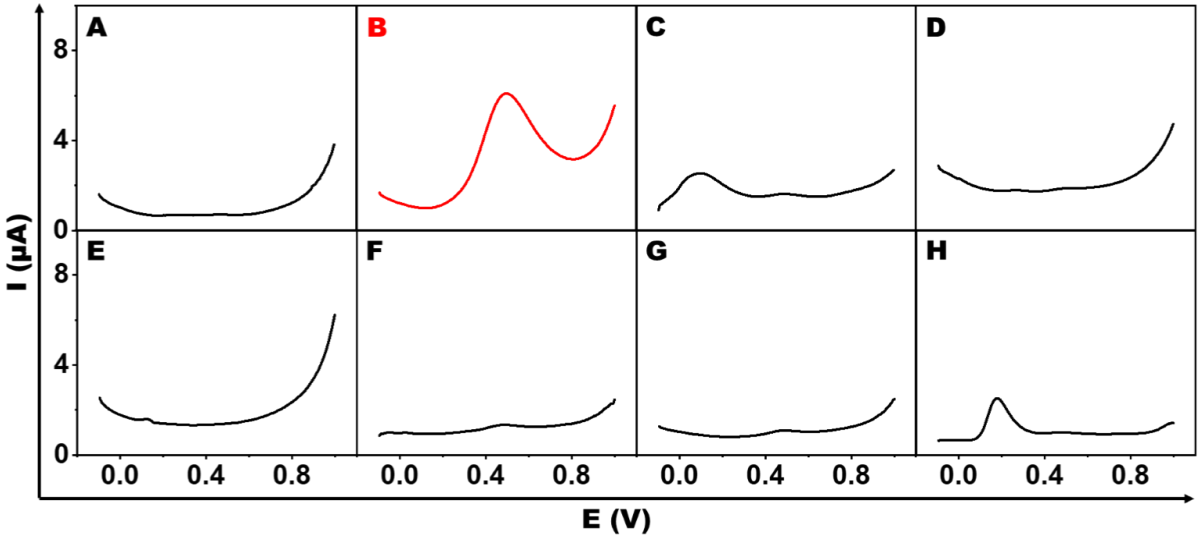


In addition to these results, using phantom-gel polymer as a mimicking skin is well known to test the viability of using the fabricated device [115]. Herein, we have applied this technique to evaluate the model in both PBS and artificial ISF mediums, which results are presented in Figure 50 and Figure 51.

**Figure 50 -** Phantom-gel mimicked skin model evaluation. (A) SWV responses of different propofol concentrations (25–100 µmol $L^{-1}$, 25 µmol $L^{-1}$ increments) with the mimicking-skin phantom-gel along with (B) the corresponding propofol calibration plot (I = 0.038 $C_{PPF}$ - 0.198, $R^2$ 0.999). SWV from -0.1 to 1.0 V vs. Ag/AgCl using a frequency of 10 Hz, amplitude of 50 mV, and step potential of 6 mV in 0.1 M PBS pH 7.4 medium (normalization of the signal was applied by baseline subtraction).

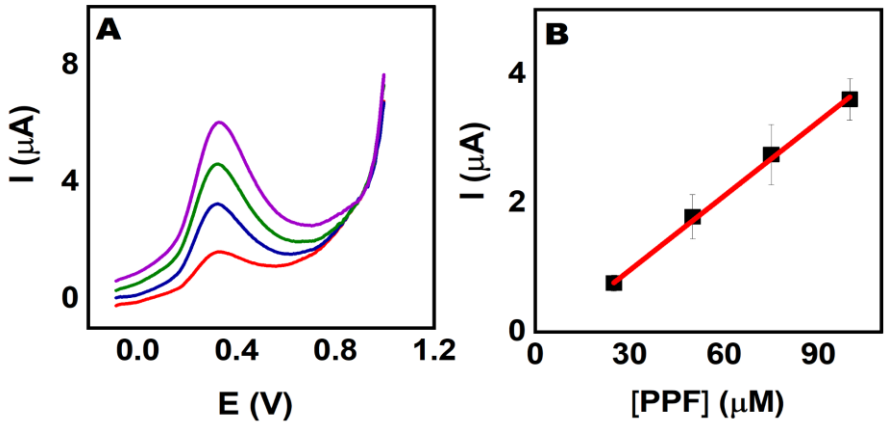


Figure 50 – A presents the SWV responses for different propofol concentrations (25–100 µmol $L^{-1}$, 25 µmol $L^{-1}$ increments) incubated in the mimicking-skin phantom-gel using 0.1 M PBS pH 7.4 medium. As observed above, the SWV current peak increases with the increment of PPF concentration incubated in the phantom gel. Thus, Figure 50 – B shows the corresponding PPF calibration plot, I = 0.038 $C_{PPF}$ - 0.198, $R^2$ 0.999, where a linear relationship is observed with a sensitivity of 0.038 µA $\mu mol^{-1}$ L, which is a similar electrochemical behavior when compared to the presented results carried out in PBS solution.

Furthermore, SWVs were also carried out in phantom-gel incubated with propofol in artificial ISF. Figure 51 - A shows a schematic representation of a phantom-gel mimicked skin model with the penetration of the developed HMNs sensor, while Figure 51 - B presents the SWV obtained in this experiment. A typical SWV for PPF response is observed, with a linear relationship between the current signal increase and PPF concentration increment (Figure 51 - C). In this case, the current response

is also higher when compared to the system evaluated in PBS due to the different composition in ISF medium, behavior also observed in the data discussed above.

**Figure 51 -** Phantom-gel mimicked skin model evaluation. (A) Schematic representation of the mimicking-skin phantom gel with the penetration of the developed HMNs sensor. (B) SWV responses of different propofol concentrations (25–100 µmol $L^{-1}$, 25 µmol $L^{-1}$ increments) with the mimicking-skin phantom gel and (C) the corresponding propofol calibration plot. SWV from -0.1 to 1.0 V vs. Ag/AgCl using a frequency of 10 Hz, amplitude of 50 mV, and step potential of 6 mV in an artificial ISF medium (normalization of the signal was applied by baseline subtraction).

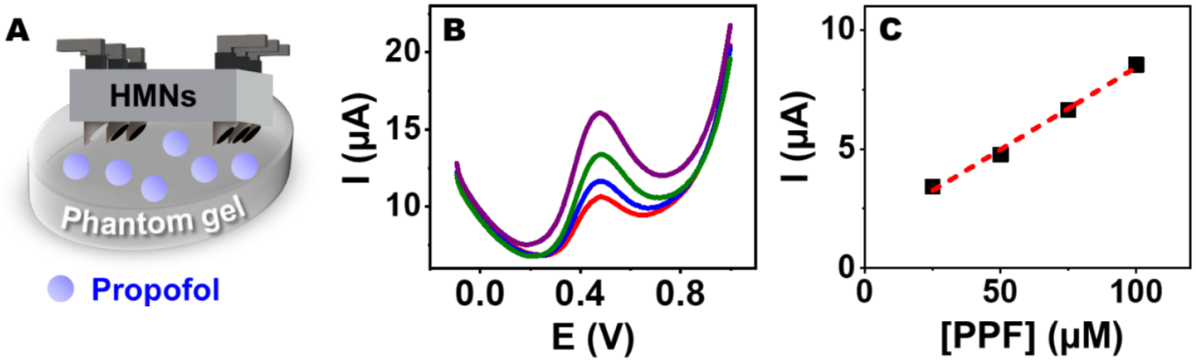


All the presented results demonstrated the viability of applying the fabricated device in a mimicked skin model, which is a crucial step when studying the development of a new wearable sensor. However, more experiments are required to calculate LOD, LOQ and evaluate the reproducibility of the mimicked skin system.

Although the results showed the potential of HMNs devices to detect PPF in the range of interest and the evaluation of the system in mimicked skin models, the obstacle for long-term PPF measurements is well known. The specie generated from PPF electrochemical oxidation can initiate other reactions over the electrode surface, responsible for forming an unwanted polymeric film and, consequently, electrode passivation [226]. It can harm stability test measurements over hours. An example of this

is shown in the stability test results recorded in PBS and ISF for the fabricated device and presented in Figure 52.

**Figure 52** -The stability performance of the developed HMNs sensor. (A) SWV responses of 50 µmol $L^{-1}$ propofol in PBS (A) and artificial ISF (C) for 12 repetitive measurements at 10-minute intervals over 120 minutes along with the corresponding transitional signal profile of the developed HMNs sensor ((B) for PBS and (D) for ISF), which decreases concerning the increasing amount of detection scans. SWV from -0.1 to 0.8 V vs. Ag/AgCl using a frequency of 10 Hz, amplitude of 50 mV, and step potential of 6 mV (normalization of the signal was applied by baseline subtraction).

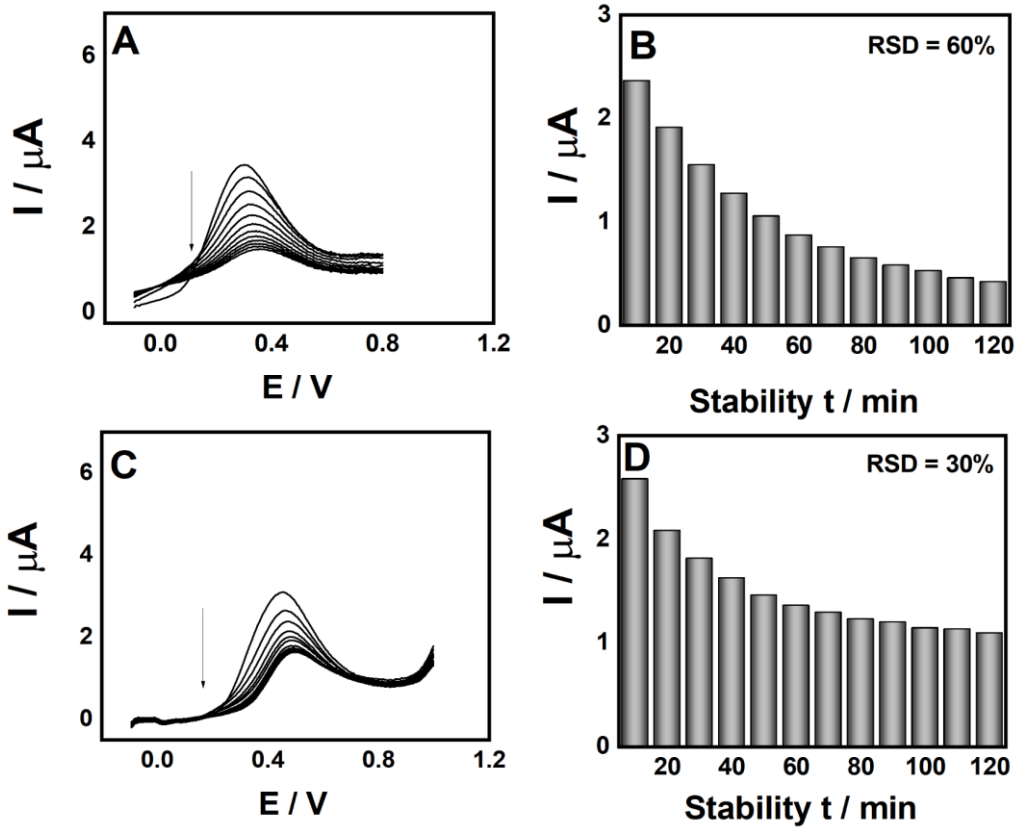


Figure 52 - A and C show SWV responses of 50 µmol $L^{-1}$ propofol in PBS and artificial ISF every 10 minutes over 120 minutes. In these graphs, it is possible to observe the current signal decreasing significantly with every measurement, where this effect is more intense in PBS than in artificial ISF due to the different molecules present in this medium. The data generated a bar chart (Figure 52 – B and D) for all

SWV current peaks recorded every 10 minutes, which we call stability time. Using this bar chart, an RSD of 60.0 and 30.0% for data obtained in PBS and ISF, respectively, was calculated, showing a high deviation between the measurements and low stability in the signal. It clearly shows the electrode passivation during the period evaluated. For every measurement, the polymerization on the electrode surface generated by the unwanted product of PPF oxidation leads to higher electrode passivation.

For this reason, many strategies were tested, including using different protective barriers such as PVC, chitosan, and glutaraldehyde, besides using different working electrode materials, such as gold and platinum. All tested protective barriers presented a significant decrease or blocked the current signal, poor reproducibility, and, most importantly, did not improve the electrode passivation problem. Furthermore, using gold or platinum material as working electrodes did not generate any PPF electrochemical response. Thus, another and more promising test was realized using a smaller working electrode area and only one working electrode in the HMNs system. Figure 53 represents how the smaller area was selected on the working electrode using only the internal hollow as diameter instead of covering the whole top of the microneedle with the conductive material.

**Figure 53 -** Schematic representation of the developed HMNs sensors along with the two options of area to use. The area of each HMN is 0.78 $mm^2$ considering the hollow diameter and 1.77 $mm^2$ considering the base size diameter.

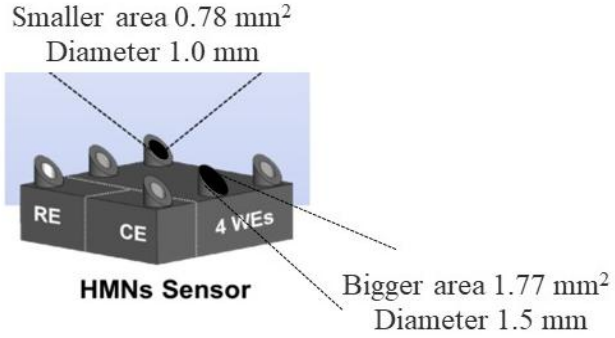

The area of each HMN is 0.78 $mm^2$ considering the hollow diameter (1.0 mm) and 1.77 $mm^2$ considering the base diameter. The stability test used a smaller area and only one working electrode. It leads to the probability of using one working electrode every 1-hour stability measurements providing a much longer-term collection of data. It would be fundamental for PPF monitoring during a surgical procedure. The new stability data is presented in Figure 54.

**Figure 54 -** The stability performance of the developed HMNs sensor using only one working in MN with a smaller area (0.78 $mm^2$). (A) SWV responses of 25 µmol $L^{-1}$ propofol in PBS (A) and artificial ISF (C) for 12 repetitive measurements at 10-minute intervals over 120 minutes along with the corresponding transitional signal profile of the developed HMNs sensor ((B) for PBS and (D) for ISF), which decreases concerning the increasing amount of detection scans. SWV from -0.1 to 0.8 V vs. Ag/AgCl using a frequency of 10 Hz, amplitude of 50 mV, and step potential of 4 mV (normalization of the signal was applied by baseline subtraction).

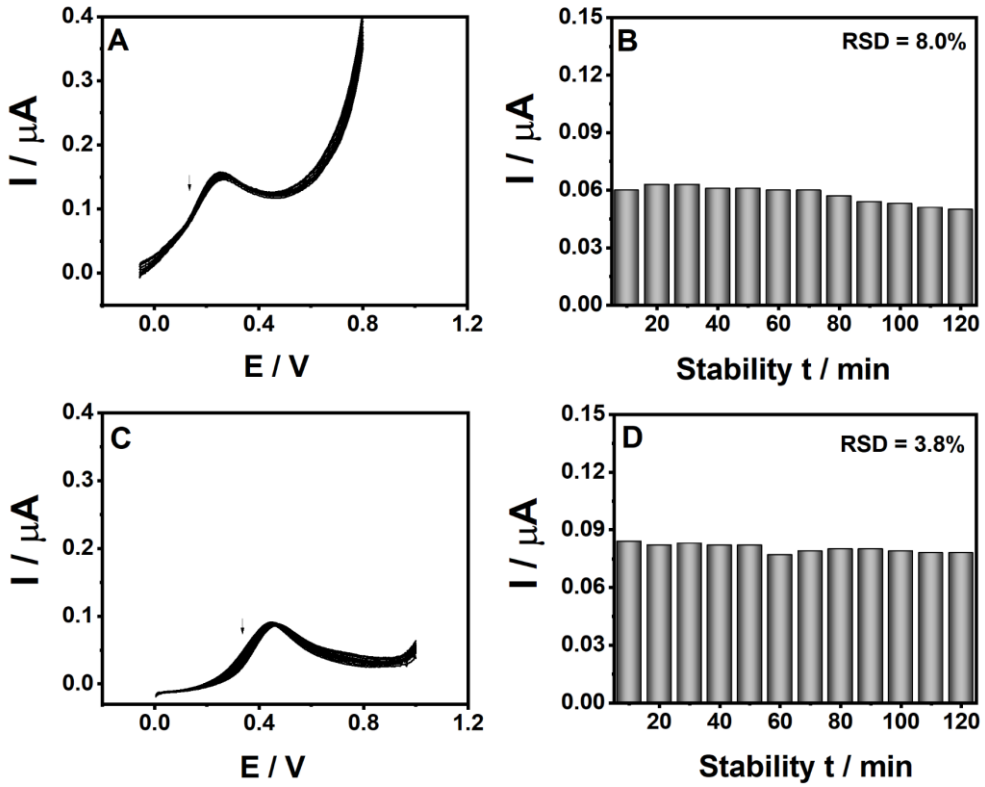

Figure 54 - A and C shows SWV responses of 25 μmol $L^{-1}$ propofol in PBS and artificial ISF every 10 minutes over 120 minutes. In this case, the current signal remains stable, and the effect can be due to the smaller size of the working electrode, which can make the diffusional mass transport more efficient [227], preventing polymerization on the electrode surface. As observed above, the stability is more evident in artificial ISF and PBS due to the different molecules present in this medium. The data also generated a bar chart (Figure 54 - B and D) for all SWV current peaks recorded every 10 minutes. Using this bar chart, an RSD of 8.0 and 3.8% for data obtained in PBS and ISF, respectively, was calculated, showing a much smaller deviation between the measurements and, consequently, high stability in the signal during 2 hours. Other studies are necessary to validate using one needle as a working electrode every 1 or 2 hours of stability measurements. However, everything indicates a significant probability of applying the MNs array sensor for PPF long-term monitoring.

With all the results presented herein, the idea is to develop a minimally invasive sensing platform looking forward to long-term propofol monitoring in ISF. The schematic representation of how the device would work during a surgical procedure for anesthesia monitoring is proposed in Figure 55. Although more efforts are still necessary, the results showed an attractive potential for future application.

**Figure 55 -** Schematic representation of the hollow microneedles (HMNs) device as a minimally invasive sensing platform for propofol detection in ISF using the SWV technique.

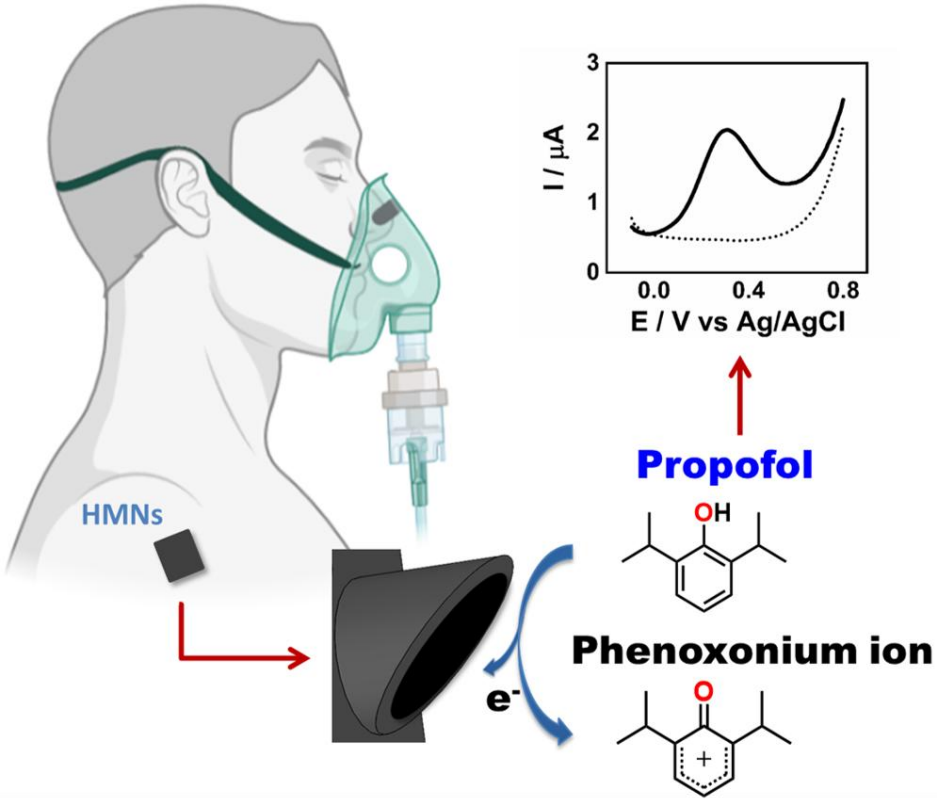


## 4.4. Conclusions

Initially, the solid MNs were used to develop the necessary skills to work with MNs. A three-electrode system was fabricated using a 3D printer and covered with Pt, where a good performance for glucose and lactate detection was observed. However, more experiments should be conducted to improve the system since reproducibility problems were presented on the electrode modification used on the biorecognition. After this initial study, another device composed of hollow microneedles was developed for propofol monitoring. This proposed method enabled selective

sensitivity for propofol measurements covering the μmol $L^{-1}$ concentration range of interest analyte. However, a better sensitivity can be reached using working electrode modifications, although that is not the purpose of the work at this stage. The long-term monitoring capability of the sensor was evaluated in PBS and artificial ISF mediums, presenting good potential to be applied for 2 hours. As the device is a microneedle array of 4 working electrodes, it allows applying one working electrode every 2 hours, leading to longer-term monitoring. Yet, more experiments are necessary to evaluate it. The potential applicability of the developed microneedle array-based sensor toward minimally invasive monitoring of propofol drug was also demonstrated by skin-mimicking phantom gel experiments. The new microneedle array sensing platform holds promising potential for the continuous, real-time, in-vivo detection of the anesthetic propofol drug during surgical procedures that can significantly improve safety and efficacy for the delivery of anesthetic drugs.

# 5. Final Considerations and Perspectives

The exposed data in this thesis showed satisfactory results regarding developing portable electrochemical devices on polymer materials using $CO_2$ laser for analytical applications. Laser-scribing is a simple, scalable, and low-cost method. Initially, phenolic paper was proposed as another alternative material for fabricating laser-scribed electrochemical divides. This material is a low-cost, rigid board that can easily be bought or recycled from used systems. Thus, robust devices with a porous structure and graphene-like domains were obtained, presenting interesting properties, such as good conductivity. The material showed satisfactory reproducibility and repeatability, with great potential for on-site analytical applications.

Furthermore, another electrochemical platform was proposed using polyimide and paper due to the necessity for new polymer-based electrochemical sensors that can be combined with paper structures to create versatile and efficient analytical devices. Thus, low-cost, versatile, and flexible devices were obtained using the laser-scribing technique and Kapton tape, an inexpensive polyimide source. The devices consisted of a miniaturized three - electrodes system, requiring only 200 µL of solution for static conditions measurements. A microfluidic system was also obtained, combining the polyimide electrochemical devices with a paper-based platform to be applied using hydrodynamic conditions. The proposed analytical platforms demonstrated satisfactory electroanalytical performance in static and hydrodynamic conditions, indicating the platforms' versatility and the system's potential to be used in analytical applications.

The research internship abroad was in the wearable sensors field at Professor Dr. Joseph Wang's laboratory. The proposal was to learn more about wearable sensors to apply this knowledge with the devices fabricated and presented in this thesis. Thus, a device composed of hollow microneedles array was proposed for propofol monitoring. The potential applicability of the developed microneedle array-based sensor toward minimally invasive monitoring of propofol drug was demonstrated by skin-mimicking phantom gel experiments. Although the new microneedle array sensing platform holds promising potential for the continuous, real-time detection of the anesthetic propofol drug during surgical procedures, more experimental data are still needed.

The laser-scribing technique demonstrated a simple, scalable, and low-cost way to obtain portable electrochemical devices in various platforms, especially using polymer materials, which are an alternative to the drawbacks of paper use. Moreover, combining different platforms is also promising, depending on the analytical applications. These devices can also be considered for electrochemical wearable sensors fabrication, although this is a future step in this project. Therefore, this work focuses on applying the knowledge obtained in wearable sensors to develop a wearable platform using the laser-scribing devices proposed herein. In addition, more experiments are still needed to finalize the propofol microneedle sensor to obtain a promising device for constantly monitoring propofol anesthesia drugs on-body.

# 6. References


1. Zarei M. Portable biosensing devices for point-of-care diagnostics: Recent developments and applications. *TrAC Trends in Analytical Chemistry*. 2017;91:26-41. doi:https://doi.org/10.1016/j.trac.2017.04.001
2. Lu Y, Shi Z, Liu Q. Smartphone-based biosensors for portable food evaluation. *Curr Opin Food Sci*. 2019;28:74-81. doi:https://doi.org/10.1016/j.cofs.2019.09.003
3. de Araujo WR, Cardoso TMG, da Rocha RG, et al. Portable analytical platforms for forensic chemistry: A review. *Anal Chim Acta*. 2018;1034:1-21. doi:10.1016/j.aca.2018.06.014
4. Marquez S, Liu J, Morales-Narváez E. Paper-based analytical devices in environmental applications and their integration with portable technologies. *Curr Opin Environ Sci Health*. 2019;10:1-8. doi:https://doi.org/10.1016/j.coesh.2019.08.002
5. Wang J. Portable electrochemical systems. *TrAC Trends in Analytical Chemistry*. 2002;21(4):226-232. doi:https://doi.org/10.1016/S0165-9936(02)00402-8
6. Henry CS, Dungchai W, Chailapakul O. Electrochemical Detection for Paper-Based Microfluidics. *Anal Chem*. 2009;81(14):5821-5826. papers://d32519d5-83a5-42d0-9481-c6b25a06c86f/Paper/p4048%5Cnpapers2://publication/uuid/92862073-E254-4D3B-99FF-595DB0090353

7. De Araujo WR, Paixão WR. Fabrication of disposable electrochemical devices using silver ink and office paper. *Analyst*. 2014;139(11):2742-2747. doi:10.1039/c4an00097h

8. Ataide VN, Mendes LF, Gama LILM, De Araujo WR, Paixaõ TRLC. Electrochemical paper-based analytical devices: Ten years of development. *Analytical Methods*. 2020;12(8):1030-1054. doi:10.1039/c9ay02350j

9. Stefano JS, Orzari LO, Silva-Neto HA, et al. Different approaches for fabrication of low-cost electrochemical sensors. *Curr Opin Electrochem*. 2022;32:100893. doi:https://doi.org/10.1016/j.coelec.2021.100893

10. Ebrahimi G, Samadi Pakchin P, Shamloo A, et al. Label-free electrochemical microfluidic biosensors: futuristic point-of-care analytical devices for monitoring diseases. *Mikrochim Acta*. 2022;189(7):252. doi:10.1007/s00604-022-05316-3

11. Hou Y, Lv CC, Guo YL, et al. Recent Advances and Applications in Paper-Based Devices for Point-of-Care Testing. *J Anal Test*. 2022;6(3):247-273. doi:10.1007/s41664-021-00204-w

12. Elder P the. *Naturalis Historia*.; 1669.

13. KUNKEL HG, TISELIUS A. Electrophoresis of proteins on filter paper. *J Gen Physiol*. 1951;35(1):89-118. doi:10.1085/jgp.35.1.89

14. Rocco RM. *Landmark Papers in Clinical Chemistry*. Elsevier; 2006.

15. Liu H, Xiang Y, Lu Y, Crooks RM. Aptamer-based origami paper analytical device for electrochemical detection of adenosine. *Angewandte Chemie - International Edition*. 2012;51(28):6925-6928. doi:10.1002/anie.201202929

16. Manuscript A, Volume L, Bioassays P. Patterned Paper as a Platform for Inexpensive, Low Volume,Portable Bioassays. 2013;46(8):1318-1320. doi:10.1002/anie.200603817.Patterned

17. Wang S, Chinnasamy T, Lifson MA, Inci F, Demirci U. Flexible Substrate-Based Devices for Point-of-Care Diagnostics. *Trends Biotechnol*. 2016;34(11):909-921. doi:10.1016/j.tibtech.2016.05.009

18. Nery EW, Kubota LT. Sensing approaches on paper-based devices: a review. *Anal Bioanal Chem*. 2013;405(24):7573-7595. doi:10.1007/s00216-013-6911-4

19. Noviana E, Carrão DB, Pratiwi R, Henry CS. Emerging applications of paper-based analytical devices for drug analysis: A review. *Anal Chim Acta*. 2020;1116:70-90. doi:https://doi.org/10.1016/j.aca.2020.03.013

20. Chen YH, Kuo ZK, Cheng CM. Paper - a potential platform in pharmaceutical development. *Trends Biotechnol*. 2015;33(1):4-9. doi:10.1016/j.tibtech.2014.11.004

21. Liana DD, Raguse B, Justin Gooding J, Chow E. Recent advances in paper-based sensors. *Sensors (Switzerland)*. 2012;12(9):11505-11526. doi:10.3390/s120911505

22. Martinez AW, Phillips ST, Whitesides GM, Carrilho E. Diagnostics for the developing world: Microfluidic paper-based analytical devices. *Anal Chem*. 2010;82(1):3-10. doi:10.1021/ac9013989

23. Rozand C. Paper-based analytical devices for point-of-care infectious disease testing. *European Journal of Clinical Microbiology & Infectious Diseases*. 2014;33(2):147-156. doi:10.1007/s10096-013-1945-2

24. Silva TG, De Araujo WR, Muñoz RAA, et al. Simple and Sensitive Paper-Based Device Coupling Electrochemical Sample Pretreatment and Colorimetric Detection. *Anal Chem*. 2016;88(10):5145-5151. doi:10.1021/acs.analchem.6b00072

25. Yakoh A, Rattanarat P, Siangproh W, Chailapakul O. Simple and selective paper-based colorimetric sensor for determination of chloride ion in environmental samples using label-free silver nanoprisms. *Talanta*. 2018;178:134-140. doi:10.1016/j.talanta.2017.09.013

26. de Araujo WR, Frasson CMR, Ameku WA, Silva JR, Angnes L, Paixão TRLC. Single-Step Reagentless Laser Scribing Fabrication of Electrochemical Paper-Based Analytical Devices. *Angewandte Chemie - International Edition*. 2017;56(47):15113-15117. doi:10.1002/anie.201708527

27. Nie J, Zhang Y, Lin L, et al. Low-Cost Fabrication of Paper-Based Microfluidic Devices by One-Step Plotting. *Anal Chem*. 2012;84(15):6331-6335. doi:10.1021/ac203496c

28. Lu Y, Shi W, Jiang L, Qin J, Lin B. Rapid prototyping of paper-based microfluidics with wax for low-cost, portable bioassay. *Electrophoresis*. 2009;30(9):1497-1500. doi:https://doi.org/10.1002/elps.200800563

29. Cardoso TMG, de Souza FR, Garcia PT, Rabelo D, Henry CS, Coltro WKT. Versatile fabrication of paper-based microfluidic devices with high chemical resistance using scholar glue and magnetic masks. *Anal Chim Acta*. 2017;974:63-68. doi:10.1016/j.aca.2017.03.043

30. Cate DM, Adkins JA, Mettakoonpitak J, Henry CS. Recent developments in paper-based microfluidic devices. *Anal Chem*. 2015;87(1):19-41. doi:10.1021/ac503968p

31. Renault C, Li X, Fosdick SE, Crooks RM. Hollow-Channel Paper Analytical Devices. *Anal Chem*. 2013;85(16):7976-7979. doi:10.1021/ac401786h

32. Mettakoonpitak J, Boehle K, Nantaphol S, et al. Electrochemistry on Paper-based Analytical Devices: A Review. *Electroanalysis*. 2016;28(7):1420-1436. doi:10.1002/elan.201501143

33. da Silva ETSG, Souto DEP, Barragan JTC, de F. Giarola J, de Moraes ACM, Kubota LT. Electrochemical Biosensors in Point-of-Care Devices: Recent Advances and Future Trends. *ChemElectroChem*. 2017;4(4):778-794. doi:10.1002/celc.201600758

34. Hu J, Wang SQ, Wang L, et al. Advances in paper-based point-of-care diagnostics. *Biosens Bioelectron*. 2014;54:585-597. doi:10.1016/j.bios.2013.10.075

35. Dungchai W, Chailapakul O, Henry CS. Electrochemical Detection for Paper-Based Microfluidics. *Anal Chem*. 2009;81(14):5821-5826. doi:10.1021/ac9007573

36. Wang S, Chen S, Shang K, Gao X, Wang X. Sensitive electrochemical detection of cholesterol using a portable paper sensor based on the synergistic effect of cholesterol oxidase and nanoporous gold. *Int J Biol Macromol*. 2021;189(August):356-362. doi:10.1016/j.ijbiomac.2021.08.145

37. Fiore L, Mazzaracchio V, Serani A, et al. Microfluidic paper-based wearable electrochemical biosensor for reliable cortisol detection in sweat. *Sens Actuators B Chem*. 2023;379:133258. doi:https://doi.org/10.1016/j.snb.2022.133258

38. Cao Q, Liang B, Yu C, et al. High accuracy determination of multi metabolite by an origami-based coulometric electrochemical biosensor. *Journal of Electroanalytical Chemistry*. 2020;873:114358. doi:https://doi.org/10.1016/j.jelechem.2020.114358

39. Prasad KS, Cao X, Gao N, et al. A low-cost nanomaterial-based electrochemical immunosensor on paper for high-sensitivity early detection of pancreatic cancer. *Sens Actuators B Chem*. 2020;305:127516. doi:https://doi.org/10.1016/j.snb.2019.127516

40. Lahcen AA, Rauf S, Beduk T, et al. Electrochemical sensors and biosensors using laser-derived graphene: A comprehensive review. *Biosens Bioelectron*. 2020;168(June):112565. doi:10.1016/j.bios.2020.112565

41. Zhang W, Zhu S, Luque R, Han S, Hu L, Xu G. Recent development of carbon electrode materials and their bioanalytical and environmental applications. *Chem Soc Rev*. 2016;45(3):715-752. doi:10.1039/c5cs00297d

42. Geim AK. Graphene: Status and Prospects. *Science (1979)*. 2009;324(5934):1530-1534. doi:10.1126/science.1158877

43. El-Kady MF, Kaner RB. Scalable fabrication of high-power graphene micro-supercapacitors for flexible and on-chip energy storage. *Nat Commun*. 2013;4(1):1475. doi:10.1038/ncomms2446

44. Lin J, Peng Z, Liu Y, et al. Laser-induced porous graphene films from commercial polymers. *Nat Commun*. 2014;5(1):5714. doi:10.1038/ncomms6714

45. Ye R, James DK, Tour JM. Laser-Induced Graphene: From Discovery to Translation. *Advanced Materials*. 2019;31(1):1-15. doi:10.1002/adma.201803621

46. Ye R, James DK, Tour JM. Laser-Induced Graphene. *Acc Chem Res*. 2018;51(7):1609-1620. doi:10.1021/acs.accounts.8b00084

47. Aparicio-Martínez E, Ibarra A, Estrada-Moreno IA, Osuna V, Dominguez RB. Flexible electrochemical sensor based on laser scribed Graphene/Ag nanoparticles for non-enzymatic hydrogen peroxide detection. *Sens Actuators B Chem*. 2019;301:127101. doi:https://doi.org/10.1016/j.snb.2019.127101

48. Kurra N, Jiang Q, Nayak P, Alshareef HN. Laser-derived graphene: A three-dimensional printed graphene electrode and its emerging applications. *Nano Today*. 2019;24:81-102. doi:10.1016/j.nantod.2018.12.003

49. Tan KW, Jung B, Werner JG, Rhoades ER, Thompson MO, Wiesner U. Transient laser heating induced hierarchical porous structures from block copolymer–directed self-assembly. *Science (1979)*. 2015;349(6243):54-58. doi:10.1126/science.aab0492

50. Khan MA, Hristovski IR, Marinaro G, Kosel J. Magnetic Composite Hydrodynamic Pump With Laser-Induced Graphene Electrodes. *IEEE Trans Magn*. 2017;53:1-4.

51. Singh SP, Li Y, Zhang J, Tour JM, Arnusch CJ. Sulfur-Doped Laser-Induced Porous Graphene Derived from Polysulfone-Class Polymers and Membranes. *ACS Nano*. 2018;12(1):289-297. doi:10.1021/acsnano.7b06263

52. Nayak P, Kurra N, Xia C, Alshareef HN. Highly Efficient Laser Scribed Graphene Electrodes for On-Chip Electrochemical Sensing Applications. *Adv Electron Mater*. 2016;2(10):1-11. doi:10.1002/aelm.201600185

53. Zhu C, Tao LQ, Wang Y, et al. Graphene oxide humidity sensor with laser-induced graphene porous electrodes. *Sens Actuators B Chem*. 2020;325:128790. doi:https://doi.org/10.1016/j.snb.2020.128790

54. Tao LQ, Tian H, Liu Y, et al. An intelligent artificial throat with sound-sensing ability based on laser induced graphene. *Nat Commun*. 2017;8(1):14579. doi:10.1038/ncomms14579

55. Stanford MG, Yang K, Chyan Y, Kittrell C, Tour JM. Laser-Induced Graphene for Flexible and Embeddable Gas Sensors. *ACS Nano*. 2019;13(3):3474-3482. doi:10.1021/acsnano.8b09622

56. Rahimi R, Ochoa M, Yu W, Ziaie B. Highly Stretchable and Sensitive Unidirectional Strain Sensor via Laser Carbonization. *ACS Appl Mater Interfaces*. 2015;7(8):4463-4470. doi:10.1021/am509087u

57. Fenzl C, Nayak P, Hirsch T, Wolfbeis OS, Alshareef HN, Baeumner AJ. Laser-Scribed Graphene Electrodes for Aptamer-Based Biosensing. *ACS Sens*. 2017;2(5):616-620. doi:10.1021/acssensors.7b00066

58. Tehrani F, Bavarian B. Facile and scalable disposable sensor based on laser engraved graphene for electrochemical detection of glucose. *Sci Rep*. 2016;6(May):1-10. doi:10.1038/srep27975

59. Zhu Y, Cai H, Ding H, Pan N, Wang X. Fabrication of Low-Cost and Highly Sensitive Graphene-Based Pressure Sensors by Direct Laser Scribing Polydimethylsiloxane. *ACS Appl Mater Interfaces*. 2019;11:6195-6200. doi:10.1021/acsami.8b17085

60. Chyan Y, Ye R, Li Y, Singh SP, Arnusch CJ, Tour JM. Laser-Induced Graphene by Multiple Lasing: Toward Electronics on Cloth, Paper, and Food. *ACS Nano*. 2018;12(3):2176-2183. doi:10.1021/acsnano.7b08539

61. Ye R, Chyan Y, Zhang J, et al. Laser-Induced Graphene Formation on Wood. *Advanced Materials*. 2017;29(37):1702211. doi:https://doi.org/10.1002/adma.201702211

62. Hui X, Xuan X, Kim J, Park JY. A highly flexible and selective dopamine sensor based on Pt-Au nanoparticle-modified laser-induced graphene. *Electrochim Acta*. 2019;328:135066. doi:https://doi.org/10.1016/j.electacta.2019.135066

63. Zhang Z, Song M, Hao J, Wu K, Li C, Hu C. Visible light laser-induced graphene from phenolic resin: A new approach for directly writing graphene-based electrochemical devices on various substrates. *Carbon N Y*. 2018;127:287-296. doi:10.1016/j.carbon.2017.11.014

64. Lei Y, Alshareef AH, Zhao W, Inal S. Laser-Scribed Graphene Electrodes Derived from Lignin for Biochemical Sensing. *ACS Appl Nano Mater*. 2020;3(2):1166-1174. doi:10.1021/acsanm.9b01795

65. Wan Z, Umer M, Lobino M, et al. Laser induced self-N-doped porous graphene as an electrochemical biosensor for femtomolar miRNA detection. *Carbon N Y*. 2020;163:385-394. doi:10.1016/j.carbon.2020.03.043

66. Zhang F, Alhajji E, Lei Y, Kurra N, Alshareef HN. Highly Doped 3D Graphene Na-Ion Battery Anode by Laser Scribing Polyimide Films in Nitrogen Ambient. *Adv Energy Mater*. 2018;8(23):1-9. doi:10.1002/aenm.201800353

67. Ko Y il, Lee G, Kim MJ, et al. Direct Pattern Growth of Carbon Nanomaterials by Laser Scribing on Spin-Coated Cu-PI Composite Films and Their Gas Sensor Application. *Materials*. 2021;14(12):3388. doi:10.3390/ma14123388

68. Cho EC, Chang-Jian CW, Huang JH, et al. Laser scribing of Ag-decorated graphene for high-performance and flexible heaters. *J Taiwan Inst Chem Eng*. 2021;119:224-231. doi:10.1016/j.jtice.2021.02.011

69. Arantes IVS, Ataide VN, Ameku WA, et al. Laser-induced fabrication of gold nanoparticles onto paper substrates and their application on paper-based electroanalytical devices. *Sens Diagn*. 2023;2(1):111-121. doi:10.1039/D2SD00176D

70. Rocha DP, Ataide VN, de Siervo A, et al. Reagentless and sub-minute laser-scribing treatment to produce enhanced disposable electrochemical sensors via additive manufacture. *Chemical Engineering Journal*. 2021;425:130594. doi:https://doi.org/10.1016/j.cej.2021.130594

71. Veloso WB, Ataide VN, Rocha DP, et al. 3D-printed sensor decorated with nanomaterials by CO2 laser ablation and electrochemical treatment for non-enzymatic tyrosine detection. *Microchimica Acta*. 2023;190(2):63. doi:10.1007/s00604-023-05648-8

72. Dubey AK, Yadava V. Laser beam machining—A review. *Int J Mach Tools Manuf*. 2008;48(6):609-628. doi:https://doi.org/10.1016/j.ijmachtools.2007.10.017

73. Ghanam A, Lahcen AA, Beduk T, Alshareef HN, Amine A, Salama KN. Laser scribed graphene: A novel platform for highly sensitive detection of electroactive biomolecules. *Biosens Bioelectron*. 2020;168:112509. doi:https://doi.org/10.1016/j.bios.2020.112509

74. Kurra N, Jiang Q, Nayak P, Alshareef HN. Laser-derived graphene: A three-dimensional printed graphene electrode and its emerging applications. *Nano Today*. 2019;24:81-102. doi:https://doi.org/10.1016/j.nantod.2018.12.003

75. Mendes LF, de Siervo A, Reis de Araujo W, Longo Cesar Paixão TR. Reagentless fabrication of a porous graphene-like electrochemical device from phenolic paper using laser-scribing. *Carbon N Y*. 2020;159:110-118. doi:10.1016/j.carbon.2019.12.016

76. Huang L, Su J, Song Y, Ye R. Laser-Induced Graphene: En Route to Smart Sensing. *Nanomicro Lett*. 2020;12(1):157. doi:10.1007/s40820-020-00496-0

77. Wang F, Wang K, Zheng B, et al. Laser-induced graphene: preparation, functionalization and applications. *Materials Technology*. 2018;33(5):340-356. doi:10.1080/10667857.2018.1447265

78. Santos NF, Pereira SO, Moreira A, et al. IR and UV Laser-Induced Graphene: Application as Dopamine Electrochemical Sensors. *Adv Mater Technol*. 2021;6(6):2100007. doi:https://doi.org/10.1002/admt.202100007

79. Guo Y, Zhang C, Chen Y, Nie Z. Research Progress on the Preparation and Applications of Laser-Induced Graphene Technology. *Nanomaterials*. 2022;12(14). doi:10.3390/nano12142336

80. Chen Y, Long J, Xie B, et al. One-Step Ultraviolet Laser-Induced Fluorine-Doped Graphene Achieving Superhydrophobic Properties and Its Application in Deicing. *ACS Appl Mater Interfaces*. 2022;14(3):4647-4655. doi:10.1021/acsami.1c18559

81. Lamberti A, Perrucci F, Caprioli M, et al. New insights on laser-induced graphene electrodes for flexible supercapacitors: tunable morphology and physical properties. *Nanotechnology*. 2017;28(17):174002. doi:10.1088/1361-6528/aa6615

82. Beduk T, Ait Lahcen A, Tashkandi N, Salama KN. One-step electrosynthesized molecularly imprinted polymer on laser scribed graphene bisphenol a sensor. *Sens Actuators B Chem*. 2020;314:128026. doi:https://doi.org/10.1016/j.snb.2020.128026

83. Soares RRA, Hjort RG, Pola CC, et al. Laser-Induced Graphene Electrochemical Immunosensors for Rapid and Label-Free Monitoring of Salmonella enterica in Chicken Broth. *ACS Sens*. 2020;5(7):1900-1911. doi:10.1021/acssensors.9b02345

84. Barman SC, Zahed MdA, Sharifuzzaman Md, et al. A Polyallylamine Anchored Amine-Rich Laser-Ablated Graphene Platform for Facile and Highly Selective Electrochemical IgG Biomarker Detection. *Adv Funct Mater*. 2020;30(14):1907297. doi:https://doi.org/10.1002/adfm.201907297

85. de Lima LF, de Araujo WR. Laser-scribed graphene on polyetherimide substrate: an electrochemical sensor platform for forensic determination of xylazine in urine and beverage samples. *Microchimica Acta*. 2022;189(12):465. doi:10.1007/s00604-022-05566-1

86. Wang Y, Guo H, Yuan M, Yu J, Wang Z, Chen X. One-step laser synthesis platinum nanostructured 3D porous graphene: A flexible dual-functional electrochemical biosensor for glucose and pH detection in human perspiration. *Talanta*. 2023;257:124362. doi:https://doi.org/10.1016/j.talanta.2023.124362

87. Vivaldi F, Dallinger A, Poma N, et al. Sweat analysis with a wearable sensing platform based on laser-induced graphene. *APL Bioeng*. 2022;6(3):036104. doi:10.1063/5.0093301

88. Min J, Sempionatto JR, Teymourian H, Wang J, Gao W. Wearable electrochemical biosensors in North America. *Biosens Bioelectron*. 2021;172:112750. doi:https://doi.org/10.1016/j.bios.2020.112750

89. Mahato K, Wang J. Electrochemical sensors: From the bench to the skin. *Sens Actuators B Chem*. 2021;344:130178. doi:https://doi.org/10.1016/j.snb.2021.130178

90. Mohan AMV, Rajendran V, Mishra RK, Jayaraman M. Recent advances and perspectives in sweat based wearable electrochemical sensors. *TrAC Trends in Analytical Chemistry*. 2020;131:116024. doi:https://doi.org/10.1016/j.trac.2020.116024

91. Teymourian H, Parrilla M, Sempionatto JR, et al. Wearable Electrochemical Sensors for the Monitoring and Screening of Drugs. *ACS Sens*. 2020;5(9):2679-2700. doi:10.1021/acssensors.0c01318

92. Heikenfeld J, Jajack A, Feldman B, et al. Accessing analytes in biofluids for peripheral biochemical monitoring. *Nat Biotechnol*. 2019;37(4):407-419. doi:10.1038/s41587-019-0040-3

93. De la Paz E, Barfidokht A, Rios S, Brown C, Chao E, Wang J. Extended Noninvasive Glucose Monitoring in the Interstitial Fluid Using an Epidermal Biosensing Patch. *Anal Chem*. 2021;93(37):12767-12775. doi:10.1021/acs.analchem.1c02887

94. Dardano P, Rea I, De Stefano L. Microneedles-based electrochemical sensors: New tools for advanced biosensing. *Curr Opin Electrochem*. 2019;17:121-127. doi:https://doi.org/10.1016/j.coelec.2019.05.012

95. Larrañeta E, Lutton REM, Woolfson AD, Donnelly RF. Microneedle arrays as transdermal and intradermal drug delivery systems: Materials science, manufacture and commercial development. *Materials Science and Engineering: R: Reports*. 2016;104:1-32. doi:https://doi.org/10.1016/j.mser.2016.03.001

96. Madden J, O'Mahony C, Thompson M, O'Riordan A, Galvin P. Biosensing in dermal interstitial fluid using microneedle based electrochemical devices. *Sens Biosensing Res*. 2020;29:100348. doi:https://doi.org/10.1016/j.sbsr.2020.100348

97. Yoon Y, Lee GS, Yoo K, Lee JB. Fabrication of a Microneedle/CNT Hierarchical Micro/Nano Surface Electrochemical Sensor and Its In-Vitro Glucose Sensing Characterization. *Sensors*. 2013;13(12):16672-16681. doi:10.3390/s131216672

98. Li Y, Aoude H. Blast response of beams built with high-strength concrete and high-strength ASTM A1035 bars. *Int J Impact Eng*. 2019;130:41-67. doi:https://doi.org/10.1016/j.ijimpeng.2019.02.007

99. Chen Z, Ye R, Yang J, et al. Rapidly Fabricated Microneedle Arrays Using Magnetorheological Drawing Lithography for Transdermal Drug Delivery. *ACS Biomater Sci Eng*. 2019;5(10):5506-5513. doi:10.1021/acsbiomaterials.9b00919

100. Skaria E, Patel BA, Flint MS, Ng KW. Poly(lactic acid)/Carbon Nanotube Composite Microneedle Arrays for Dermal Biosensing. *Anal Chem*. 2019;91(7):4436-4443. doi:10.1021/acs.analchem.8b04980

101. Krieger KJ, Bertollo N, Dangol M, Sheridan JT, Lowery MM, O'Cearbhaill ED. Simple and customizable method for fabrication of high-aspect ratio microneedle molds using low-cost 3D printing. *Microsyst Nanoeng*. 2019;5(1):42. doi:10.1038/s41378-019-0088-8

102. García-Guzmán JJ, Pérez-Ràfols C, Cuartero M, Crespo GA. Microneedle based electrochemical (Bio)Sensing: Towards decentralized and continuous health status monitoring. *TrAC Trends in Analytical Chemistry*. 2021;135:116148. doi:https://doi.org/10.1016/j.trac.2020.116148

103. Erdem Ö, Eş I, Akceoglu GA, Saylan Y, Inci F. Recent Advances in Microneedle-Based Sensors for Sampling, Diagnosis and Monitoring of Chronic Diseases. *Biosensors (Basel)*. 2021;11(9). doi:10.3390/bios11090296

104. Goud KY, Mahato K, Teymourian H, Longardner K, Litvan I, Wang J. Wearable electrochemical microneedle sensing platform for real-time continuous interstitial fluid monitoring of apomorphine: Toward Parkinson

management. *Sens Actuators B Chem*. 2022;354:131234. doi:https://doi.org/10.1016/j.snb.2021.131234

105. Abdullah H, Phairatana T, Jeerapan I. Tackling the challenges of developing microneedle-based electrochemical sensors. *Microchimica Acta*. 2022;189(11):440. doi:10.1007/s00604-022-05510-3
106. Mahato K, Wang J. Electrochemical sensors: From the bench to the skin. *Sens Actuators B Chem*. 2021;344(April):130178. doi:10.1016/j.snb.2021.130178
107. Promphet N, Ummartyotin S, Ngeontae W, Puthongkham P, Rodthongkum N. Non-invasive wearable chemical sensors in real-life applications. *Anal Chim Acta*. 2021;(xxxx):338643. doi:10.1016/j.aca.2021.338643
108. Min J, Sempionatto JR, Teymourian H, Wang J, Gao W. Wearable electrochemical biosensors in North America. *Biosens Bioelectron*. 2021;172:112750. doi:10.1016/j.bios.2020.112750
109. Wang S, Chen S, Shang K, Gao X, Wang X. Sensitive electrochemical detection of cholesterol using a portable paper sensor based on the synergistic effect of cholesterol oxidase and nanoporous gold. *Int J Biol Macromol*. 2021;189:356-362. doi:https://doi.org/10.1016/j.ijbiomac.2021.08.145
110. Torrente-Rodríguez RM, Tu J, Yang Y, et al. Investigation of Cortisol Dynamics in Human Sweat Using a Graphene-Based Wireless mHealth System. *Matter*. 2020;2(4):921-937. doi:https://doi.org/10.1016/j.matt.2020.01.021

111. Chen TW, Rajaji U, Chen SM, Li YL, Ramalingam RJ. Ultrasound-assisted synthesis of α-MnS (alabandite) nanoparticles decorated reduced graphene oxide hybrids: Enhanced electrocatalyst for electrochemical detection of Parkinson's disease biomarker. *Ultrason Sonochem*. 2019;56:378-385. doi:https://doi.org/10.1016/j.ultsonch.2019.04.010

112. Bandookwala M, Sengupta P. 3-Nitrotyrosine: a versatile oxidative stress biomarker for major neurodegenerative diseases. *International Journal of Neuroscience*. 2020;130(10):1047-1062. doi:10.1080/00207454.2020.1713776

113. Moura SL, Martín CG, Martí M, Pividori MI. Electrochemical immunosensing of nanovesicles as biomarkers for breast cancer. *Biosens Bioelectron*. 2020;150:111882. doi:https://doi.org/10.1016/j.bios.2019.111882

114. Yang Y, Song Y, Bo X, et al. A laser-engraved wearable sensor for sensitive detection of uric acid and tyrosine in sweat. *Nat Biotechnol*. 2020;38(2):217-224. doi:10.1038/s41587-019-0321-x

115. Goud KY, Moonla C, Mishra RK, et al. Wearable Electrochemical Microneedle Sensor for Continuous Monitoring of Levodopa: Toward Parkinson Management. *ACS Sens*. 2019;4(8):2196-2204. doi:10.1021/acssensors.9b01127

116. Mugo SM, Lu W, Wood M, Lemieux S. Wearable microneedle dual electrochemical sensor for simultaneous pH and cortisol detection in sweat. *Electrochemical Science Advances*. 2022;2(1):e2100039. doi:https://doi.org/10.1002/elsa.202100039

117. Kiang TKL, Schmitt V, Ensom MHH, Chua B, Häfeli UO. Therapeutic drug monitoring in interstitial fluid: A feasibility study using a comprehensive panel of drugs. *J Pharm Sci*. 2012;101(12):4642-4652. doi:https://doi.org/10.1002/jps.23309

118. Mishra RK, Goud KY, Li Z, et al. Continuous Opioid Monitoring along with Nerve Agents on a Wearable Microneedle Sensor Array. *J Am Chem Soc*. 2020;142(13):5991-5995. doi:10.1021/jacs.0c01883

119. Tiwari N, Chatterjee S, Kaswan K, Chung JH, Fan KP, Lin ZH. Recent advancements in sampling, power management strategies and development in applications for non-invasive wearable electrochemical sensors. *Journal of Electroanalytical Chemistry*. 2022;907:116064. doi:https://doi.org/10.1016/j.jelechem.2022.116064

120. Ghanam A, Lahcen AA, Beduk T, Alshareef HN, Amine A, Salama KN. Laser scribed graphene: A novel platform for highly sensitive detection of electroactive biomolecules. *Biosens Bioelectron*. 2020;168:112509. doi:https://doi.org/10.1016/j.bios.2020.112509

121. Ma W, Zhu J, Wang Z, Song W, Cao G. Recent advances in preparation and application of laser-induced graphene in energy storage devices. *Mater Today Energy*. 2020;18:100569. doi:https://doi.org/10.1016/j.mtener.2020.100569

122. Sharma S, Kamath R, Madou M. Porous glassy carbon formed by rapid pyrolysis of phenol-formaldehyde resins and its performance as electrode material for electrochemical double layer capacitors. *J Anal Appl Pyrolysis*. 2014;108:12-18. doi:https://doi.org/10.1016/j.jaap.2014.05.025

123. Xue R, Yan J, Liu X, Tian Y, Yi B. Effect of activation on the carbon fibers from phenol–formaldehyde resins for electrochemical supercapacitors. *J Appl Electrochem*. 2011;41:1357-1366.

124. Tang K, Zhang A, Ge T, Liu X, Tang X, Li Y. Research progress on modification of phenolic resin. *Mater Today Commun*. 2021;26:101879. doi:https://doi.org/10.1016/j.mtcomm.2020.101879

125. Kim YM, Han TU, Watanabe C, et al. Analytical pyrolysis of waste paper laminated phenolic-printed circuit board (PLP-PCB). *J Anal Appl Pyrolysis*. 2015;115:87-95. doi:https://doi.org/10.1016/j.jaap.2015.06.013

126. RAYMING Group Subordinate Enterprise. PHENOLIC PCB – THE ADVANTAGES, USES AND MANUFACTURING PROCESS.

127. Ingerslev F, Vaclavik E, Halling-Sørensen B. Pharmaceuticals and personal care products - A source of endocrine disruption in the environment? 2003;75(11-12):1881-1893. doi:doi:10.1351/pac200375111881

128. Ciślak M, Kruszelnicka I, Zembrzuska J, Ginter-Kramarczyk D. Estrogen pollution of the European aquatic environment: A critical review. *Water Res*. 2023;229:119413. doi:https://doi.org/10.1016/j.watres.2022.119413

129. Torres NH, de Oliveira Santiago Santos G, Romanholo Ferreira LF, Américo-Pinheiro JHP, Eguiluz KIB, Salazar-Banda GR. Environmental aspects of hormones estriol, 17β-estradiol and 17α-ethinylestradiol: Electrochemical processes as next-generation technologies for their removal in water matrices. *Chemosphere*. 2021;267:128888. doi:https://doi.org/10.1016/j.chemosphere.2020.128888

130. Moraes FC, Rossi B, Donatoni MC, de Oliveira KT, Pereira EC. Sensitive determination of 17β-estradiol in river water using a graphene based electrochemical sensor. *Anal Chim Acta*. 2015;881:37-43. doi:https://doi.org/10.1016/j.aca.2015.04.043

131. da Silva DN, Pereira AC. Development of a Chemically Modified Electrode with Magnetic Molecularly Imprinted Polymer (MagMIP) for 17-β-Estradiol Determination in Water Samples. *Electrochem*. 2022;3(4):809-819. doi:10.3390/electrochem3040053

132. Moraes FC, Rossi B, Donatoni MC, de Oliveira KT, Pereira EC. Sensitive determination of 17β-estradiol in river water using a graphene based electrochemical sensor. *Anal Chim Acta*. 2015;881:37-43. doi:10.1016/j.aca.2015.04.043

133. Tanimoto S, Ichimura A. Discrimination of Inner- and Outer-Sphere Electrode Reactions by Cyclic Voltammetry Experiments. *J Chem Educ*. 2013;90(6):778-781. doi:10.1021/ed200604m

134. Brownson DAC, Varey SA, Hussain F, Haigh SJ, Banks CE. Electrochemical properties of CVD grown pristine graphene: monolayer- vs. quasi-graphene. *Nanoscale*. 2014;6(3):1607-1621. doi:10.1039/C3NR05643K

135. Casero E, Parra-Alfambra AM, Petit-Domínguez MD, Pariente F, Lorenzo E, Alonso C. Differentiation between graphene oxide and reduced graphene by electrochemical impedance spectroscopy (EIS). *Electrochem commun*. 2012;20(1):63-66. doi:10.1016/j.elecom.2012.04.002

136. Randviir EP, Banks CE. Electrochemical impedance spectroscopy: an overview of bioanalytical applications. *Anal Methods*. 2013;5(5):1098-1115. doi:10.1039/C3AY26476A

137. Selva TMG, de Araujo WR, Bacil RP, Paixão TRLC. Study of Electrochemical Oxidation and Quantification of the Pesticide Pirimicarb Using a Boron-Doped Diamond Electrode. *Electrochim Acta*. 2017;246:588-596. doi:10.1016/j.electacta.2017.06.051

138. Akyazi T, Basabe-Desmonts L, Benito-Lopez F. Review on microfluidic paper-based analytical devices towards commercialisation. *Anal Chim Acta*. 2018;1001:1-17. doi:10.1016/j.aca.2017.11.010

139. Mahadeva SK, Walus K, Stoeber B. Paper as a platform for sensing applications and other devices: A review. *ACS Appl Mater Interfaces*. 2015;7(16):8345-8362. doi:10.1021/acsami.5b00373

140. Ferrari AC, Basko DM. Raman spectroscopy as a versatile tool for studying the properties of graphene. *Nat Nanotechnol*. 2013;8(4):235-246. doi:10.1038/nnano.2013.46

141. Hodkiewicz J. Characterizing Carbon Materials with Raman Spectroscopy - Application Note: 51901. *Prog Mater Sci*. 2010;50. doi:10.1088/0022-3727/46/12/122001

142. Kakihana M, Osada M. Chapter 18 - Raman Spectroscopy as a Characterization Tool for Carbon Materials. In: YASUDA E ichi, INAGAKI M, KANEKO K, ENDO M, OYA A, TANABE Y, eds. *Carbon Alloys*. Elsevier Science; 2003:285-298. doi:https://doi.org/10.1016/B978-008044163-4/50018-8

143. Pumera M, Ambrosi A, Bonanni A, Chng ELK, Poh HL. Graphene for electrochemical sensing and biosensing. *TrAC - Trends in Analytical Chemistry*. 2010;29(9):954-965. doi:10.1016/j.trac.2010.05.011

144. Mariotti D, Švrček V, Mathur A, Dickinson C, Matsubara K, Kondo M. Carbon nanotube growth activated by quantum-confined silicon nanocrystals. *J Phys D Appl Phys*. 2013;46(12):122001. doi:10.1088/0022-3727/46/12/122001

145. Sherwood PMA. Surface analysis of carbon and carbon fibers for composites. *J Electron Spectros Relat Phenomena*. 1996;81(3):319-342. doi:https://doi.org/10.1016/0368-2048(95)02529-4

146. Desimoni E, Casella GI, Morone A, Salvi AM. XPS determination of oxygen-containing functional groups on carbon-fibre surfaces and the cleaning of these surfaces. *Surface and Interface Analysis*. 1990;15(10):627-634. doi:https://doi.org/10.1002/sia.740151011

147. Oda H, Yamashita A, Minoura S, Okamoto M, Morimoto T. Modification of the oxygen-containing functional group on activated carbon fiber in electrodes of an electric double-layer capacitor. *J Power Sources*. 2006;158(2):1510-1516. doi:https://doi.org/10.1016/j.jpowsour.2005.10.061

148. Pandolfo AG, Hollenkamp AF. Carbon properties and their role in supercapacitors. *J Power Sources*. 2006;157(1):11-27. doi:https://doi.org/10.1016/j.jpowsour.2006.02.065

149. Rajaura RS, Srivastava S, Sharma V, et al. Role of interlayer spacing and functional group on the hydrogen storage properties of graphene oxide

and reduced graphene oxide. *Int J Hydrogen Energy*. 2016;41(22):9454-9461. doi:https://doi.org/10.1016/j.ijhydene.2016.04.115

150. Qiu R, Yuan S, Xiao J, et al. Effects of Edge Functional Groups on Water Transport in Graphene Oxide Membranes. *ACS Appl Mater Interfaces*. 2019;11(8):8483-8491. doi:10.1021/acsami.9b00492
151. Tong WL, Hung YM, Yu H, et al. Ultrafast Water Permeation in Graphene Nanostructures Anomalously Enhances Two-Phase Heat Transfer. *Adv Mater Interfaces*. 2018;5(13):1800286. doi:https://doi.org/10.1002/admi.201800286
152. Ji X, Dong Y, Nguyen TT, Chen X, Guo M. Environment-friendly wood fibre composite with high bonding strength and water resistance. *R Soc Open Sci*. 2018;5(4):172002. doi:10.1098/rsos.172002
153. Lin J, Peng Z, Liu Y, et al. Laser-induced porous graphene films from commercial polymers. *Nat Commun*. 2014;5(1):5714. doi:10.1038/ncomms6714
154. Noviana E, McCord CP, Clark KM, Jang I, Henry CS. Electrochemical paper-based devices: sensing approaches and progress toward practical applications. *Lab Chip*. 2020;20(1):9-34. doi:10.1039/C9LC00903E
155. Salcı B, Biryol I. Voltammetric investigation of β-estradiol. *J Pharm Biomed Anal*. 2002;28(3):753-759. doi:https://doi.org/10.1016/S0731-7085(01)00676-8
156. Mohan JM, Amreen K, Javed A, Dubey SK, Goel S. Emerging trends in miniaturized and microfluidic electrochemical sensing platforms. *Curr Opin Electrochem*. 2022;33:100930. doi:https://doi.org/10.1016/j.coelec.2021.100930

157. Keyvani F, Debnath N, Ayman Saleh M, Poudineh M. An integrated microfluidic electrochemical assay for cervical cancer detection at point-of-care testing. *Nanoscale*. 2022;14(18):6761-6770. doi:10.1039/D1NR08252C

158. Podunavac I, Djocos M, Vejin M, et al. 3D-Printed Microfluidic Chip for Real-Time Glucose Monitoring in Liquid Analytes. *Micromachines (Basel)*. 2023;14(3). doi:10.3390/mi14030503

159. Wisitsoraat A, Sritongkham P, Karuwan C, Phokharatkul D, Maturos T, Tuantranont A. Fast cholesterol detection using flow injection microfluidic device with functionalized carbon nanotubes based electrochemical sensor. *Biosens Bioelectron*. 2010;26(4):1514-1520. doi:https://doi.org/10.1016/j.bios.2010.07.101

160. Mettakoonpitak J, Khongsoun K, Wongwan N, et al. Simple biodegradable plastic screen-printing for microfluidic paper-based analytical devices. *Sens Actuators B Chem*. 2021;331:129463. doi:https://doi.org/10.1016/j.snb.2021.129463

161. Fiore L, Mazzaracchio V, Serani A, et al. Microfluidic paper-based wearable electrochemical biosensor for reliable cortisol detection in sweat. *Sens Actuators B Chem*. 2023;379:133258. doi:https://doi.org/10.1016/j.snb.2022.133258

162. da Silva ENT, Ferreira VS, Lucca BG. Rapid and inexpensive method for the simple fabrication of PDMS-based electrochemical sensors for detection in microfluidic devices. *Electrophoresis*. 2019;40(9):1322-1330. doi:https://doi.org/10.1002/elps.201800478

163. Nie Z, Nijhuis CA, Gong J, et al. Electrochemical sensing in paper-based microfluidic devices †. 2010;(c):477-483. doi:10.1039/b917150a

164. Ruecha N, Lee J, Chae H, et al. Paper-Based Digital Microfluidic Chip for Multiple Electrochemical Assay Operated by a Wireless Portable Control System. *Adv Mater Technol*. 2017;2(3):1600267. doi:https://doi.org/10.1002/admt.201600267

165. Wu Y, Xue P, Hui KM, Kang Y. A paper-based microfluidic electrochemical immunodevice integrated with amplification-by-polymerization for the ultrasensitive multiplexed detection of cancer biomarkers. *Biosens Bioelectron*. 2014;52:180-187. doi:https://doi.org/10.1016/j.bios.2013.08.039

166. Carvalhal RF, Simão Kfouri M, de Oliveira Piazetta MH, Gobbi AL, Kubota LT. Electrochemical Detection in a Paper-Based Separation Device. *Anal Chem*. 2010;82(3):1162-1165. doi:10.1021/ac902647r

167. Santhiago M, Kubota LT. A new approach for paper-based analytical devices with electrochemical detection based on graphite pencil electrodes. *Sens Actuators B Chem*. 2013;177:224-230. doi:https://doi.org/10.1016/j.snb.2012.11.002

168. Pradela-Filho LA, Araújo DAG, Takeuchi RM, Santos AL. Nail polish and carbon powder: An attractive mixture to prepare paper-based electrodes. *Electrochim Acta*. 2017;258:786-792. doi:https://doi.org/10.1016/j.electacta.2017.11.127

169. Pradela-Filho LA, Andreotti IAA, Carvalho JHS, et al. Glass varnish-based carbon conductive ink: A new way to produce disposable electrochemical

sensors. *Sens Actuators B Chem*. 2020;305:127433. doi:https://doi.org/10.1016/j.snb.2019.127433

170. Freitas RC, Orzari LO, Ferreira LMC, et al. Electrochemical determination of melatonin using disposable self-adhesive inked paper electrode. *Journal of Electroanalytical Chemistry*. 2021;897:115550. doi:https://doi.org/10.1016/j.jelechem.2021.115550
171. Araújo DAG, Camargo JR, Pradela-Filho LA, et al. A lab-made screen-printed electrode as a platform to study the effect of the size and functionalization of carbon nanotubes on the voltammetric determination of caffeic acid. *Microchemical Journal*. 2020;158:105297. doi:https://doi.org/10.1016/j.microc.2020.105297
172. Noviana E, Ozer T, Carrell CS, et al. Microfluidic Paper-Based Analytical Devices: From Design to Applications. *Chem Rev*. 2021;121(19):11835-11885. doi:10.1021/acs.chemrev.0c01335
173. Nesakumar N, Kesavan S, Li CZ, Alwarappan S. Microfluidic Electrochemical Devices for Biosensing. *J Anal Test*. 2019;3(1):3-18. doi:10.1007/s41664-019-0083-y
174. Channon RB, Menger RF, Wang W, et al. Design and application of a self-pumping microfluidic staggered herringbone mixer. *Microfluid Nanofluidics*. 2021;25(4):31. doi:10.1007/s10404-021-02426-x
175. Griesche C, Hoecherl K, Baeumner AJ. Substrate-Independent Laser-Induced Graphene Electrodes for Microfluidic Electroanalytical Systems. *ACS Appl Nano Mater*. 2021;4(3):3114-3121. doi:10.1021/acsanm.1c00299

176. Nasraoui S, Al-Hamry A, Teixeira PR, et al. Electrochemical sensor for nitrite detection in water samples using flexible laser-induced graphene electrodes functionalized by CNT decorated by Au nanoparticles. *Journal of Electroanalytical Chemistry*. 2021;880:114893. doi:https://doi.org/10.1016/j.jelechem.2020.114893

177. Nayak P, Kurra N, Xia C, Alshareef HN. Highly Efficient Laser Scribed Graphene Electrodes for On-Chip Electrochemical Sensing Applications. *Adv Electron Mater*. 2016;2(10):1600185. doi:https://doi.org/10.1002/aelm.201600185

178. Getachew BA, Bergsman DS, Grossman JC. Laser-Induced Graphene from Polyimide and Polyethersulfone Precursors as a Sensing Electrode in Anodic Stripping Voltammetry. *ACS Appl Mater Interfaces*. 2020;12(43):48511-48517. doi:10.1021/acsami.0c11725

179. Pradela-Filho LA, Noviana E, Araújo DAG, Takeuchi RM, Santos AL, Henry CS. Rapid Analysis in Continuous-Flow Electrochemical Paper-Based Analytical Devices. *ACS Sens*. 2020;5(1):274-281. doi:10.1021/acssensors.9b02298

180. Mutyala S, Mathiyarasu J. A reagentless non-enzymatic hydrogen peroxide sensor presented using electrochemically reduced graphene oxide modified glassy carbon electrode. *Materials Science and Engineering: C*. 2016;69:398-406. doi:https://doi.org/10.1016/j.msec.2016.06.069

181. Burke M, Larrigy C, Vaughan E, et al. Fabrication and Electrochemical Properties of Three-Dimensional (3D) Porous Graphitic and Graphenelike

Electrodes Obtained by Low-Cost Direct Laser Writing Methods. *ACS Omega*. 2020;5(3):1540-1548. doi:10.1021/acsomega.9b03418

182. Bobinger MR, Romero FJ, Salinas-Castillo A, et al. Flexible and robust laser-induced graphene heaters photothermally scribed on bare polyimide substrates. *Carbon N Y*. 2019;144:116-126. doi:https://doi.org/10.1016/j.carbon.2018.12.010
183. Wang P Sen, Wittberg TN, Wolf JD. A characterization of Kapton polyimide by X-ray photoelectron spectroscopy and energy dispersive spectroscopy. *J Mater Sci*. 1988;23(11):3987-3991. doi:10.1007/BF01106825
184. Romero FJ, Salinas-Castillo A, Rivadeneyra A, et al. In-Depth Study of Laser Diode Ablation of Kapton Polyimide for Flexible Conductive Substrates. *Nanomaterials*. 2018;8(7). doi:10.3390/nano8070517
185. Zhang W, Lei Y, Ming F, Jiang Q, Costa PMFJ, Alshareef HN. Lignin Laser Lithography: A Direct-Write Method for Fabricating 3D Graphene Electrodes for Microsupercapacitors. *Adv Energy Mater*. 2018;8(27):1801840. doi:https://doi.org/10.1002/aenm.201801840
186. Zeng DW, Yung KC, Xie CS. XPS investigation of the chemical characteristics of Kapton films ablated by a pulsed TEA CO2 laser. *Surf Coat Technol*. 2002;153(2):210-216. doi:https://doi.org/10.1016/S0257-8972(01)01696-6
187. Brett C, Brett AMO. Electrochemistry: principles, methods, and applications. *(No Title)*. Published online 1993.
188. Teixeira D, Fernandes R, Prudêncio C, Vieira M. 3-Nitrotyrosine quantification methods: Current concepts and future challenges.

*Biochimie*. 2016;125:1-11. doi:https://doi.org/10.1016/j.biochi.2016.02.011

189. Martins G V, Marques AC, Fortunato E, Sales MGF. Wax-printed paper-based device for direct electrochemical detection of 3-nitrotyrosine. *Electrochim Acta*. 2018;284:60-68. doi:https://doi.org/10.1016/j.electacta.2018.07.150
190. Roy E, Patra S, Madhuri R, Sharma PK. Developing electrochemical sensor for point-of-care diagnostics of oxidative stress marker using imprinted bimetallic Fe/Pd nanoparticle. *Talanta*. 2015;132:406-415. doi:https://doi.org/10.1016/j.talanta.2014.09.033
191. MacDonald SM, Roscoe SG. Electrochemical oxidation reactions of tyrosine, tryptophan and related dipeptides. *Electrochim Acta*. 1997;42(8):1189-1200. doi:https://doi.org/10.1016/S0013-4686(96)00285-X
192. Yokoyama K, Uhlin U, Stubbe J. Site-Specific Incorporation of 3-Nitrotyrosine as a Probe of pKa Perturbation of Redox-Active Tyrosines in Ribonucleotide Reductase. *J Am Chem Soc*. 2010;132(24):8385-8397. doi:10.1021/ja101097p
193. Roy E, Patra S, Madhuri R, Sharma PK. Developing electrochemical sensor for point-of-care diagnostics of oxidative stress marker using imprinted bimetallic Fe/Pd nanoparticle. *Talanta*. 2015;132:406-415. doi:https://doi.org/10.1016/j.talanta.2014.09.033
194. Wang S, Sun G, Chen Z, et al. Constructing a novel composite of molecularly imprinted polymer-coated AuNPs electrochemical sensor for

the determination of 3-nitrotyrosine. *Electrochim Acta*. 2018;259:893-902. doi:https://doi.org/10.1016/j.electacta.2017.11.033

195. Govindasamy M, Manavalan S, Chen SM, Umamaheswari R, Chen TW. Determination of oxidative stress biomarker 3-nitro-l-tyrosine using CdWO4 nanodots decorated reduced graphene oxide. *Sens Actuators B Chem*. 2018;272:274-281. doi:https://doi.org/10.1016/j.snb.2018.05.138
196. Chen SM, Umamaheswari R, Mani G, et al. Hierarchically structured CuFe2O4 ND@RGO composite for the detection of oxidative stress biomarker in biological fluids. *Inorg Chem Front*. 2018;5(4):944-950. doi:10.1039/C7QI00799J
197. Zhai H, Wang S, Zhou J, et al. A Simple and Sensitive Electrochemical Sensor for 3-Nitrotyrosine Based on Electrochemically Anodic Pretreated Glassy Carbon Electrode in Anionic Surfactant Medium. *J Electrochem Soc*. 2019;166(15):B1426. doi:10.1149/2.0281915jes
198. Martins G V, Marques AC, Fortunato E, Sales MGF. Paper-based (bio)sensor for label-free detection of 3-nitrotyrosine in human urine samples using molecular imprinted polymer. *Sens Biosensing Res*. 2020;28:100333. doi:https://doi.org/10.1016/j.sbsr.2020.100333
199. Maheshwaran S, Akilarasan M, Chen SM, et al. An Ultra-sensitive Electrochemical Sensor for the Detection of Oxidative Stress Biomarker 3-Nitro-l-tyrosine in Human Blood Serum and Saliva Samples Based on Reduced Graphene Oxide Entrapped Zirconium (IV) Oxide. *J Electrochem Soc*. 2020;167(6):66517. doi:10.1149/1945-7111/ab847d
200. Ju J, Liu X, Yu JJ, Sun K, Fathi F, Zeng X. Electrochemistry at Bimetallic Pd/Au Thin Film Surfaces for Selective Detection of Reactive Oxygen

Species and Reactive Nitrogen Species. *Anal Chem*. 2020;92(9):6538-6547. doi:10.1021/acs.analchem.0c00140

201. Martins G V, Riveiro A, Chiussi S, Sales MGF. Flexible sensing devices integrating molecularly-imprinted polymers for the detection of 3-nitrotyrosine biomarker. *Biosens Bioelectron X*. 2022;10:100107. doi:https://doi.org/10.1016/j.biosx.2022.100107
202. Samoson K, Soleh A, Saisahas K, et al. Facile fabrication of a flexible laser induced gold nanoparticle/chitosan/ porous graphene electrode for uric acid detection. *Talanta*. 2022;243:123319. doi:https://doi.org/10.1016/j.talanta.2022.123319
203. Ji D, Liu Z, Liu L, et al. Smartphone-based integrated voltammetry system for simultaneous detection of ascorbic acid, dopamine, and uric acid with graphene and gold nanoparticles modified screen-printed electrodes. *Biosens Bioelectron*. 2018;119:55-62. doi:https://doi.org/10.1016/j.bios.2018.07.074
204. Zhang YM, Xu PL, Zeng Q, Liu YM, Liao X, Hou MF. Magnetism-assisted modification of screen printed electrode with magnetic multi-walled carbon nanotubes for electrochemical determination of dopamine. *Materials Science and Engineering: C*. 2017;74:62-69. doi:https://doi.org/10.1016/j.msec.2017.01.005
205. Paixão GA, Souza TG, Pradela Filho LA, et al. Low-cost conductive films based on graphite and cellulose acetate as promising electroanalytical platforms. *Polym Adv Technol*. 2021;32(9):3714-3723. doi:https://doi.org/10.1002/pat.5391

206. Kivlehan F, Chaum E, Lindner E. Propofol detection and quantification in human blood: the promise of feedback controlled, closed-loop anesthesia. *Analyst*. 2015;140(1):98-106. doi:10.1039/C4AN01483A

207. Ferrier DC, Kiely J, Luxton R. Propofol detection for monitoring of intravenous anaesthesia: a review. *J Clin Monit Comput*. 2022;36(2):315-323. doi:10.1007/s10877-021-00738-5

208. Akbar M, Agah M. A Microfabricated Propofol Trap for Breath-Based Anesthesia Depth Monitoring. *Journal of Microelectromechanical Systems*. 2013;22(2):443-451. doi:10.1109/JMEMS.2012.2227949

209. Ayad MM, Belal F, Hosney MM, Elmansi H, Elsayed N. Simultaneous HPLC Determination of Cisatracurium and Propofol in Human Plasma via Fluorometric Detection. *J Chromatogr Sci*. 2018;56(6):524-530. doi:10.1093/chromsci/bmy027

210. Sørensen LK, Hasselstrøm JB. Simultaneous determination of propofol and its glucuronide in whole blood by liquid chromatography–electrospray tandem mass spectrometry and the influence of sample storage conditions on the reliability of the test results. *J Pharm Biomed Anal*. 2015;109:158-163. doi:https://doi.org/10.1016/j.jpba.2015.02.035

211. Vaiano F, Serpelloni G, Focardi M, Fioravanti A, Mari F, Bertol E. LC–MS/MS and GC–MS methods in propofol detection: Evaluation of the two analytical procedures. *Forensic Sci Int*. 2015;256:1-6. doi:https://doi.org/10.1016/j.forsciint.2015.07.013

212. Li L, Li Y. Study of azo-coupling derivatization by sequential injection coupled with spectrophotometric optical fibre detection for propofol

analysis. *Analytical Methods*. 2016;8(32):6176-6184. doi:10.1039/C6AY01047D

213. Li L, Ding H, Di B, Li W, Chen J. Rapid detection of propofol in whole blood using an automated on-line molecularly imprinted pretreatment coupled with optical fibre detection. *Analyst*. 2012;137(23):5632-5638. doi:10.1039/C2AN35523J

214. Langmaier J, Garay F, Kivlehan F, Chaum E, Lindner E. Electrochemical quantification of 2,6-diisopropylphenol (propofol). *Anal Chim Acta*. 2011;704(1):63-67. doi:https://doi.org/10.1016/j.aca.2011.08.003

215. Yang X, Kirsch J, Fergus J, Simonian A. Modeling analysis of electrode fouling during electrolysis of phenolic compounds. *Electrochim Acta*. 2013;94:259-268. doi:https://doi.org/10.1016/j.electacta.2013.01.019

216. Hong CC, Lin CC, Hong CL, Lin ZX, Chung MH, Hsieh PW. Handheld analyzer with on-chip molecularly-imprinted biosensors for electrical detection of propofol in plasma samples. *Biosens Bioelectron*. 2016;86:623-629. doi:https://doi.org/10.1016/j.bios.2016.07.032

217. Stradolini F, Kilic T, Taurino I, De Micheli G, Carrara S. Cleaning strategy for carbon-based electrodes: Long-term propofol monitoring in human serum. *Sens Actuators B Chem*. 2018;269:304-313. doi:https://doi.org/10.1016/j.snb.2018.04.082

218. Moonla C, Goud KY, Teymourian H, et al. An integrated microcatheter-based dual-analyte sensor system for simultaneous, real-time measurement of propofol and fentanyl. *Talanta*. 2020;218:121205. doi:https://doi.org/10.1016/j.talanta.2020.121205

219. Park J, Sempionatto JR, Kim J, et al. Microscale Biosensor Array Based on Flexible Polymeric Platform toward Lab-on-a-Needle: Real-Time Multiparameter Biomedical Assays on Curved Needle Surfaces. *ACS Sens*. 2020;5(5):1363-1373. doi:10.1021/acssensors.0c00078

220. Bretag AH. Synthetic interstial fluid for isolated mammalian tissue. *Life Sci*. 1969;8(5, Part 1):319-329. doi:https://doi.org/10.1016/0024-3205(69)90283-5

221. Evans SAG, Elliott JM, Andrews LM, Bartlett PN, Doyle PJ, Denuault G. Detection of Hydrogen Peroxide at Mesoporous Platinum Microelectrodes. *Anal Chem*. 2002;74(6):1322-1326. doi:10.1021/ac011052p

222. Valentini F, Amine A, Orlanducci S, Terranova ML, Palleschi G. Carbon Nanotube Purification: Preparation and Characterization of Carbon Nanotube Paste Electrodes. *Anal Chem*. 2003;75(20):5413-5421. doi:10.1021/ac0300237

223. Švancara I, Vytřas K, Kalcher K, Walcarius A, Wang J. Carbon Paste Electrodes in Facts, Numbers, and Notes: A Review on the Occasion of the 50-Years Jubilee of Carbon Paste in Electrochemistry and Electroanalysis. *Electroanalysis*. 2009;21(1):7-28. doi:https://doi.org/10.1002/elan.200804340

224. Moonla C, Goud KY, Teymourian H, et al. An integrated microcatheter-based dual-analyte sensor system for simultaneous, real-time measurement of propofol and fentanyl. *Talanta*. 2020;218:121205. doi:https://doi.org/10.1016/j.talanta.2020.121205

225. Stradolini F, Kilic T, Di Consiglio A, Ozsoz M, De Micheli G, Carrara S. Long-term Monitoring of Propofol and Fouling Effect on Pencil Graphite Electrodes. *Electroanalysis*. 2018;30(7):1363-1369. doi:https://doi.org/10.1002/elan.201700834

226. Stradolini F, Kilic T, Taurino I, De Micheli G, Carrara S. Cleaning strategy for carbon-based electrodes: Long-term propofol monitoring in human serum. *Sens Actuators B Chem*. 2018;269:304-313. doi:https://doi.org/10.1016/j.snb.2018.04.082

227. Forster RJ. Microelectrodes: new dimensions in electrochemistry. *Chem Soc Rev*. 1994;23(4):289-297. doi:10.1039/CS9942300289

# SUMMARIZED CV


## Letícia Francine Mendes

242 Amabile Miosso St.

Votorantim City - Santos Dumont – SP

Brazil

leticiafrancinemendes@gmail.com


---

### Education

**2018 – present** **Institute of Chemistry - University of São Paulo**

*Graduate degree (Ph.D.) in chemistry (in progress)*

Supervisor: Prof. Dr. Thiago Regis Longo Cesar da Paixão.

**2016 - 2018** **Institute of Chemistry - University of São Paulo**

*Graduate degree (MSc) in chemistry*

Supervisor: Prof. Dr. Thiago Regis Longo Cesar da Paixão.

**2011 - 2015** **Federal University of São Carlos**

*Undergraduate degree in chemistry*

Supervisor: Prof. Dr. Francisco Trivinho Strixino.

### Complementary Education

**2022 – 2023** **University of California San Diego**

*Research internship abroad*

Supervisor: Prof. Dr. Joseph Wang

### Professional History

**2018 – Present** **Institute of Chemistry - University of São Paulo**

*Ph.D. student*
Research Project: “Development of portable electrochemical devices on polymer materials using $CO_2$ laser for analytical applications”.

Supervisor: Prof. Dr. Thiago Regis Longo Cesar da Paixão.

Scholarship: FAPESP Grant # 2018/16250-0

**2016 – 2018 Institute of Chemistry - University of São Paulo**

*Master's degree student*
Research Project: “Development of electrochemical sensor modified with molecularly imprinted polymers (MIP) aiming cortisol quantification”.

Supervisor: Prof. Dr. Thiago Regis Longo Cesar da Paixão.

Scholarship: FAPESP Grant # 2016/07416-6

**2012 – 2015 Federal University of São Carlos**

*Undergraduate research student*
Research Project: “Melhoramento do processo de eletropolimento de substratos de alumínio”.

Supervisor: Prof. Dr. Francisco Trivinho Strixino.

Scholarship: FAPESP Grant # 2012/01997-6

## Teaching experience

### TEACHING EXPERIENCE

**2019 – 2021 Teaching, Degree: Secondary Education**.

Volunteer teacher

Disciplines Taught: Chemistry

### AUXILIARY TEACHER

**07/2019 - 12/2019 Chemistry discipline: QFL230 – Analytical chemistry**

Presented colloquiums for undergraduate students. Monitored laboratory classes and tests of the students enrolled in the chemistry course at the University of São Paulo.

**03/2019 - 06/2019 Chemistry discipline: QFL1212 – II Analytical chemistry**

Presented colloquiums for undergraduate students. Monitored laboratory classes and tests of the students enrolled in the chemistry course at the University of São Paulo.

**07/2018 - 12/2018 Chemistry discipline: QFL1200 – Analytical chemistry**

Presented colloquiums for undergraduate students. Monitored laboratory classes and tests of the students enrolled in the chemistry course at the University of São Paulo.

**06/2016 - 11/2016 Chemistry discipline: QFL1111 – Analytical chemistry**

Presented colloquiums for undergraduate students. Monitored laboratory classes and tests of the students enrolled in the chemistry course at the University of São Paulo.

## Awards

**2021 -** A prize for the Chemistry Graduate Program for the top 10 high-impact articles published in the Chemistry Graduate Program 2020 and top 1 student video selected by Chemistry Graduate Program: https://youtu.be/JbMvaeTODUI.

**2016 -** Lavoisier Award - Best Student of the Degree in Chemistry, Regional Council of Chemistry.

**2013 -** Best Poster Award in the area of surface treatment of the work presented in XIX SIBEE (Simpósio Brasileiro de Eletroquímica e Eletroanalítica), corrosion and passivation, The International Society of Electrochemistry (ISE).

**Complete scientific results**

**Researcher ID:** U-9267-2019

## Revised Manuscript Submitted

Laochai, Thidarut; Moonla, Chochanon; Moon, Jongmin; Sakdaphetsiri, Kittiya; Yin, Lu; Mendes, Leticia Francine; Abbas, Amal; Djassemi, Omeed; Seker, Sumeyye; Mahato, Kuldeep; Chailapakul, Orawon; Wang, Joseph; Rodthongkum, Nadnudda. Touch-Based Potentiometric Sensors for Simultaneous Detection of Urea and Ammonium from Fingertip Sweat.
Manuscript Status: Submitted to ACS Sensors

## Articles in Scientific Journals

Stefano, Jéssica Santos; Orzari, Luiz Otávio; Silva-Neto, Habdias Araujo; de Ataíde, Vanessa Neiva; Mendes, Letícia Francine; Coltro, Wendell Karlos Tomazelli; Longo Cesar Paixão, Thiago Regis; Janegitz, Bruno Campos. Different approaches for fabrication of low-cost electrochemical sensors. Current Opinion In Electrochemistry, v. 32, p. 100893, 2022.

De Ataide, Vanessa; Arantes, Iana; Mendes, Letícia; Baldo, Thaísa; Rocha, Danielly; Paixao, Thiago R L C; Coltro, Wendell K. T. Review: A Pencil Drawing Overview: From Graphite to Electrochemical Sensors/Biosensors Applications. Journal of the Electrochemical Society, v. 169, p. 047524, 2022.

Mendes, Letícia F.; Pradela-Filho, Lauro A.; Paixão, Thiago R.L.C. Polyimide adhesive tapes as a versatile and disposable substrate to produce $CO_2$ laser-induced carbon sensors for batch and microfluidic analysis. Microchemical Journal, v. 182, p. 107893, 2022.

Moon, Jong-Min; Del Caño, Rafael; Moonla, Chochanon; Sakdaphetsiri, Kittiya; Saha, Tamoghna; Francine Mendes, Letícia; Yin, Lu; Chang, An-Yi; Seker,

Sumeyye; Wang, Joseph. Self-Testing of Ketone Bodies, along with Glucose, Using Touch-Based Sweat Analysis. ACS Sensors, v. 7, p. 3973-3981, 2022.

Baldo, Thaisa A.; De Lima, Lucas Felipe; Mendes, Letícia F.; De Araujo, William R.; Paixão, Thiago R. L. C.; Coltro, Wendell K. T. Wearable and Biodegradable Sensors for Clinical and Environmental Applications. ACS Applied Electronic Materials, v. 3, p. 68-100, 2021.

Ataide, Vanessa N.; Mendes, Letícia F.; Gama, Lillia I. L. M.; De Araujo, William R.; Paixão, Thiago R. L. C. Electrochemical paper-based analytical devices: ten years of development. Analytical Methods, v. 12, p. 1030-1054, 2020.

Clark, Kaylee M.; Skrajewski, Lauren; Benavidez, Tomás E.; Mendes, Letícia F.; Bastos, Erick L.; Dörr, Felipe A.; Sachdeva, Rakesh; Ogale, Amod A.; Paixão, Thiago R. L. C.; Garcia, Carlos D. Fluorescent patterning of paper through laser engraving. Soft Matter, v. 16, p. 7659-7666, 2020.

Mendes, Letícia Francine; De Siervo, Abner; Reis De Araujo, William; Longo Cesar Paixão, Thiago Regis. Reagentless fabrication of a porous graphene-like electrochemical device from phenolic paper using laser-scribing. Carbon, v. 159, p. 110-118, 2019.

Mendes, Letícia Francine; Souza e Silva, Ângela Rodrigues; Bacil, Raphael Prata; Serrano, Silvia Helena Pires; Angnes, Lúcio; Paixão, Thiago Regis Longo Cesar; De Araujo, William Reis. Forensic electrochemistry: Electrochemical study and quantification of xylazine in pharmaceutical and urine samples. Electrochimica Acta, v. 295, p. 726-734, 2018.

Mendes, Letícia F.; Moraes, Ariana S.; Santos, Janaina S.; Leite, Fábio L.; Trivinho-Strixino, Francisco. Investigation of roughness and specular quality of commercial aluminum (6061 alloy) for fabrication of nanoporous anodic alumina films. Surface & Coatings Technology, v. 310, p. 199-206, 2017.

Garcia, U. M.; Mendes, L. F.; Santos, J. S.; Trivinho-Strixino, F. Comparison and construction of Mild and Hard Anodisation reactors for porous alumina synthesis. Química Nova (Online), v. 1, p. 1-5, 2015.

**Book Chapter Published**

V.S. Arantes, I.; L.M. Gongoni, J.; Mendes, Letícia F.; Ataide, V. N. ; A. Ameku, W.; T. Garcia, P.; Araujo, W. R.; R.L.C. Paixao, T. Chapter 5 - Electrochemical paper-based analytical devices. 1 ed.:, 2021, v. 1, p. 81-116.

V.S. Arantes, I.; Mendes, Letícia F.; Ataide, V. N.; Araujo, W. R.; R.L.C. Paixao, T. Chapter 11 - Conclusions, challenges, and next steps. 1 ed.: , 2021, v. 1, p. 259-274.

**Relevant contributions to scientific conferences**

**Oral presentation**

Mendes, L. F.; Pradela Filho, L.; Paixao, Thiago R L C. Laser-induced disposable electrochemical devices based on Kapton adhesive tape for sensing applications. 2023. Philadelphia. Pittcon Conference, 2023.

Mendes, L. F.; Paixao, Thiago R L C. Portable and Flexible Electrochemical Devices Fabrication Using Laser-Scribing Technique on Polyimide Tape. 2021. Simpósio Brasileiro de Eletroquímica e Eletroanalitica, 2021.

Mendes, L. F.; Moraes, A. S.; Santos, J. S.; Leite, F. L.; Trivinho-Strixino, F. Study of electropolishing parameters on aluminum samples and the influence on Porous Anodic Alumina (PAA) preparation. XX SIBEE, 2015

**Poster presentation**

Mendes, Letícia F.; Albuquerque, J. J.; Paixão, Thiago R. L. C. Laser-Scribing Fabrication of Portable, Robust and Nernstian pH Electrodes on polymeric platforms. Chicago, Pittcon Conference, 2020.

Mendes, L. F.; W. R. Araujo; Paixão, Thiago Regis Longo Cesar. Laser-Scribing Fabrication of Portable Electrochemical Devices on Non-Conductive Polymer Materials. Philadelphia. Pittcon Conference, 2019

Mendes, L. F.; W. R. Araujo; Paixão, Thiago Regis Longo Cesar. Fabrication of Portable Electrochemical Devices Using Laser-Scribing Technique on Phenolic Paper Sheets. Ribeirão Preto. XXII Simpósio Brasileiro de Eletroquímica e Eletroanalítica, 2019.

Mendes, L. F.; W. R. Araujo; T. R. L. C. Paixão. Fabrication of a disposable electrochemical paper-based device for cortisol quantification. 41ª Reunião Anual da Sociedade Brasileira de Química, 2018.

Mendes, L. F.; W. R. Araujo; T. R. L. C. Paixão. Laser-Scribing Fabrication of Electrochemical device based in polymeric material for analytical applications. Electrochemistry, from Sensing to Energy Conversion and Storage, 2018.

Mendes, L. F.; W. R. Araujo; T. R. L. C. Paixão. Development of molecularly imprinted polymer (MIP) modified electrode for cortisol recognition. XXI Simpósio Brasileiro de Eletroquímica e Eletroanalítica, 2017.

Mendes, L. F.; Ferreira, M.; Trivinho-Strixino, F. Monitoring the growth kinetics of self-assembled PEI/GOx films over porous anodic alumina. 38ª Reunião Anual da Sociedade Brasileira de Química, 2015.

Mendes, L. F.; Ferreira, M.; Trivinho-Strixino, F. Crescimento de filme LBL de PEI/GOx sobre a Alumina Anodica Porosa (AAP) observado a partir de Espectroscopia de Fluorescência. 22° Congresso de Iniciação Científica, 2014.

Mendes, L. F.; Trivinho-Strixino, F. Study of experimental parameters on aluminum electropolishing using reflectance spectroscopy. XIX Simpósio Brasileiro de Eletroquímica e Eletroanalítica, 2013.

Mendes, L. F.; Trivinho-Strixino, F. Study of experimental parameters on aluminum electropolishing using diffuse reflectance spectroscopy. XI Brazilian MRS Meeting, 2012.

SPRINGER NATURE LICENSE
TERMS AND CONDITIONS

Jul 24, 2023

---

This Agreement between Letícia Mendes ("You") and Springer Nature ("Springer Nature") consists of your license details and the terms and conditions provided by Springer Nature and Copyright Clearance Center.

| | |
|---|---|
| License Number | 5595460957920 |
| License date | Jul 24, 2023 |
| Licensed Content Publisher | Springer Nature |
| Licensed Content Publication | Nature Communications |
| Licensed Content Title | Laser-induced porous graphene films from commercial polymers |
| Licensed Content Author | Jian Lin et al |
| Licensed Content Date | Dec 10, 2014 |
| Type of Use | Thesis/Dissertation |
| Requestor type | academic/university or research institute |
| Format | electronic |
| Portion | figures/tables/illustrations |
| Number of figures/tables/illustrations | 1 |
| Would you like a high resolution image with your order? | no |
| Will you be translating? | no |

| | |
|---|---|
| Circulation/distribution | 30 - 99 |
| Author of this Springer Nature content | no |
| Title | Development of portable electrochemical devices on polymer materials using CO2 laser for analytical applications |
| Institution name | University of Sao Paulo |
| Expected presentation date | Sep 2023 |
| Order reference number | 44 |
| Portions | Figure 1 |
| Requestor Location | Letícia Mendes<br>Rua Amabile Miosso 242<br><br>Votorantim, São Paulo 18117-070<br>Brazil<br>Attn: University of São Paulo |
| Total | 0.00 USD |

Terms and Conditions

**Springer Nature Customer Service Centre GmbH Terms and Conditions**

The following terms and conditions ("Terms and Conditions") together with the terms specified in your [RightsLink] constitute the License ("License") between you as Licensee and Springer Nature Customer Service Centre GmbH as Licensor. By clicking 'accept' and completing the transaction for your use of the material ("Licensed Material"), you confirm your acceptance of and obligation to be bound by these Terms and Conditions.

**1. Grant and Scope of License**

1. 1. The Licensor grants you a personal, non-exclusive, non-transferable, non-sublicensable, revocable, world-wide License to reproduce, distribute, communicate to the public, make available, broadcast, electronically transmit or create derivative works using the Licensed Material for the purpose(s) specified in your RightsLink Licence Details only. Licenses are granted for the specific use requested in the order and for no other use, subject to these Terms and Conditions. You acknowledge and agree that the rights granted to you under this License do not include the right to

modify, edit, translate, include in collective works, or create derivative works of the Licensed Material in whole or in part unless expressly stated in your RightsLink Licence Details. You may use the Licensed Material only as permitted under this Agreement and will not reproduce, distribute, display, perform, or otherwise use or exploit any Licensed Material in any way, in whole or in part, except as expressly permitted by this License.

1. 2. You may only use the Licensed Content in the manner and to the extent permitted by these Terms and Conditions, by your RightsLink Licence Details and by any applicable laws.

1. 3. A separate license may be required for any additional use of the Licensed Material, e.g. where a license has been purchased for print use only, separate permission must be obtained for electronic re-use. Similarly, a License is only valid in the language selected and does not apply for editions in other languages unless additional translation rights have been granted separately in the License.

1. 4. Any content within the Licensed Material that is owned by third parties is expressly excluded from the License.

1. 5. Rights for additional reuses such as custom editions, computer/mobile applications, film or TV reuses and/or any other derivative rights requests require additional permission and may be subject to an additional fee. Please apply to journalpermissions@springernature.com or bookpermissions@springernature.com for these rights.

**2. Reservation of Rights**

Licensor reserves all rights not expressly granted to you under this License. You acknowledge and agree that nothing in this License limits or restricts Licensor's rights in or use of the Licensed Material in any way. Neither this License, nor any act, omission, or statement by Licensor or you, conveys any ownership right to you in any Licensed Material, or to any element or portion thereof. As between Licensor and you, Licensor owns and retains all right, title, and interest in and to the Licensed Material subject to the license granted in Section 1.1. Your permission to use the Licensed Material is expressly conditioned on you not impairing Licensor's or the applicable copyright owner's rights in the Licensed Material in any way.

**3. Restrictions on use**

3. 1. Minor editing privileges are allowed for adaptations for stylistic purposes or formatting purposes provided such alterations do not alter the original meaning or intention of the Licensed Material and the new figure(s) are still accurate and representative of the Licensed Material. Any other changes including but not limited to, cropping, adapting, and/or omitting material that affect the meaning, intention or moral rights of the author(s) are strictly prohibited.

3. 2. You must not use any Licensed Material as part of any design or trademark.

3. 3. Licensed Material may be used in Open Access Publications (OAP), but any such reuse must include a clear acknowledgment of this permission visible at the same time as the figures/tables/illustration or abstract and which must indicate that the Licensed Material is not part of the governing OA license but has been reproduced with permission. This may be indicated according to any standard referencing system but must include at a minimum 'Book/Journal title, Author, Journal Name (if applicable), Volume (if applicable), Publisher, Year, reproduced with permission from SNCSC'.

**4. STM Permission Guidelines**

4. 1. An alternative scope of license may apply to signatories of the STM Permissions Guidelines ("STM PG") as amended from time to time and made available at https://www.stm-assoc.org/intellectual-property/permissions/permissions-guidelines/.

4. 2. For content reuse requests that qualify for permission under the STM PG, and which may be updated from time to time, the STM PG supersede the terms and conditions contained in this License.

4. 3. If a License has been granted under the STM PG, but the STM PG no longer apply at the time of publication, further permission must be sought from the Rightsholder. Contact journalpermissions@springernature.com or bookpermissions@springernature.com for these rights.

**5. Duration of License**

5. 1. Unless otherwise indicated on your License, a License is valid from the date of purchase ("License Date") until the end of the relevant period in the below table:

| | |
|---|---|
| Reuse in a medical communications project | Reuse up to distribution or time period indicated in License |
| Reuse in a dissertation/thesis | Lifetime of thesis |
| Reuse in a journal/magazine | Lifetime of journal/magazine |
| Reuse in a book/textbook | Lifetime of edition |
| Reuse on a website | 1 year unless otherwise specified in the License |
| Reuse in a presentation/slide kit/poster | Lifetime of presentation/slide kit/poster. Note: publication whether electronic or in print of presentation/slide kit/poster may require further permission. |
| Reuse in conference proceedings | Lifetime of conference proceedings |
| Reuse in an annual report | Lifetime of annual report |
| Reuse in training/CME materials | Reuse up to distribution or time period indicated in License |
| Reuse in newsmedia | Lifetime of newsmedia |
| Reuse in coursepack/classroom materials | Reuse up to distribution and/or time period indicated in license |

**6. Acknowledgement**

6. 1. The Licensor's permission must be acknowledged next to the Licensed Material in print. In electronic form, this acknowledgement must be visible at the same time as the figures/tables/illustrations or abstract and must be hyperlinked to the journal/book's homepage.

6. 2. Acknowledgement may be provided according to any standard referencing system and at a minimum should include "Author, Article/Book Title, Journal name/Book imprint, volume, page number, year, Springer Nature".

**7. Reuse in a dissertation or thesis**

7. 1. Where 'reuse in a dissertation/thesis' has been selected, the following terms apply: Print rights of the Version of Record are provided for; electronic rights for use only on institutional repository as defined by the Sherpa guideline (www.sherpa.ac.uk/romeo/) and only up to what is required by the awarding institution.

7. 2. For theses published under an ISBN or ISSN, separate permission is required. Please contact journalpermissions@springernature.com or bookpermissions@springernature.com for these rights.

7. 3. Authors must properly cite the published manuscript in their thesis according to current citation standards and include the following acknowledgement: '*Reproduced with permission from Springer Nature*'.

**8. License Fee**

You must pay the fee set forth in the License Agreement (the "License Fees"). All amounts payable by you under this License are exclusive of any sales, use, withholding, value added or similar taxes, government fees or levies or other assessments. Collection and/or remittance of such taxes to the relevant tax authority shall be the responsibility of the party who has the legal obligation to do so.

**9. Warranty**

9. 1. The Licensor warrants that it has, to the best of its knowledge, the rights to license reuse of the Licensed Material. **You are solely responsible for ensuring that the material you wish to license is original to the Licensor and does not carry the copyright of another entity or third party (as credited in the published version).** If the credit line on any part of the Licensed Material indicates that it was reprinted or adapted with permission from another source, then you should seek additional permission from that source to reuse the material.

9. 2. EXCEPT FOR THE EXPRESS WARRANTY STATED HEREIN AND TO THE EXTENT PERMITTED BY APPLICABLE LAW, LICENSOR PROVIDES THE LICENSED MATERIAL "AS IS" AND MAKES NO OTHER REPRESENTATION OR WARRANTY. LICENSOR EXPRESSLY DISCLAIMS ANY LIABILITY FOR ANY CLAIM ARISING FROM OR OUT OF THE CONTENT, INCLUDING BUT NOT LIMITED TO ANY ERRORS, INACCURACIES, OMISSIONS, OR DEFECTS CONTAINED THEREIN, AND ANY IMPLIED OR EXPRESS WARRANTY AS TO MERCHANTABILITY OR FITNESS FOR A PARTICULAR PURPOSE. IN NO EVENT SHALL LICENSOR BE LIABLE TO YOU OR ANY OTHER PARTY OR ANY OTHER PERSON OR FOR ANY SPECIAL, CONSEQUENTIAL, INCIDENTAL, INDIRECT, PUNITIVE, OR EXEMPLARY DAMAGES, HOWEVER CAUSED, ARISING OUT OF OR IN CONNECTION WITH THE DOWNLOADING, VIEWING OR USE OF THE LICENSED MATERIAL REGARDLESS OF THE FORM OF ACTION, WHETHER FOR BREACH OF CONTRACT, BREACH OF WARRANTY, TORT, NEGLIGENCE, INFRINGEMENT OR OTHERWISE (INCLUDING, WITHOUT LIMITATION, DAMAGES BASED ON LOSS OF PROFITS, DATA, FILES, USE, BUSINESS OPPORTUNITY OR CLAIMS OF THIRD PARTIES), AND WHETHER OR NOT THE PARTY HAS BEEN ADVISED OF THE POSSIBILITY OF SUCH DAMAGES. THIS LIMITATION APPLIES NOTWITHSTANDING ANY FAILURE OF ESSENTIAL PURPOSE OF ANY LIMITED REMEDY PROVIDED HEREIN.

**10. Termination and Cancellation**

10. 1. The License and all rights granted hereunder will continue until the end of the applicable period shown in Clause 5.1 above. Thereafter, this license will be

terminated and all rights granted hereunder will cease.

10. 2. Licensor reserves the right to terminate the License in the event that payment is not received in full or if you breach the terms of this License.

**11. General**

11. 1. The License and the rights and obligations of the parties hereto shall be construed, interpreted and determined in accordance with the laws of the Federal Republic of Germany without reference to the stipulations of the CISG (United Nations Convention on Contracts for the International Sale of Goods) or to Germany´s choice-of-law principle.

11. 2. The parties acknowledge and agree that any controversies and disputes arising out of this License shall be decided exclusively by the courts of or having jurisdiction for Heidelberg, Germany, as far as legally permissible.

11. 3. This License is solely for Licensor's and Licensee's benefit. It is not for the benefit of any other person or entity.

**Questions?** For questions on Copyright Clearance Center accounts or website issues please contact springernaturesupport@copyright.com or +1-855-239-3415 (toll free in the US) or +1-978-646-2777. For questions on Springer Nature licensing please visit https://www.springernature.com/gp/partners/rights-permissions-third-party-distribution

**Other Conditions**:

Version 1.4 - Dec 2022

**Questions? customercare@copyright.com.**

JOHN WILEY AND SONS LICENSE
TERMS AND CONDITIONS

Jul 24, 2023

---

This Agreement between Letícia Mendes ("You") and John Wiley and Sons ("John Wiley and Sons") consists of your license details and the terms and conditions provided by John Wiley and Sons and Copyright Clearance Center.

| | |
|---|---|
| License Number | 5595470205547 |
| License date | Jul 24, 2023 |
| Licensed Content Publisher | John Wiley and Sons |
| Licensed Content Publication | Angewandte Chemie International Edition |
| Licensed Content Title | Single-Step Reagentless Laser Scribing Fabrication of Electrochemical Paper-Based Analytical Devices |
| Licensed Content Author | Thiago R. L. C. Paixão, Lúcio Angnes, José R. Silva, et al |
| Licensed Content Date | Oct 23, 2017 |
| Licensed Content Volume | 56 |
| Licensed Content Issue | 47 |
| Licensed Content Pages | 5 |
| Type of use | Dissertation/Thesis |
| Requestor type | University/Academic |
| Format | Electronic |

| | |
|---|---|
| Portion | Figure/table |
| Number of figures/tables | 1 |
| Will you be translating? | No |
| Title | Development of portable electrochemical devices on polymer materials using CO2 laser for analytical applications |
| Institution name | University of Sao Paulo |
| Expected presentation date | Sep 2023 |
| Order reference number | 26 |
| Portions | Figure 1 |
| Requestor Location | Letícia Mendes<br>Rua Amabile Miosso 242<br><br>Votorantim, São Paulo 18117-070<br>Brazil<br>Attn: University of São Paulo |
| Publisher Tax ID | EU826007151 |
| Total | 0.00 USD |
| Terms and Conditions | |

## TERMS AND CONDITIONS

**Terms and Conditions**

- The materials you have requested permission to reproduce or reuse (the "Wiley Materials") are protected by copyright.

- You are hereby granted a personal, non-exclusive, non-sub licensable (on a stand-alone basis), non-transferable, worldwide, limited license to reproduce the Wiley Materials for the purpose specified in the licensing process. This license, **and any CONTENT (PDF or image file) purchased as part of your order,** is for a one-time use only and limited to any maximum distribution number specified in the license. The first instance of republication or reuse granted by this license must be completed within two years of the date of the grant of this license (although copies prepared before the end date may be distributed thereafter). The Wiley Materials shall not be used in any other manner or for any other purpose, beyond what is granted in the license. Permission is granted subject to an appropriate acknowledgement given to the author, title of the material/book/journal and the publisher. You shall also duplicate the copyright notice that appears in the Wiley publication in your use of the Wiley Material. Permission is also granted on the understanding that nowhere in the text is a previously published source acknowledged for all or part of this Wiley Material. Any third party content is expressly excluded from this permission.

- With respect to the Wiley Materials, all rights are reserved. Except as expressly granted by the terms of the license, no part of the Wiley Materials may be copied, modified, adapted (except for minor reformatting required by the new Publication), translated, reproduced, transferred or distributed, in any form or by any means, and no derivative works may be made based on the Wiley Materials without the prior permission of the respective copyright owner.**For STM Signatory Publishers clearing permission under the terms of the STM Permissions Guidelines only, the terms of the license are extended to include subsequent editions and for editions in other languages, provided such editions are for the work as a whole in situ and does not involve the separate exploitation of the permitted figures or extracts,** You may not alter, remove or suppress in any manner any copyright, trademark or other notices displayed by the Wiley Materials. You may not license, rent, sell, loan, lease, pledge, offer as security, transfer or assign the Wiley Materials on a stand-alone basis, or any of the rights granted to you hereunder to any other person.

- The Wiley Materials and all of the intellectual property rights therein shall at all times remain the exclusive property of John Wiley & Sons Inc, the Wiley Companies, or their respective licensors, and your interest therein is only that of having possession of and the right to reproduce the Wiley Materials pursuant to Section 2 herein during the continuance of this Agreement. You agree that you own no right, title or interest in or to the Wiley Materials or any of the intellectual property rights therein. You shall have no rights hereunder other than the license as provided for above in Section 2. No right, license or interest to any trademark, trade name, service mark or other branding ("Marks") of WILEY or its licensors is granted hereunder, and you agree that you shall not assert any such right, license or interest with respect thereto

- NEITHER WILEY NOR ITS LICENSORS MAKES ANY WARRANTY OR REPRESENTATION OF ANY KIND TO YOU OR ANY THIRD PARTY, EXPRESS, IMPLIED OR STATUTORY, WITH RESPECT TO THE MATERIALS OR THE ACCURACY OF ANY INFORMATION CONTAINED IN THE MATERIALS, INCLUDING, WITHOUT LIMITATION, ANY IMPLIED WARRANTY OF MERCHANTABILITY, ACCURACY, SATISFACTORY QUALITY, FITNESS FOR A PARTICULAR PURPOSE, USABILITY, INTEGRATION OR NON-INFRINGEMENT AND ALL SUCH WARRANTIES ARE HEREBY EXCLUDED BY WILEY AND ITS LICENSORS AND WAIVED BY YOU.

- WILEY shall have the right to terminate this Agreement immediately upon breach of this Agreement by you.

- You shall indemnify, defend and hold harmless WILEY, its Licensors and their respective directors, officers, agents and employees, from and against any actual or threatened claims, demands, causes of action or proceedings arising from any breach of this Agreement by you.

- IN NO EVENT SHALL WILEY OR ITS LICENSORS BE LIABLE TO YOU OR ANY OTHER PARTY OR ANY OTHER PERSON OR ENTITY FOR ANY SPECIAL, CONSEQUENTIAL, INCIDENTAL, INDIRECT, EXEMPLARY OR PUNITIVE DAMAGES, HOWEVER CAUSED, ARISING OUT OF OR IN CONNECTION WITH THE DOWNLOADING, PROVISIONING, VIEWING OR USE OF THE MATERIALS REGARDLESS OF THE FORM OF ACTION, WHETHER FOR BREACH OF CONTRACT, BREACH OF WARRANTY, TORT, NEGLIGENCE, INFRINGEMENT OR OTHERWISE (INCLUDING, WITHOUT LIMITATION, DAMAGES BASED ON LOSS OF PROFITS, DATA, FILES, USE, BUSINESS OPPORTUNITY OR CLAIMS OF THIRD PARTIES), AND WHETHER OR NOT THE PARTY HAS BEEN ADVISED OF THE POSSIBILITY OF SUCH DAMAGES. THIS LIMITATION SHALL APPLY NOTWITHSTANDING ANY FAILURE OF ESSENTIAL PURPOSE OF ANY LIMITED REMEDY PROVIDED HEREIN.

- Should any provision of this Agreement be held by a court of competent jurisdiction to be illegal, invalid, or unenforceable, that provision shall be deemed amended to achieve as nearly as possible the same economic effect as the original provision, and the legality, validity and enforceability of the remaining provisions of this Agreement shall not be affected or impaired thereby.

- The failure of either party to enforce any term or condition of this Agreement shall not constitute a waiver of either party's right to enforce each and every term and condition of this Agreement. No breach under this agreement shall be deemed waived or excused by either party unless such waiver or consent is in writing signed by the party granting such waiver or consent. The waiver by or consent of a party to a breach of any provision of this Agreement shall not operate or be construed as a waiver of or consent to any other or subsequent breach by such other party.

- This Agreement may not be assigned (including by operation of law or otherwise) by you without WILEY's prior written consent.

- Any fee required for this permission shall be non-refundable after thirty (30) days from receipt by the CCC.

- These terms and conditions together with CCC's Billing and Payment terms and conditions (which are incorporated herein) form the entire agreement between you and WILEY concerning this licensing transaction and (in the absence of fraud) supersedes all prior agreements and representations of the parties, oral or written. This Agreement may not be amended except in writing signed by both parties. This Agreement shall be binding upon and inure to the benefit of the parties' successors, legal representatives, and authorized assigns.

- In the event of any conflict between your obligations established by these terms and conditions and those established by CCC's Billing and Payment terms and conditions, these terms and conditions shall prevail.

- WILEY expressly reserves all rights not specifically granted in the combination of (i) the license details provided by you and accepted in the course of this licensing transaction, (ii) these terms and conditions and (iii) CCC's Billing and Payment terms

and conditions.

- This Agreement will be void if the Type of Use, Format, Circulation, or Requestor Type was misrepresented during the licensing process.

- This Agreement shall be governed by and construed in accordance with the laws of the State of New York, USA, without regards to such state's conflict of law rules. Any legal action, suit or proceeding arising out of or relating to these Terms and Conditions or the breach thereof shall be instituted in a court of competent jurisdiction in New York County in the State of New York in the United States of America and each party hereby consents and submits to the personal jurisdiction of such court, waives any objection to venue in such court and consents to service of process by registered or certified mail, return receipt requested, at the last known address of such party.

**WILEY OPEN ACCESS TERMS AND CONDITIONS**

Wiley Publishes Open Access Articles in fully Open Access Journals and in Subscription journals offering Online Open. Although most of the fully Open Access journals publish open access articles under the terms of the Creative Commons Attribution (CC BY) License only, the subscription journals and a few of the Open Access Journals offer a choice of Creative Commons Licenses. The license type is clearly identified on the article.

**The Creative Commons Attribution License**

The Creative Commons Attribution License (CC-BY) allows users to copy, distribute and transmit an article, adapt the article and make commercial use of the article. The CC-BY license permits commercial and non-

**Creative Commons Attribution Non-Commercial License**

The Creative Commons Attribution Non-Commercial (CC-BY-NC)License permits use, distribution and reproduction in any medium, provided the original work is properly cited and is not used for commercial purposes.(see below)

**Creative Commons Attribution-Non-Commercial-NoDerivs License**

The Creative Commons Attribution Non-Commercial-NoDerivs License (CC-BY-NC-ND) permits use, distribution and reproduction in any medium, provided the original work is properly cited, is not used for commercial purposes and no modifications or adaptations are made. (see below)

**Use by commercial "for-profit" organizations**

Use of Wiley Open Access articles for commercial, promotional, or marketing purposes requires further explicit permission from Wiley and will be subject to a fee.

Further details can be found on Wiley Online Library
http://olabout.wiley.com/WileyCDA/Section/id-410895.html

**Other Terms and Conditions:**

**v1.10 Last updated September 2015**

**Questions? customercare@copyright.com.**

SPRINGER NATURE LICENSE
TERMS AND CONDITIONS

Jul 24, 2023

---

This Agreement between Letícia Mendes ("You") and Springer Nature ("Springer Nature") consists of your license details and the terms and conditions provided by Springer Nature and Copyright Clearance Center.

| | |
|---|---|
| License Number | 5595480009063 |
| License date | Jul 24, 2023 |
| Licensed Content Publisher | Springer Nature |
| Licensed Content Publication | Microchimica Acta |
| Licensed Content Title | Tackling the challenges of developing microneedle-based electrochemical sensors |
| Licensed Content Author | Hilmee Abdullah et al |
| Licensed Content Date | Nov 3, 2022 |
| Type of Use | Thesis/Dissertation |
| Requestor type | academic/university or research institute |
| Format | electronic |
| Portion | figures/tables/illustrations |
| Number of figures/tables/illustrations | 1 |
| Will you be translating? | no |
| Circulation/distribution | 30 - 99 |

| | |
|---|---|
| Author of this Springer Nature content | no |
| Title | Development of portable electrochemical devices on polymer materials using CO2 laser for analytical applications |
| Institution name | University of Sao Paulo |
| Expected presentation date | Sep 2023 |
| Order reference number | 104 |
| Portions | Fig. 1 |
| Requestor Location | Letícia Mendes<br>Rua Amabile Miosso 242<br><br>Votorantim, São Paulo 18117-070<br>Brazil<br>Attn: University of São Paulo |
| Total | 0.00 USD |

Terms and Conditions

**Springer Nature Customer Service Centre GmbH Terms and Conditions**

The following terms and conditions ("Terms and Conditions") together with the terms specified in your [RightsLink] constitute the License ("License") between you as Licensee and Springer Nature Customer Service Centre GmbH as Licensor. By clicking 'accept' and completing the transaction for your use of the material ("Licensed Material"), you confirm your acceptance of and obligation to be bound by these Terms and Conditions.

**1. Grant and Scope of License**

1. 1. The Licensor grants you a personal, non-exclusive, non-transferable, non-sublicensable, revocable, world-wide License to reproduce, distribute, communicate to the public, make available, broadcast, electronically transmit or create derivative works using the Licensed Material for the purpose(s) specified in your RightsLink Licence Details only. Licenses are granted for the specific use requested in the order and for no other use, subject to these Terms and Conditions. You acknowledge and agree that the rights granted to you under this License do not include the right to modify, edit, translate, include in collective works, or create derivative works of the Licensed Material in whole or in part unless expressly stated in your RightsLink

Licence Details. You may use the Licensed Material only as permitted under this Agreement and will not reproduce, distribute, display, perform, or otherwise use or exploit any Licensed Material in any way, in whole or in part, except as expressly permitted by this License.

1. 2. You may only use the Licensed Content in the manner and to the extent permitted by these Terms and Conditions, by your RightsLink Licence Details and by any applicable laws.

1. 3. A separate license may be required for any additional use of the Licensed Material, e.g. where a license has been purchased for print use only, separate permission must be obtained for electronic re-use. Similarly, a License is only valid in the language selected and does not apply for editions in other languages unless additional translation rights have been granted separately in the License.

1. 4. Any content within the Licensed Material that is owned by third parties is expressly excluded from the License.

1. 5. Rights for additional reuses such as custom editions, computer/mobile applications, film or TV reuses and/or any other derivative rights requests require additional permission and may be subject to an additional fee. Please apply to journalpermissions@springernature.com or bookpermissions@springernature.com for these rights.

**2. Reservation of Rights**

Licensor reserves all rights not expressly granted to you under this License. You acknowledge and agree that nothing in this License limits or restricts Licensor's rights in or use of the Licensed Material in any way. Neither this License, nor any act, omission, or statement by Licensor or you, conveys any ownership right to you in any Licensed Material, or to any element or portion thereof. As between Licensor and you, Licensor owns and retains all right, title, and interest in and to the Licensed Material subject to the license granted in Section 1.1. Your permission to use the Licensed Material is expressly conditioned on you not impairing Licensor's or the applicable copyright owner's rights in the Licensed Material in any way.

**3. Restrictions on use**

3. 1. Minor editing privileges are allowed for adaptations for stylistic purposes or formatting purposes provided such alterations do not alter the original meaning or intention of the Licensed Material and the new figure(s) are still accurate and representative of the Licensed Material. Any other changes including but not limited to, cropping, adapting, and/or omitting material that affect the meaning, intention or moral rights of the author(s) are strictly prohibited.

3. 2. You must not use any Licensed Material as part of any design or trademark.

3. 3. Licensed Material may be used in Open Access Publications (OAP), but any such reuse must include a clear acknowledgment of this permission visible at the same time as the figures/tables/illustration or abstract and which must indicate that the Licensed Material is not part of the governing OA license but has been reproduced with permission. This may be indicated according to any standard referencing system but must include at a minimum 'Book/Journal title, Author, Journal Name (if applicable), Volume (if applicable), Publisher, Year, reproduced with permission from SNCSC'.

**4. STM Permission Guidelines**

4. 1. An alternative scope of license may apply to signatories of the STM Permissions Guidelines ("STM PG") as amended from time to time and made available at https://www.stm-assoc.org/intellectual-property/permissions/permissions-guidelines/.

4. 2. For content reuse requests that qualify for permission under the STM PG, and which may be updated from time to time, the STM PG supersede the terms and conditions contained in this License.

4. 3. If a License has been granted under the STM PG, but the STM PG no longer apply at the time of publication, further permission must be sought from the Rightsholder. Contact journalpermissions@springernature.com or bookpermissions@springernature.com for these rights.

**5. Duration of License**

5. 1. Unless otherwise indicated on your License, a License is valid from the date of purchase ("License Date") until the end of the relevant period in the below table:

| | |
|---|---|
| Reuse in a medical communications project | Reuse up to distribution or time period indicated in License |
| Reuse in a dissertation/thesis | Lifetime of thesis |
| Reuse in a journal/magazine | Lifetime of journal/magazine |
| Reuse in a book/textbook | Lifetime of edition |
| Reuse on a website | 1 year unless otherwise specified in the License |
| Reuse in a presentation/slide kit/poster | Lifetime of presentation/slide kit/poster. Note: publication whether electronic or in print of presentation/slide kit/poster may require further permission. |
| Reuse in conference proceedings | Lifetime of conference proceedings |
| Reuse in an annual report | Lifetime of annual report |
| Reuse in training/CME materials | Reuse up to distribution or time period indicated in License |
| Reuse in newsmedia | Lifetime of newsmedia |
| Reuse in coursepack/classroom materials | Reuse up to distribution and/or time period indicated in license |

**6. Acknowledgement**

6. 1. The Licensor's permission must be acknowledged next to the Licensed Material in print. In electronic form, this acknowledgement must be visible at the same time as the figures/tables/illustrations or abstract and must be hyperlinked to the journal/book's homepage.

6. 2. Acknowledgement may be provided according to any standard referencing system and at a minimum should include "Author, Article/Book Title, Journal name/Book imprint, volume, page number, year, Springer Nature".

**7. Reuse in a dissertation or thesis**

7. 1. Where 'reuse in a dissertation/thesis' has been selected, the following terms apply: Print rights of the Version of Record are provided for; electronic rights for use only on institutional repository as defined by the Sherpa guideline

(www.sherpa.ac.uk/romeo/) and only up to what is required by the awarding institution.

7. 2. For theses published under an ISBN or ISSN, separate permission is required. Please contact journalpermissions@springernature.com or bookpermissions@springernature.com for these rights.

7. 3. Authors must properly cite the published manuscript in their thesis according to current citation standards and include the following acknowledgement: '*Reproduced with permission from Springer Nature*'.

**8. License Fee**

You must pay the fee set forth in the License Agreement (the "License Fees"). All amounts payable by you under this License are exclusive of any sales, use, withholding, value added or similar taxes, government fees or levies or other assessments. Collection and/or remittance of such taxes to the relevant tax authority shall be the responsibility of the party who has the legal obligation to do so.

**9. Warranty**

9. 1. The Licensor warrants that it has, to the best of its knowledge, the rights to license reuse of the Licensed Material. **You are solely responsible for ensuring that the material you wish to license is original to the Licensor and does not carry the copyright of another entity or third party (as credited in the published version).** If the credit line on any part of the Licensed Material indicates that it was reprinted or adapted with permission from another source, then you should seek additional permission from that source to reuse the material.

9. 2. EXCEPT FOR THE EXPRESS WARRANTY STATED HEREIN AND TO THE EXTENT PERMITTED BY APPLICABLE LAW, LICENSOR PROVIDES THE LICENSED MATERIAL "AS IS" AND MAKES NO OTHER REPRESENTATION OR WARRANTY. LICENSOR EXPRESSLY DISCLAIMS ANY LIABILITY FOR ANY CLAIM ARISING FROM OR OUT OF THE CONTENT, INCLUDING BUT NOT LIMITED TO ANY ERRORS, INACCURACIES, OMISSIONS, OR DEFECTS CONTAINED THEREIN, AND ANY IMPLIED OR EXPRESS WARRANTY AS TO MERCHANTABILITY OR FITNESS FOR A PARTICULAR PURPOSE. IN NO EVENT SHALL LICENSOR BE LIABLE TO YOU OR ANY OTHER PARTY OR ANY OTHER PERSON OR FOR ANY SPECIAL, CONSEQUENTIAL, INCIDENTAL, INDIRECT, PUNITIVE, OR EXEMPLARY DAMAGES, HOWEVER CAUSED, ARISING OUT OF OR IN CONNECTION WITH THE DOWNLOADING, VIEWING OR USE OF THE LICENSED MATERIAL REGARDLESS OF THE FORM OF ACTION, WHETHER FOR BREACH OF CONTRACT, BREACH OF WARRANTY, TORT, NEGLIGENCE, INFRINGEMENT OR OTHERWISE (INCLUDING, WITHOUT LIMITATION, DAMAGES BASED ON LOSS OF PROFITS, DATA, FILES, USE, BUSINESS OPPORTUNITY OR CLAIMS OF THIRD PARTIES), AND WHETHER OR NOT THE PARTY HAS BEEN ADVISED OF THE POSSIBILITY OF SUCH DAMAGES. THIS LIMITATION APPLIES NOTWITHSTANDING ANY FAILURE OF ESSENTIAL PURPOSE OF ANY LIMITED REMEDY PROVIDED HEREIN.

**10. Termination and Cancellation**

10. 1. The License and all rights granted hereunder will continue until the end of the applicable period shown in Clause 5.1 above. Thereafter, this license will be terminated and all rights granted hereunder will cease.

10. 2. Licensor reserves the right to terminate the License in the event that payment is not received in full or if you breach the terms of this License.

**11. General**

11. 1. The License and the rights and obligations of the parties hereto shall be construed, interpreted and determined in accordance with the laws of the Federal Republic of Germany without reference to the stipulations of the CISG (United Nations Convention on Contracts for the International Sale of Goods) or to Germany´s choice-of-law principle.

11. 2. The parties acknowledge and agree that any controversies and disputes arising out of this License shall be decided exclusively by the courts of or having jurisdiction for Heidelberg, Germany, as far as legally permissible.

11. 3. This License is solely for Licensor's and Licensee's benefit. It is not for the benefit of any other person or entity.

**Questions?** For questions on Copyright Clearance Center accounts or website issues please contact springernaturesupport@copyright.com or +1-855-239-3415 (toll free in the US) or +1-978-646-2777. For questions on Springer Nature licensing please visit https://www.springernature.com/gp/partners/rights-permissions-third-party-distribution

**Other Conditions**:

Version 1.4 - Dec 2022

**Questions? customercare@copyright.com.**

ELSEVIER LICENSE
TERMS AND CONDITIONS

Jul 24, 2023

---

This Agreement between Letícia Mendes ("You") and Elsevier ("Elsevier") consists of your license details and the terms and conditions provided by Elsevier and Copyright Clearance Center.

| | |
|---|---|
| License Number | 5595480390711 |
| License date | Jul 24, 2023 |
| Licensed Content Publisher | Elsevier |
| Licensed Content Publication | Sensors and Actuators B: Chemical |
| Licensed Content Title | Wearable electrochemical microneedle sensing platform for real-time continuous interstitial fluid monitoring of apomorphine: Toward Parkinson management |
| Licensed Content Author | K. Yugender Goud,Kuldeep Mahato,Hazhir Teymourian,Katherine Longardner,Irene Litvan,Joseph Wang |
| Licensed Content Date | Mar 1, 2022 |
| Licensed Content Volume | 354 |
| Licensed Content Issue | n/a |
| Licensed Content Pages | 1 |
| Start Page | 131234 |
| End Page | 0 |
| Type of Use | reuse in a thesis/dissertation |

| | |
|---|---|
| Portion | figures/tables/illustrations |
| Number of figures/tables/illustrations | 2 |
| Format | electronic |
| Are you the author of this Elsevier article? | No |
| Will you be translating? | No |
| Title | Development of portable electrochemical devices on polymer materials using CO2 laser for analytical applications |
| Institution name | University of Sao Paulo |
| Expected presentation date | Sep 2023 |
| Order reference number | 105 |
| Portions | Graphical Abstract, Fig. 1 |
| Requestor Location | Letícia Mendes<br>Rua Amabile Miosso 242<br><br>Votorantim, São Paulo 18117-070<br>Brazil<br>Attn: University of São Paulo |
| Publisher Tax ID | GB 494 6272 12 |
| Total | 0.00 USD |

Terms and Conditions

**INTRODUCTION**

1. The publisher for this copyrighted material is Elsevier. By clicking "accept" in connection with completing this licensing transaction, you agree that the following terms and conditions apply to this transaction (along with the Billing and Payment terms and conditions

established by Copyright Clearance Center, Inc. ("CCC"), at the time that you opened your RightsLink account and that are available at any time at https://myaccount.copyright.com).

**GENERAL TERMS**

2. Elsevier hereby grants you permission to reproduce the aforementioned material subject to the terms and conditions indicated.

3. Acknowledgement: If any part of the material to be used (for example, figures) has appeared in our publication with credit or acknowledgement to another source, permission must also be sought from that source. If such permission is not obtained then that material may not be included in your publication/copies. Suitable acknowledgement to the source must be made, either as a footnote or in a reference list at the end of your publication, as follows:

"Reprinted from Publication title, Vol /edition number, Author(s), Title of article / title of chapter, Pages No., Copyright (Year), with permission from Elsevier [OR APPLICABLE SOCIETY COPYRIGHT OWNER]." Also Lancet special credit - "Reprinted from The Lancet, Vol. number, Author(s), Title of article, Pages No., Copyright (Year), with permission from Elsevier."

4. Reproduction of this material is confined to the purpose and/or media for which permission is hereby given. The material may not be reproduced or used in any other way, including use in combination with an artificial intelligence tool (including to train an algorithm, test, process, analyse, generate output and/or develop any form of artificial intelligence tool), or to create any derivative work and/or service (including resulting from the use of artificial intelligence tools).

5. Altering/Modifying Material: Not Permitted. However figures and illustrations may be altered/adapted minimally to serve your work. Any other abbreviations, additions, deletions and/or any other alterations shall be made only with prior written authorization of Elsevier Ltd. (Please contact Elsevier's permissions helpdesk here). No modifications can be made to any Lancet figures/tables and they must be reproduced in full.

6. If the permission fee for the requested use of our material is waived in this instance, please be advised that your future requests for Elsevier materials may attract a fee.

7. Reservation of Rights: Publisher reserves all rights not specifically granted in the combination of (i) the license details provided by you and accepted in the course of this licensing transaction, (ii) these terms and conditions and (iii) CCC's Billing and Payment terms and conditions.

8. License Contingent Upon Payment: While you may exercise the rights licensed immediately upon issuance of the license at the end of the licensing process for the transaction, provided that you have disclosed complete and accurate details of your proposed use, no license is finally effective unless and until full payment is received from you (either by publisher or by CCC) as provided in CCC's Billing and Payment terms and conditions. If full payment is not received on a timely basis, then any license preliminarily granted shall be deemed automatically revoked and shall be void as if never granted. Further, in the event that you breach any of these terms and conditions or any of CCC's Billing and Payment terms and conditions, the license is automatically revoked and shall be void as if never granted. Use of materials as described in a revoked license, as well as any use of the materials beyond the scope of an unrevoked license, may constitute copyright infringement and publisher reserves the right to take any and all action to protect its copyright in the materials.

9. Warranties: Publisher makes no representations or warranties with respect to the licensed material.

10. Indemnity: You hereby indemnify and agree to hold harmless publisher and CCC, and their respective officers, directors, employees and agents, from and against any and all claims arising out of your use of the licensed material other than as specifically authorized pursuant to this license.

11. No Transfer of License: This license is personal to you and may not be sublicensed, assigned, or transferred by you to any other person without publisher's written permission.

12. No Amendment Except in Writing: This license may not be amended except in a writing signed by both parties (or, in the case of publisher, by CCC on publisher's behalf).

13. Objection to Contrary Terms: Publisher hereby objects to any terms contained in any purchase order, acknowledgment, check endorsement or other writing prepared by you, which terms are inconsistent with these terms and conditions or CCC's Billing and Payment terms and conditions. These terms and conditions, together with CCC's Billing and Payment terms and conditions (which are incorporated herein), comprise the entire agreement between you and publisher (and CCC) concerning this licensing transaction. In the event of any conflict between your obligations established by these terms and conditions and those established by CCC's Billing and Payment terms and conditions, these terms and conditions shall control.

14. Revocation: Elsevier or Copyright Clearance Center may deny the permissions described in this License at their sole discretion, for any reason or no reason, with a full refund payable to you. Notice of such denial will be made using the contact information provided by you. Failure to receive such notice will not alter or invalidate the denial. In no event will Elsevier or Copyright Clearance Center be responsible or liable for any costs, expenses or damage incurred by you as a result of a denial of your permission request, other than a refund of the amount(s) paid by you to Elsevier and/or Copyright Clearance Center for denied permissions.

## LIMITED LICENSE

The following terms and conditions apply only to specific license types:

15. **Translation**: This permission is granted for non-exclusive world **English** rights only unless your license was granted for translation rights. If you licensed translation rights you may only translate this content into the languages you requested. A professional translator must perform all translations and reproduce the content word for word preserving the integrity of the article.

16. **Posting licensed content on any Website**: The following terms and conditions apply as follows: Licensing material from an Elsevier journal: All content posted to the web site must maintain the copyright information line on the bottom of each image; A hyper-text must be included to the Homepage of the journal from which you are licensing at http://www.sciencedirect.com/science/journal/xxxxx or the Elsevier homepage for books at http://www.elsevier.com; Central Storage: This license does not include permission for a scanned version of the material to be stored in a central repository such as that provided by Heron/XanEdu.

Licensing material from an Elsevier book: A hyper-text link must be included to the Elsevier homepage at http://www.elsevier.com . All content posted to the web site must maintain the copyright information line on the bottom of each image.

**Posting licensed content on Electronic reserve**: In addition to the above the following clauses are applicable: The web site must be password-protected and made available only to bona fide students registered on a relevant course. This permission is granted for 1 year only. You may obtain a new license for future website posting.

17. **For journal authors:** the following clauses are applicable in addition to the above:

**Preprints:**

A preprint is an author's own write-up of research results and analysis, it has not been peer-reviewed, nor has it had any other value added to it by a publisher (such as formatting, copyright, technical enhancement etc.).

Authors can share their preprints anywhere at any time. Preprints should not be added to or enhanced in any way in order to appear more like, or to substitute for, the final versions of articles however authors can update their preprints on arXiv or RePEc with their Accepted Author Manuscript (see below).

If accepted for publication, we encourage authors to link from the preprint to their formal publication via its DOI. Millions of researchers have access to the formal publications on ScienceDirect, and so links will help users to find, access, cite and use the best available version. Please note that Cell Press, The Lancet and some society-owned have different preprint policies. Information on these policies is available on the journal homepage.

**Accepted Author Manuscripts:** An accepted author manuscript is the manuscript of an article that has been accepted for publication and which typically includes author-incorporated changes suggested during submission, peer review and editor-author communications.

Authors can share their accepted author manuscript:

- immediately
    - via their non-commercial person homepage or blog
    - by updating a preprint in arXiv or RePEc with the accepted manuscript
    - via their research institute or institutional repository for internal institutional uses or as part of an invitation-only research collaboration work-group
    - directly by providing copies to their students or to research collaborators for their personal use
    - for private scholarly sharing as part of an invitation-only work group on commercial sites with which Elsevier has an agreement
- After the embargo period
    - via non-commercial hosting platforms such as their institutional repository
    - via commercial sites with which Elsevier has an agreement

In all cases accepted manuscripts should:

- link to the formal publication via its DOI
- bear a CC-BY-NC-ND license - this is easy to do
- if aggregated with other manuscripts, for example in a repository or other site, be shared in alignment with our hosting policy not be added to or enhanced in any way to appear more like, or to substitute for, the published journal article.

**Published journal article (JPA):** A published journal article (PJA) is the definitive final record of published research that appears or will appear in the journal and embodies all value-adding publishing activities including peer review co-ordination, copy-editing, formatting, (if relevant) pagination and online enrichment.

Policies for sharing publishing journal articles differ for subscription and gold open access articles:

**Subscription Articles:** If you are an author, please share a link to your article rather than the full-text. Millions of researchers have access to the formal publications on ScienceDirect, and so links will help your users to find, access, cite, and use the best available version.

Theses and dissertations which contain embedded PJAs as part of the formal submission can be posted publicly by the awarding institution with DOI links back to the formal publications on ScienceDirect.

If you are affiliated with a library that subscribes to ScienceDirect you have additional private sharing rights for others' research accessed under that agreement. This includes use for classroom teaching and internal training at the institution (including use in course packs and courseware programs), and inclusion of the article for grant funding purposes.

**Gold Open Access Articles:** May be shared according to the author-selected end-user license and should contain a CrossMark logo, the end user license, and a DOI link to the formal publication on ScienceDirect.

Please refer to Elsevier's posting policy for further information.

18. **For book authors** the following clauses are applicable in addition to the above: Authors are permitted to place a brief summary of their work online only. You are not allowed to download and post the published electronic version of your chapter, nor may you scan the printed edition to create an electronic version. **Posting to a repository:** Authors are permitted to post a summary of their chapter only in their institution's repository.

19. **Thesis/Dissertation**: If your license is for use in a thesis/dissertation your thesis may be submitted to your institution in either print or electronic form. Should your thesis be published commercially, please reapply for permission. These requirements include permission for the Library and Archives of Canada to supply single copies, on demand, of the complete thesis and include permission for Proquest/UMI to supply single copies, on demand, of the complete thesis. Should your thesis be published commercially, please reapply for permission. Theses and dissertations which contain embedded PJAs as part of the formal submission can be posted publicly by the awarding institution with DOI links back to the formal publications on ScienceDirect.

## Elsevier Open Access Terms and Conditions

You can publish open access with Elsevier in hundreds of open access journals or in nearly 2000 established subscription journals that support open access publishing. Permitted third party re-use of these open access articles is defined by the author's choice of Creative Commons user license. See our open access license policy for more information.

**Terms & Conditions applicable to all Open Access articles published with Elsevier:**

Any reuse of the article must not represent the author as endorsing the adaptation of the article nor should the article be modified in such a way as to damage the author's honour or reputation. If any changes have been made, such changes must be clearly indicated.

The author(s) must be appropriately credited and we ask that you include the end user license and a DOI link to the formal publication on ScienceDirect.

If any part of the material to be used (for example, figures) has appeared in our publication with credit or acknowledgement to another source it is the responsibility of the user to ensure their reuse complies with the terms and conditions determined by the rights holder.

**Additional Terms & Conditions applicable to each Creative Commons user license:**

**CC BY:** The CC-BY license allows users to copy, to create extracts, abstracts and new works from the Article, to alter and revise the Article and to make commercial use of the Article (including reuse and/or resale of the Article by commercial entities), provided the user gives appropriate credit (with a link to the formal publication through the relevant

DOI), provides a link to the license, indicates if changes were made and the licensor is not represented as endorsing the use made of the work. The full details of the license are available at http://creativecommons.org/licenses/by/4.0.

**CC BY NC SA:** The CC BY-NC-SA license allows users to copy, to create extracts, abstracts and new works from the Article, to alter and revise the Article, provided this is not done for commercial purposes, and that the user gives appropriate credit (with a link to the formal publication through the relevant DOI), provides a link to the license, indicates if changes were made and the licensor is not represented as endorsing the use made of the work. Further, any new works must be made available on the same conditions. The full details of the license are available at http://creativecommons.org/licenses/by-nc-sa/4.0.

**CC BY NC ND:** The CC BY-NC-ND license allows users to copy and distribute the Article, provided this is not done for commercial purposes and further does not permit distribution of the Article if it is changed or edited in any way, and provided the user gives appropriate credit (with a link to the formal publication through the relevant DOI), provides a link to the license, and that the licensor is not represented as endorsing the use made of the work. The full details of the license are available at http://creativecommons.org/licenses/by-nc-nd/4.0. Any commercial reuse of Open Access articles published with a CC BY NC SA or CC BY NC ND license requires permission from Elsevier and will be subject to a fee.

Commercial reuse includes:

- Associating advertising with the full text of the Article
- Charging fees for document delivery or access
- Article aggregation
- Systematic distribution via e-mail lists or share buttons

Posting or linking by commercial companies for use by customers of those companies.

20. **Other Conditions**:

v1.10

**Questions? customercare@copyright.com.**